

# **The role of residual antigen and of the alarmin IL-33 in shaping the antiviral immune response**

## **Inauguraldissertation**

zur

Erlangung der Würde eines Doktors der Philosophie vorgelegt  
der Philosophisch-Naturwissenschaftlichen Fakultät der  
Universität Basel

von

**Anna-Friederike Marx**

2023

Original document stored on the publication server of the University of Basel

[edoc.unibas.ch](https://edoc.unibas.ch)



This work is licensed under a [Creative Commons Attribution 4.0 International License](https://creativecommons.org/licenses/by/4.0/).

Genehmigt von der Philosophisch-Naturwissenschaftlichen Fakultät  
auf Antrag von

Erstbetreuer: Prof. Dr. Daniel Pinschewer

Zweitbetreuer: Prof. Dr. Christoph Dehio

Externer Experte: Dr. Peter Aichele

Basel, den 25.05.2021

Prof. Dr. Marcel Mayor

Dekan

# Table of Contents

<b>Table of Contents</b> .....	<b>2</b>
<b>List of Figures</b> .....	<b>7</b>
<b>List of Supplementary Figures</b> .....	<b>8</b>
<b>List of Graphical abstracts</b> .....	<b>9</b>
<b>Abbreviations</b> .....	<b>10</b>
<b>I Introduction</b> .....	<b>13</b>
<b>I.I Arenaviruses and their biological implications</b> .....	<b>13</b>
<b>I.II The Lymphocytic choriomeningitis model of viral infection</b> .....	<b>14</b>
<b>I.III Arenavirus-based vector platform</b> .....	<b>15</b>
<b>I.IV The adaptive immune responses in acute and chronic LCMV infection and the importance of T- cell factor-1 expressing CD8 T cells for viral clearance</b> .....	<b>16</b>
<b>I.V The role of cytokines and antigen availability in adaptive immune response</b> .....	<b>19</b>
<b>I.VI The diverse role of the IL-33-ST2 axis in viral infection</b> .....	<b>19</b>
<b>I.VII The role of type I interferon in controlling virus replication and fostering effective antiviral immunity</b> .....	<b>21</b>
<b>I.VIII LCMV-derived antigen-availability and -retention shape T and B- cell differentiation</b> .....	<b>23</b>
<b>II. Aim of the Thesis</b> .....	<b>24</b>
<b>1. Residual LCMV antigen in transiently CD4<sup>+</sup> T cell-depleted mice induces high levels of virus-specific antibodies but only limited B cell memory</b> .....	<b>25</b>
<b>1.1 Abstract</b> .....	<b>26</b>
<b>1.2 Introduction</b> .....	<b>27</b>
<b>1.3 Results</b> .....	<b>27</b>
<b>1.3.1 Anti-LCMV immune response in mice transiently depleted of CD4<sup>+</sup> T cells during acute infection</b> ...	<b>27</b>
<b>1.3.2 Antigen-binding avidity and IgG subclass distribution</b> .....	<b>28</b>
<b>1.3.3 Induction of LCMV GP-specific IgG Ab with delayed kinetics</b> .....	<b>29</b>

1.3.4 Antigen-induced proliferation of LCMV GP-specific KL25HL B cells in LCMV immune hosts .....	29
1.3.5 Role of FcγR and complement receptors CD21/CD35 .....	30
1.3.6 LCMV NP-specific IgG Ab secreting cells and plasma cells .....	30
1.3.7 LCMV NP-specific B cell memory in transiently CD4 <sup>+</sup> T cell depleted mice is strongly impaired .....	31
<b>1.4 Discussion .....</b>	<b>32</b>
<b>1.5 Material and Methods .....</b>	<b>35</b>
1.5.1 Mice and infections .....	35
1.5.2 LCMV qPCR .....	35
1.5.3 Adoptive transfer of B cells from KL25HL/VI10 BCR knock-in / tg mice .....	35
1.5.4 Flow cytometry .....	36
1.5.5 Determination of LCMV GP- and NP-specific Abs .....	36
1.5.6 Quantification of LCMV NP-specific Ab secreting cells by ELISPOT .....	37
<b>1.6 Acknowledgements .....</b>	<b>37</b>
<b>1.7 Conflict of Interest .....</b>	<b>37</b>
<b>1.8 Figures .....</b>	<b>38</b>
<b>1.9 Supplementary Figures .....</b>	<b>45</b>
<b>2. <i>Heterologous arenavirus vector prime – boost overrules self-tolerance for efficient tumor-specific CD8 T cell attack</i> .....</b>	<b>49</b>
<b>2.1 Summary .....</b>	<b>50</b>
<b>2.2 Introduction .....</b>	<b>51</b>
<b>2.3 Results .....</b>	<b>52</b>
2.3.1 Arenavirus vector backbone candidates and their genetic and phenotypic stability .....	52
2.3.2 artARENA vectors are attenuated in guinea pig and in a mouse pathogenesis model .....	54
2.3.3 Immunogenicity and epitope dominance in heterologous artARENA prime – boost vaccination .....	55
2.3.4 Phenotype of artARENA-induced CTLs and their dependence on IL-33 – ST2 alarmin signaling .....	56
2.3.5 Genealogic artARENA vector backbone relatedness dictates interference by pre-existing immunity and potency in heterologous prime – boost immunization .....	57
2.3.6 Interference by vector backbone-specific CTLs rather than by neutralizing antibodies .....	58
2.3.7 Heterologous artARENA vector immunotherapy increases TIL numbers and tumor cure rates resulting in long-term anti-tumor immunity .....	59
<b>2.4 Discussion .....</b>	<b>60</b>
<b>2.5 Limitations of the study .....</b>	<b>62</b>



<b>2.6 Acknowledgements .....</b>	<b>62</b>
<b>2.7 Author contributions .....</b>	<b>62</b>
<b>2.8 Declaration of interests .....</b>	<b>63</b>
<b>2.9 Results-Figures .....</b>	<b>64</b>
<b>2.10 Results-Supplementary Figures .....</b>	<b>73</b>
<b>2.11 Material and Methods .....</b>	<b>81</b>
2.11.1 Animals and ethics statement.....	81
2.11.2 Cell lines .....	81
2.11.3 Viruses, titration and neutralization test .....	82
2.11.4 Viral virulence testing.....	82
2.11.5 Tumor implantation and tumor measurement.....	82
2.11.6 Virus engineering, infection and immunization .....	83
2.11.7 Assessment of blood-brain-barrier integrity.....	83
2.11.8 Virus sequencing and genealogy tree building.....	84
2.11.9 Flow cytometry .....	84
2.11.10 Statistical testing.....	85
<b>3.     <i>Alarmins and type I interferon synergistically potentiate antiviral CD8 T cell responses by promoting stemness .....</i></b>	<b>86</b>
<b>3.1 Abstract.....</b>	<b>87</b>
<b>3.2 Introduction .....</b>	<b>88</b>
<b>3.3 Material and Methods .....</b>	<b>89</b>
3.3.1 Mice and animal experimentation .....	89
3.3.2 Viruses, virus titrations, infections and immunizations .....	90
3.3.3 Flow cytometry and intracellular staining for transcription factors.....	90
3.3.4 Next generation RNA sequencing and bioinformatic data analyses .....	91
3.3.5 Adoptive cell transfer and FACS sorting.....	92
3.3.6 <i>In vivo</i> antibody blockade.....	93
3.3.7 <i>In vitro</i> activation of P14 Wt cells with or without IL-33.....	93
3.3.8 Histology .....	94
3.3.9 Statistical analysis .....	94
<b>3.4 Results.....</b>	<b>95</b>
3.4.1 The expansion and fate of CD8 T cells depends on IL-33 signaling .....	95
3.4.2 IL-33 signaling promotes the formation of stem-like CD8 T cells.....	96

3.4.3 IL-33 signaling balances IFN-I effects to maintain CD8 T cell stemness .....	96
3.4.4 IL-33 balances IFN-I effects for efficient expansion and self-renewal of early CD8 T <sub>SCL</sub> cells.....	98
3.4.5 IL-33 signals at the onset of infection impact the quality of emerging CD8 T <sub>SCL</sub> cells .....	99
<b>3.5 Discussion.....</b>	<b>100</b>
<b>3.6 Figures.....</b>	<b>102</b>
<b>3.7 Supplementary Figures .....</b>	<b>112</b>
<b>3.8 Author contributions .....</b>	<b>115</b>
<b>3.9 Acknowledgements .....</b>	<b>115</b>
<b>4. <i>Supplementary data for: Alarmins and type I interferon synergistically potentiate antiviral CD8 T cell responses by promoting stemness.....</i></b>	<b>116</b>
<b>4.1 Introduction .....</b>	<b>116</b>
<b>4.2 Material and Methods .....</b>	<b>117</b>
4.2.1 Mice and animal experimentations.....	117
4.2.2 Viruses.....	117
4.2.3 Flow cytometry and intracellular staining for cytokines .....	117
4.2.4 Adoptive cell transfer .....	118
4.2.5 Bone marrow chimeric mice .....	118
4.2.6 <i>In vivo</i> antibody blockade.....	118
4.2.7 Statistics .....	119
<b>4.3 Results.....</b>	<b>119</b>
4.3.1 The interplay of type I interferon and IL-33 in fostering an effective CD8 T cell response upon chronic antigen exposure .....	119
4.3.2 IFN-I sensing by hematopoietic cells results in an inflammatory environment in which ST2 <sup>-/-</sup> CD8 T cells expand poorly .....	120
4.3.3 The impaired expansion of ST2 <sup>-/-</sup> CD8 T cell cannot be explained by a higher sensitivity towards the immunosuppressive cytokine IL-10.....	120
<b>4.4 Discussion.....</b>	<b>121</b>
<b>4.5 Figures.....</b>	<b>123</b>
<b>III. Global Discussion and Perspectives .....</b>	<b>127</b>
<b>IV. References.....</b>	<b>133</b>
<b>V. Appendix .....</b>	<b>153</b>

<b>V.1 Background .....</b>	<b>154</b>
<b>V.2 Case presentation .....</b>	<b>154</b>
<b>V.3 Conclusions .....</b>	<b>154</b>
<b>V.4 Author contribution .....</b>	<b>154</b>
<b><i>VI. Contributions to the work.....</i></b>	<b><i>155</i></b>
<b><i>Curriculum vitae .....</i></b>	<b><i>156</i></b>
<b><i>Acknowledgment.....</i></b>	<b><i>159</i></b>

## List of Figures

<i>Figure 1-1 Anti-LCMV immune response in mice that had been transiently depleted of CD4 T cells during acute infection</i> .....	38
<i>Figure 1-2 Antigen-binding avidity and IgG subclass distribution</i> .....	39
<i>Figure 1-3 Induction of LCMV-GP specific IgG with a delayed kinetics</i> .....	40
<i>Figure 1-4 Proliferation of LCMV GP-specific KL25HL B cells induced by residual LCMV antigen</i> .....	41
<i>Figure 1-5 Role of FcR and the complement receptors CD21/CD35</i> .....	42
<i>Figure 1-6 LCMV NP-specific IgG ASC and plasma cells in BM</i> .....	43
<i>Figure 1-7 LCMV NP-specific memory B cell response</i> .....	44
<i>Figure 2-1 Arenavirus vector backbone candidates and their genetic and phenotypic stability</i> .....	64
<i>Figure 2-2 artARENA vectors are attenuated in guinea pig and mouse pathogenesis models</i> .....	66
<i>Figure 2-3 Immunogenicity and epitope dominance in heterologous artARENA prime – boost vaccination</i> .....	67
<i>Figure 2-4 Phenotype of artARENA-induced CTLs and their dependence on IL-33 – ST2 alarmin signaling</i> .....	68
<i>Figure 2-5 Genealogic artARENA vector backbone relatedness dictates interference by pre-existing immunity and potency in heterologous prime – boost immunization</i> .....	70
<i>Figure 2-6 Interference by vector backbone-specific CTLs rather than by nAbs</i> .....	71
<i>Figure 2-7 Heterologous artARENA vector immunotherapy increases TIL numbers and tumor cure rates resulting in long-term anti-tumor immunity</i> .....	72
<i>Figure 3-1 CD8 T cell-intrinsic IL-33 signaling is essential for the response to chronic viral infection</i> .....	102
<i>Figure 3-2 IL-33 is required to preserve the Tcf-1 expressing population</i> .....	104
<i>Figure 3-3 Upon type I interferon exposure, IL-33 signaling enables differentiation of CD8 T cells into CD8 T<sub>SCL</sub></i> .....	106
<i>Figure 3-4 The proliferative as well as the generation capacity of CD8 T<sub>SCL</sub> cells and the differentiation into effector CD8 T cells is clearly IL-33 dependent</i> .....	108
<i>Figure 3-5 Self-generation of CD8 T<sub>SCL</sub> as well as the proliferative capacity rely on IL-33 signaling within the first 4 days</i> .....	110
<i>Figure 4-1 Comparison of the expansion kinetics of P14 Wt and P14 ST2<sup>-/-</sup> CD8 T cells in type I interferon depleted mice in comparison to IFNAR<sup>-/-</sup> mice</i> .....	123
<i>Figure 4-2 IL-33 signaling is compensating IFN-I signaling on a single cell level</i> .....	124
<i>Figure 4-3 Understanding the role of hematopoietic and non-hematopoietic IFNAR signaling for the expansion of P14 ST2<sup>-/-</sup> CD8 T cells</i> .....	125
<i>Figure 4-4 Comparison of the expansion kinetics of P14 Wt and P14 ST2<sup>-/-</sup> CD8 T cells in IL-10<sup>-/-</sup> mice compared to Wt recipients</i> .....	126

## List of Supplementary Figures

<i>S 1-1 Control of LCMV Armstrong infection is independent of CD4+ T cells</i> .....	45
<i>S 1-2 Lack of a LCMV NP-specific IgM response in mice that had been transiently depleted of CD4+ T cells during acute infection</i> .....	45
<i>S 1-3 MHC class II-deficient mice fail to generate LCMV NP-specific IgG Ab</i> .....	46
<i>S 1-4 Repeated administration of anti-CD4 Ab prevents induction of LCMV NP-specific IgG</i> .....	46
<i>S 1-5 T<sub>FH</sub> phenotype (PD-1<sup>+</sup>CXCR5<sup>+</sup>) of LCMV NP309-specific CD4<sup>+</sup> T cells</i> .....	47
<i>S 1-6 Numbers of LCMV NP309-tet<sup>+</sup> CD4<sup>+</sup> T cells in CD4 Ab-treated and control LCMV immune mice 5 days after LCMV rechallenge</i> .....	48
<i>S 1-7 Supporting Fig. 7A</i> .....	48
<i>S 1-8 Supporting Fig. 7B</i> .....	48
<i>S 2-1 Genetic and phenotypic stability of artARENA and r3ARENA vectors. Related to Figure 2-1</i> .....	73
<i>S 2-2 artARENA vectors are attenuated in guinea pigs. Related to Figure 2-2</i> .....	75
<i>S 2-3 Functionality of CD8 T cell response to heterologous artARENA prime – boost vaccination. Related to Figure 2-3</i> .....	76
<i>S 2-4 Impact of heterologous artARENA vector prime – boost interval on CTL responses, and efficient artPICV boost of artLCMV-primed responses after a long interval. Related to Figure 2-3</i> .....	77
<i>S 2-5 Phenotype of artARENA-induced CTLs one month after boost. Related to Figure 2-4</i> .....	78
<i>S 2-6 Dependence of artARENA-induced CTL responses on IL-33 – ST2 alarmin signaling. Related to Figure 2-4</i> .....	79
<i>S 2-7 Cell culture growth curve of artMOPV-P1A. Related to Figure 2-5</i> .....	80
<i>S 3-1 Impaired T cell maintenance in the absence of IL-33</i> .....	112
<i>S 3-2 Gating strategy for FACS sorting of P14 Wt and P14 ST2<sup>-/-</sup> CD8 T cells</i> .....	112
<i>S 3-3 Impaired Tcf-1 expression in the absence of IL-33 signaling</i> .....	113
<i>S 3-4 Upon type I interferon exposure, the antigen-specific repertoire of antigen-specific CD8 T cells in Wt and ST2<sup>-/-</sup> mice is equalized</i> .....	113
<i>S 3-5 Gating strategy for IL-33 reporting stroma cells in the spleen</i> .....	114
<i>S 3-6 IL-33 protein levels are unaffected upon IFN-I blockade</i> .....	114
<i>S 3-7 Gating strategy for sorting of GFP<sup>+</sup> and GFP<sup>-</sup> CD8 Tcf7<sup>gfp</sup> T cells</i> .....	115
<i>S 0-1 Schematic overview summarizing the potential parameters leading to the induction of an IL-33 dependent antiviral CD8 T cell response</i> .....	130

## List of Graphical abstracts

<i>Graphical abstract 1-1 Residual LCMV antigen in transiently CD4<sup>+</sup> T cell-depleted mice induces high levels of virus-specific antibodies but only limited B cell memory.....</i>	<i>26</i>
<i>Graphical abstract 2-1 Heterologous arenavirus vector prime – boost overrules self-tolerance for efficient tumor-specific CD8 T cell attack .....</i>	<i>50</i>
<i>Graphical abstract 3-1 Alarmins and type I interferon synergistically potentiate antiviral CD8 T cell responses by promoting stemness .....</i>	<i>87</i>

## Abbreviations

AAC	Adeno-associated virus
Ab	Antibody
AIDS	Acquired Immunodeficiency Syndrome
APC	Antigen presenting cell
Arm	Armstrong
Art	artificial
BEC	Blood endothelial cells
Bcl-2	B cell lymphoma 2
BM	Bone marrow
CAND	Candid#1
CAR	Chimeric antigen receptor
CD8 T <sub>EX</sub>	Exhausted CD8 T cells
CD8 T <sub>SCL</sub>	Stem-cell like CD8 T cells
CFSE	Carboxyfluorescein succinimidyl ester
Cl-13	Clone 13
CMV	Cytomegalovirus
CNS	central nervous system
COVID-19	Coronavirus Disease 19
CSF	Cerebrospinal fluid
CTLA-4	Cytotoxic T-lymphocyte-associated protein 4
CTL	Cytotoxic T lymphocyte
DAMP	Damage-associated molecular patterns
DNA	Deoxyribonucleic acid
ELISA	Enzyme-linked Immunosorbent Assay
FACS	Fluorescent-activated cell sorting
GC	Germinal Center
GFP	Green fluorescent protein
GP	Glycoprotein
HBV	Hepatitis B virus
HCV	Hepatitis C virus
HIV	Human Immunodeficiency virus
IFN-I	Type I interferon
IFN- $\alpha$	Interferon alpha
IFN- $\gamma$	Interferon gamma
Ig	Immunoglobulin

IL	Interleukin
IL1rl1	Interleukin-1 Receptor like 1
i.p.	Intraperitoneal
i.v.	Intravenous injection
JNK	c-Jun N-terminal kinase
kD	Kilodalton
ko	Knockout
LAG-3	Lymphocyte-activation gene 3
LASV	Lassa virus
LCMV	Lymphocytic choriomeningitis virus
MAPK	Mitogen-activated protein kinase
MFI	Mean fluorescent intensity
mg	milligram
ml	milliliter
MOI	Multiplicity of infection
MHC	Major histocompatibility complex
nAb	Neutralizing antibody
mAb	Non-neutralizing antibody
NF- $\kappa$ B	Nuclear factor-kappa B
NK cell	Natural killer cell
NP	Nucleoprotein
NW	New world
OVA	Ovalbumin
OW	Old world
PAMP	Pathogen-associated molecular patterns
PCR	Polymerase chain reaction
PD-1	Programmed cell death protein 1
p.i.	Post infection
PICV	Pichinde
PFU	Plaque forming unit
PRR	Pathogen recognition receptor
RIG-1	Retinoid acid inducible gene 1
RLR	Retinoid acid inducible gene 1 (RIG-1) like receptors
RNA	Ribonucleic acid
RT-PCR	Reverse transcriptase PCR
SD	Standard Deviation
SEC	second



## Abbreviations

SEM	Standard Error of the Mean
SIV	Simian immunodeficiency virus
TCR	T cell receptor
Tfh	T follicular helper
TGF- $\beta$	Transforming growth factor beta
TLR	Toll like receptor
TIGIT	T cell immunoreceptor with Ig and ITIM domains
Tim-3	T cell immunoglobulin and mucin domain-containing protein 3
VV	Vaccinia
wk	week
wt	Wild-type

# I Introduction

## II Arenaviruses and their biological implications

The worldwide presence of arenaviruses combined with their human pathogenic potential makes their study an utmost importance. This is further impressed by the fact that certain arenaviruses, such as Lymphocytic choriomeningitis virus (LCMV), are the natural pathogens of *mus musculus*, which makes LCMV easily translatable to the most developed mammalian research model. Arenaviruses belong to the *arenaviridae* virus family and are characterized by being a bi-segmented ambisense single-stranded RNA virus (1). These viruses can infect a broad range of mammals and, as more recently discovered, reptiles (2). Indeed, due to this wide tropism, multiple species of arenaviruses can be encountered in every inhabited continent of the world. However, mammalian arenaviruses, despite being capable of infecting a wide range of mammalian species, are mostly found in rodents. Each species of arenavirus is carried by one or a limited number of rodent species and is contiguous to its reservoir's geographic range. This geographic constriction contributed to the arenavirus's ample phylogenetic diversity and has ultimately driven the separation of the mammalian arenaviruses into two subfamilies: the "New-World" (NW) arenaviruses (present exclusively in North and South America); and the "Old-world" (OW) arenaviruses (present on all other continents) (3, 4). The exception to this is LCMV, which despite having a phylogenetic resemblance with OW arenaviruses, can be found world-wide (5). This again, is reflective of its host's geographic spread, the house mouse (*mus musculus*). A further driver of diversification are genetic recombination events and vertical and horizontal transfer of viruses within and between populations (4, 6). The estimated emergence of new arenaviruses species every three years is a further testimony to their diversification potential (3).

Despite arenaviruses being able to infect humans, such events are considered an incidental and are usually contained with little human-to-human transmission reported (7). Infection occurs primarily by exposure to urine, feces or saliva from infected animals, most frequently in rural or underdeveloped settings. After human infection by an arenavirus, a broad spectrum of clinical manifestations can be observed in humans, from mild or asymptomatic infection to fatal hemorrhagic fever. The first arenavirus identified to cause hemorrhagic disease was Junin, a NW arenavirus, which incidentally is the only arenavirus for which a vaccine is currently in clinical use (8-10). This was followed by the identification of other hemorrhagic fever causing arenaviruses such as Guanarito, Machupo, and Lassa viruses (LASV) (11). The LASV is currently considered as the most important human pathogen amongst the arenaviruses for which little to no effective therapy or prevention is available (12). Yearly, thousands of infections with LASV and subsequent deaths are reported in Africa with plenty more estimated to be underreported.

As for the prototypical arenavirus, LCMV, rare cases of adult human LCMV infection have been reported with most being manifested with neurological disease such as meningitis or encephalitis, perfectly matching LCMV's namesake (13). In immunocompetent individuals infection with LCMV is described as mostly

moderate and full recovery is achieved after several weeks. Indeed, up to one third of LCMV infected people report no symptoms, despite serological evidence of infection (14).

When an infection with LCMV causes disease symptoms, the progression of the disease is described as a biphasic illness with initial symptoms such as fever and general malaise, followed by a second phase with symptoms typical of aseptic meningitis such as fever, headache, nausea and photophobia (15). In immunocompromised individuals, such as transplant patients, infection with LCMV can further progress to lethal meningoencephalitis (16). Another clinically relevant scenario is the case of prenatal infection, in which LCMV infects the fetal brain and retina leading to substantial injury and neurological malformation (17-19). In summary, the clinical manifestations of a LCMV infection are dependent on the developmental stage and immunocompetence degree of the patient. Given that the most severe LCMV infections are observed in immunocompromised individuals or infants infected in utero, this speaks towards the theory that competent cellular immunity is critical for viral clearance.

Infection with LCMV can be diagnosed indirectly by serological testing or directly by PCR. If active infection is suspected, a direct confirmation of viral presence in the blood or cerebrospinal fluid (CSF) can be confirmed by an RT-PCR directed to LCMV mRNA (20). However, PCR based diagnosis relies on active viral infection, which can lead to false negative results in the process of viral clearance. Therefore, if proof of prior infection is required, an Enzyme-linked Immunosorbent Assay (ELISA) directed at LCMV specific antibodies can be performed.

As it is the case for other arenavirus-associated diseases, an effective antiviral therapy for LCMV is still not developed. Although the off-label use of an extremely high dose of ribavirin is used for Lassa fever treatment, its usage is greatly limited by the severe side-effects and therapy efficacy is only proven if given in an early time window post infection (21). The recently developed drug favipiravir was shown to have a better antiviral activity against arenavirus in both cell cultural and animal studies with less cytotoxicity in comparison to ribavirin, and might thereby be a promising therapeutic approach (22-24).

### **I.II The Lymphocytic choriomeningitis model of viral infection**

Infection of mice with LCMV is one of the best-studied models for virus-induced immunity. Major milestones in the understanding of the mammalian immune system, such as the MHC class system (25) and T cell exhaustion (26), were reached through the use of the LCMV infection model. By having a diverse set of LCMV strains available which translate into different lengths of viral persistence in mice, the molecular mechanisms that underpin acute versus chronic infection can be duly dissected in a standardized model. Moreover, due to the non-cytolytic nature of LCMV there is a better distinction between virus mediated versus host mediated cellular destruction for the cause of tissue pathogenesis (27). Due to such a versatility, it is thus not surprising that many of the immunological findings using the LCMV infection model had a major impact in the understanding of human chronic diseases that go beyond virus infections, such as cancer or autoimmune diseases (28-30). Indeed, the mechanisms governing CD8 T cell exhaustion, which were

discovered and greatly studied using the LCMV model (discussed in section I.IV) formed the basis for cancer therapies targeting immune cell checkpoint inhibitors such as programmed cell death protein 1 (PD-1) (reviewed in (31, 32)).

Originally three different LCMV-strains were isolated: Traub, WE/UBC and Armstrong (Arm). Other strains that were derived from the original three and that are used in research are: Docile, a highly replicating strain derived from LCMV-WE (UBC) (33) and LCMV Clone 13 (LCMV Cl-13) (34). In comparison to its parent strain LCMV-Arm, which causes a transient infection, LCMV Cl-13 is characterized by causing chronic viral infection (>20 days) (34). By using reverse genetic tools three coding mutations were identified between Cl-13 and Arm, from which two of them contribute to viral persistence and immunosuppression, one in the viral polymerase (35) and the other in the glycoprotein (36, 37). Whereas the polymerase mutation conferred faster replication capacity in LCMV Cl-13, the glycoprotein mutation increased the receptor binding affinity with the former having a much greater impact on pathogenicity. Moreover, the mutation located in the glycoprotein allows LCMV Cl-13 to preferentially infect dendritic cells (38-40). Therefore, on the basis of differential replication kinetics, vastly different outcomes in terms of viral persistence are observed between Arm and Cl-13. Infection with high doses of highly disseminating strains such as LCMV Cl-13 or Docile result in prolonged viremia while LCMV-Arm is acutely cleared independently of the dosage (34, 41). Importantly, the T cell epitopes between LCMV Arm and LCMV Cl-13 are identical allowing a side-by-side comparison of an acute and chronic infection (42, 43). Importantly, as it was shown by the group of Lehman-Grube, acutely infected CD8-deficient mice are unable to clear the infection pointing out that CD8 T cells are the driving force of early viral clearance in a LCMV infection (44).

### **I.III Arenavirus-based vector platform**

CD8 T cells are a critical component of protective immunity against exogenous agents, such as viral infections, or endogenous threats, such as cancer cells. Thus, a major goal of vaccines against chronic infections such as Human immunodeficiency virus (HIV), Hepatitis C as well as tumor cells is the induction of a potent and durable CD8 T cell response. With the advent of recombinant viral vector technology, a panoply of viral vaccine delivery platforms became available, several of which are currently in clinical use (45, 46). Yet, a major challenge for the translation of various viral vectors into human therapy is the pre-existing immunity targeting the parental viral vector (47).

Since the development of arenavirus reverse genetic tools (48, 49), these vectors became a promising vaccine platform against both chronic diseases and cancer. Indeed, given the low seroprevalence of arenaviruses in the human population (50-52) combined with a glycan shield which strongly evades humoral immunity (53), arenavirus-based vectors are an optimal candidate for clinical use. In addition, LCMV was shown to directly infect antigen-presenting cells (APC), which is essential for the activation of CD8 T cells (54, 55). Due to the arenavirus unique transcription strategy, arenavirus-based vectors can only carry foreign genetic material if one of the genes is replaced in their original bi-segment arrangement. This led to the first generation of

LCMV-based vectors to be pseudotyped, with the LCMV glycoprotein (GP) gene replaced by the antigen of choice. However, such strategy greatly limits *in vivo* replication of these vectors (56).

Although these vectors are inherently safe, they are only able to deliver the genetic material in a single round of infection, having thus a limited antigenic delivery capacity. For this reason, further research was absolutely necessary. In the past the antigenic capacity of LCMV-based vectors was improved by switching to a tri-segmented genomic configuration (57). These vectors were further optimized leading to stably expressing LCMV-based attenuated immunotherapy vectors (artLCMV). As it was shown by (58), artLCMV shows both a stable attenuation and a constant expression of the transgene, thereby fulfilling the criteria for a potential vaccine vector. In addition to their natural tropism for antigen presenting cells, it was shown that artLCMV vectors are able to trigger the release of IL-33, which is an important stimulator for CD8 T cell proliferation (58, 59).

Importantly, the vector-induced cytotoxic T lymphocyte (CTL) response can be further optimized by repeated administration of hetero- or homologous boosts (discussed in (60)). Over the past years, the use of heterologous prime-boost approaches has gained significant momentum against a wide range of pathogens (61-64). By combining two distantly related arenaviruses with minimal genetic overlap the immunotherapeutic potential of the arenavirus-based vaccine platform can be further potentiated as demonstrated in chapter 2 (65).

Recently, replication-deficient LCMV vectors expressing the human cytomegalovirus antigen glycoprotein B and the 65-kD phosphoprotein were tested in a dose-escalation Phase I clinical trial (66). The fact that the vaccine was well tolerated and induced a cytomegalovirus-specific CD8 and neutralizing antibody (nAb) response in most of the healthy adult volunteers, further justified the clinical evaluation of replication-deficient LCMV vectors. Moreover, this study could clearly highlight the benefit of replication-deficient LCMV vectors by being able to induce a humoral as well as a cellular immune response.

#### **I.IV The adaptive immune responses in acute and chronic LCMV infection and the importance of T- cell factor-1 expressing CD8 T cells for viral clearance**

As mentioned in I.II, LCMV infection, particularly by the acute infection causing strains, is strictly controlled by CD8 T cells (67). Viral clearance by CD8 T cells is achieved by eliminating the infected host cells via perforin-mediated lysis (68) as well as the production of IFN- $\gamma$ , TNF- $\alpha$  and IL-2 that help to shape the developing immune response. Most of the effector CD8 T cells that peaks around day 8-10 post infection (p.i)., undergo a contraction phase, where only 5-10 % will persist and form the memory CD8 T cell pool that protect the host against reinfection (69-71). The clearance of an acute LCMV infection is depended on CD8 T cells and viral clearance can be achieved in the absence of CD4 T cells (72) and a humoral immune response (73). In contrast to the primary CD8 T cell response, which does not require CD4 T cell help, the LCMV specific B cell response is strictly CD4 T cell dependent (74). In the first weeks after LCMV infection (either acute or chronic) the vast majority of the induced LCMV-specific Abs show no antiviral activity in

cell culture neutralizing assays, and are thus referred to as non-neutralizing Abs (nnAbs) (75). The majority of described nnAbs bind either to the LCMV-nucleoprotein (NP) or LCMV-GP and are thought to provide protection by shaping the adaptive immune response (76-78). Similar to chronic infection in humans, infection of mice with LCMV strains which cause a persistent infection are associated with a compromised T-cell response (79) and have an ambivalent effect on the B cell response. Even though high affinity LCMV neutralizing antibodies are described to be generated only in the context of chronic infection (75) their appearance in physiological settings, coincides with the later stages of infection or even after clearance. This suggests that although chronic infection drives successful B cell responses, high viral loads might still be detrimental towards B cell development in the initial stages of infection (80).

Unlike to an acute infection, in a chronic LCMV infection CD8 T cells are exposed to an excessive amount of antigen and inflammatory signals. This leads to a hierarchical loss of CD8 T cell effector functions, a state called in literature “T cell exhaustion” (26, 81). Initially, CD8 T cell exhaustion was described as a clonal deletion of CD8 T cells occurring during high antigen-persistence (82). More recently, with the development of advanced methods such as major histocompatibility complex multimers (tetramer) to detect antigen-specific CD8 T cells, it became clearer that exhausted CD8 T cells are not necessarily physically deleted but are instead functionally impaired with a reduced ability to produce cytokines as well as killing infected target cells (83). Moreover, exhausted CD8 T cells (CD8 T<sub>ex</sub>) differ in their transcriptome, metabolism (84) and epigenetic imprint (85, 86) when compared to effector CD8 T cells generated upon an acute infection. Besides these aspects, CD8 T<sub>ex</sub> show high expression of multiple co-inhibitory receptors such as PD-1, TIGIT, LAG-3, CTLA-4, TIM-3 or CD39 (87-92) which dampen T cell activation by the following mechanism: changes at transcriptional level (PD-1), inhibition of competitive fitness resulting in impaired proliferation (93), altering T cell metabolism (94, 95), limiting co-stimulation (92) as well as inhibition of the signal cascade downstream of TCR signaling (96).

Several factors dictate the development of CD8 T cell exhaustion, including antigen-persistence (97), the presence of CD4 T cells (98, 99), T-cell receptor (TCR) signaling (100) and the expression of certain immunosuppressive cytokines such as IL-10 (101, 102) and TGF- $\beta$  (103). Notably, the state of CD8 T cell exhaustion is distinct from tolerance and anergy, two mechanisms that are acquired via central and peripheral immune tolerance mechanisms (104).

As previously mentioned, exhaustion of CD8 T cells has been also reported in human chronic diseases. It is now a recognizable hallmark in patients with chronic hepatitis B (105, 106), C (107) or human immunodeficiency virus (HIV) (108, 109) infection as well as oncologic diseases. Moreover, in cancer immunology reversion of intra-tumoral CD8 T cell exhaustion has been one of the major therapeutical objectives of the last decade. However, exhaustion can also be seen as a functional adaptation of the immune system to high antigen stimulation. Studies from mice deficient for PD-1 (110), clearly suggested a protective role of the inhibitory receptor PD-1. In this regard, CD8 T cell exhaustion can be seen as a mechanism to prevent immunopathology in the presence of high antigenic load and therapeutic interventions have to be chosen carefully.

As shown by (111, 112) depletion of CD8 T cells during the chronic phase of simian immunodeficiency virus (SIV) infection immediately led to increased viral titer. Such data clearly point out that CD8 T<sub>EX</sub> are not functionally inert, moreover they play an important role to keep chronic viral infection in check.

Since the parameters that lead to CD8 T cell exhaustion have been defined, methods that prevent CD8 T cell exhaustion but also enhance the effector function have become available. Indeed, inhibition of inhibitory receptors such as PD-1, Tim-3, CTLA-4 or Tim-3 showed a beneficial effect on exhausted CD8 T cells by restoring their ability to proliferate, secrete cytokines and kill infected target cells (28, 113). Several studies aimed to identify the CD8 T cell subset that provides the proliferative burst upon anti-PD-1/PDL-1 administration to further optimize the PD-1 directed immunotherapy. In 2016, several groups revealed at least two different groups of exhausted CD8 T cells. One subset is classified as a terminal differentiated CD8 T cells that perform cytotoxic functions but are unable to persist in the long term. The second subset, called stem cell-like CD8 T cells (CD8 T<sub>SCL</sub>), is characterized by the following three features: proliferative capacity, self-regeneration and ability to produce differentiated cells (discussed in (114)). Moreover, this subpopulation of virus-specific CD8 T cells was shown to sustain the ongoing immune response and exhibit increased proliferative capacity in response to checkpoint blockade. Phenotypically, CD8 T<sub>SCL</sub> display high expression of the transcription factor Tcf-1 (encoded by *Tcf7*), a transcription factor that was shown to be critical for T cell development, mature T cell differentiation and memory formation (discussed in (115)). Importantly, the generation as well as persistence of CD8 T<sub>SCL</sub> is dependent on Tcf-1 as shown by studying the phenotype of Tcf-1 deficient CD8 T cells. Besides high expression of Tcf-1, CD8 T<sub>SCL</sub> are characterized by high expression of ID3 (116), Bcl-6 (117), FOXO1 (118) and TOX (119) and the surface marker CXCR5, giving them access to B cell follicles. CXCR5 expression goes along with a significant enrichment of CD4 T follicular helper (Tfh)-related genes. Further transcriptional profiling provided evidence for a significant enrichment of a memory and exhausted gene signature, whereas genes related to effector CD8 T cells (CD8 T<sub>EF</sub>) were not upregulated (120, 121). Besides the substantial differences on a transcriptional level, these two CD8 T cell subsets showed a unique epigenetic signature (116, 122). Collectively, these data clearly point towards a heterogeneity within the pool of CD8 T cells in a chronic viral infection (discussed in (114)). To further study the interconnection between the different CD8 T cell compartments, transfer experiments of both subsets were performed. In contrast to terminal differentiated CD8 T cells, CD8 T<sub>SCL</sub> retained their proliferative capacity, regenerated and gave rise to more differentiated CD8 T cells. Recent studies suggested that the divergence of these two CD8 T cell subsets occur rapidly after CD8 T cell activation in the early phase of the chronic viral infection (116).

In summary, the observations made in 2016 were confirmed and extended by several studies highlighting the presence of stem-like CD8 T cells also in chronic infections in humans as well as in tumors (123-126). Remarkably, Tcf-1 defines CD8 T cells responding to checkpoint blockade therapy in melanoma patients highlighting the importance of Tcf-1 in preserving CD8 T cell functionality in the context of chronic tumor antigen exposure.



#### **I.V The role of cytokines and antigen availability in adaptive immune response**

Identifying molecular pathways that contribute to the generation of a potent CD8 T cell response in a chronic infection is important to confer live-long protective immunity. Throughout the course of a viral infection, CD8 T cells receive instructions from the cytokine milieu that initially operate as immunological warning signs. At later stages of the infection, a delicate balance of pro- and anti-inflammatory cytokines supports the survival and maintenance of CD8 T cells while simultaneously dampening their antiviral activity. Moreover, cytokines act in conjunction with antigenic signals to determine the fate of lymphocytes (127). Upon viral clearance, cytokines play a crucial role in maintaining the memory T cell population without further need of an antigen stimulus (128, 129).

Based on their pleiotropic functions, cytokines are attractive therapeutic candidates to improve viral control and immunity (130). To modulate the biological action, it is of high importance to study the stage dependent effects on CD8 T cells but also how these signals integrate other factors.

In the course of a LCMV infection, the first cytokines that serve as immunological warning signs are type I interferon (IFN-I) and Interleukin 33 (IL-33). Based on the aim of the study to further characterize the importance of IL-33 for the induction of a potent antiviral CD8 T cell response and to understand the interplay between IL-33 and IFN-I (discussed in chapter 3 and 4), the next two paragraphs will briefly summarize how both cytokines regulate the antiviral CD8 T cell response.

#### **I.VI The diverse role of the IL-33-ST2 axis in viral infection**

Initiation of a protective CD8 T cell response is dependent on various pro-inflammatory cytokines. This includes also members of the IL-1 family to which the IL-33 belongs (131). Based on the fact that IL-33 lacks a traditional signal sequence that would allow secretion by a conventional secretory pathway, cell death by necrosis and/or active necroptosis are considered as the key mechanism by which IL-33 reaches the extracellular milieu (132). IL-33 is considered to function as an endogenous danger signal to alert the immune system and is therefore classified as an alarmin (133). Moreover, as pointed out by (132), release of IL-33 may also reflect a physiological response to biomechanically stressed conditions. By this, IL-33 may function not only as an inflammatory cytokine but also as a mechano-sensitive paracrine factor. However, IL-33 might behave differentially depending on the cell type as well as on the stimulus applied. This cytokine is constitutively expressed as a nuclear precursor-protein in epithelial and endothelial cells (134, 135). In the spleen and in lymph nodes, fibroblastic reticular cells (FRC) were identified as the primary source of IL-33 (58, 136). Based on its nuclear localization and binding of DNA-associated histones, IL-33 was shown to be able to regulate gene transcription (137, 138) in addition to its function as an alarm mediator when released into the extracellular space. The full-length IL-33 protein consists of an N-terminal chromatin-binding motif with an IL-1 cytokine domain at its C-terminus (139). Comparison of the human and the mouse full-length protein showed 55% homology (131). In 2009, it was reported that the release of IL-33, unlike other IL-1 family members, is independent of Caspase-1 cleavage (140, 141). Subsequently, it was shown



that the proteolytic cleavage of the C-terminal cytokine domain is mediated by neutrophil elastase and cathepsin G (142, 143) resulting in an augmented bioreactivity of the alarmin. IL-33 activity is regulated by several mechanisms, including alternative splicing that leads to the production of a soluble ST2 (sST2) that act as a decoy receptor to limit IL-33 signaling (144). Another mechanism by which IL-33 activity is controlled is the formation of two disulfide-bridges that result in the disruption of the receptor-binding site (145). To avoid inappropriate inflammatory reactions in the context of apoptotic cell death, caspase-3 cleavage inactivates IL-33 (146).

After its release IL-33 binds to a heterodimeric cell surface receptor, consisting of a ubiquitous IL1R accessory protein (IL-1RAcP) and a selectively expressed receptor ST2 (131). The IL-33 receptor is expressed on various immune cell types such as eosinophils, basophils (147), innate lymphoid cells (148), regulatory cells (149), mast cells (150, 151), macrophages as well as Th1 (152) and Th2 CD4 T cells (153-155). Expression on CD8 T cells is only detectable upon activation (59).

Originally, IL-33 was described as a potent inducer of type II immunity, such as in the context of allergy or immunity to parasites and is therefore described as a cytokine elucidating mainly Th2 associated immune responses. However, over the years it became clear that IL-33 is a central mediator that is involved in a huge variety of infections and pathologies as well as tissue homeostasis (144, 153). IL-33 was also described to recruit antigen-presenting cells (156) and to mediate diverse pro-inflammatory responses (157, 158) but has also been shown to promote rheumatoid arthritis (159) and neuroinflammation (160). In addition, IL-33 is also linked to pulmonary viral infections and chronic lung diseases (161). More recently, it was published that IL-33 expression correlates with seropositivity in COVID-19 convalescent individuals. However, to which extent IL-33 play a role in SARS-CoV-2 infection is not clear and further work is needed (162). Signaling of IL-33 can be activated through either p38 mitogen activated protein kinase (MAPK), c-Jun-N terminal kinase (JNK) or nuclear factor kappa-B (NF- $\kappa$ B) cascades (163).

In 2012, our lab was able to highlight the importance of IL-33 as an CD8 T cell stimulator for several RNA and DNA viruses, amongst them LCMV (59). In an acute infection, ST2 deficient CD8 T cells showed reduced cytotoxic potential combined with an inability to differentiate into multi-functional effector cells. The fact that ST2-deficient CD8 T cells showed decreased expression of the anti-apoptotic protein Bcl-2 pointed towards a pro-survival effect of IL-33. In the same study, it was shown that exogenous IL-33, in form of recombinant protein, can augment CD8 T cell responses to vaccination and serves thereby as an adjuvant in vaccines designed to boost CD8 T cell immune responses. Based on this result, further studies reported that IL-33 co-delivered in DNA vaccines or triggered by viral vectors represents as a promising immunoadjuvant at improving antiviral as well as tumor T cell immunity (58, 164-167).

Beyond their effector-promoting activity, the alarmin was shown to be critical for memory reexpansion as well as for the differentiation of reactivated memory T cells into effector cells (168). By this, IL-33 was found to be critical for memory T cell recall responses what has important implications for immunity to recurrent diseases.

Overall, the pleotropic actions of IL-33 open new possibilities for harnessing the power of IL-33 to increase the efficiency of vaccines.

## **I.VII The role of type I interferon in controlling virus replication and fostering effective antiviral immunity**

Once emerging viruses have broken the host barrier and invaded the target organism, recognition is initiated by pathogen associated molecular patterns (PAMPs) which bind to the pattern recognition receptors (PRRs). In case of a LCMV infection, two classes of PRRs play a role. Toll-like receptors (TLR) and the retinoid acid inducible gene 1 (RIG-1) like receptors (RLRs). Both receptors signal through IRF3 and IRF7 resulting in a robust production of type I interferon (IFN-I), which signals in an autocrine and paracrine manner to induce the expression of interferon-stimulated genes, a hallmark of microbial diseases (reviewed in (169)).

The IFN-I family, which includes several IFN $\alpha$ s and a single IFN $\beta$  amongst other subtypes, is one of the key components of the antiviral host response. All IFN-I subtypes signal through the same receptor, comprised of IFNAR1 and IFNAR2, that is found on most nucleated cells. Upon ligation, several signal transduction pathways including STAT-1-homodimers, STAT-3 homodimers, PI3K-AKT, MAPK pathway, PI3K-AKT and the IFN-stimulated gene factor 3 consisting of the STAT-1-STAT-2 heterodimers and the transcription factor interferon regulatory factor 9 are activated (170, 171).

Similar to other viruses, LCMV has evolved strategies to counteract the induction of IFN-I (172, 173). However, this inhibition is not complete based on the observation that a robust production upon infection is observed (174).

In many aspects the LCMV model has enabled us to get a broader understanding of the importance of IFN- I in the innate as well as the adaptive immune response against viral infection. The earliest possible detection of IFN-I is after 6h post infection, reaching a maximum level 24h after virus-inoculum (174-176).

The action of IFN-I in the outcome of LCMV infection dramatically differ depending on 1) timing of administration or blockade, 2) used virus strain and 3) route of infection and can be either beneficial or harmful.

For an acute infection, such as caused by LCMV-Arm, it was shown that deficiency in IFN-I results in viral persistence. Besides the increased replication, the virus spreads to all organs including the CNS (174, 177, 178). Comparable need for IFN-I in controlling viral replication in an acute setting is also seen for other viruses and by this not restricted to the LCMV model (179-181). Coinciding with the inability to clear the virus, IFN-I deficiency in LCMV-Arm infected mice resulted in exhaustion of CD8 T cells (177, 179). Similar to what was observed for the effector CD8 T cell response, long-lasting memory CD8 T cells are dependent on IFN-I signaling what might coincide with an inability of the host to clear a secondary infection (182).

To understand to which extent intrinsic IFN-I is influencing the overall phenotype of antigen-specific CD8 T cells, transfer studies with IFNAR-deficient P14 TCR transgenic CD8 T cells specific for the LCMV glycoprotein (P14, (183) ) were performed. In contrast to their wild-type (Wt) counterparts, P14 IFNAR<sup>-/-</sup> CD8 T cells were severely impaired in their capacity to expand, however cell division, expression of activation markers as well as effector cell function was were not impaired (182, 184).

Later on, microarray analysis showed that IFN-I expressed on CD8 T cells triggered the expression of selected inhibitory NK-cell receptor ligands. Consequently, transferred P14 IFNAR<sup>-/-</sup> cells were eliminated

by NK-cells in a perforin-dependent manner. By this, IFN-I was identified as a key player regulating the protection of T cells against NK-cells. Accordingly, NK-cell depletion prevented the rapid elimination of transferred P14 IFNAR<sup>-/-</sup> CD8 T cells (182, 185).

In comparison to an acute infection, where IFN-I is critical to prevent persistent infection, in chronic LCMV infection it was reported that loss of IFN-I signaling leads to reduced viral loads and enhanced viral clearance (174, 186). However, a reduction in viral titers was not observed within the first days after infection. Moreover, blockade of IFNAR increased initially viral titers. Further analysis clearly pointed towards the extensive role that IFN-I plays in immunomodulation by inhibiting multiple pro-inflammatory cytokines and chemokines as well as negative regulatory molecules. In more detail, it was shown that IFNAR blockade resulted in a significant suppression of the immunosuppressive molecules IL-10 as well as PDL-1 and preserved the lymphoid architecture. Both studies concluded that the accelerated control of persistent infection induced by blocking IFN-I signaling, is not based on an increased anti-viral CD8 T cell response, but is dependent on CD4 T cells. In addition, it was shown that an enhanced IFN- $\gamma$  production is associated with viral clearance (174, 186).

While a lot has been learnt from dampening the IFN-I response, other studies focused on augmenting the IFN-I response such as by administration of recombinant IFN-I. Such treatment during the first week post LCMV CI-13 infection showed a beneficial effect on the CD8 T cell response as well as on the control of the infection (175). However, the treatment after the first week of LCMV CI-13 infection showed no impact on the outcome in terms of viral control (175, 187). In contrast, when CD8 T cells were primed with IFN-I prior to LCMV CI-13 infection, a robust CD8 T cell response was observed that results in viral clearance of LCMV CI-13 within two weeks (188). Overall, these data clearly indicate that IFN-I mediated clearance of LCMV CI-13 coincides with the priming of the antiviral CD8 T cell response.

In terms of therapeutic benefit, blockade of IFN-I as a therapeutic approach showed mixed outcomes in pre-clinical settings, with potentially severe drawbacks that would preclude its clinical use. Even though type I interferon blockade was shown to enhance clearance of chronic LCMV infection, blockade of IFN-I during simian immunodeficiency virus infection resulted in enhanced viral replication (189), whereas treatment with IFN-I in humanized mice showed an increase of the anti-HIV CD8 T cell response (190). Additionally, IFN-I therapy (alpha) is a clinically approved treatment for chronic hepatitis C and B infection, and is used worldwide due to its cost-effective results (191, 192).

In summary, given the fact that studies revealed both negative as well as positive effects of IFN-I, it is imperative to critically delineate the effect of IFN-I in chronic disease settings.

### **I.VIII LCMV-derived antigen-availability and -retention shape T and B- cell differentiation**

Besides the inflammatory milieu, the antigen-availability is one of the key elements shaping an adaptive immune response. The levels and duration of antigen stimulation is a critical determinant for the initiation of a protective immune response, as it has been observed when comparing the CD8 T cell response in an acute versus a chronic LCMV infection. In case of an acute infection, the level of antigen is sufficient to promote an effective immune response that finally enables the host to clear the infection. However, in the context of a chronic viral infection, the high amount of antigen over a longer time-period is one of the major causes of CD8 T cell exhaustion as discussed in section I.IV. Studies from other infections highlighted that a short-term antigen presentation negatively impact the magnitude of the CD8 T cell response (193). Delivery of a maximal amount of antigen at a single dose is thereby considered as the most efficient strategy for the induction of a potent CD8 T cell response.

Upon clearance of an acute infection, it was not known whether the viral antigen is stored and might be even capable of regulating an immune response. Antigen-retention in the LCMV infection model was first shown for CD4 T cells by transferring CFSE-labelled TCR-transgenic CD4 T cells specific for the LCMV-GP protein (referred as SMARTA CD4 T cells (194)) in initially LCMV-Arm infected mice at different time points after infection. Up to 2 months after infection transferred SMARTA CD4 T cells were still capable to undergo cell division (195). Such data clearly point towards the existence of a natural antigen-depot. Similar results were shown for an acute vesicular stomatitis virus infection (196) and influenza infection (197, 198). In comparison to CD4 T cells, CD8 T cells were not stimulated by resident LCMV-derived antigen (195). Based on the observation that residual viral antigen is present for several weeks at sufficient levels to stimulate antigen-specific CD4 T cells, we studied to which extent the residual antigen is sufficient to induce a functional T cell help for differentiation of B cells into antibody-secreting cells and forming a protective memory pool (see chapter 2).

Overall, these studies provided important aspects for the development of effective vaccines. Moreover, they are important for our understanding on how the period immediately following the peak of an acute infection is shaping the immune response in terms of transmission into an adaptive memory response.

In the context of vaccination, facilitating a persistent depot of the protein of interest is still challenging. Often the antigen is cleared from the injection side and/or lymph nodes. Besides this, in comparison to an acute infection the antigen kinetics differ and has probably to mimicked to the natural conditions to achieve maximum vaccine potency.

## **II. Aim of the Thesis**

The aims of the thesis were threefold:

Firstly, we were interested in studying the potency of residual LCMV antigen-depots in transiently CD4 T cell depleted mice for the induction of an antiviral B cell response.

Secondly, we studied whether a heterologous arenavirus vector prime-boost was beneficial for the establishment of an effective tumor-specific CD8 T cell response.

Thirdly, we aimed to define the role of the IL-33 ST2 axis for the formation of an anti-viral CD8 T cell response in the context of a chronic viral infection.

# 1. Residual LCMV antigen in transiently CD4<sup>+</sup> T cell-depleted mice induces high levels of virus-specific antibodies but only limited B cell memory

Oliver Schweier<sup>1\*</sup>, Ulrike Aichele<sup>1\*</sup>, Anna-Friederike Marx<sup>1,3\*</sup>, Tobias Straub<sup>1</sup>, J. Sijf Verbeek<sup>2</sup>, Daniel D. Pinschewer<sup>3</sup> and Hanspeter Pircher<sup>1</sup>

<sup>1</sup>Institute for Immunology, Medical Center - University of Freiburg, Faculty of Medicine, University of Freiburg, Germany

<sup>2</sup>Department of Human Genetics, Leiden University Medical Center, Leiden, the Netherlands

<sup>3</sup>Division of Experimental Virology, Department of Biomedicine, University of Basel, Switzerland.

\* equal contribution

Keywords: antibodies, CD4<sup>+</sup> T cell depletion, LCMV, memory B cells, residual antigen

Correspondence: Hanspeter Pircher, Institute for Immunology, Hermann-Herder-Str.11, D-79104 Freiburg, Germany, Phone: +49 761 203 6521, Fax: +49 761 203 6577 e-mail: hanspeter.pircher@uniklinik-freiburg.de

This article has been published in

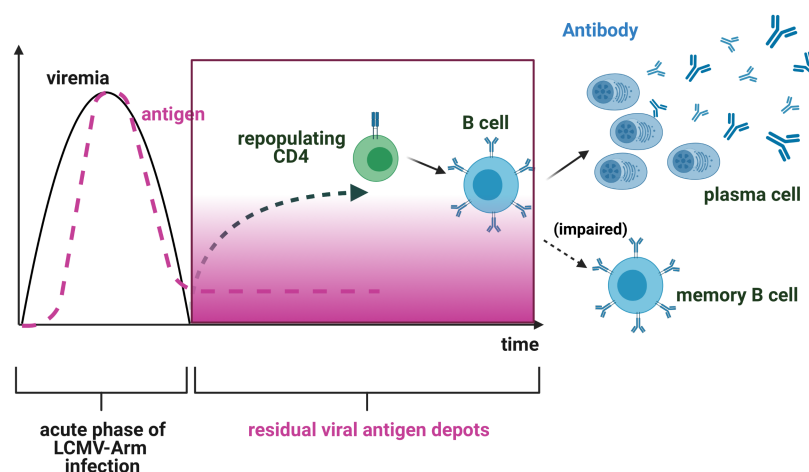
Eur. J. Immunol. 2019 Jan 19; 49: 626-637

### Abbreviations:

Ab, antibody; AF, AlexaFluor; ASC, antibody secreting cells; Arm, Armstrong; B6, C57BL/6; BCR, B cell receptor; BM, bone marrow; GC, germinal center; GP, glycoprotein; IC, immune complexes; i.p., *intraperitoneally*; LCMV, lymphocytic choriomeningitis virus; mAb, monoclonal Ab; min., minutes; NP, nucleoprotein; OVA, ovalbumin; PC, plasma cells; PE, *phycoerythrin*; tg, transgenic; p.i., post infection; pfu, plaque forming unit; PBS, phosphate buffered saline; VSV, vesicular stomatitis virus; wk, week; wt, wild-type;

## 1.1 Abstract

Infection of C57BL/6 mice with lymphocytic choriomeningitis virus (LCMV) strain Armstrong (Arm) induces an acute infection with rapid virus clearance by CD8<sup>+</sup> T cells independently of CD4<sup>+</sup> T cell help. Residual viral antigen may, however, persist for a prolonged time. Here, we demonstrate that mice that had been transiently depleted of CD4<sup>+</sup> T cells during acute LCMV Arm infection generated high levels of virus-specific IgG antibodies (Ab) after viral clearance. Robust induction of LCMV-specific IgG after transient CD4<sup>+</sup> T cell depletion was dependent on Fc $\gamma$  receptors but not on the complement receptors CD21/CD35. In contrast to the potent production of LCMV-specific IgG, the generation of LCMV-specific isotype-switched memory B cells after transient CD4<sup>+</sup> T cell depletion was considerably reduced. Moreover, mice depleted of CD4<sup>+</sup> T cells during acute infection were strongly impaired in generating a secondary LCMV-specific B cell response upon LCMV rechallenge. In conclusion, our data indicate that LCMV antigen depots after viral clearance were capable of inducing high levels of virus-specific IgG. They failed, however, to induce robust virus-specific B cell memory revealing a previously unappreciated dichotomy of specific Ab production and memory cell formation after priming with residual antigen.



Graphical abstract 1-1 Residual LCMV antigen in transiently CD4<sup>+</sup> T cell-depleted mice induces high levels of virus-specific antibodies but only limited B cell memory

(Generated with biorender.com)

## 1.2 Introduction

Presentation of antigen is often rapidly down-regulated after pathogen elimination (193, 199, 200). In certain viral infections, however, prolonged antigen presentation after pathogen clearance has been observed. In mice infected with influenza virus, residual viral antigen has been shown to promote CD4<sup>+</sup> T cell memory formation and to control migration and activation state of virus-specific cytotoxic T lymphocytes (197, 198). In this infection model, migrating respiratory dendritic cells were identified as essential for both sampling and presenting the viral antigen (201). In the vesicular stomatitis virus (VSV) model, ovalbumin (OVA)-specific OT-1 CD8<sup>+</sup> T cells adoptively transferred into VSV<sub>OVA</sub> immune mice 4 weeks (wk) post infection (p.i.) have been demonstrated to undergo antigen-specific cell division and acquisition of memory cell markers (196). In the LCMV model, virus-specific CD4<sup>+</sup> but not CD8<sup>+</sup> T cells have been shown to divide upon transfer into LCMV immune mice 6 wk p.i. (195). It is, however, unclear whether residual LCMV antigen is “sufficient” to induce functional T cell help for specific antibody (Ab) production and memory B cell formation. Here, we addressed this question using the LCMV Arm infection model. Infection of mice with LCMV Arm induces an acute infection with rapid viral clearance. Furthermore, transient Ab-mediated depletion of CD4<sup>+</sup> T cells during the acute phase prevents the induction of a LCMV-specific IgG response without affecting virus control (202). We here demonstrate that in such mice residual viral antigen after viral clearance was able to induce high levels of LCMV-specific IgG Ab with time. In contrast to the potent induction of virus-specific Ab, LCMV antigen depots failed, however, to generate a solid virus-specific B cell memory.

## 1.3 Results

### 1.3.1 Anti-LCMV immune response in mice transiently depleted of CD4<sup>+</sup> T cells during acute infection

To examine whether residual LCMV antigen is able to prime CD4<sup>+</sup> T cells for B cell help, we used the following experimental system: CD4<sup>+</sup> T cells in C57BL/6 (B6) mice were transiently depleted by injection of CD4-specific Ab. Afterwards, mice were infected with LCMV Arm and LCMV nucleoprotein (NP)-specific IgG levels in serum were determined at different time points after infection. Control of LCMV Arm infection has been shown to be independent of CD4<sup>+</sup> T cells (202). Also in our hands, infectious LCMV particles were below detection limit in spleens of anti-CD4 Ab-treated mice at day 9 p.i. (Supporting Information Fig. S 1-1). Nonetheless, copies of viral RNA in this organ could be detected by qPCR up to wk 4 p.i.. The copy numbers at day 7 p.i. were 10<sup>2</sup>-10<sup>3</sup>-fold lower when compared to day 5, but did not significantly differ in anti-CD4 Ab-treated and control mice (Fig. 1-1 A). In non-depleted control mice, high levels of LCMV NP-specific IgG were generated within 2 wk p.i. and these levels were maintained for a prolonged time. In anti-CD4 Ab-treated mice, LCMV NP-specific IgG levels were strongly reduced (~50 to ~100-fold) in the first 2 wk after infection, confirming previous findings that the generation of LCMV Arm-specific IgG is CD4<sup>+</sup> T cell-dependent (202). Interestingly, anti-CD4 Ab-treated mice were also strongly



impaired to generate a IgM response against LCMV NP (Supporting Information Fig. S 1-2). Most strikingly, however, LCMV NP-specific IgG levels in anti-CD4 Ab-treated mice steadily increased and by 5 to 10 wk p.i. reached similar levels as in control mice (Fig. 1-1 B). The kinetics of the LCMV NP-specific IgG response in anti-CD4 Ab-treated mice coincided with the reemergence of CD4<sup>+</sup> T cells (Fig. 1-1 C).

In addition, LCMV NP-specific IgG were not detected at all in MHC class II-deficient mice that permanently lack CD4<sup>+</sup> T cells (Supporting Information Fig. S 1-3). These findings suggested that the *de novo* generated CD4<sup>+</sup> T cells in anti-CD4 Ab-treated mice were primed by residual viral antigen and provided help to LCMV NP-specific B cells. The observation that repeated administration of anti-CD4 Ab prevented the development of NP-specific Ab (Supporting Information Fig. 1-4) is further consistent with this interpretation.

To enumerate the LCMV NP-specific CD4<sup>+</sup> T cell response in anti-CD4 Ab-treated mice we used MHC II tetramer (I-A<sup>b</sup>/NP<sub>309-328</sub>) staining. Although the NP<sub>309-328</sub> peptide represents the immunodominant CD4<sup>+</sup> T cell epitope of NP in B6 mice, frequencies of NP<sub>309</sub>-specific CD4<sup>+</sup> T cells in LCMV immune mice are rather low (203, 204). Therefore, we used tetramer-based cell enrichment to increase the sensitivity of the read-out (205). NP<sub>309</sub>-specific CD4<sup>+</sup> T cell frequencies in naïve B6 mice ranged from 1-2 cells per million CD4<sup>+</sup> T cells. At wk 11 p.i., these numbers were increased similarly (~100-fold) in anti-CD4 Ab-treated and control mice, indicating that residual LCMV antigen was able to prime LCMV NP-specific CD4<sup>+</sup> T cells (Fig. 1-1 D). At an earlier time point (wk 6 p.i.), we observed a considerable variation between individual mice in the anti-CD4 Ab-treated group and numbers of NP<sub>309</sub>-specific CD4<sup>+</sup> T cells tended to be lower than in the control group. The fraction of NP<sub>309</sub>-specific CD4<sup>+</sup> T cells that displayed a T<sub>FH</sub> phenotype (PD-1<sup>+</sup>CXCR5<sup>+</sup>) were comparable in both groups (Fig. 1-1 E). However, PD-1 levels (mean fluorescence) of LCMV NP<sub>309</sub>-specific CD4<sup>+</sup> T cells from anti-CD4 Ab-treated were increased when compared to controls (Supporting Information Fig. S 1-5). The numbers of germinal center (GC) B cells (Fas<sup>+</sup>GL7<sup>+</sup>) in spleen of infected mice at day 10 p.i. were strongly reduced by transient CD4<sup>+</sup> T cell depletion. At later time points (wk 6-11), these numbers increased but remained ~2-fold lower than in non-depleted control mice (Fig. 1-1 F). Taken together, these data show that mice depleted of CD4<sup>+</sup> T cells during acute infection generated a robust LCMV NP-specific IgG response with time reaching Ab levels similar to that of non-depleted control mice. LCMV NP<sub>309</sub>-specific CD4<sup>+</sup> T cells were also induced in anti-CD4 Ab-treated mice with a similar magnitude as in control mice. The GC response was nearly absent in anti-CD4 Ab-treated mice at day 10 after infection and although it increased with time, it remained ~2-fold lower than in non-depleted control mice.

### 1.3.2 Antigen-binding avidity and IgG subclass distribution

To assess the antigen-binding avidity of LCMV NP-specific IgG, we used ELISA combined with an urea wash step after the serum Ab had bound to LCMV NP on the plate (206). In non-depleted B6 mice, the avidity of NP-specific IgG as determined by the fraction of specific Ab bound after an urea wash step increased with time of infection. Remarkably, the avidity of LCMV NP-specific IgG in mice that were CD4<sup>+</sup> T cell-depleted during acute infection also increased with time and at 8-10 wk p.i. no significant difference

in LCMV NP-binding avidity of both groups could be observed any longer (Fig. 1-2 A). Thus, transient CD4<sup>+</sup> T cell depletion during the acute phase did not prevent the induction of LCMV NP-specific Ab with high antigen-binding avidity by residual viral antigen. IgG2c is known to be the major IgG subclass of LCMV-specific Ab in sera of LCMV-infected B6 mice (207). Interestingly, anti-CD4 Ab-treated mice showed an increase in LCMV NP-specific IgG1 Ab when compared to controls (Fig. 1-2 B).

### 1.3.3 Induction of LCMV GP-specific IgG Ab with delayed kinetics

In LCMV-infected mice, Ab specific for the viral glycoprotein (GP) are also induced albeit at lower levels when compared to NP-specific Ab (75). At wk 5-8 p.i. GP-specific IgG levels in mice that were depleted of CD4<sup>+</sup> T cells during acute infection were still considerably lower compared to controls (Fig. 1-3 A, left). This was in contrast to NP-specific IgG that were similar between the two groups at this time point (Fig. 1-3 A, right). Remarkably, GP-specific IgG levels in the anti-CD4 Ab-treated group increased with time and by 12-15 wk p.i. reached almost comparable levels to those in the control group (Fig. 1-3 B). Hence, these data indicate that LCMV GP-specific IgG were also induced by residual LCMV antigen but with a slower kinetics when compared to NP-specific IgG.

### 1.3.4 Antigen-induced proliferation of LCMV GP-specific KL25HL B cells in LCMV immune hosts

To examine whether residual LCMV antigen is able to activate antigen-inexperienced B cells, we transferred CFSE-labeled LCMV GP-specific B cells from KL25 B cell receptor (BCR) heavy chain knock-in / light chain transgenic (tg) KL25HL mice into LCMV immune mice 5 wk p.i.. Since the KL25 BCR is specific for GP of the LCMV strain WE, a recombinant LCMV Arm virus engineered to express GP of WE (LCMV-Arm/WE-GP) was used (208). Cell division and recovery of KL25HL B cells were determined 4 days after cell transfer into LCMV-Arm/WE-GP-infected and, as a control, into non-infected recipient mice. The data show that KL25HL B cells divided extensively in LCMV-Arm/WE-GP-infected but not in non-infected recipient mice (Fig. 1-4 A). To control for antigen specificity, we also transferred CFSE-labeled B cells from CD45.1<sup>+</sup> VI10 H heavy chain knock-in mice into LCMV-Arm/WE-GP-infected and non-infected recipient mice. VI10 H mice carry the rearranged V<sub>H</sub>DJ<sub>H</sub> region from the VSV-specific mAb VI10 on both alleles in the IgH locus (209). In comparison to KL25 HL B cells, VI10 H B cells showed significantly reduced cell division and ~10-fold decreased cell recovery in spleen of the infected recipient mice (Fig. 1-4 B, C). The presence of CFSE<sup>low</sup> cells and the slight increase of VI10 H B cells in infected compared to non-infected recipients is most likely due to the proliferative response of a few LCMV-specific B cells in VI10 H mice that exhibit a restricted but not a monoclonal BCR repertoire. In sum, these data indicate that residual antigen in LCMV immune mice 5 wk p.i. was able to induce a strong proliferative response of B cells expressing a LCMV GP-specific antigen receptor.

### 1.3.5 Role of FcγR and complement receptors CD21/CD35

Fcγ receptors and the complement receptors CD21/35 are considered to be important for antigen retention (210-214). To assess the role of Fcγ-receptors (FcγR) in our model, FcγR<sup>-/-</sup> mice deficient in all four FcγR (FcγRI<sup>-/-</sup>RIIB<sup>-/-</sup>RIII<sup>-/-</sup>RIV<sup>-/-</sup>) were used. Similar to wild-type (wt) mice, FcγR<sup>-/-</sup> mice also generated a robust CD4<sup>+</sup> T cell-dependent LCMV NP-specific IgG response after LCMV infection. In contrast to wt mice, however, LCMV NP-specific IgG in anti-CD4 Ab-treated FcγR<sup>-/-</sup> mice failed to reach levels equivalent to those in control FcγR<sup>-/-</sup> mice, even when assessed late after infection (wk 15-18, Fig. 1-5 A). The role of complement receptors was examined in CD21/CD35<sup>-/-</sup> mice. Similar to wt mice, LCMV NP-specific IgG levels in transiently CD4<sup>+</sup> T cell-depleted CD21/CD35<sup>-/-</sup> mice reached control levels >5 wk p.i. (Fig. 1-5 B). At later time points, NP-specific IgG levels in transiently CD4<sup>+</sup> T cell-depleted CD21/CD35<sup>-/-</sup> mice were even increased as compared to non-depleted CD21/CD35<sup>-/-</sup> mice. The underlying reason of this phenomenon is unclear, but may involve compensatory mechanisms in mice that completely lack CD21/CD35 expression. Of note, LCMV NP-specific IgG levels in LCMV-infected CD21/CD35<sup>-/-</sup> mice were lower than in wt mice, which was most likely due to the well-known function of CD21/CD35 in enhancing humoral immunity (215-217). Taken together, these findings suggest that induction of a potent LCMV NP-specific IgG response by residual viral antigen requires FcγR- but not CD21/35-mediated retention of immune complexes.

### 1.3.6 LCMV NP-specific IgG Ab secreting cells and plasma cells

The bone marrow (BM) is the major site of long-term Ab production after LCMV infection (207). We thus determined the numbers of LCMV NP-specific IgG Ab-secreting cells (ASC) in BM of anti-CD4 Ab-treated and control LCMV immune B6 mice 7-11 wk p.i.. Importantly, the mice used for these experiments showed similar levels of LCMV NP-specific IgG in serum (133±16 AU/ml in anti-CD4 Ab-treated versus 127±40 AU/ml in control mice). Nonetheless, the numbers of LCMV NP-specific IgG ASC as assessed by ELISPOT were decreased about 3-fold in anti-CD4 Ab-treated mice as compared to controls (Fig. 1-6 A). To substantiate these data, we also determined the numbers of LCMV NP-specific CD138<sup>+</sup>TACI<sup>+</sup> plasma cells (PC) by flow cytometry. Antigen-specific PC were identified by intracellular staining with AlexaFluor (AF) 647-conjugated recombinant LCMV NP to identify cells that contain LCMV NP-specific Ab. This analysis revealed that LCMV NP-specific PC in BM were reduced about 2-fold in anti-CD4 Ab-treated compared to control mice (Fig. 1-6 B). Of note, the numbers of LCMV NP-specific PC measured by flow cytometry were roughly comparable to the numbers of LCMV NP-specific ASC derived from ELISPOT analysis (Fig. 1-6 A versus Fig. 1-6 B). Plasma cell differentiation negatively correlates with B220 expression (218). Notably, we observed that the ratio of B220<sup>negative</sup> to B220<sup>intermediate</sup> NP<sup>+</sup>CD138<sup>+</sup>TACI<sup>+</sup> cells in BM were ~2-fold decreased in anti-CD4 Ab-treated mice (Fig. 1-6 C). This suggested that PC differentiation in anti-CD4 Ab-treated mice was somewhat impaired. Overall, these data show that irrespectively of unimpaired Ab

responses, LCMV NP-specific IgG ASC and PC in BM remained ~2-3-fold decreased in anti-CD4 Ab-treated mice.

### **1.3.7 LCMV NP-specific B cell memory in transiently CD4<sup>+</sup> T cell depleted mice is strongly impaired**

So far, our data show that mice that had been transiently depleted of CD4<sup>+</sup> T cells during acute infection generated high levels of LCMV NP-specific IgG Ab after viral clearance. Therefore, it was of interest to examine the generation of LCMV NP-specific B cell memory under these conditions. Firstly, we determined the numbers of isotype-switched (IgM<sup>-</sup>D<sup>+</sup>) memory B cells specific for LCMV NP in these mice. For this, spleen cells from anti-CD4 Ab-treated and control LCMV immune B6 mice (7-11 wk p.i.) were stained with B220-, IgM- and IgD-specific mAb and with AF 647-conjugated recombinant LCMV NP to identify antigen-specific (LCMV NP<sup>+</sup>) B cells. This analysis revealed that the numbers of LCMV NP-specific isotype-switched memory B cells in transiently CD4<sup>+</sup> T cell-depleted mice were ~8-fold lower than in controls (Fig. 1-7 A).

Secondly, we performed LCMV rechallenge experiments in mice that had been depleted of CD4<sup>+</sup> T cells during primary infection and measured the LCMV NP-specific memory B cell recall response. As controls, non-depleted infection-matched (13-20 wk p.i.) LCMV immune mice were used. Strikingly, the numbers of LCMV NP-specific IgG ASC in spleen determined 5 days after LCMV rechallenge were strongly decreased (~36-fold) in formerly anti-CD4 Ab-treated mice (Fig. 1-7 B). These ELISPOT data were confirmed by flow cytometric analyses. For that, Ab secreting cells were identified by CD138 and TACI expression and antigen specificity was determined by cytoplasmic LCMV NP staining. This analysis revealed that the number of cytoplasmic LCMV NP-positive CD138<sup>+</sup>TACI<sup>+</sup> cells in spleen were also strongly reduced (~24-fold) in the anti-CD4 Ab-treated group (Fig. 1-7 C). Of note, most of the CD138<sup>+</sup>TACI<sup>+</sup> cells at day 5 post reinfection expressed B220, characterizing them as plasmablasts. Finally, we also assessed the LCMV NP-specific CD4<sup>+</sup> T cell response in anti-CD4 Ab-treated and control mice after LCMV rechallenge using MHC II tetramer (I-A<sup>b</sup>/NP<sub>309-328</sub>) staining in combination with tetramer-based cell enrichment. The data show that the numbers of NP<sub>309</sub>-specific CD4<sup>+</sup> T cells after LCMV rechallenge were ~5-fold lower in anti-CD4 Ab-treated compared to control mice (Supporting Information Fig. S-1-6). Hence, mice that had been transiently CD4<sup>+</sup> T cell-depleted during primary infection showed a strongly decreased LCMV NP-specific B cell memory response despite high serum levels of LCMV NP-specific IgG. In addition, the recall LCMV NP-specific CD4<sup>+</sup> T cell response was also impaired that likely contributes to the observed poor memory B cell response in these mice after LCMV rechallenge.

## 1.4 Discussion

In this study, we demonstrate that mice that had been transiently depleted of CD4<sup>+</sup> T cells during acute LCMV infection generated a robust LCMV-specific IgG response after viral clearance with Ab levels similar to non-depleted control mice. In contrast, LCMV-specific isotype-switched memory B cells were significantly reduced and the secondary LCMV-specific B cell response after LCMV rechallenge was severely impaired. These findings indicate that LCMV antigen depots present after the acute phase of the infection were capable of inducing robust LCMV-specific IgG production. They were, however, inefficient in the generation of a LCMV-specific memory B cell response.

There are a number of earlier studies that analyzed the induction of Ab responses after previous antigen exposure under the “umbrella” anti-CD4 Ab (219-223). In some but not all cases, tolerance was induced when soluble antigens were used. The induction of LCMV-specific IgG and the expansion of LCMV-specific CD4<sup>+</sup> T cells indicate that tolerance was not induced in anti-CD4 Ab-treated mice after LCMV infection. Our data show similarities but also differences to a recent study examining the Ab response in transiently CD4<sup>+</sup> T cell-depleted mice after intramuscular immunization with an adenovirus vector (224). Similar to our data, virus-specific IgG Ab titers developed with time and finally reach concentrations equivalent to those of non-depleted controls. In contrast to our findings, the secondary B cell response in adenovirus immunized mice as determined by measuring Ab titers after boost was similar in control and anti-CD4 Ab-treated mice. It is, however, important to note that ASC, PC and antigen-specific memory B cells were not directly enumerated in the adenovirus study. In addition, the secondary Ab response was determined at a rather late time point (1 month) after boost.

To explain this discrepancy further, one may also argue that intramuscular vaccination with a non-replicative adenoviral vector likely provides different triggers for B cell activation when compared to systemic infection with replicative LCMV.

What is the fate of LCMV-specific B cells that are exposed to high antigen levels during acute infection without CD4<sup>+</sup> T cell help? The observation that anti-CD4 Ab-treated mice failed to generate a IgM response against LCMV NP indicates that LCMV-specific B cells were not properly activated under these conditions. Nonetheless, we cannot exclude the possibility that some B cells in anti-CD4 Ab-treated mice were primed early in infection and were reinvigorated upon reemergence of LCMV-specific CD4<sup>+</sup> T cells. Alternatively, it is possible that B cells were generated *de novo* and were subsequently activated by residual LCMV antigen. The observation that LCMV GP-specific KL25HL B cells proliferated vigorously after transfer into LCMV immune recipients (5 wk p.i.) indicates that LCMV antigen depots present at this time point were sufficient for robust B cell activation.

The antigen-binding avidity of LCMV NP-specific IgG as determined by urea wash ELISA is known to increase with time (206). Although delayed, we yet observed a similar increase in antigen-binding avidity of LCMV NP-specific IgG Ab in anti-CD4 Ab-treated as in control mice. This result fits to the observation that CD4<sup>+</sup> T cell depletion during the acute phase of the LCMV infection delayed but did not completely abolish the generation of splenic GC B cells. Due to their low numbers in the polyclonal system, the antigen

specificity of GC B cells could, however, not be evaluated. Thus, these findings may suggest that residual LCMV antigen was capable to drive hypermutation and GC reaction after transient CD4<sup>+</sup> T cell depletion. Nevertheless, we cannot formally exclude the possibility that the increase in antigen-binding avidity of LCMV NP-specific IgG in anti-CD4 Ab-treated mice was due to non GC-driven selection of high avidity B cells by limiting antigen.

IgG Ab specific for LCMV GP were also induced in anti-CD4 Ab-treated mice at wk 12-15 post LCMV infection but with a significant time delay when compared to the NP-specific IgG that were already present at high levels at wk 5-8 p.i.. This indicates that residual LCMV GP was still present at a rather late time point (> wk 5-8) to stimulate the production of GP-specific Ab. In contrast to NP, GP is heavily glycosylated and the generation of GP-specific Ab is hampered by a glycan shield (53). Also in normal mice without CD4<sup>+</sup> T cell depletion, NP-specific Ab are generated more quickly and reach higher titers than GP-specific Ab (75). The decreased production of GP- in comparison to NP-specific Ab is most likely explained by the low precursor frequency of GP-specific B cells and/or the necessity of these cells to considerably undergo somatic hypermutations to generate decent binding antigen receptors. In anti-CD4 Ab-treated mice, the generation of GP-specific Ab may be further delayed by the limited T cell help at the initiation of the GC response and possibly also by low GP levels.

Our study further demonstrates that LCMV NP-specific IgG in anti-CD4 Ab-treated FcγR<sup>-/-</sup> mice did not reach the levels found in non-treated littermate controls. This suggests that residual LCMV is stored in the form of immune complexes (IC) that are retained by FcγR. In the absence of FcγR, the amount of residual LCMV antigen available for T/B cell activation may be too limiting. Due to the low levels of virus-specific Ab present at wk 1-2 p.i., the formation of IC in anti-CD4 Ab-treated mice is likely to be impaired. However, virus-specific Ab titers quickly increased thereafter enabling efficient IC formation also in anti-CD4 Ab-treated mice. Of note, injection of anti-CD4 Ab into FcγR<sup>-/-</sup> mice did not lead to physical depletion of CD4<sup>+</sup> T cells due to the lack of FcγR (data not shown). Instead, the helper function of CD4<sup>+</sup> T cells was functionally blocked as evident by the reduced levels of LCMV NP-specific IgG. This implies that CD4<sup>+</sup> T cell recovery in FcγR<sup>-/-</sup> mice did not require *de novo* generation of CD4<sup>+</sup> T cells as in wt mice. Although unlikely, we cannot completely rule out the possibility that the inefficient induction of LCMV NP-specific IgG Ab in anti-CD4 Ab-treated FcγR<sup>-/-</sup> mice was due to this effect.

Despite similar levels of LCMV NP-specific IgG in serum, LCMV NP-specific IgG ASC and plasma cells in the BM of anti-CD4 Ab-treated mice were decreased by a factor of 2-3 when compared to control mice. This suggests that a substantial fraction of LCMV NP-specific IgG in serum of anti-CD4 Ab-treated mice originated from plasmablasts or short-lived plasma cells that did not efficiently home to the BM. However, LCMV NP-specific IgG ASC in spleen of anti-CD4 Ab-treated mice were also significantly lower than in control mice (data not shown). We thus favor the notion that plasmablasts or short-lived plasma cells were underestimated in our ELISPOT assays and flow cytometric analyses possibly due to a higher degree of spontaneous cell death when compared to fully differentiated long-lived plasma cells from control mice. The observation that LCMV NP-specific plasma cells from anti-CD4 Ab-treated mice showed a less differentiated phenotype with respect to B220 expression would be compatible with such an interpretation.



Despite similar anti-LCMV NP Ab levels in serum, isotype-switched memory B cells specific for the same antigen were clearly decreased (~8-fold) in anti-CD4 Ab-treated mice. This indicates that LCMV antigen depots were quite efficient in inducing Ab production but clearly less in generating memory B cells. The impaired ability to induce memory B cells by residual antigen could be due to lower antigen levels and/or decreased inflammatory signals when compared to the priming conditions at the acute phase of the LCMV infection. In this context, the increased IgG1 levels of LCMV NP-specific Ab in anti-CD4 Ab-treated mice is noteworthy. It probably reflects the lower IFN- $\gamma$  levels during priming with residual viral antigen when compared to the acute infection (225). The role of persisting antigen for maintenance of memory B cells is still controversially discussed (226). Our finding that residual LCMV antigen was inefficient in inducing LCMV-specific memory B cells is more compatible with the concept that memory B cells are independent of persisting antigen as demonstrated previously (227).

The secondary LCMV NP-specific B cell response in anti-CD4 Ab-treated mice after LCMV rechallenge as determined by assessing the numbers of ASC and plasmablasts shortly (day 5) after antigen boost was strongly decreased (~24 to ~36-fold). This impressive decrease clearly exceeds the ~8-fold reduced number of LCMV NP-specific memory B cells in these mice. Thus, LCMV NP-specific memory B cells generated under conditions of limited T cell help and/or in the absence of inflammatory signals may also be impaired in their ability to differentiate into ASC after antigen boost. In addition, the secondary response of LCMV NP-specific CD4<sup>+</sup> T cells in mice that were transiently depleted of CD4<sup>+</sup> T cells during acute infection was considerably lower than in control mice. This likely contributes to the poor memory B cell response in transiently CD4<sup>+</sup> T cell-depleted mice after LCMV re challenge.

In conclusion, we here demonstrate that CD4<sup>+</sup> T cell help to B cells for antibody production can be provided weeks after an acute LCMV infection. Hence, residual LCMV antigen depots can prime CD4<sup>+</sup> T cells for B cell help probably in a Fc $\gamma$ R-depend manner. Finally, our study unravels a previously unappreciated dichotomy of specific Ab production and memory B cell formation after priming with residual viral antigen.

## 1.5 Material and Methods

### 1.5.1 Mice and infections

B6 mice were obtained from Janvier (Le Genest St-Isle, France). FcγR<sup>-/-</sup> (228), CD21/CD35<sup>-/-</sup> (217), KL25HL BCR knock-in / tg (229) and VI10 H heavy chain knock-in (209) mice were bred and kept in our animal facilities under specific pathogen-free conditions. Unless stated otherwise, mice were infected *intraperitoneally* (i.p.) with 2x10<sup>5</sup> plaque forming unit (pfu) LCMV Arm. For depletion of CD4<sup>+</sup> T cells, mice were treated i.p. with 200 μg CD4-specific mAb YTS191 (BioXCell) at day -3 and day -1 before LCMV infection. For LCMV rechallenge, immune mice were infected i.p. with 8x10<sup>5</sup> pfu LCMV Arm and analyzed at day 5 post secondary infection. LCMV was propagated on baby hamster kidney cells (BHK) and viral titers were determined by focus-forming assay (230). Mice at the age of 8-20 wk were used for primary LCMV infection. Animal experiments were performed at the University of Freiburg and the University of Basel, in accordance with the laws of animal protection and with authorization of the Regierungspräsidium Freiburg and the cantonal authorities of Basel.

### 1.5.2 LCMV qPCR

RNA was prepared from ~30 mg splenic tissue using phenol (TriReagent, Sigma)-chloroform-extraction followed by EtOH-sodium acetate-precipitation. To transcribe the viral RNA genome, single-stranded cDNA from 1 μg of total RNA was generated with the High Capacity cDNA Reverse Transcription Kit (Applied Biosystems) using random primers. The qPCR reaction was performed with KAPA<sup>™</sup> SyBR<sup>®</sup> FAST qPCR Kit Master Mix in MicroAmp<sup>®</sup> Optical 384-well reaction plate (Applied Biosystems) with the following LCMV GP<sub>Arm</sub> primers: forward: CATTACCTGGACTTTGTCAGACTC; reverse: GCAACTGCTGTGTTCCCGAAAC (231). PCR conditions: 50°C 2 min.; 95°C 10 min.; 40 cycles of 95°C 15 sec.; 60°C 20 sec.. Samples were run on a ABI Prism<sup>®</sup> 7900 sequence detector and analyzed with SDS2.4 Software and RQ manager (all Applied Biosystems). Copy numbers were determined with a plasmid containing LCMV GP<sub>Arm</sub>.

### 1.5.3 Adoptive transfer of B cells from KL25HL/VI10 BCR knock-in / tg mice

B6 recipients were infected i.p. with 2x10<sup>5</sup> pfu recombinant LCMV Arm expressing the glycoprotein of the LCMV strain WE (LCMV-Arm/WE-GP) (208). Five weeks later, 2x10<sup>6</sup> MACS-purified (Milteny, Biotec, Germany), CFSE (carboxyfluorescein succinimidyl ester, Thermo Fischer)-labeled untouched resting B cells from CD45.1<sup>+</sup> KL25HL BCR tg mice (209) were transferred (i.v.). As a control, B cells from CD45.1<sup>+</sup> VI10



knock-in mice were also transferred. These mice carry on both alleles the rearranged V<sub>H</sub>DJ<sub>H</sub> region from the VSV-specific mAb VI10 (209). Mice were analyzed 4 days after cell transfer.

### 1.5.4 Flow cytometry

Flow cytometry was performed according to the guidelines as published by Cossarizza et al. (232). Single cell suspensions were stained with fluorophore-conjugated mAb specific for the following molecules: B220 (Ra3-6B2; AF488, BV421, PE), CD4 (RM4-5; BV650), CD8 (53-6.7; AF488), CD11b (M1/70; AF488), CD19 (6D5, PE-Cy7), CD45.1 (A20, BV421), CD45.2 (104, BV786), CD138 (281-2; PE-Cy7), CXCR5 (L138D7; PE), Fas (SA367H8, AF488), GL7 (GL7, BV412), IgD (11-26c2A; AF700), IgM (RMM-1; A488), PD-1 (29F.1A12; APC) and TACI (8F10; PE), all purchased from BioLegend. Tetramer enrichment was performed as described previously (205) with some modifications. In brief, splenic single-cell suspensions were labelled at room temperature in 300  $\mu$ l PBS with 6.5  $\mu$ g I-A<sup>b</sup>/NP<sub>309-328</sub> tetramers coupled to PE (*phycoerythrin*) in the presence of 5  $\mu$ g Fc-block (clone 2.4G2), 6% mouse and 6% rat serum for 1 hour. I-A<sup>b</sup>/NP<sub>309-328</sub> tetramers were obtained from the NIH Tetramer Core Facility. Cell enrichment was performed with anti-PE beads applying MACS technology (Milteny, Biotec, Germany). The enriched cell population was stained on ice for 30 minutes (min.) with a cocktail of fluorochrome-labelled mAb specific for B220, CD4, CD8, CD11b, CXCR5 and PD-1. The entire stained sample was collected on a LSRFortessa flow cytometer using DAPI (4',6-diamidino-2-phenylindole) staining to exclude dead cells. The percentage of tetramer-positive cells was multiplied by the total number of cells in the enriched fraction to calculate the number of tetramer-positive cells per 10<sup>6</sup> CD4<sup>+</sup> T cells in the starting spleen cell suspension.

To identify LCMV NP-specific plasma cells, BM cells were first surface stained on ice for 30 min. with mAb specific for B220, CD138 and TACI. Afterwards, cells were fixed and permeabilized using Inside Stain Kit (Milteny, Biotec, Germany). After a blocking step with PBS containing 2% FCS (on ice for 10 min.), cells were incubated on ice for 45 min. with bacteria-derived and AF 647-conjugated recombinant LCMV NP (3-5  $\mu$ g/ml). To identify LCMV NP-specific isotype-switched (IgM<sup>-</sup>D<sup>+</sup>) memory B cells, spleen cells were first surface stained on ice for 30 min. with mAb specific for B220, IgD and IgM. After a wash step, cells were incubated with AF 647-labelled recombinant LCMV NP (3-5  $\mu$ g/ml) on ice for 1 hour. Cells were analyzed on LSRFortessa flow cytometer using DAPI staining to exclude dead cells (DAPI staining was omitted in intracellular staining) and FlowJo software (Treestar). Gating strategies are shown directly in the corresponding figures or in Supporting Information Fig.S 1- 7.

### 1.5.5 Determination of LCMV GP- and NP-specific Abs

GP- and NP-specific IgG were measured by ELISA using a GPc-Fc construct (75) and recombinant bacterial expressed LCMV NP (53), respectively, as described. The levels of NP-specific IgG were expressed as

arbitrary unit (AU) per ml serum. These values were interpolated from a standard curve. This curve was generated from a serial dilution of purified polyclonal mouse IgG (100-3 ng/ml, Jackson ImmunoResearch) incubated on wells coated with rabbit anti-mouse IgG F(ab')<sub>2</sub> (Jackson ImmunoResearch). One AU corresponds to the OD values obtained with 1 µg purified polyclonal mouse IgG upon serial dilution. To determine the antigen-binding avidity of NP-specific IgG, conventional ELISA combined with a 8 M urea wash step was used as described previously (206).

To calculate the percent bound IgG Ab after urea wash, we used area under the curve (AUC) analysis of OD<sub>492</sub> values of PBS and urea-treated samples over a range of six serum dilutions (1:900 to 1: 72.900). For detection of IgG subtypes, biotinylated goat anti-mouse IgG1-, IgG2b- and IgG2c-specific Ab (Jackson ImmunoResearch) were used.

### **1.5.6 Quantification of LCMV NP-specific Ab secreting cells by ELISPOT**

Single-cell suspension of BM were cleared of erythrocytes by a single round of 0.83% NH<sub>4</sub>Cl treatment and resuspended in cell culture medium (IMDM, Iscove's Modified Dulbecco's Medium + 10% fetal calf sera). 96-well Multiscreen Assay plates (Merck Millipore) were activated by adding 35% ethanol (15 µl/well) for 1 minute. The activated plates were washed twice with phosphate buffered saline (PBS) and coated with 3 µg/ml recombinant LCMV NP (100 µl/well) at 4°C overnight. Afterwards, the plates were washed twice with PBS and blocked with cell culture medium (200 µl/well) at room temperature for 2 hours. Blocking medium was replaced with 100 µl cell culture medium containing threefold dilutions of BM cells starting with a cell density of 10<sup>7</sup> cells/ml. After incubation at 37°C in humid atmosphere with 5% CO<sub>2</sub> for 5 hours, plates were emptied by being flicked and washed 3-times with PBS containing 0.05% Tween 20 (PBST). A 100 µl volume of *horseradish peroxidase-labeled* rabbit anti-mouse Fcγ-specific Ab (Jackson ImmunoResearch) diluted into PBS was added to each well and incubated overnight at 4°C. The plates were washed 4-times with PBST and 4-times with PBS, and detection was carried out by adding freshly made AEC (3-amino-9-ethylcarbazole; BD Bioscience) solution (100µl/well) at room temperature for 20 min.. The reaction was terminated by extensive washing with water. After drying in the dark, spots were enumerated using a stereomicroscope (Stemi 508, Zeiss) with an integrated camera (AxioCam 105).

### **1.6 Acknowledgements**

We thank the NIH Tetramer Core Facility for providing I-A<sup>b</sup>/NP<sub>309-328</sub> tetramers. The work was supported by the Deutsche Forschungsgemeinschaft DFG (SFB 1160/P3 to HP).

### **1.7 Conflict of Interest**

The authors declare no financial or commercial conflict of interest.

## 1.8 Figures

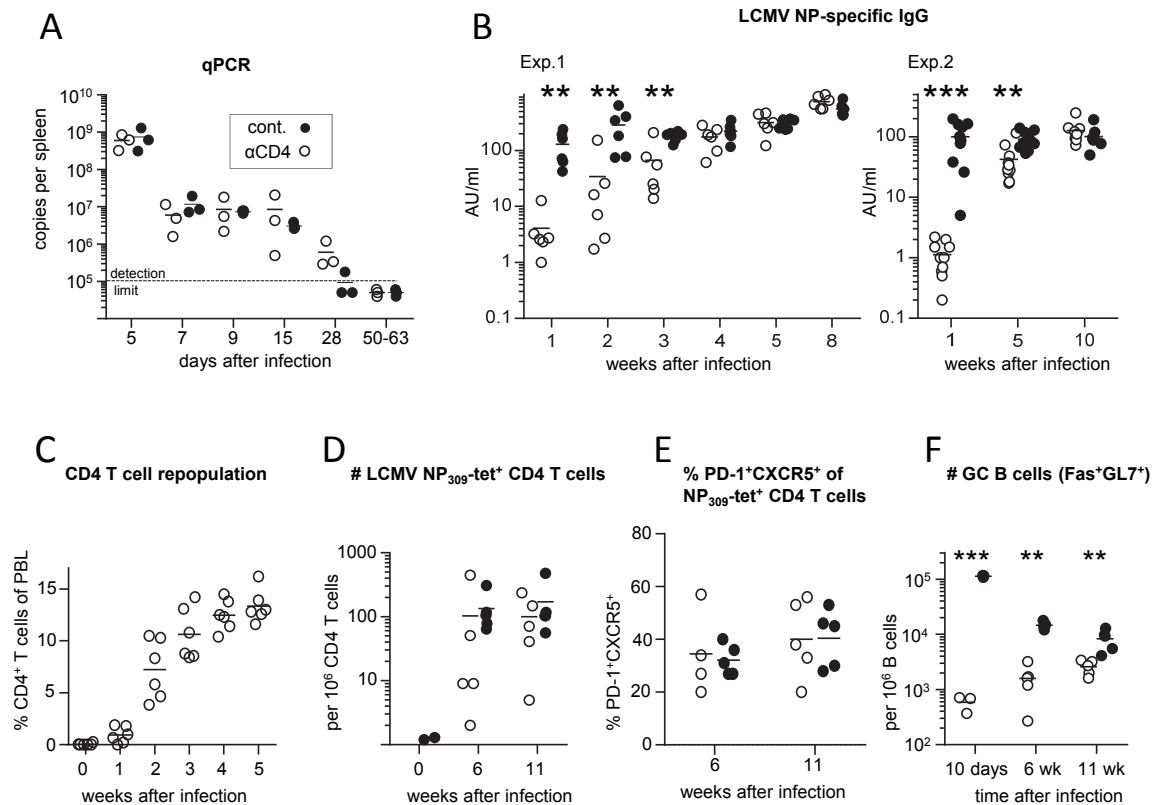


Figure 1-1 Anti-LCMV immune response in mice that had been transiently depleted of CD4 T cells during acute infection

Anti-CD4 Ab-treated ( $\alpha$ CD4, open circles) and control (cont., closed circles) B6 mice were infected with LCMV and analyzed at the indicated time points p.i.. (A) Viral load in genome copies per spleen determined by qPCR. Data are pooled from 2 independent experiments with 3 mice per group. (B) Serum concentrations of LCMV NP-specific IgG as arbitrary units (AU) per ml serum. Data from 2 independent experiments with 6-9 mice per group are shown. (C) Percent CD4<sup>+</sup> T cells of peripheral blood lymphocytes (PBL) in anti-CD4 Ab-treated mice at the indicated time points after CD4<sup>+</sup> T cell depletion and LCMV infection. Data are pooled from 2 independent experiments with 3 mice per group. (D) Numbers of LCMV NP<sub>309</sub>-tet<sup>+</sup> CD4<sup>+</sup> T cells per 10<sup>6</sup> CD4<sup>+</sup> T cells from naïve and LCMV immune mice. Data are pooled from 2 independent experiments with 5 mice per group. (E) T<sub>FH</sub> phenotype of LCMV NP<sub>309</sub>-tet<sup>+</sup> CD4<sup>+</sup> T cells determined by PD-1/CXCR5 co-expression analysis. Data are pooled from 2 independent experiments with 5 mice per group. (F) Numbers of GC (Fas<sup>+</sup>GL7<sup>+</sup>) B cells per 10<sup>6</sup> B220<sup>+</sup> B cells in spleen. Data are pooled from 2 experiments with 3-5 mice per group. Symbols represent the values from individual mice. Horizontal lines indicate the mean, horizontal dashed lines indicate the detection limit. \*\*p < 0.01, \*\*\*p < 0.001; Mann-Whitney U-test.

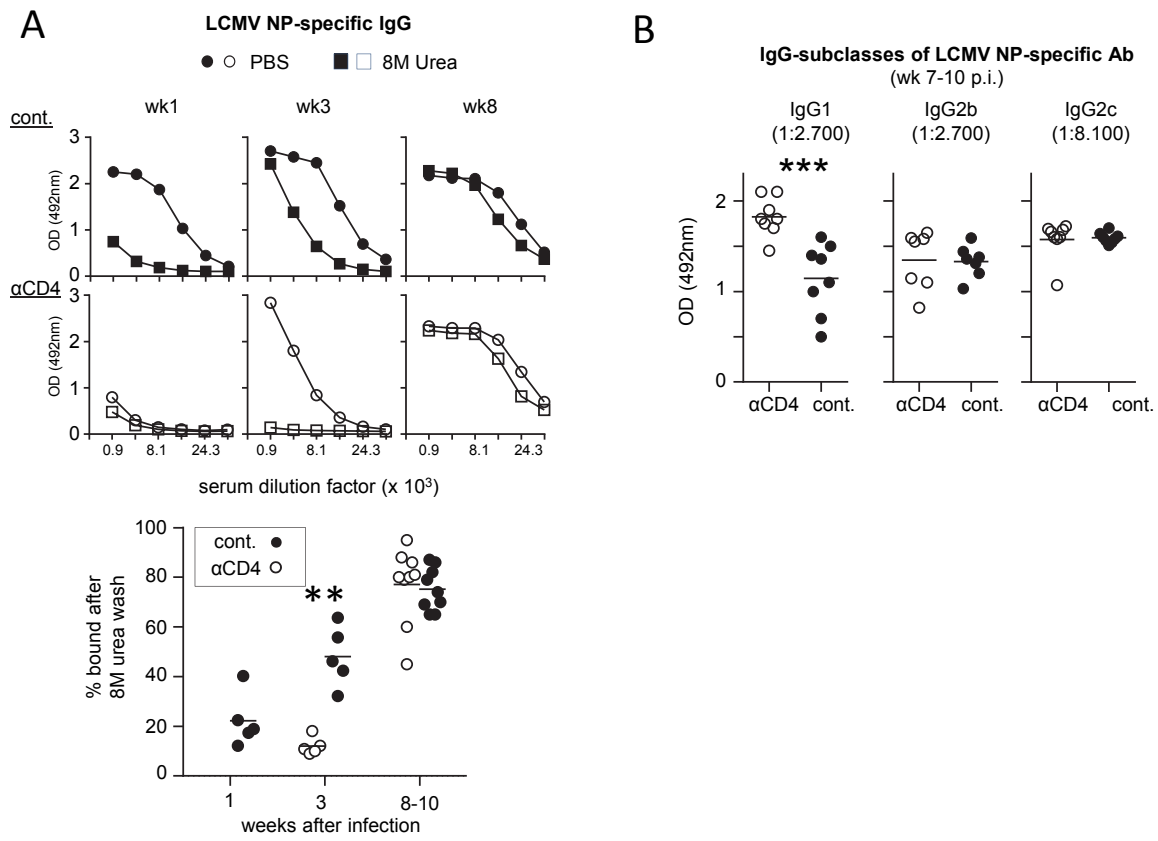
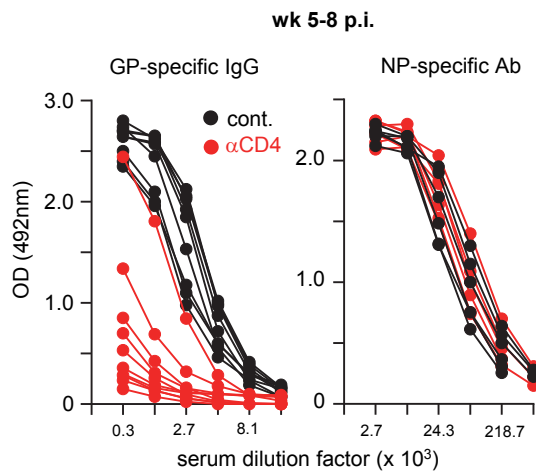


Figure 1-2 Antigen-binding avidity and IgG subclass distribution

Anti-CD4 Ab-treated ( $\alpha$ CD4, open symbols) and control (cont., closed symbols) B6 mice were infected with LCMV and analyzed at the indicated time points. (A) Top: LCMV NP-specific IgG in serum as detected by ELISA. Antigen-captured serum IgG was washed with PBS (circles) or urea (squares) before detection. ELISA profiles from one individual mouse per group are displayed. Data are representative from 2 independent experiments with 5-9 mice per group. Bottom: Avidity of LCMV NP-specific IgG Ab determined by ELISA with and without an urea wash step. Data shown are pooled from 2 independent experiments with 5-9 mice per group. (B) IgG subclasses of LCMV NP-specific IgG determined by ELISA using subclass-specific secondary Ab to detect antigen-captured serum IgG. OD (492nm) values at the indicated serum dilution in the linear range are displayed. Symbols represent the values of individual mice. Horizontal lines indicate the mean. Data shown are pooled from 2-3 independent experiments with 5-9 mice per group. \* $p < 0.05$ , \*\* $p < 0.01$ ; Mann-Whitney U-test.

A



B

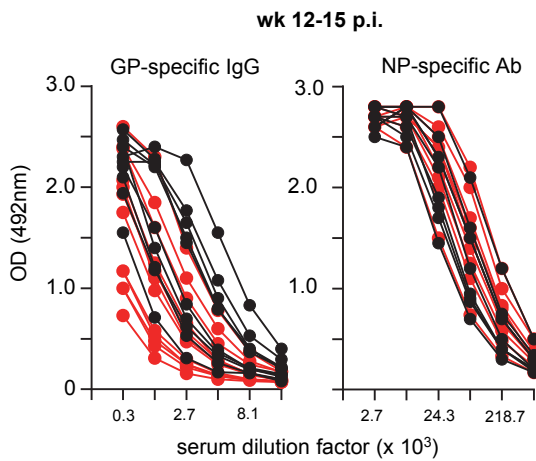


Figure 1-3 Induction of LCMV-GP specific IgG with a delayed kinetics

Anti-CD4 Ab-treated (red) and control B6 (black) mice were infected with LCMV. LCMV GP- (left) and NP-specific IgG levels (right) in serum were determined by ELISA at wk 5-8 (A) and wk 12-15 (B) after infection. ELISA profiles from individual mice are depicted. Pooled data from 3 independent experiments are shown. n= 7-9 mice per group.

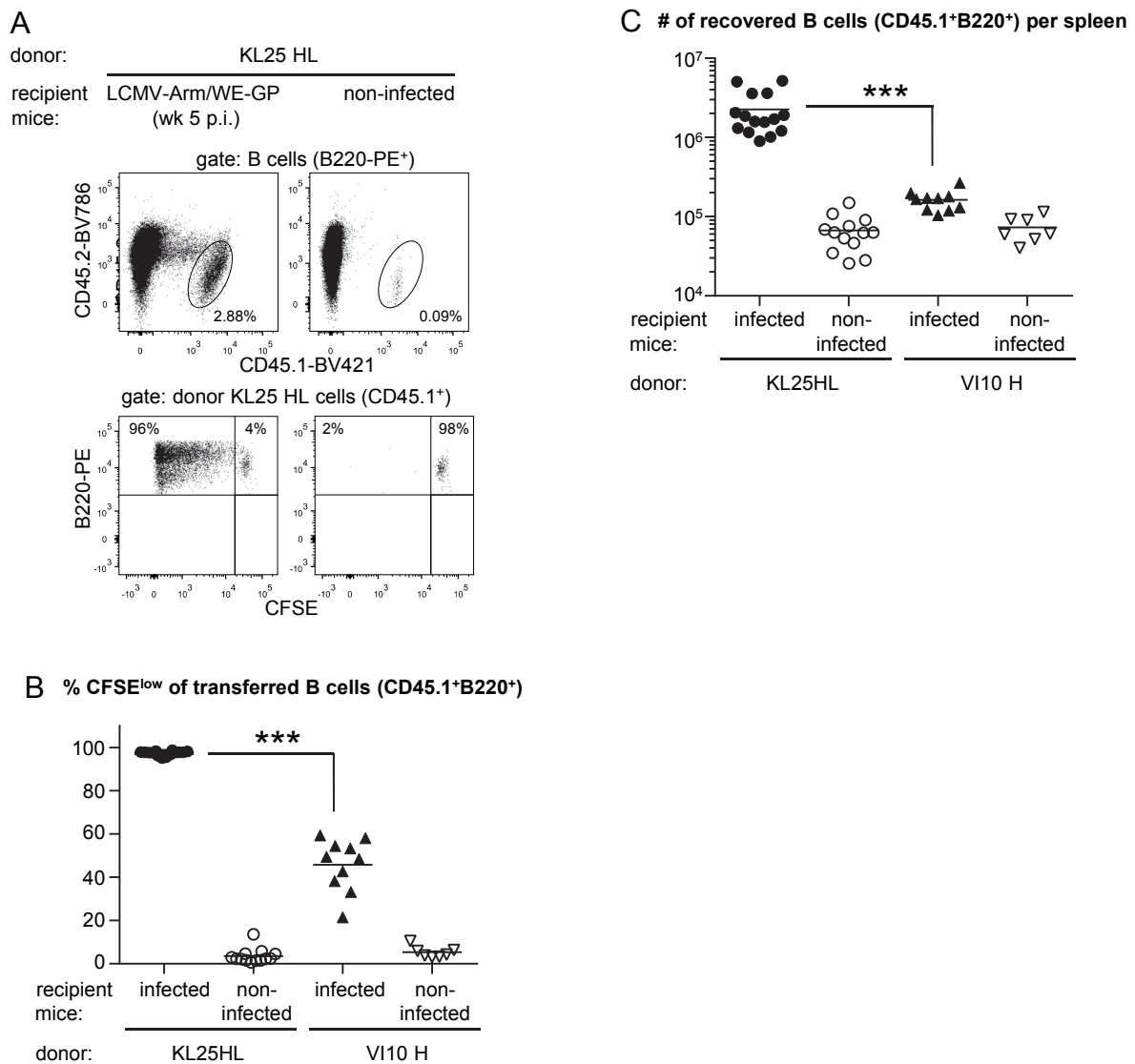


Figure 1-4 Proliferation of LCMV GP-specific KL25HL B cells induced by residual LCMV antigen

CFSE-labeled B cells from CD45.1<sup>+</sup> KL25HL and from CD45.1<sup>+</sup> VI10 H mice were transferred into LCMV-Arm/WE-GP-infected (wk 5 p.i.) and non-infected CD45.2<sup>+</sup> recipient mice. Mice were analyzed by flow cytometry 4 days after cell transfer.

(A) FACS plots gated on B220<sup>+</sup> B cells (top) and on KL25 HL donor cells (bottom) from spleen. Data are representative from 3 independent experiments with 15 mice per group. Numbers indicate the percentages of the respective cell populations. (B) Percentage distribution of CFSE<sup>low</sup> cells among donor KL25HL and VI10 H B cells in spleen of infected and non-infected recipients as indicated. (C) Absolute cell numbers of recovered KL25HL and VI10 H B cells in spleen of infected and non-infected recipients as indicated. (B-C) Data are pooled from 3 independent experiments with KL25 HL B cells and 2 independent experiments with VI10 H B cells. Symbols represent the values of individual mice. As indicated, a total of 7-15 mice per group were analyzed. \*\*\*p < 0.001; Mann-Whitney U-test.

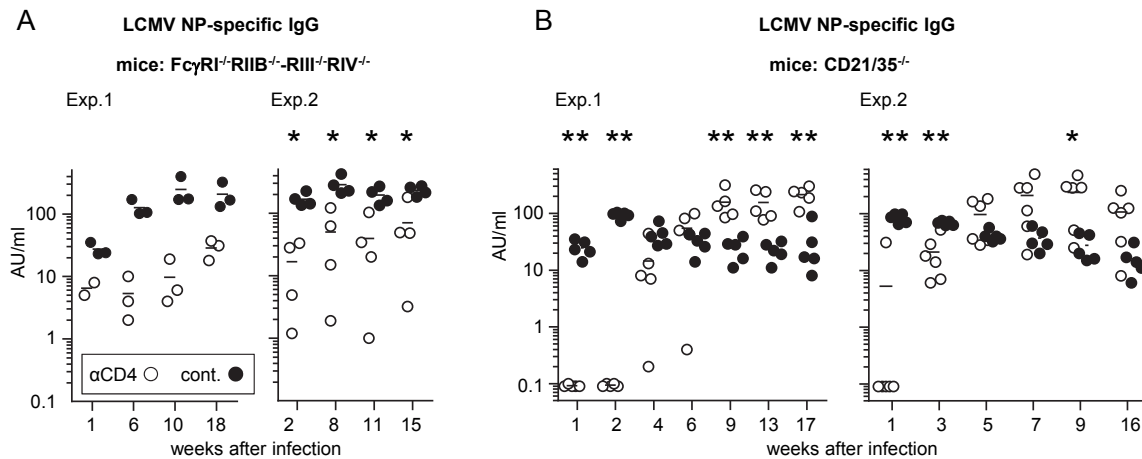


Figure 1-5 Role of FcR and the complement receptors CD21/CD35

(A)  $Fc\gamma R^{-/-}$  and (B)  $CD21/CD35^{-/-}$  mice were treated with anti-CD4 Ab ( $\alpha CD4$ , open circles) or were left untreated (cont., closed circles). Afterwards, mice were infected with LCMV and the amount of LCMV NP-specific IgG in serum was determined by ELISA at the indicated time points. Pooled data from 2 independent experiments for each mouse line are shown. Symbols represent the values of individual mice, horizontal lines indicate the mean.  $n=3-5$  per group. \* $p < 0.05$ , \*\* $p < 0.01$ ; Mann-Whitney U-test. Statistics was omitted when  $<4$  values per group were present.

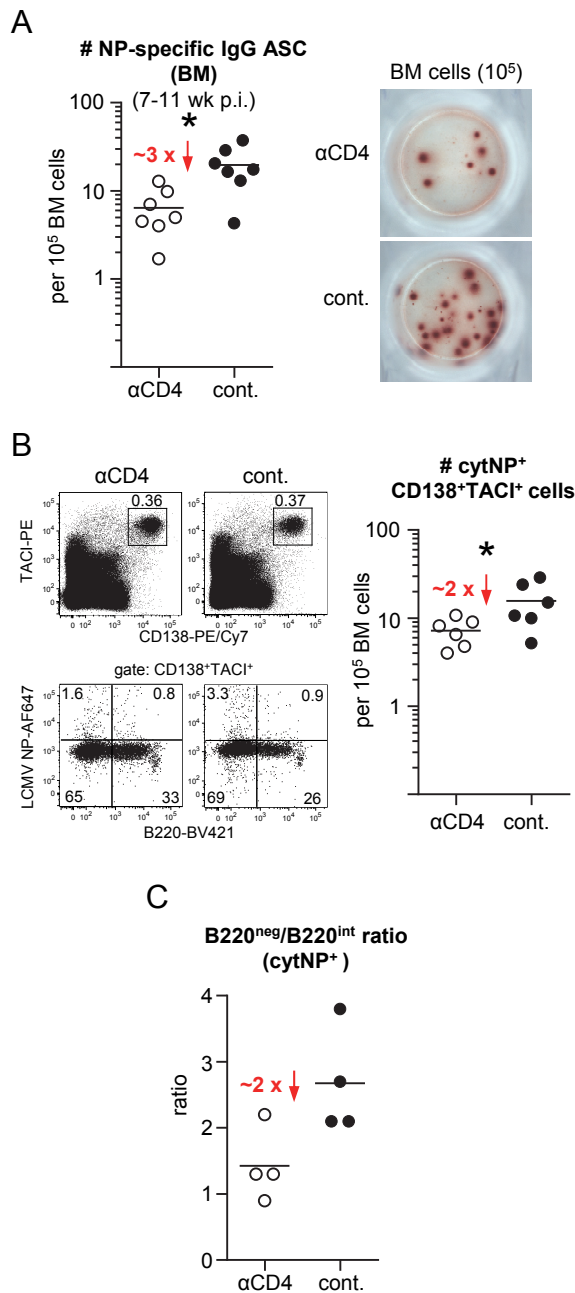


Figure 1-6 LCMV NP-specific IgG ASC and plasma cells in BM

Anti-CD4 Ab-treated ( $\alpha$ CD4, open circles) and control (cont., closed circles) B6 mice were infected with LCMV and analyzed at 7-11 wk p.i.. (A) Numbers (#) of NP-specific IgG ASC per 10<sup>5</sup> BM cells as determined by ELISPOT. On the right, representative ELISPOT demonstrating LCMV NP-specific ASC; as indicated 10<sup>5</sup> BM cells were added per well. (B) Representative FACS plots of BM cells illustrating the gating strategy to analyze LCMV NP-specific plasma cells. On the right, numbers (#) of cytoplasmic (cyt) LCMV NP<sup>+</sup> CD138<sup>+</sup>TACI<sup>+</sup> cells per 10<sup>5</sup> BM cells. (C) Ratio of B220<sup>negative</sup> to B220<sup>intermediate</sup> cells within the subset of LCMV NP<sup>+</sup>CD138<sup>+</sup>TACI<sup>+</sup> BM cells. (A-C) Data are pooled from 2 independent experiments with 4-7 mice per group. Symbols represent the values of individual mice, horizontal lines indicate the mean. The value in red beside the red arrow in graph indicates the fold reduction of the means from the control to the anti-CD4 Ab-treated group. \* $p < 0.05$ , Mann-Whitney U-test.



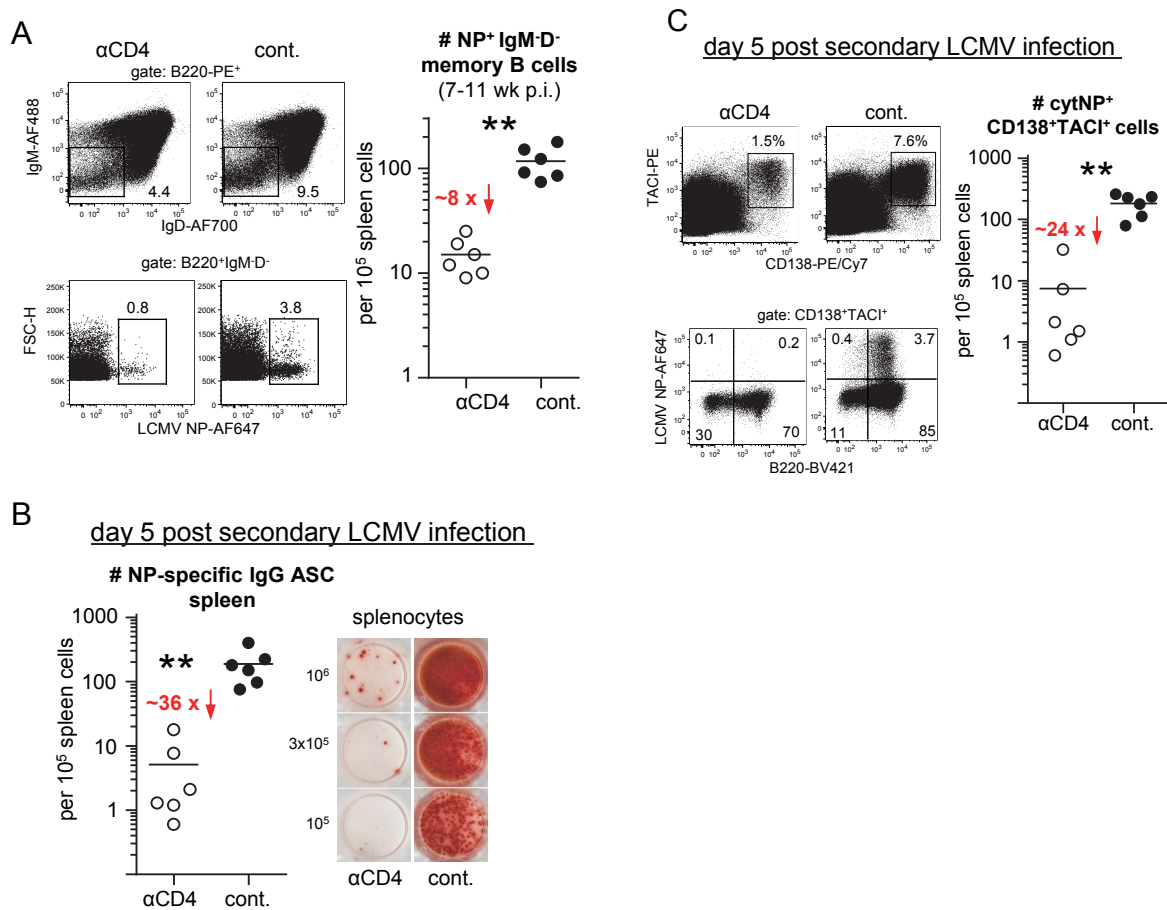


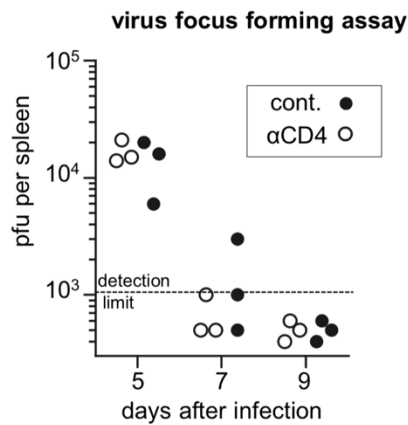
Figure 1-7 LCMV NP-specific memory B cell response

(A) Anti-CD4 Ab-treated ( $\alpha$ CD4, open circles) and control (cont., closed circles) B6 mice were infected with LCMV and analyzed at 7-11 wk p.i.. Representative FACS plots of spleen cells depicting the gating strategy to analyze LCMV NP-specific isotype-switched (IgM-D<sup>-</sup>) memory B cells. On the right, numbers (#) of LCMV NP-specific isotype-switched memory B cells per 10<sup>5</sup> spleen cells. Data are pooled from 2 independent experiments with 6 mice per group. (B, C) LCMV immune B6 mice (18-20 wk p.i.) that had been transiently depleted of CD4<sup>+</sup> T cells ( $\alpha$ CD4, open circles) during primary infection were re-infected with LCMV. Non-depleted infection-matched LCMV immune mice were used as controls (cont., closed circles).

(B) Numbers (#) of LCMV NP-specific IgG ASC per 10<sup>5</sup> spleen cells as determined by ELISPOT at day 5 post re-challenge. On the right, representative ELISPOT demonstrating LCMV NP-specific ASC; the indicated numbers of spleen cells were added per well. (C) Representative FACS plots of spleen cells illustrating the gating strategy to analyze LCMV NP-specific plasma cells/plasmablasts. On the right, numbers (#) of cytoplasmic (cyt) LCMV NP<sup>+</sup> CD138<sup>+</sup>TACI<sup>+</sup> cells per 10<sup>5</sup> BM cells. (B-C) Data are pooled from 2 independent experiments with 6 mice per group. Symbols repre

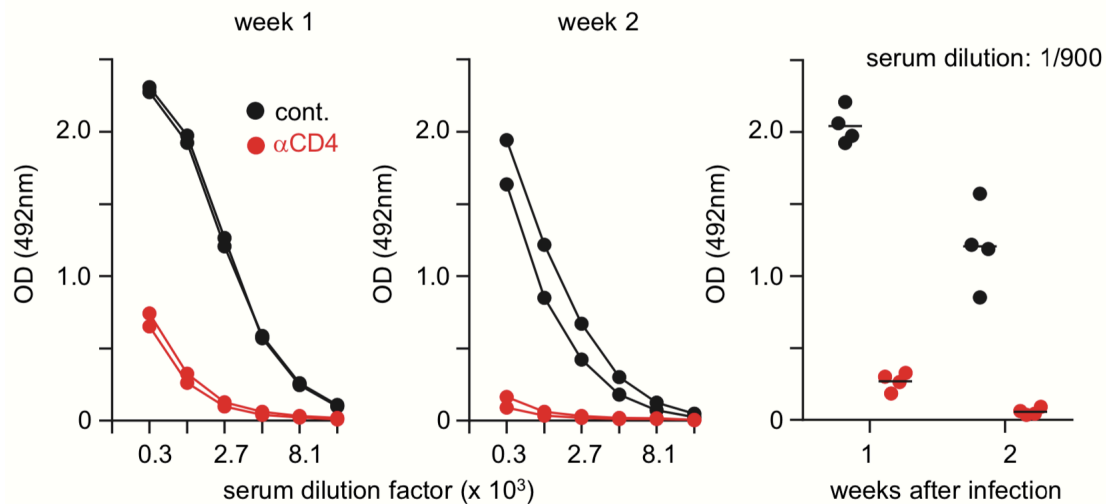
sent the values of individual mice, horizontal lines indicate the mean. The value in red beside the red arrow in the graph indicates the fold reduction of the means from the control to the anti-CD4 Ab-treated group. \*\*p < 0.01, Mann-Whitney U-test.

## 1.9 Supplementary Figures



S 1-1 Control of LCMV Armstrong infection is independent of CD4+ T cells

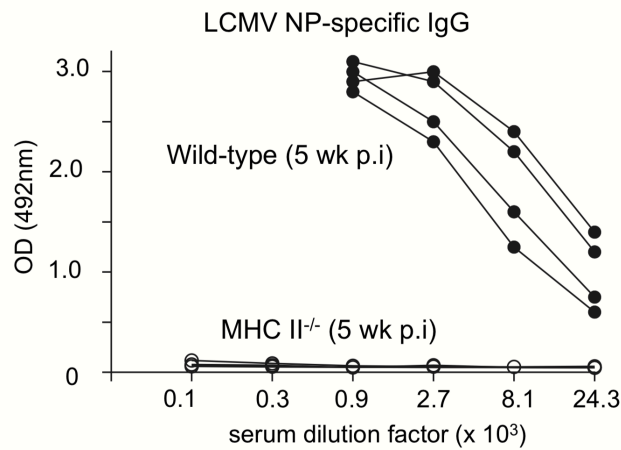
Anti-CD4 Ab-treated ( $\alpha$ CD4, open circles) and control (cont., closed circles) B6 mice were infected with  $2 \times 10^5$  pfu LCMV Armstrong i.p. and analyzed at the indicated time points after infection. Viral titers in spleen were determined by focus-forming assay.



S 1-2 Lack of a LCMV NP-specific IgM response in mice that had been transiently depleted of CD4+ T cells during acute infection

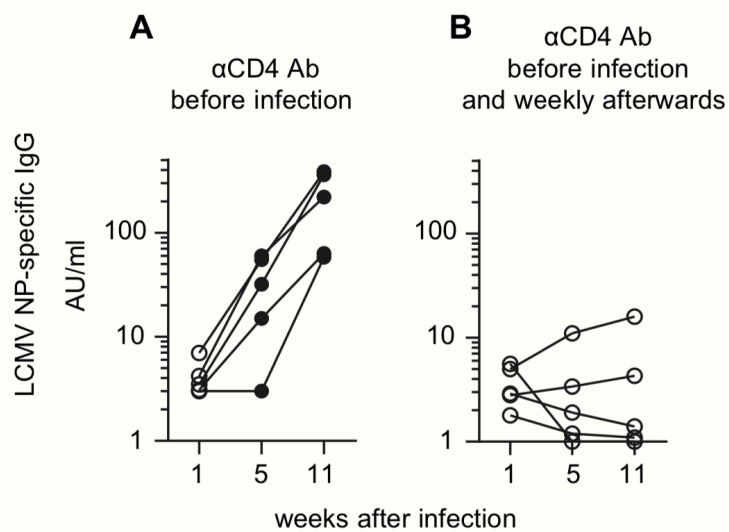
Anti-CD4 Ab-treated ( $\alpha$ CD4, red) and control (cont., black) B6 mice were infected i.p. with  $2 \times 10^5$  pfu LCMV Armstrong. LCMV NP-specific IgM levels in serum were determined by ELISA at week 1 and 2 p.i.. On the left, ELISA profiles from individual mice at the indicated time points p.i. are depicted. On the right, pooled data with 4 mice per group are displayed.

Residual LCMV antigen in transiently CD4+ T cell-depleted mice induces high levels of virus-specific antibodies but only limited B cell memory



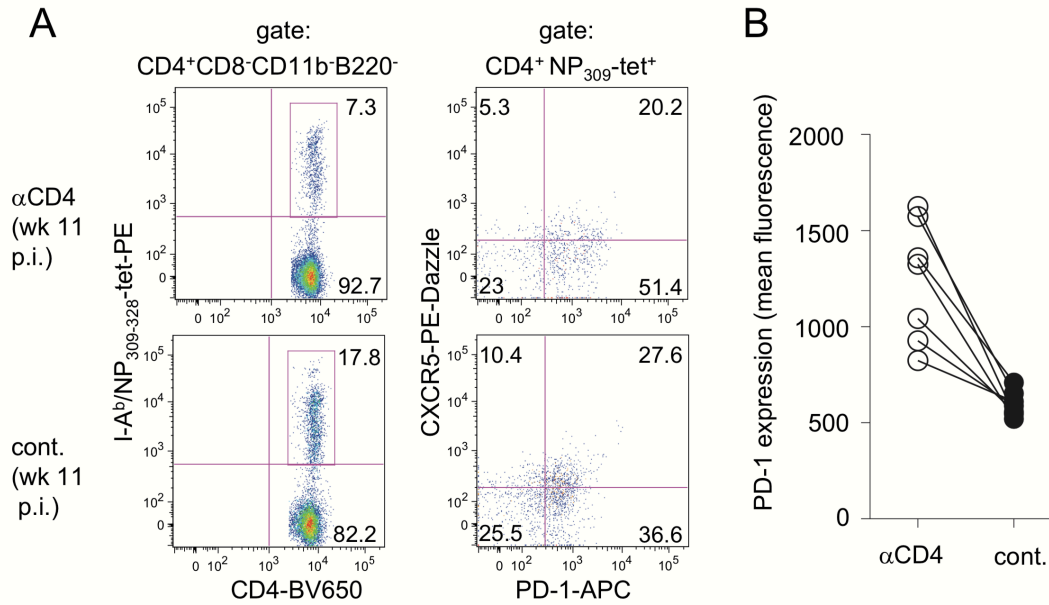
*S 1-3 MHC class II-deficient mice fail to generate LCMV NP-specific IgG Ab*

B6 (closed circles) and MHC class II-deficient mice (B6.129S2-*H2<sup>dlAb1-Ea</sup>J*, open circles) were infected i.p. with  $2 \times 10^2$  pfu LCMV Armstrong. After 5 weeks, LCMV NP-specific IgG levels in serum were determined by ELISA. ELISA profiles from individual mice are depicted.



*S 1-4 Repeated administration of anti-CD4 Ab prevents induction of LCMV NP-specific IgG*

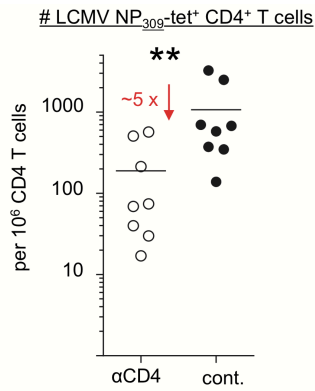
(A) B6 mice were treated with anti-CD4 Ab before infection with  $2 \times 10^5$  pfu LCMV Armstrong i.p.. (B) B6 mice were treated with anti-CD4 Ab before and repeatedly with weekly intervals after infection with  $2 \times 10^5$  pfu LCMV Armstrong i.p.. At the indicated time points, LCMV NP-specific IgG levels in serum were determined. Symbols represent the values from individual mice.



*S 1-5 T<sub>FH</sub> phenotype (PD-1<sup>+</sup>CXCR5<sup>+</sup>) of LCMV NP309-specific CD4<sup>+</sup> T cells*

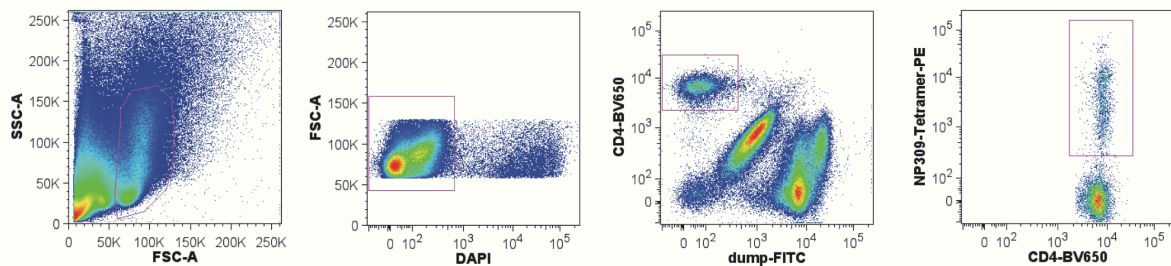
CD4 Ab-treated and control B6 mice were infected with  $2 \times 10^5$  pfu LCMV Armstrong. After 11 weeks, LCMV NP<sub>309</sub>-specific CD4<sup>+</sup> T cells from spleen were enriched and their PD-1/CXCR5 phenotype were determined by flow cytometry. (A) Representative FACS plots of tetramer-based enriched LCMV NP<sub>309</sub>-specific CD4<sup>+</sup> T cells. (B) PD-1 expression (mean fluorescence) of LCMV NP<sub>309</sub>-specific CD4<sup>+</sup> T cells from CD4 Ab-treated and control B6 mice analyzed 6-11 wk p.i.. Data are shown as pairs from the 2 groups that were analyzed side-by-side on the same day.

Residual LCMV antigen in transiently CD4+ T cell-depleted mice induces high levels of virus-specific antibodies but only limited B cell memory



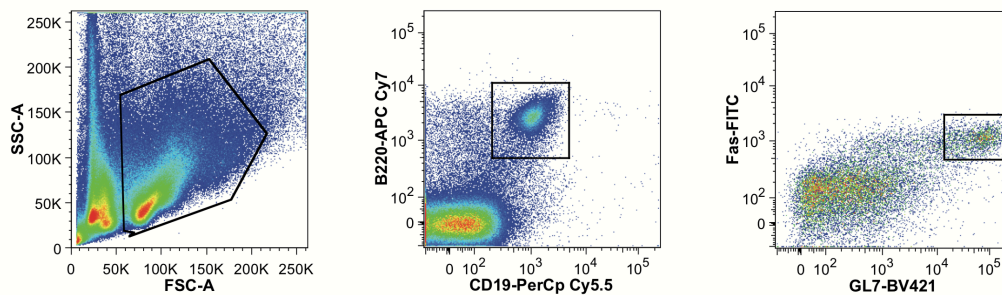
S 1-6 Numbers of LCMV NP309-tet<sup>+</sup> CD4<sup>+</sup> T cells in CD4 Ab-treated and control LCMV immune mice 5 days after LCMV rechallenge

LCMV immune B6 mice (11-14 wk p.i.) that had been transiently depleted of CD4<sup>+</sup> T cells (αCD4, open circles) during primary infection were re-infected with LCMV. Non-depleted infection-matched LCMV immune mice were used as controls (cont., closed circles). Numbers of LCMV NP<sub>309</sub>-tet<sup>+</sup> CD4<sup>+</sup> T cells were determined by MHC II tetramer (I-A<sup>b</sup>/NP<sub>309</sub>- 328) staining in combination with tetramer-based cell enrichment. Data shown are pooled from 2 independent experiments with 8 mice per group. Symbols represent the values from individual mice. \*\*p < 0.01, Mann-Whitney U-test.



S 1-7 Supporting Fig. 7A

Gating strategy used in Figure 1-1 D.



S 1-8 Supporting Fig. 7B

Gating strategy used in Figure 1-1 F.

## **2. Heterologous arenavirus vector prime – boost overrules self-tolerance for efficient tumor-specific CD8 T cell attack**

Weldy V. Bonilla<sup>1</sup>, Nicole Kirchhammer<sup>1†</sup>, Anna-Friederike Marx<sup>1†</sup>, Sandra M. Kallert<sup>1</sup>, Magdalena A. Krzyzaniak<sup>1</sup>, Min Lu<sup>1</sup>, Stéphanie Darbre<sup>2</sup>, Sarah Schmidt<sup>3</sup>, Josipa Raguz<sup>3</sup>, Ursula Berka<sup>3</sup>, Ilena Vincenti<sup>2</sup>, Mindaugas Pauzuolis<sup>2</sup>, Romy Kerber<sup>4</sup>, Sabine Hoepner<sup>5</sup>, Stephan Günther<sup>4</sup>, Carsten Magnus<sup>6,7</sup>, Doron Merkler<sup>2</sup>, Klaus K. Orlinger<sup>3</sup>, Alfred Zippelius<sup>1,8</sup>, Daniel D. Pinschewer<sup>1\*</sup>

<sup>1</sup> University of Basel, Department of Biomedicine, Basel, Switzerland

<sup>2</sup> University of Geneva, Department of Pathology and Immunology, Geneva, Switzerland

<sup>3</sup> Hookipa Pharma Inc., Vienna, Austria

<sup>4</sup> Bernhard Nocht Institute for Tropical Medicine, Hamburg, Germany

<sup>5</sup> Tumor Immunology, Department of Clinical Research, University of Bern, 3008 Bern, Switzerland.

<sup>6</sup> University of Zurich, Institute of Virology, Zurich, Switzerland

<sup>7</sup> Current address: F. Hoffmann-La Roche AG, Diagnostics Information Solution, Grenzacherstrasse 124, 4070 Basel, Switzerland

<sup>8</sup> Medical Oncology, University Hospital Basel, Basel, Switzerland

† These authors contributed equally to the present work

\* Corresponding author and lead contact:

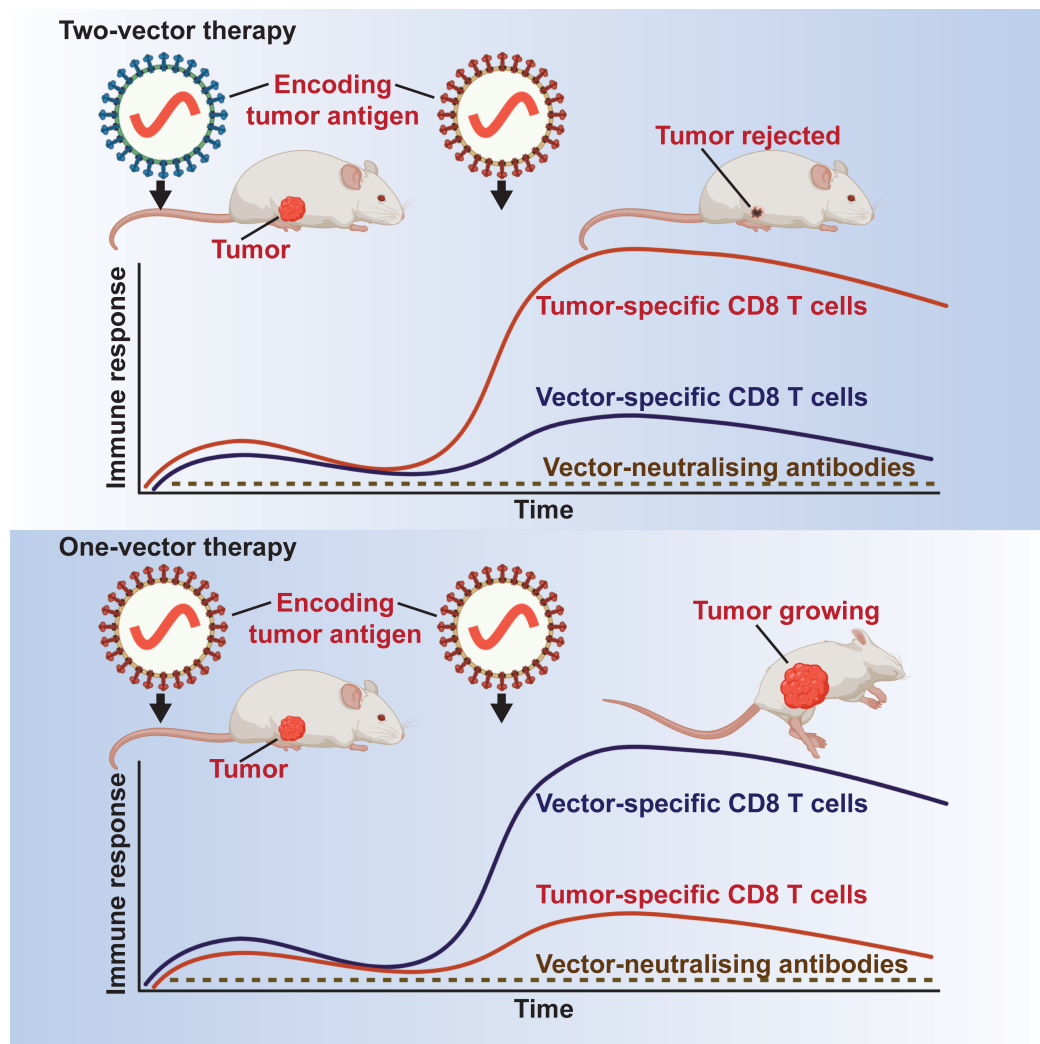
Daniel D. Pinschewer

Email: Daniel.Pinschewer@unibas.ch

Phone: +41-79-543 39 70

This article has been published in

Cell Rep Med. 2021 Mar 3;2(3):100209



Graphical abstract 2-1 Heterologous arenavirus vector prime – boost overrules self-tolerance for efficient tumor-specific CD8 T cell attack

## 2.1 Summary

Therapeutic vaccination regimens inducing clinically effective tumor-specific CD8 T cell (CTL) responses represent an unmet medical need. We engineer two distantly related arenaviruses, Pichinde virus and lymphocytic choriomeningitis virus, for therapeutic cancer vaccination. In mice, life-replicating vector formats of these two viruses delivering a self-antigen in a heterologous prime-boost regimen induce tumor-specific CTL responses up to 50% of the circulating CD8 T cell pool. This CTL attack eliminates established solid tumors in a significant proportion of animals, accompanied by protection against tumor re-challenge. The magnitude of CTL responses is alarmin-driven and requires combining two genealogically distantly related arenaviruses. Vector-neutralizing antibodies do not inhibit booster immunizations by the same vector or by closely related vectors. Rather, CTL immunodominance hierarchies favor vector backbone-targeted responses at the expense of self-reactive CTLs. These findings establish a powerful arenavirus-based immunotherapy regimen which allows to reshuffle immunodominance hierarchies and break self-directed tolerance for efficient tumor control.

## 2.2 Introduction

Cytotoxic CD8<sup>+</sup> T lymphocytes (CTL) are central mediators of adaptive immunity. Tumor-infiltrating CTLs in several tumor types are associated with clinical outcome (233-235) and pre-existing CTL infiltration may predict responsiveness to immune checkpoint inhibition (236). Analogously, CTLs are key players in HIV elite control and hepatitis B virus clearance (111, 112, 237).

Therapeutic vaccination for CTL induction holds great promise for cancer therapy (238, 239), but has delivered inconsistent therapeutic benefit including the failure of large clinical trials (240-243). Despite the induction of sizeable tumor antigen-specific CD8<sup>+</sup> T cell frequencies by modalities such as adjuvanted peptide(244), inefficient tumor infiltration has curtailed the clinical efficacy of these cells (245, 246). Delivering tumor-associated antigens (TAAs) in the context of virus-induced inflammation (247) bears significant potential to overcome these hurdles. Accordingly, several viral vector platforms have been developed for therapeutic use against solid tumors (243, 248-255). Inbuilt immunostimulatory properties of the viral particles themselves, exhibiting pathogen-associated molecular patterns, activate antigen-presenting cells (APCs) to augment and differentiate immune responses (256, 257). In addition, certain replicating viral delivery systems trigger the release of damage-associated molecular patterns or alarmins such as interleukin-33 (IL-33) (58, 258). These signals critically augment the activated T cells' expansion, effector differentiation and anti-tumor efficacy (59, 152).

Anti-vector immunity can inhibit viral delivery systems, impeding their re-administration to augment immune responses. A single immunization with vaccinia virus or modified vaccinia virus Ankara (MVA) elicits neutralizing antibody (nAb) responses in the majority of individuals (259) and inhibits vaccinia-vectored immunization (260). The seroprevalence to common adenoviral (Ad) serotypes such as Ad5 can regionally exceed 90%. Ad5-nAbs dampen or even abrogate responses to recombinant Ad5-based vaccines (261), and the use of simian adenovirus (sAd) backbones with lower seroprevalence has increased immunological response rates in clinical trials (262, 263). Still, also sAd vectors induce vector-specific nAbs when used for vaccination and have failed to demonstrate efficient homologous boosting capacity (264). More surprisingly, even serologically distinct adenovectors did not efficiently boost upon each other (263, 264), and adenoviral vectors are nowadays commonly combined with poxvirus-based platforms for heterologous prime-boost vaccination (264).

For several decades members of the arenavirus family have found widespread use in basic immunological research owing to their capacity of inducing CTL responses of exceptional magnitude, functionality and longevity (265). In the new millennium reverse genetic techniques have enabled the tailored design of this virus family and its exploitation for vaccination (48, 266). Replication-deficient vectors (rLCMV) based on the prototypic arenavirus lymphocytic choriomeningitis virus (LCMV) have demonstrated excellent CTL and nAb induction against vectorized transgenes in mice, non-human primates and recently also in humans (66, 267-269). As an important differentiation from other viral vector technologies, rLCMV-based immunization only rarely induced vector-nAbs, facilitating the vector's repeated administration in homologous prime-boost vaccination (66, 267, 269). This peculiarity of LCMV-based vectors is due to an N-linked "glycan shield" on the outer globular domain of the viral envelope glycoprotein domain, which



impairs antibody accessibility to critical neutralizing epitopes (53). rLCMV vectors are currently in clinical Phase 2 testing for the prevention of cytomegalovirus-associated disease in transplant recipients (270).

We and others have developed replication-attenuated tri-segmented arenavirus-based vector formats (artLCMV, r3LCMV, r3PICV, Fig. 2-1 A-C), which induce even more potent effector CTL responses than replication-deficient rLCMV or commonly used poxviral and adenoviral vector systems (57, 58, 271). An artLCMV based vector has recently entered early-stage clinical testing (272). When used to deliver tumor self-antigens to tumor-bearing mice, artLCMV induced potent anti-tumor CTL responses and extended the animals' survival (58). Tumor-specific CTL responses were, however, lower in magnitude than those induced against vectorized non-self-antigens and complete tumor remission was not achieved. This suggested that self-tolerance limited the therapeutic efficacy of artLCMV-based immunization (58).

Here we systematically explore a range of additional arenavirus vector backbones for vaccine delivery. We report that, counter to commonly held concepts, anti-vector CTL responses rather than neutralizing antibodies curtail the immunogenicity of homologous arenavirus vector prime – boost vaccination. Accordingly, backbones of distant genealogic relationship offered most potent heterologous prime – boost combinations, resulting in considerable rates of complete tumor rejection.

## 2.3 Results

### 2.3.1 Arenavirus vector backbone candidates and their genetic and phenotypic stability

Arenaviruses form enveloped particles and contain two segments of negative-stranded RNA. The large (L) segment encodes for the viral polymerase L and the matrix protein Z, whereas the short (S) segment carries the envelope glycoprotein (GP) and nucleoprotein (NP) genes, separated by intergenic regions, respectively (Fig. 2-1 A). We and others have incorporated transgenic sequences such as tumor-associated antigens (TAAs) into replicating arenavirus vectors by segregating the NP and GP genes onto artificially duplicated S segments ( $S_{NP}$ ,  $S_{GP}$ , Fig. 2-1 B, C) (57, 58, 271). This can be achieved by either the artARENA (e.g. artLCMV) or r3ARENA (e.g. r3LCMV) design strategy (Fig. 2-1 B, C). Here we vectorized additional mammalian arenaviruses (mammarenaviruses) to exploit their immunotherapeutic potential when combined in heterologous prime-boost combinations. Based on phylogenetic relationship, mammarenaviruses can be subdivided into the Old World group of viruses and four clades (A-D) of New World viruses (Fig. 2-1 D). For vector generation (see STAR Methods) we selected three mutually very distantly related viruses representing the main branches of the phylogenetic tree, namely the prototypic Old World virus lymphocytic choriomeningitis virus (LCMV), the widely studied New World Clade A virus Pichinde (PICV) and the Junin virus vaccine strain Candid#1 (CAND). CAND is in clinical use as a prophylactic vaccine against Junin virus, the causative agent of Argentine hemorrhagic fever (9), and PICV has no human disease correlate but can infect humans as documented in accidentally exposed laboratory workers (273).

LCMV infection is mostly asymptomatic or manifests as a flu-like infection (274). Rare cases of choriomeningitis are generally self-limiting and, despite documented cases of protracted central nervous system manifestations, commonly heal without persisting sequels (275, 276). From a safety perspective all three viruses are therefore valid vector backbone candidates for immunotherapeutic use in humans. We generated both, artARENA (artLCMV, artPICV, artCAND) as well as r3ARENA (r3LCMV, r3PICV, r3CAND) vectors expressing fluorescent reporter proteins. In cell culture, artARENA vectors as well as their respective r3ARENA counterparts reached lower titers than their respective parental wildtype (wt) viruses (Fig. 2-1 E-G). These observations extended and generalized earlier findings on attenuated artARENA and r3ARENA vector growth (57, 58, 271).

Genetic and phenotypic stability are key criteria for the clinical utility of replicating viral vector systems. We have previously reported that artLCMV stably retained its genome organization and transgene expression over extended periods of in vivo replication, whereas r3LCMV underwent inter-segmental recombination, reverting to a non-transgenic bisegmented wildtype-like virus (58). Here we used artPICV-GFP, r3PICV-GFP and wildtype PICV virus (PICVwt) to infect highly immunodeficient AGRAG mice, which lack the type I and type II interferon receptors and are devoid of T and B cells owing to RAG deficiency. In the first 30 days of persistent infection, total viral loads (determined as PICV-NP-expressing infectivity) in blood of artPICV-GFP- and r3PICV-GFP-infected animals were similar and below those of PICVwt-infected controls (Fig. 2-1 H). By day 70, however, r3PICV-GFP viremia exceeded the levels in artPICV-GFP-infected animals and increased continuously thereafter, eventually reaching levels equivalent to PICVwt. Conversely, artPICV viremia remained consistently below PICVwt controls. GFP transgene-expressing viral infectivity in r3PICV-GFP- and artPICV-GFP infected mice was at comparable levels up to around day 70 of infection (Fig. 2-1 I). Thereafter it declined continuously in r3PICV-GFP infection but remained stable in artPICV-infected animals. The resulting ratio of total PICV infectivity to GFP-transgenic infectivity documented that r3PICV-GFP progressively lost its transgene while transgene expression by artPICV-GFP remained stable throughout the observation period of >200 days (Fig. 2-1 J). We performed RT-PCR to detect supposedly recombined wildtype-like S segments containing both PICV NP and GP sequences (Fig. 2-1 K). Such RNA species were absent from artPICV-GFP-infected mice but were consistently detected in the blood of r3PICV-infected animals (Fig. 2-1 L). Sequence analysis of amplicons revealed that some of them contained one or two GFP remnants, flanked by partially or completely duplicated viral intergenic regions, thus identifying them as inter-segmental recombination products of the  $S_{NP}$  and  $S_{GP}$  segments of r3PICV-GFP (Fig. 2-1 M). On day 224 after infection, RT-PCR assays detected the  $S_{NP}$  and  $S_{GP}$  segments of artPICV-GFP but not the corresponding GFP-containing segments of r3PICV-GFP (Fig. S 2-1 A-D), further supporting the notion of r3PICV-GFP transgene loss. When re-isolated after >200 days of persistent infection and propagated in cell culture, r3PICV-GFP reached titers equivalent to PICVwt virus, whereas re-isolated artPICV-GFP growth was attenuated. This contrasted with the cell culture behavior of the inoculum of r3PICV-GFP and artPICV-GFP vectors, both of which grew to lower titers than the corresponding PICVwt viruses (Fig. 2-1 N). These findings indicated that the genetic instability of r3PICV-GFP was accompanied by phenotypic reversion to PICVwt-like growth, whereas artPICV-GFP was genetically and phenotypically stable. Analogous findings

were made with CAND-based vectors.  $S_{NP} - S_{GP}$  recombination products and loss of GFP-containing segments was also observed in r3CAND-infected AGRAG mice but not in artCAND-infected animals (Fig. S 2-1 E-K). Re-isolated r3CAND-GFP exhibited CANDwt-like cell culture growth behavior (Fig. S 2-1 L) while artCAND replication in AGRAG mice was at too low levels as to allow for the virus' re-isolation. Altogether, these studies generalized the finding (58) that artARENA vectors are genetically and phenotypically stable, while r3ARENA vectors are prone to transgene loss and phenotypic reversion to wildtype-like virus.

### 2.3.2 artARENA vectors are attenuated in guinea pig and in a mouse pathogenesis model

Next we tested whether artPICV and artLCMV were attenuated in animal models. Guinea pigs were infected with titrated doses of either PICVwt, known to cause lethal disease in these animals, or with artPICV-E7E6 expressing a non-oncogenic fusion construct consisting of the HPV16 E7 and E6 ORFs (277) (see chart in Fig. 2-2 A). Animals receiving diluent were included as a further control. At PICVwt doses of  $3 \times 10^2$  or 3 PFU, three out of eight animals reached humane endpoints (Fig. 2-2 A), a disease which was always accompanied by high-level viremia ( $>10^3$  PFU; Fig. 2-2 B, C). At the highest PICVwt dose ( $3 \times 10^4$  PFU), seven out of eight guinea pigs developed high-level viremia and terminal disease (Fig. 2-2 A, D). In contrast, artPICV-E7E6 infection at  $3 \times 10^2$  PFU was aviremic (Fig. 2-2 E) and doses of  $3 \times 10^4$  or even  $3 \times 10^6$  PFU (100-fold higher than the highest PICVwt dose tested) did not result in high-level viremia (Fig. 2-2 F, G). Transient low-level viremia was detected in only 1 out of 8 animals in both of these latter cohorts (Fig. 2-2 F, G) and none of these animals developed terminal disease (Fig. 2-2 A). When administered  $3 \times 10^2$  PFU artPICV-E7E6, the lowest dose tested, seven out of eight animals were free of disease throughout the 27-day observation period and none of the animals had detectable viremia (Fig. 2-2 E). On day 24 after vector inoculation one of these aviremic animals suddenly exhibited signs of disease corresponding to humane study endpoints, thus necessitating its euthanasia on day 25. The absence of detectable viral loads in this animal suggested, however, that its disease was unrelated to artPICV-E7E6 vector administration. Measurements of body weight loss, a commonly used parameter of PICV-induced disease in guinea pigs, provided additional independent support to the conclusion that artPICV-E7E6 was substantially attenuated (Fig. S 2-2).

Intracranial inoculation of mice represents the standard model to assess the neurovirulence of LCMV-based vectors (58, 267, 278). In agreement with earlier data demonstrating attenuation of artLCMV vectors (58) we found that 100 – 1000 PFU of artLCMV-E7E6 had to be administered intracranially to elicit terminal choriomeningitis in about half of the animals whereas 1 PFU of LCMVwt resulted in terminal disease in all mice (Fig. 2-2 I). LCMV-induced choriomeningitis is mediated by CD8 T cells, which attack virus-infected meningeal cells and astrocytes resulting in blood-brain-barrier (BBB) breakdown and brain edema (279-281). To investigate the mechanisms underlying reduced artLCMV neurovirulence we infected wildtype mice intracranially with 10 PFU of either artLCMV-E7E6 or LCMVwt or with diluent.

Seven days later, at the peak of disease in LCMVwt-infected animals, we determined immunoglobulin deposits in the brain parenchyma as a surrogate of BBB integrity (Fig. 2-2 J, K). The brain area affected by BBB breakdown was significantly larger in LCMVwt- than in artLCMV-E7E6-infected mice (Fig. 2-2 L). Regions of dense immunoglobulin deposits were evident in LCMVwt-infected brains, notably around the longitudinal fissure with substantial extension into deeper cortical layers, whereas in artLCMV-E7E6-infected brains only small immunoglobulin deposits were detected in proximity to the longitudinal fissure. This morphological correlate of reduced immunopathological damage furthers our understanding of attenuated artLCMV neurovirulence (279).

### 2.3.3 Immunogenicity and epitope dominance in heterologous artARENA prime – boost vaccination

Next we tested the utility of artPICV – artLCMV as a heterologous prime – boost regimen. We primed C57BL/6 mice with either artLCMV-E7E6 or artPICV-E7E6, followed by artLCMV-E7E6 boost on day 13. E7-specific CTL responses in blood on day 9 were somewhat higher upon artLCMV-E7E6 prime than after artPICV-E7E6 prime (Fig. 2-3 A). Seven days after heterologous artLCMV-E7E6 boost (d20), artPICV-E7E6 primed animals reached E7-specific CTL frequencies >50% of the total circulating CD8<sup>+</sup> T cell pool, with only limited contraction over a one-month-period (Fig. 2-3 A-C, Fig. S 2-3). These CTL frequencies vastly exceeded those induced by homologous artLCMV-E7E6 prime – boost, which remained in the 6-7% range, similar to the frequencies after prime. All of these responses were polyfunctional as determined by IFN- $\gamma$ , TNF- $\alpha$  and IL-2 secretion upon peptide stimulation and comprised E7- as well as E6-specific CTLs (Fig. S 2-3). The majority of tumors, however, do not exhibit viral determinants such as HPV E7 and E6 and active immunization therefore has to rely on other classes of TAAs, for which immune responses can be affected by self-tolerance. Studies on the P815 mouse tumor cell-derived cancer-testis antigen P1A, for example, have shown post-natal expression is restricted to spermatogonia, placenta and thymic medullary epithelial cells, the latter being key to central tolerance induction (282, 283). Accordingly, P1A-knockout mice spontaneously rejected P815 tumors, mounting P1A-specific CD8 T cell responses of significantly higher magnitude and functional avidity than wildtype animals (284). To test whether heterologous artARENA immunization facilitates breaking self-tolerance we immunized BALB/c mice with P1A-expressing artLCMV-P1A or artPICV-P1A. By day 38 after prime the P1A-specific responses induced by either vector had leveled off in the range of 2-3% of circulating CD8<sup>+</sup> T cells (Fig. 2-3 F). Upon heterologous artLCMV-P1A boost, artPICV-P1A-primed mice mounted P1A-specific CTL responses exceeding 50% of the circulating CD8<sup>+</sup> T cell pool, thus substantially higher than upon artLCMV-P1A homologous boost (Fig. 2-3 F-H). These heterologous prime – boost induced CTL responses contracted slowly, with frequencies >20% persisting in peripheral blood for >3 months (Fig. 2-3 F). Besides vector transgene-specific responses (E7E6, P1A) we determined also dominant vector backbone-specific responses directed against the NP-derived epitopes NP396 in C57BL/6 mice (H-2D<sup>b</sup>-restricted) and NP118 in BALB/c mice (H-2L<sup>d</sup>-restricted). Interestingly, these responses of C57BL/6 and BALB/c mice, respectively, were substantially lower in

animals receiving heterologous artPICV – artLCMV immunization as compared to homologous artLCMV prime – boost (Fig. 2-3 D, I). Based on these measurements we calculated the transgene: backbone epitope dominance ratio (E7 : NP396, Fig. 2-3 E; P1A : NP118, Fig. 2-3 J). It was substantially higher in heterologous as compared to homologous prime – boost immunization (~50-fold in Fig. 2-3E; >200-fold in Fig. 2-3 J), indicated that heterologous prime – boost immunization biased vaccine-induced CTL responses towards transgene-derived epitopes. In the context of active immunization for immunotherapy it is important to induce high-frequency CTL responses within a short time window. artPICV-P1A – artLCMV-P1A heterologous prime – boost, administered at an interval of only four to ten days, induced P1A-specific CTL responses of higher frequencies than were obtained in homologous prime – boost immunization given at the same interval (Fig. S 2-4 A-D). A trend for higher P1A-specific CTL frequencies at longer prime – boost intervals (7-10 days as compared to 4 days) was accompanied by an inverse trend in NP118 backbone-targeting responses. Of note, artPICV-P1A prime followed by artLCMV-P1A boost clearly outperformed the inverse sequence of administration when administered at intervals of 4-10 days (Fig. S 2-4 A-D). The prime – boost regimen of artPICV followed by artLCMV rather than the inverse sequence of administration was, therefore, used for the subsequent studies. Only when the interval between the two vaccinations was substantially longer, artPICV-P1A boost of artLCMV-P1A-primed responses was effective (Fig. S 2-4 E, F).

### 2.3.4 Phenotype of artARENA-induced CTLs and their dependence on IL-33 – ST2 alarmin signaling

Next we determined how heterologous artPICV – artLCMV prime-boost influenced the magnitude and phenotype of P1A-specific CTL populations. Seven days after boost, CD62L<sup>lo</sup> effector / effector-memory cells dominated the responses of BALB/c mice to both homologous artLCMV-P1A prime – boost and heterologous artPICV-P1A – artLCMV-P1A immunization (Fig. 2-4 A-D). Importantly, heterologous prime – boost elicited not only higher P1A-specific CD62L<sup>lo</sup> effector / effector-memory CTL populations than homologous prime – boost but also the CD62L<sup>hi</sup> central memory population was more abundant (Fig. 2-4 C, D). We studied the phenotype of both CTL subsets by determining the cells' expression of the surface markers KLRG1, CX3CR1, CD27, CD43, CD127 and of the transcription factors Tcf-1, Tbet and Eomes (Fig. 2-4 E, Fig. S-2-5 G). Within both, the CD62L<sup>hi</sup> and CD62L<sup>lo</sup> subset of CTLs, heterologous prime – boost immunization promoted the expression of the effector differentiation markers KLRG1, CX3CR1 and CD43 (285-289), with a concomitant reduction in the proportion of cells expressing the memory markers CD27 and CD127 (288, 290). We observed also that CTLs emerging from heterologous prime – boost expressed higher average Tbet levels and lower levels of Tcf-1, thus further supporting the conclusion that heterologous prime - boost augmented the effector differentiation of CTLs. Irrespective of this relative effector differentiation bias, heterologous prime – boost augmented not only the total number of CTLs expressing the effector differentiation markers KLRG1, CX3CR1 and CD43 but also the population of cells expressing memory precursor markers (CD27, CD127) and the stemness-defining transcription factor Tcf-1

(120) (Fig. 2-4 F). When analyzed four weeks after boost (Fig. S 2-5 A-F), most of the differences between CTLs emerging from homologous and heterologous prime – boost persisted, but overall were less pronounced than on day seven after boost. Of note also, prominent populations of effector-like memory populations, characterized by the marker combinations CD43<sup>-</sup>CD27<sup>-</sup>, CX3CR1<sup>+</sup>CD27<sup>-</sup> and KLRG1<sup>+</sup>CD27<sup>-</sup> (285-289), were particularly abundant upon heterologous prime – boost immunization (Fig. S-2-5 G). Taken together these observations indicated that CTL responses induced by heterologous prime – boost differed from those emerging from homologous prime – boost primarily by their higher cellularity, paired with more pronounced effector differentiation.

IL-33 signals through its receptor ST2 are key for protective CTL responses to replicating viruses(59), and IL-33 signals critically augment CTL responses to artLCMV-vectored immunization and resulting tumor control (58). Here we compared the ST2 dependence of artARENA-induced CTL responses by immunizing ST2-deficient and wt control mice with artLCMV-E7E6, artPICV-E7E6 or artCAND-E7E6. artLCMV- and artPICV-induced CTL responses to E7 were significantly lower in blood of ST2-deficient mice than in wt controls (Fig. 2-4 G, H). Conversely, ST2-deficiency had no clear effect on artCAND-induced CTL responses. ST2-dependent differences in artLCMV- and artPICV-induced CTL responses were also evident when enumerating IFN- $\gamma$  and TNF- $\alpha$  co-producing CTLs in spleen (Fig. S 2-6). These findings indicated that besides artLCMV also artPICV- but not artCAND-induced CTL responses benefited from IL-33 signaling.

### **2.3.5 Genealogic artARENA vector backbone relatedness dictates interference by pre-existing immunity and potency in heterologous prime – boost immunization**

Our observations in Figs. 2-3 E, J suggested that heterologous artARENA prime – boost immunization overruled the immunodominance of vector backbone-directed CTL responses to focus immune responses on vaccine targets. To systematically investigate this hypothesis we preimmunized mice with either LCMVwt, PICVwt, CANDwt or with wildtype Mopeia virus (MOPVwt) and studied the animals' ability of responding to artLCMV-E7E6 vaccination one month later. MOPV is an Old World mammarenavirus and thus stands in close genealogic relationship to LCMV, while the New World viruses PICV and CAND are only distantly related to LCMV (Fig. 2-1 D). Owing to epitope sequence homology between LCMV and MOPV (Fig. 2-5 A), both viruses elicited clearly detectable CTL responses to NP396, whereas the more distantly related PICVwt and CANDwt did not (Fig. 2-5 B). Pre-existing immunity to LCMV or MOPV almost completely abrogated E7-specific CTL induction by artLCMV-E7E6, whereas the responses of PICVwt- or CANDwt-immune mice were only modestly below those of control mice without prior arenavirus infection (Fig. 2-5 C). This interference by LCMVwt and MOPVwt immunity was accompanied by high-frequency NP396-directed responses and a biased E7 : NP396 immunodominance hierarchy upon artLCMV-E7E6 vaccination (Fig. 2-5 D,E). Of note, we relied on the immunodominant NP396 epitope as an indicator of backbone cross-reactivity, which likely comprised additional epitopes in the four viral backbone proteins NP, GP, L and Z.



Next we tested whether these interference and immunodominance hierarchies correlated with the immunogenicity of heterologous artARENA vector prime – boost combinations. To further expand the quiver of artARENA vectors we generated a reverse genetic system for MOPV, and based thereupon developed an artMOPV-P1A vector. Cell culture experiments demonstrated attenuated growth of artMOPV-P1A when compared to its parental virus (Fig. S 2-7), analogously to the artARENA vectors described in Fig. 2-1 E-G. We compared the ability of artLCMV-P1A to boost P1A-specific CTL responses induced by artPICV-P1A, artCAND-P1A or artMOPV-P1A in BALB/c mice. Animals undergoing homologous artLCMV-P1A, artPICV-P1A or artCAND-P1A prime – boost immunizations served as comparators and after boost remained in the 10% range or below (Fig. 2-5 F). Amongst the heterologous artARENA vector combinations, artPICV-P1A and artCAND-P1A primed animals were efficiently boosted by artLCMV-P1A, reaching frequencies in the 20-30% range. Conversely, P1A-specific CTL responses of artMOPV-P1A-primed and artLCMV-P1A-boosted animals remained below 3%, thus failed to exceed the responses upon homologous artLCMV-P1A prime – boost. This indicated that the immunogenic benefit of heterologous prime – boost over homologous prime – boost was abolished when the closely related MOPV and LCMV vector backbones were combined. The above hierarchy of heterologous prime – boost combinations correlated inversely with the LCMV NP118-specific CTL responses to prime and boost (Fig. 2-5 G). artPICV-P1A und artCAND-P1A prime did not induce NP118-specific CTLs above technical background and repressed NP118-directed responses upon artLCMV-P1A boost. Conversely, artMOPV-P1A primed and artLCMV-P1A boosted animals had >50% NP118-specific CD8<sup>+</sup> T cells in peripheral blood with a corresponding P1A: NP118 epitope dominance ratio <0.1 (Fig. 2-5 H). Thus, genealogic vector backbone relatedness and vector backbone-biased CTL responses correlated with the inefficient induction of P1A-specific responses.

### **2.3.6 Interference by vector backbone-specific CTLs rather than by neutralizing antibodies**

Next we investigated the induction and cross-reactive neutralizing activity of artARENA vector-induced antibody responses. Homologous prime – boost immunization with artCAND induced sizeable vector-nAb titers (Fig. 2-6 A). On the contrary we failed to detect artLCMV- or artPICV-nAbs after homologous prime – boost immunization (Fig. 2-6 A), and neither artLCMV-, nor artPICV- nor artCAND-immune sera cross-neutralized any of the other viruses. nAb induction by artCAND but not artLCMV or artPICV was in line with differentially dense glycan shields on the respective viruses' envelope proteins (53).

These findings argued against vector-nAbs as a limiting factor in artLCMV- or artPICV-based homologous or heterologous prime – boost immunization. To formally rule out antibody-mediated inhibition we performed homologous and heterologous prime – boost immunizations in B cell-deficient JHT and wt control mice. E7-specific responses to artPICV-E7E6 and artLCMV-E7E6 prime were indistinguishable in the two strains of mice (Fig. 2-6 B). More importantly, however, JHT and wt mice showed a virtually identical response pattern to homologous artLCMV-E7E6 or heterologous artPICV-E7E6 boost,

respectively. Superior immunogenicity of heterologous as compared to homologous prime – boost despite a lack of anti-vector antibodies in JHT mice excluded anti-vector antibody responses as a major limitation in homologous artLCMV prime – boost immunization (Fig. 2-6 B).

To address whether anti-vector CTL responses, independently of other components of anti-vector immunity, can interfere with artLCMV-based vaccination we “preimmunized” mice with a recombinant vaccinia virus expressing the NP396 epitope as a minigene (VACC-NP396). Control animals were either given vaccinia virus expressing an irrelevant transgene (Vacc-lacZ) as preimmunization or were left unimmunized. As expected, VACC-NP396 preimmunization but not VACC-lacZ induced a CTL response to NP396 (Fig. 2-6 C), while both viruses triggered CTLs to the immunodominant vaccinia virus backbone epitope B8R<sub>20-27</sub> (Fig. 2-6 D). When subsequently vaccinated with artLCMV-E7E6, the E7-specific CTL responses of VACC-NP396-preimmune animals were 7-8-fold lower than those of VACC-lacZ-preimmune or not previously vaccinia-exposed controls (Fig. 2-6 E). Conversely, the NP396-specific CTL response of VACC-NP396-preimmune mice approached 50% of the circulating CD8<sup>+</sup> T cell pool, vastly exceeding the responses of VACC-lacZ-preimmune or vaccinia virus-naïve mice (Fig. 2-6 F). Thus, pre-existing immunity to one immunodominant CD8 T cell epitope in the artLCMV backbone was sufficient to repress E7-directed CTL responses upon vaccination, with a concomitant shift in the E7: NP396 epitope dominance (Fig. 2-6 G).

### **2.3.7 Heterologous artARENA vector immunotherapy increases TIL numbers and tumor cure rates resulting in long-term anti-tumor immunity**

To assess whether the augmented immunogenicity of heterologous artARENA vector prime – boost translated into superior therapeutic efficacy we exploited two transplantable syngeneic mouse tumor models. The P815 mastocytoma cell line is derived from a DBA/2 mouse and expresses the P1A cancer-testis antigen, whereas the C57BL/6-derived TC-1 cell lines serves as a model of HPV16 E7E6-expressing cancer. We implanted P815 and TC-1 tumors subcutaneously into the flank of mice and initiated artPICV or artLCMV vector therapy when tumors were palpable (P815: day 9) or had reached an average critical volume (~100 mm<sup>3</sup>, TC-1:day 8). artPICV – artLCMV heterologous therapy delivering the respective tumor antigen, P1A or E7E6, was compared to homologous artPICV – artPICV or artLCMV – artLCMV prime – boost, all administered at an interval of seven days (P815 model) or ten days (TC-1 model). Homologous artPICV and homologous artLCMV immunotherapy afforded clear tumor volume control when compared to untreated control animals (Fig. 2-7 A, B). In both tumor models, however, the most pronounced and durable effect on tumor volume was seen upon heterologous artPICV – artLCMV therapy. This therapeutic effect depended on the vectorized antigen: a control group of P815 tumor-bearing mice, which was given artPICV-GFP – artLCMV-GFP prime – boost, delivering the irrelevant GFP transgene instead of a TAA, did not show a clear therapeutic effect. Homologous prime – boost with either TAA-expressing artLCMV or artPICV extended the survival of tumor-bearing mice, albeit to a lesser extent than heterologous prime – boost, and all mice receiving homologous prime – boost immunization eventually reached humane endpoints



(Fig. 2-7 C, D). In contrast, eighteen percent of mice with P815 tumors and 37.5 percent of animals with TC-1 tumors rejected their respective tumors when undergoing heterologous TAA-vectorizing artPICV – artLCMV immunotherapy (P1A, E7E6; not GFP), resulting in the animals' survival for >125 days (Fig. 2-7 C, D). When these long-term survivors were re-challenged with the same tumor cells, no tumor growth was recorded, while tumor- and therapy-naïve control animals rapidly progressed to humane endpoints (Fig. 2-7 E, F). This observation indicated that the elimination of established tumors by artPICV – artLCMV immunotherapy resulted in long-term anti-tumor immunity.

We enumerated and characterized tumor-infiltrating CTLs on day 5 after homologous or heterologous artARENA vector immunotherapy of P815 tumors (Fig. 2-7 G-L). Heterologous artPICV-P1A – artLCMV-P1A immunotherapy did not substantially augment total tumor-infiltrating CTL numbers as compared to homologous immunotherapy with either one of these vectors (Fig. 2-7 G), but P1A-specific CTLs inside tumors were significantly more numerous upon heterologous than upon homologous artARENA immunotherapy (Fig. 2-7 H). In line with this observation we found an increase in proliferating (Ki67<sup>+</sup>) and granzyme B-expressing (cytotoxic) P1A-specific tumor infiltrating CTLs in mice with heterologous artARENA immunotherapy (Fig. 2-7 I, J). On the contrary, heterologous artPICV-P1A – artLCMV-P1A therapy triggered significantly less NP118-specific TILs than homologous artLCMV-P1A prime – boost vaccination (Fig. 2-7 K), with a corresponding shift in P1A : NP118 epitope dominance inside the tumor (Fig. 2-7 L). Taken together, these data indicated that heterologous artARENA vector immunization shifted TAA : vector backbone immunodominance patterns of tumor-infiltrating CTLs.

## 2.4 Discussion

The elicitation of clinically effective tumor-specific CTL responses remains an important unmet medical need. Here we identify epitope dominance and interference by vector backbone-directed T cell responses as an important hurdle in vectored vaccine delivery. Based on this concept in conjunction with arenaviral genealogy analyses we have developed potent heterologous artARENA-based immunization regimens inducing effective anti-tumor immunity.

Therapeutic cancer vaccination represents a particularly demanding field of active immunization. The induction of high-frequency CTL responses against TAAs is often encumbered by central as well as peripheral tolerance mechanisms, limiting the available T cell repertoire and its responsiveness (291). Additional challenges arise from chronic antigenic exposure, which can lead to the functional adaptation or impairment of specific T cell responses (292-294). In this context, potent viral vector systems and their optimal combination are of particular importance. While poxviral delivery systems have been clinically evaluated as cancer vaccines for more than two decades (248, 295) a wide variety of viral vector systems have entered clinical testing in recent years. These approaches comprise alphavirus vectors (250), human and simian adenovirus-based vectors (251, 252), lentiviral delivery systems (253), rhabdoviral vectors (254,

255) as well as combinations thereof, attesting to the promise of and broad interest in virally vectored cancer vaccination.

Animal studies have shown that arenavirus vectors are immunogenic when administered either intravenously, intradermally, subcutaneously or intramuscularly (267, 269), and the latter route has also been clinically validated in a human trial (66). Earlier studies from our lab revealed, however, that the IL-33 – ST2 alarmin pathway contributes essentially to the effectiveness of artARENA vectored cancer immunotherapy (58), and the vector's ability to trigger this pathway correlated with its spread into IL-33-expressing splenic stromal cells. In line with other investigators' work (296), these findings highlighted the importance of vaccine delivery to specialized compartments of secondary lymphoid organs. The intravenous route warrants optimal access to these tissues and, therefore, has been used here and is also exploited in an ongoing clinical trial for artLCMV-based therapy of HPV16-positive head-and-neck cancer (272).

A discriminating feature of artLCMV and artPICV vector technology consists in the lack of vector-nAb induction (58, 66, 267, 269) – owing to the viral glycan shield(53) – and globally low arenavirus seroprevalence (50-52, 297). The reasons for the latter lie in the natural host range of mammarenaviruses being restricted to rodents, combined with only rare transmission from rodents to humans. Albeit not eliciting nAbs against its own glycan-shielded envelope protein, replication-deficient rLCMV vectors elicit potent antibody immunity against vectorized cargo (53, 58, 66, 267, 269). While future work should investigate the utility of replicating artARENA vector technology for prophylactic antibody induction against infectious diseases, potent CD8 T cell responses position heterologous artARENA vector prime - boost immunization as a promising strategy for therapeutic vaccination in persistent microbial diseases, notably HIV and hepatitis B (237, 298).

Our findings highlight anti-vector T cell immunity as a mechanism of interference in artARENA vector homologous prime – boost vaccination. For delivery systems such as adenoviral and poxviral vectors, which readily elicit potent vector-nAbs (259, 299), the latter are commonly taken as surrogate and supposed main mechanism of interference by anti-vector immunity. Several observations suggest, however, that pre-existing anti-vector T cells impede responses to adenoviral and poxviral vector systems, too. Inefficient responses to MVA-vectored TAAs has been accredited to epitope dominance and competition by vector backbone-directed T cell responses (300). Similarly, the inhibitory activity of adenovirus vector-nAbs (299) may have obscured the contribution of additional interference mechanisms. Certain pairs of adenoviral vectors, although serologically distinct, failed to effectively boost upon each other (263, 264). This indicated that the mere absence of vector-nAbs cannot predict efficient boosting. Conversely, pre-existing adenovirus-specific T cell immunity correlated inversely with HIV-specific CTL induction by rAd5 vectors in human vaccine trials (301). Pre-existing T cell reactivity to Ad5 is found in >80 percent of healthy adults, irrespective of Ad5-specific serostatus (302). It originates from prior exposure to adenoviruses of unrelated serotypes, targets epitopes in conserved regions of the viral genome (303) and expands significantly upon rAd5-vectored vaccination (302). These considerations highlight advantages of viral vector platforms based on viral families such as the arenaviruses, which circulate almost exclusively in the animal kingdom.

## 2.5 Limitations of the study

We relied on the transgene: backbone epitope dominance ratio of CD8 T cell responses as an indicator and correlate of backbone-directed T cell interference. Besides inter-clonal competition of transgene- and backbone-specific T cells (304), an alternative and not mutually exclusive mechanism may consist in the accelerated elimination of vector-transduced antigen presenting cells by pre-existing anti-vector T cells (305).

The present data obtained in mice may imperfectly predict efficacy in man, yet they call for an immediate clinical evaluation of heterologous artPICV – artLCMV prime – boost immunization regimens to the benefit of patients. artPICV-E7E6 and artLCMV-E7E6 are currently entering clinical Phase 1 testing as a repeated alternating prime – boost immunization regimen for HPV16-positive head-and-neck cancer (272). Irrespective of the limited predictive value of transplantable mouse tumor models, our findings on potent CTL induction to self-antigens such as P1A suggest that self-tolerance can efficiently be broken and thus provide incentive to our plans of applying artARENA vector technology to a broader range of cancers, most of which do not express viral target antigens. The arenavirus vector platform accommodates transgenes up to ~2000 bp (58, 269), thus lending itself to the delivery of all types of proteinaceous cancer targets (306), but it remains unknown which ones provide best clinical efficacy.

## 2.6 Acknowledgements

We wish to thank Nadège Lagarde, Beatrice Dolder Schlienger, Felix Stemeseder und Sophie Schulha for excellent technical assistance, Theresa Kleissner, Goran Bekic, Daniel Oeler and Sonja Feher for diligent implementation of animal studies.

This work was supported by the Swiss National Science Foundation (grants 310030\_185318/1 to DDP; CRSII3\_160772/1 to DDP and DM; 310030\_173010 to DM; CRSII5\_170929 to AZ), by Hookipa Pharma, Inc. (to DDP, AZ and DM) and by the Austrian Research Promotion Agency (Österreichische Forschungsförderungsgesellschaft, FFG).

## 2.7 Author contributions

WVB, NK, AFM, SMK, SS, JR, UB, IV, SG, CM, DM, KKO, AZ and DDP contributed to experimental conception and design. WVB, NK, AFM, SMK, MAK, ML, SD, JR, IV, MP, RK, SH, CM performed experiments. WVB, NK, AFM, SMK, SS, JR, UB, IV, MP, CM, DM, KKO, AZ and DDP analyzed and/or interpreted the data. WVB, NK, AZ and DDP wrote the manuscript.

## **2.8 Declaration of interests**

SS, JR, UB and KKO are employees and stock option holders of Hookipa Pharma, Inc., DDP is a founder, consultant, shareholder and stock option holder of Hookipa Pharma, Inc. WVB, SMK, SS, SD, UB, DDP, DM and KKO are listed as inventors on patents describing artARENA vector technology. WVB and DDP are married.

## 2.9 Results-Figures

Figure 1

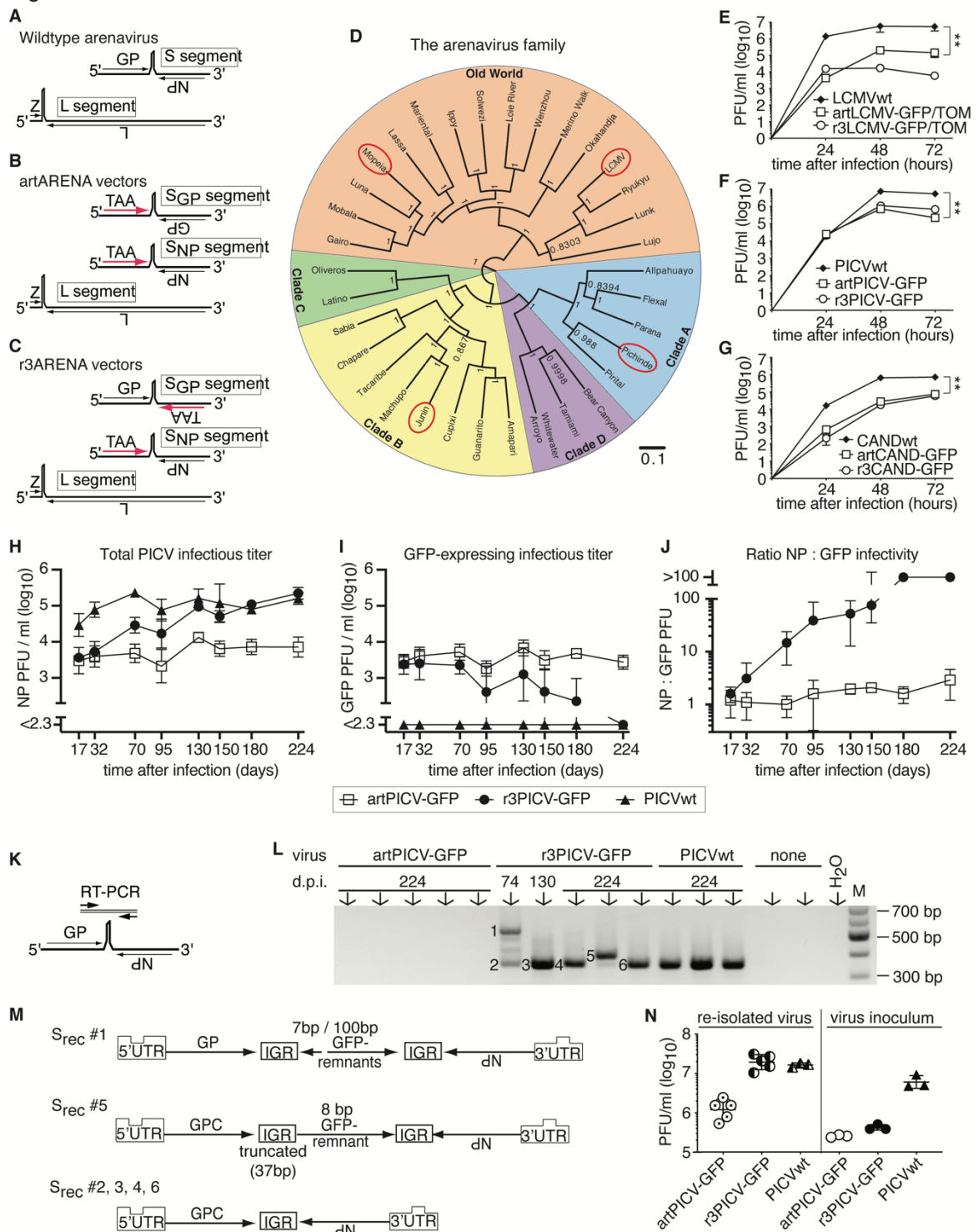


Figure 2-1 Arenavirus vector backbone candidates and their genetic and phenotypic stability

A-C: Schematic of the genome organization of wildtype arenaviruses (A), artARENA vectors (B) and r3ARENA vectors (C).

TAA: tumor associated antigen.

D: Genealogy tree of the mammarenavirus family with its clades. Red circles indicate viruses used in this study.

E-G: Growth curves of the indicated viruses and vectors in BHK-21 cells (E,F) and 293T cells (G) infected at multiplicity of infection (MOI) of 0.01. Symbols show the mean $\pm$ SD of three cell culture wells (error bars mostly within symbol size). \*\*  $p < 0.01$  by unpaired two-tailed Student's *t* test.

H-J: AGRAG mice were infected with the indicated viruses i.v. and viremia was monitored by immunofocus assays detecting either PICV-NP (H) or GFP (I) to calculate the NP : GFP infectivity ratio (J). Symbols represent means $\pm$ SD of 3-5 mice.

K-M: RT-PCR strategy (K) to amplify recombined wildtype-like PICV S segment RNA species re-uniting NP and GP sequences. Gel electrophoresis image of RT-PCR products (L) obtained from serum samples collected on the indicated time points. Each lane represents an individual mouse. Sera from uninfected mice (“none”) and water were included as negative controls. Sequence analysis of the bands numbered in (L) suggested recombination products as schematically depicted in (M). IGR: S segment intergenic region; UTR: untranslated region.

N: BHK-21 cells were infected with viruses re-isolated from individual AGRAG mice on d224 of the experiment shown in (H-J) or with the viral stocks originally used to infect the animals. Titers after 72h are shown. Symbols represent individual viral cultures from one mouse each. Mean $\pm$ SD is indicated. Number of independent data sets (N) for panels H-N=2. See also Fig. S 1-1.

Figure 2

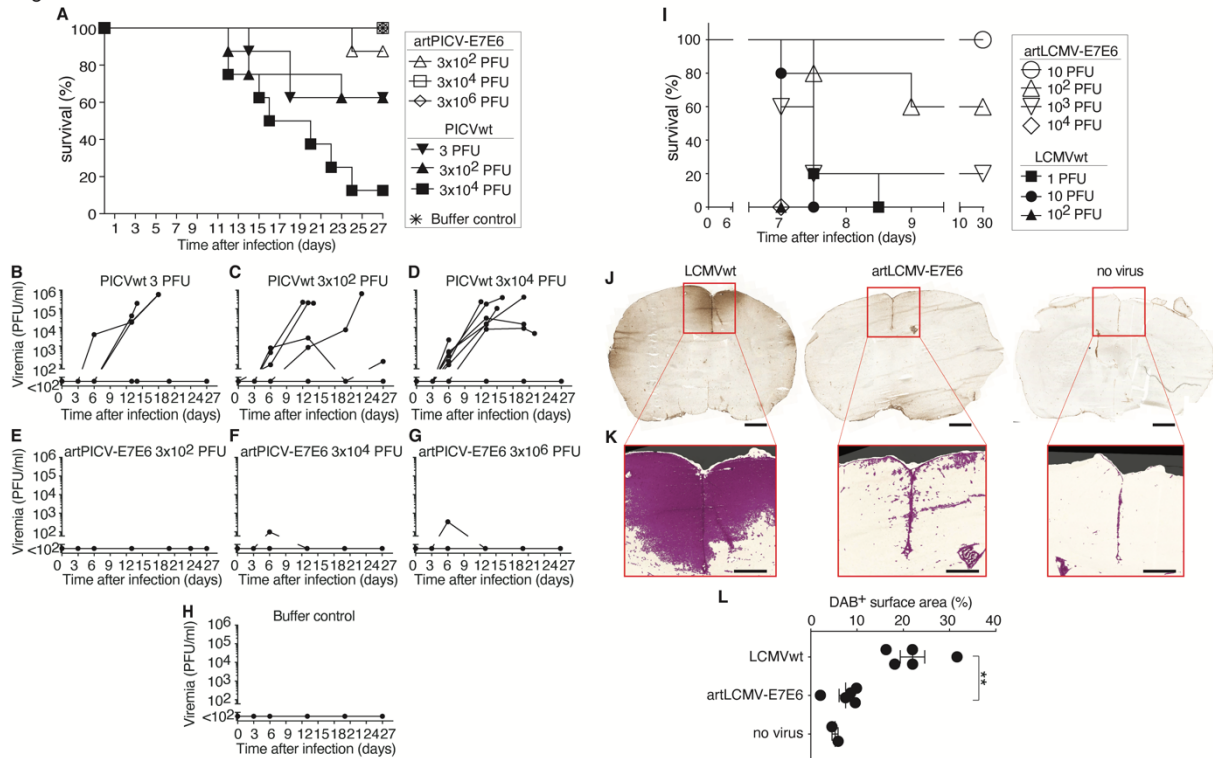


Figure 2-2 artARENA vectors are attenuated in guinea pig and mouse pathogenesis models

A-H: We infected groups of 8 adult Hartley guinea pigs, four of each sex, with either artPICV-E7E6 or PICVwt at the indicated doses intraperitoneally and monitored humane endpoints (“survival”). A group of six control animals (three of each sex) was administered diluent.

A: The animals were monitored until reaching humane endpoints or until the end of the study on d27.

B-H: Viral loads in blood of the same eight or six animals per group, respectively, as shown in (A) were determined by immunofocus assay.

I: We inoculated groups of five C57BL/6 mice intracranially with titrated doses of LCMVwt or artLCMV-E7E6 as indicated and monitored signs of choriomeningitis (“survival”).

J-L: To analyze the impact of viral infection on blood-brain-barrier permeability, animals were intracranially inoculated with 10 PFU of LCMVwt, 10 PFU of artLCMV-E7E6 or with diluent. Seven days later, IgG inside the brain parenchyma, indicating leakage across the blood-brain-barrier, was detected by peroxidase-based immunohistochemistry on histological sections. Representative images of coronary brain sections are shown (J), with an enlargement of computer-assisted detection of IgG-positive surface (K). A quantitation of the detected area is shown in (L). Error bars in (L) show the mean±SEM, while dots representing individual mice. Scale bars show 1000 μm (J) and 500 μm (K). See also Fig. S-2 2.



Figure 3

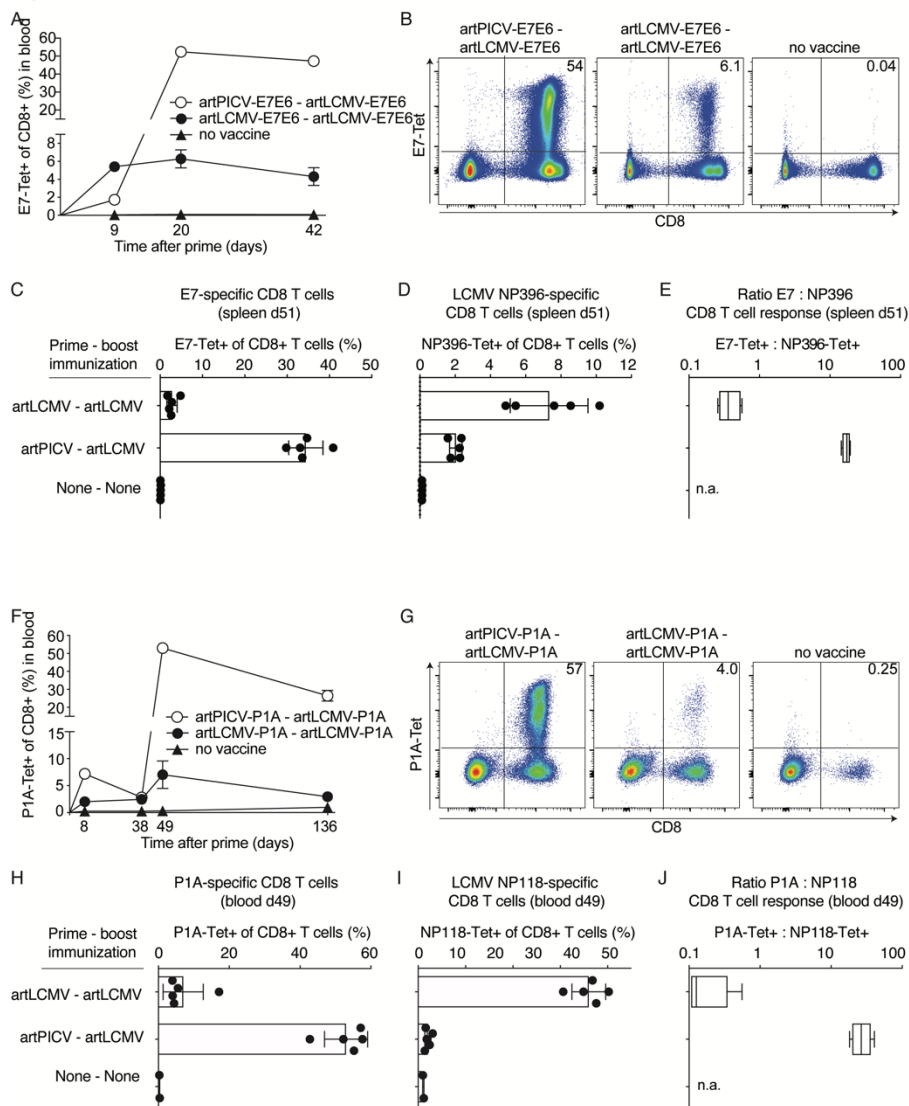


Figure 2-3 Immunogenicity and epitope dominance in heterologous artARENA prime – boost vaccination

A-E: C57BL/6 mice were given artPICV-E7E6 and artLCMV-E7E6 homologous or heterologous prime – boost vaccination i.v. on d0 and d13. E7-tetramer-binding CD8<sup>+</sup> T cell frequencies in blood were determined at the indicated time points (A). Representative FACS plots from blood gated on B220<sup>-</sup> lymphocytes analyzed on d20 (B). Splenic frequencies of E7-specific (C) or NP396-specific (D) CD8<sup>+</sup> T cells on d51 served to calculate the epitope dominance ratio displayed in (E).

F-J: BALB/c mice were given artPICV-P1A and artLCMV-P1A homologous or heterologous prime – boost vaccination i.v. on d0 and d39. P1A-tetramer-binding CD8<sup>+</sup> T cell frequencies in blood were determined at the indicated time points (F). Representative FACS plots from blood gated on B220<sup>-</sup> lymphocytes on d49 (G). Frequencies of P1A-specific (H) or NP118-specific (I) CD8<sup>+</sup> T cells in blood on d49 served to calculate epitope dominance ratios as displayed in (J). Symbols in (A, F) represent the mean±SEM of five mice, except “no vaccine” groups: 4 mice in (A), 2 mice in (F). Symbols in (C, D, H, I) display individual mice, bars indicate the mean±SD. Boxes in (E, J) display the minimal and maximal values. Numbers in (B, G) indicate the percentage of tetramer-binding cells amongst CD8<sup>+</sup>B220<sup>-</sup> T cells. See also Figs. S-2 [3](#) and S-2 [4](#).



Figure 4

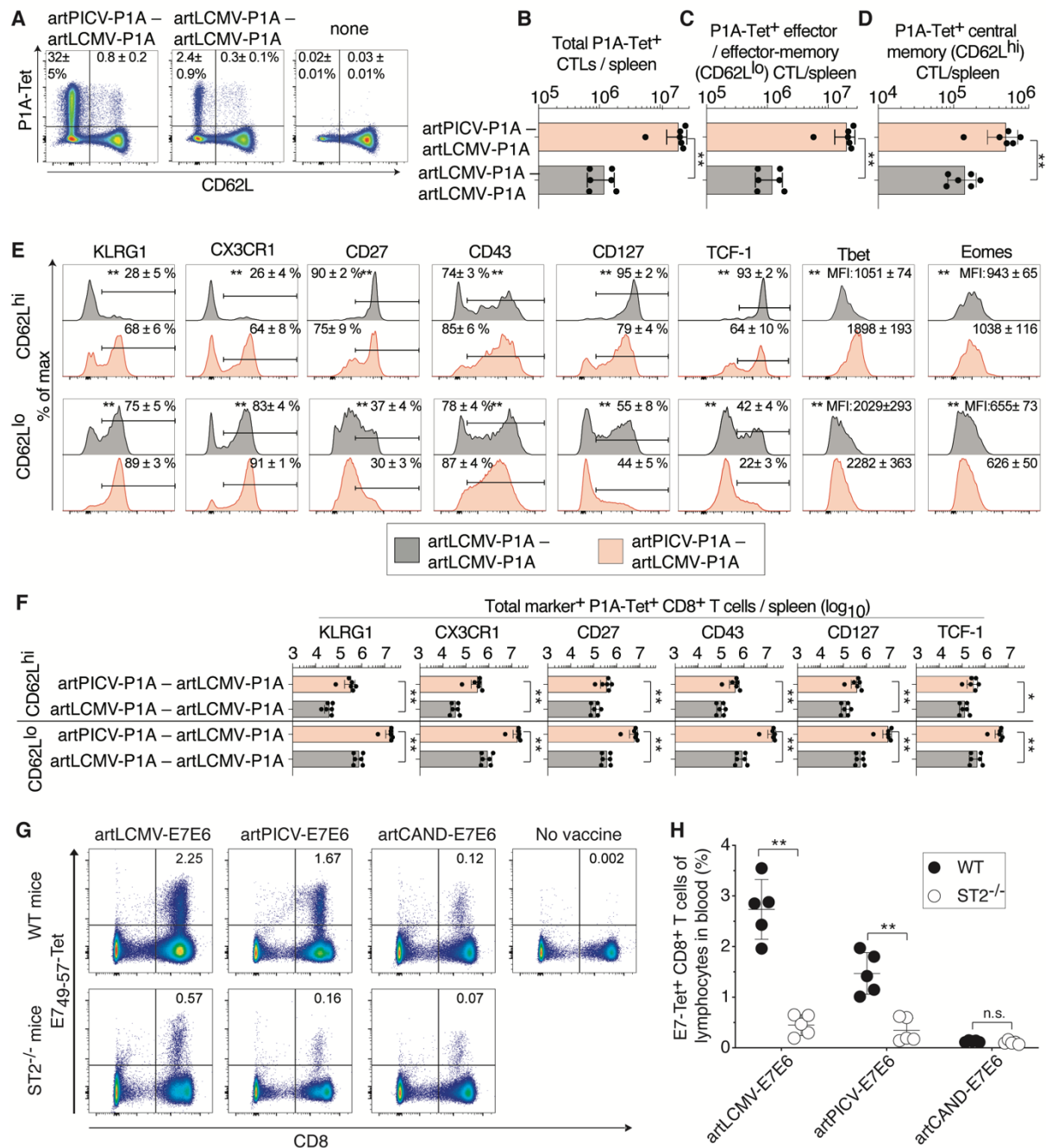


Figure 2-4 Phenotype of artARENA-induced CTLs and their dependence on IL-33 – ST2 alarmin signaling

A-F: We immunized BALB/c mice with artPICV-P1A and artLCMV-P1A in homologous or heterologous prime – boost vaccination i.v. on d0 and d27. On d34 we analyzed P1A-Tet-binding and CD62L expression by splenic CD8<sup>+</sup> T cells (A, gated on CD8<sup>+</sup>B220<sup>-</sup> lymphocytes). Unimmunized control mice are shown for comparison in (A) only. Numbers in (A) indicate the percentage of cells in the respective quadrant. Total P1A-Tet<sup>+</sup> CTLs (B), P1A-specific effector/effector-memory CTLs (CD62L<sup>lo</sup>, C) and P1A-specific central memory CTLs (CD62L<sup>hi</sup>, D) were enumerated in spleen on d34. In both subsets of P1A-specific CTLs, CD62L<sup>hi</sup> and CD62L<sup>lo</sup>, we determined the surface expression of KLRG1, CX3CR1, CD27, CD43 and CD127 as well as the master transcription factors Tcf-1, Tbet and Eomes (E). Total numbers of marker-expressing P1A-specific CTLs were enumerated in (F). (A) shows representative FACS plots from individual mice. Symbols in (B-D) represent individual mice, bars in (B-D, F) indicate the mean±SD.

Numbers in (A, E) indicate the percentage of gated cells (mean±SD) or the mean fluorescence intensity (MFI±SD). Means were calculated from six mice per immunization group (A-F) or from three unimmunized controls (A). N=2. \*\* p<0.01 by unpaired two-tailed Student's *t* test.

G, H: We immunized ST2<sup>-/-</sup> and wt mice with artLCMV-E7E6, artPICV-E7E6 or arCAND-E7E6 i.v. Controls were left unimmunized (“no vaccine” in (G)). E7-tetramer-binding cells in blood were determined on d7. Representative FACS plots are shown in (G), values indicate E7-Tet<sup>+</sup>CD8<sup>+</sup> T cells as a percentage of lymphocytes. Symbols in (H) represent individual mice (n=5 per group) with mean±SD. N=2. \*\* p<0.01 by two-way ANOVA with Sidak's post-test. See also Figs. S 2-5 and S 2-6.

Figure 5

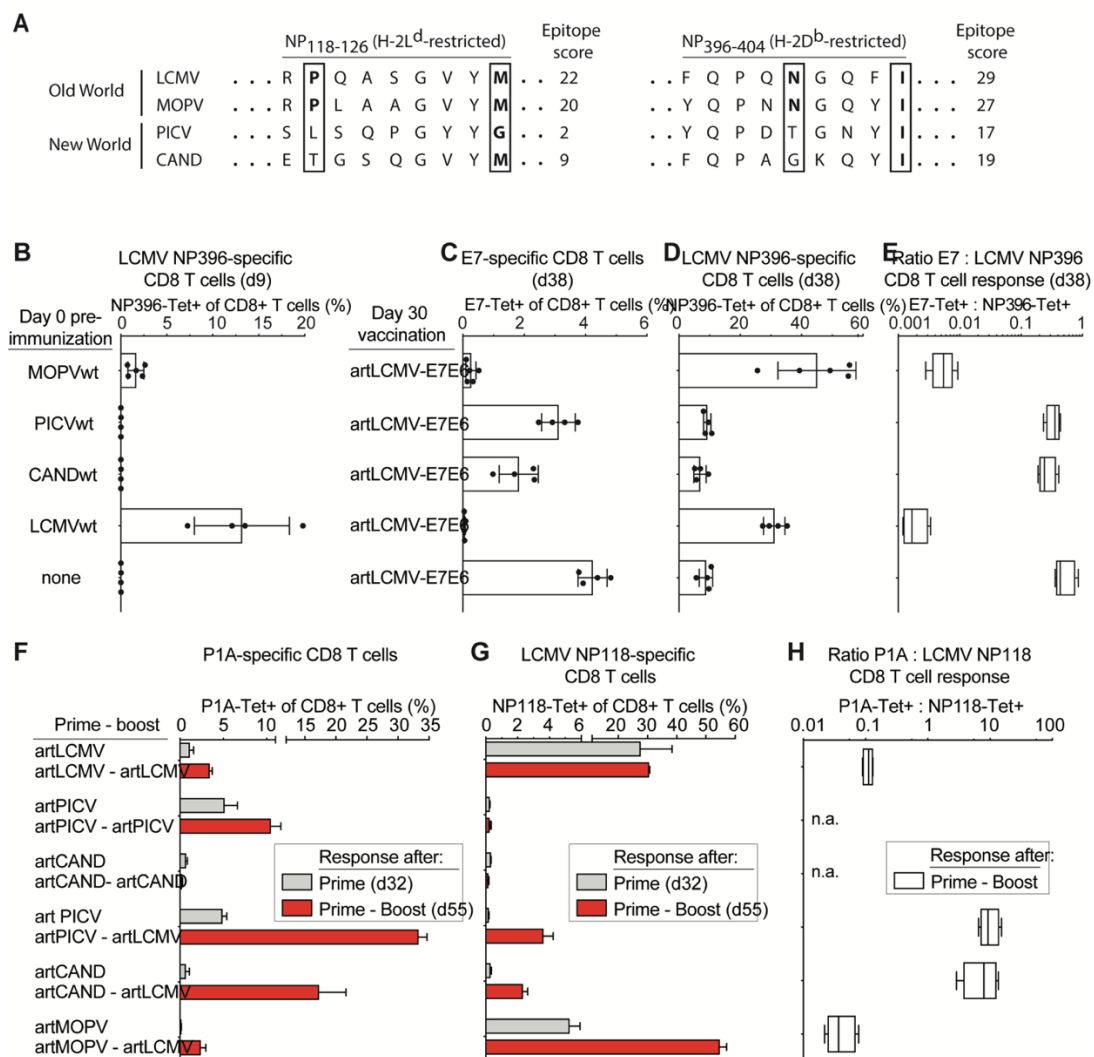


Figure 2-5 Genealogic artARENA vector backbone relatedness dictates interference by pre-existing immunity and potency in heterologous prime – boost immunization

A: Alignment of the LCMV NP118-126 and NP396-404 epitope sequences with the respective homologous sequences in the Old World arenavirus MOPV and the New World arenaviruses PICV and CAND. Epitope scores were predicted by the SYFPEITHI algorithm (307). MHC anchor positions are boxed, amino acids corresponding to consensus anchor residues for H-2L<sup>d</sup> and H-2D<sup>b</sup>, respectively, are shown in bold (308).

B-E: We preimmunized C57BL/6 mice on d0 with 10e5 PFU of MOPV, PICV, CAND or LCMV i.v. or left them uninfected. On d9 we determined NP396-specific CD8<sup>+</sup> T cell frequencies in peripheral blood (B). On d30 all mice were vaccinated with artLCMV-E7E6. Frequencies of E7-specific (C) and NP396-specific (D) CD8<sup>+</sup> T cells in blood on d38 served to calculate the epitope dominance ratio as displayed in (E). Symbols in (B-D) represent individual mice, bars in (B-D) show their mean±SD. F-H: We immunized BALB/c mice with 10e5 PFU of artARENA-P1A vectors i.v. in various homologous and heterologous prime (d0) – boost (d35) combinations as indicated. On d32 after prime and on d55 (20 days after boost) we determined the frequencies of P1A-specific (F) and NP118-specific (G) CD8<sup>+</sup> T cells in blood and calculated the P1A : NP118 epitope dominance ratio on d55 (H). The lack of NP118-specific responses over technical background in artPICV – artPICV and artCAND – artCAND immunized mice precluded this latter assessment (“n.a.”). Bars in (F, G) represent the mean±SEM of 3 (artPICV – artPICV) - 4 mice (other groups). Boxes in (E, H) display the minimal and maximal values. N=2. See also Fig. S-2-7.

Figure 6

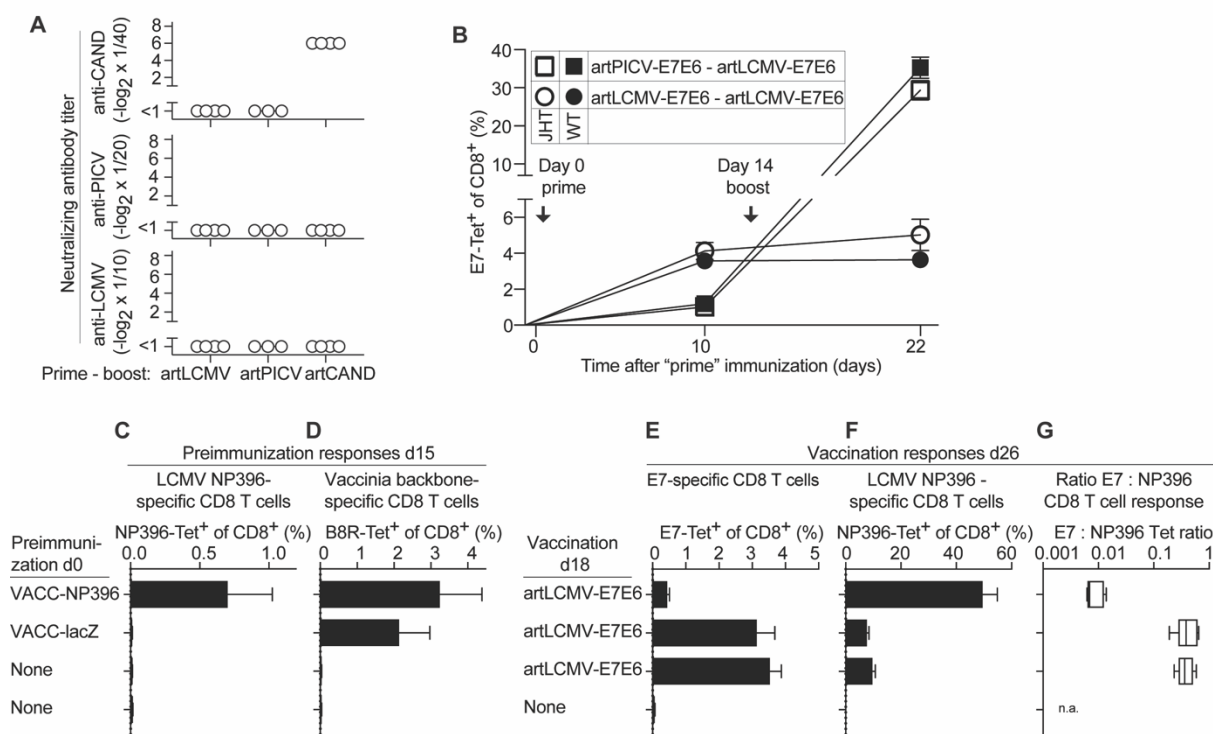


Figure 2-6 Interference by vector backbone-specific CTLs rather than by nAbs

A: We immunized BALB/c mice i.v. with artLCMV-, artPICV- or artCAND-based vectors on d0 and d35. Sera collected on d45 (d10 after homologous boost) were assayed for neutralizing activity against LCMV, PICV and CAND. Symbols represent individual mice. One representative of two similar experiments is shown.

B: We immunized B cell-deficient JHT and B cell-sufficient wt control mice with artLCMV-E7E6 and artPICV-E7E6 in homologous and heterologous prime – boost combinations on d0 and d14 as indicated in the chart. The frequencies of E7-specific CD8<sup>+</sup> T cells in blood was determined on d10 (post prime) and d22 (post boost). Symbols show the mean±SEM of 4 mice. N=2.

C-G: On d0 we preimmunized C57BL/6 mice i.v. with VACC-NP396 or VACC-lacZ or left them without preimmunization (“none”). On d15 we determined LCMV NP396-specific (C) and vaccinia B8R-specific (D) CTLs in blood by MHC class I tetramer staining. On d18 artLCMV-E7E6 i.v. vaccination was performed. Eight days later (d26) we determined E7-specific (E) as well as NP396-specific (F) CD8<sup>+</sup> T cell frequencies in blood and calculated the E7 : NP396 epitope dominance ratio (G). Bars represent the mean±SEM of 5 mice per group. Boxes display the minimal and maximal values. N=2.

Figure 7

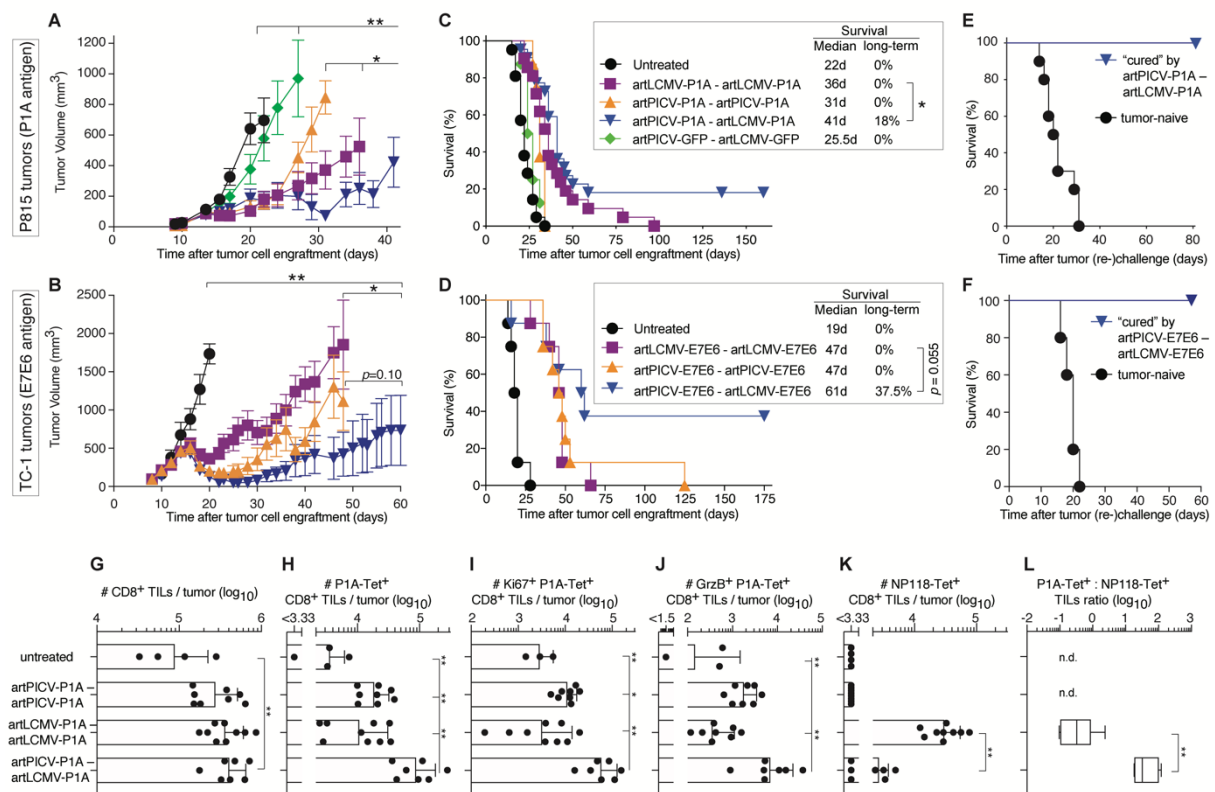


Figure 2-7 Heterologous artARENA vector immunotherapy increases TIL numbers and tumor cure rates resulting in long-term anti-tumor immunity

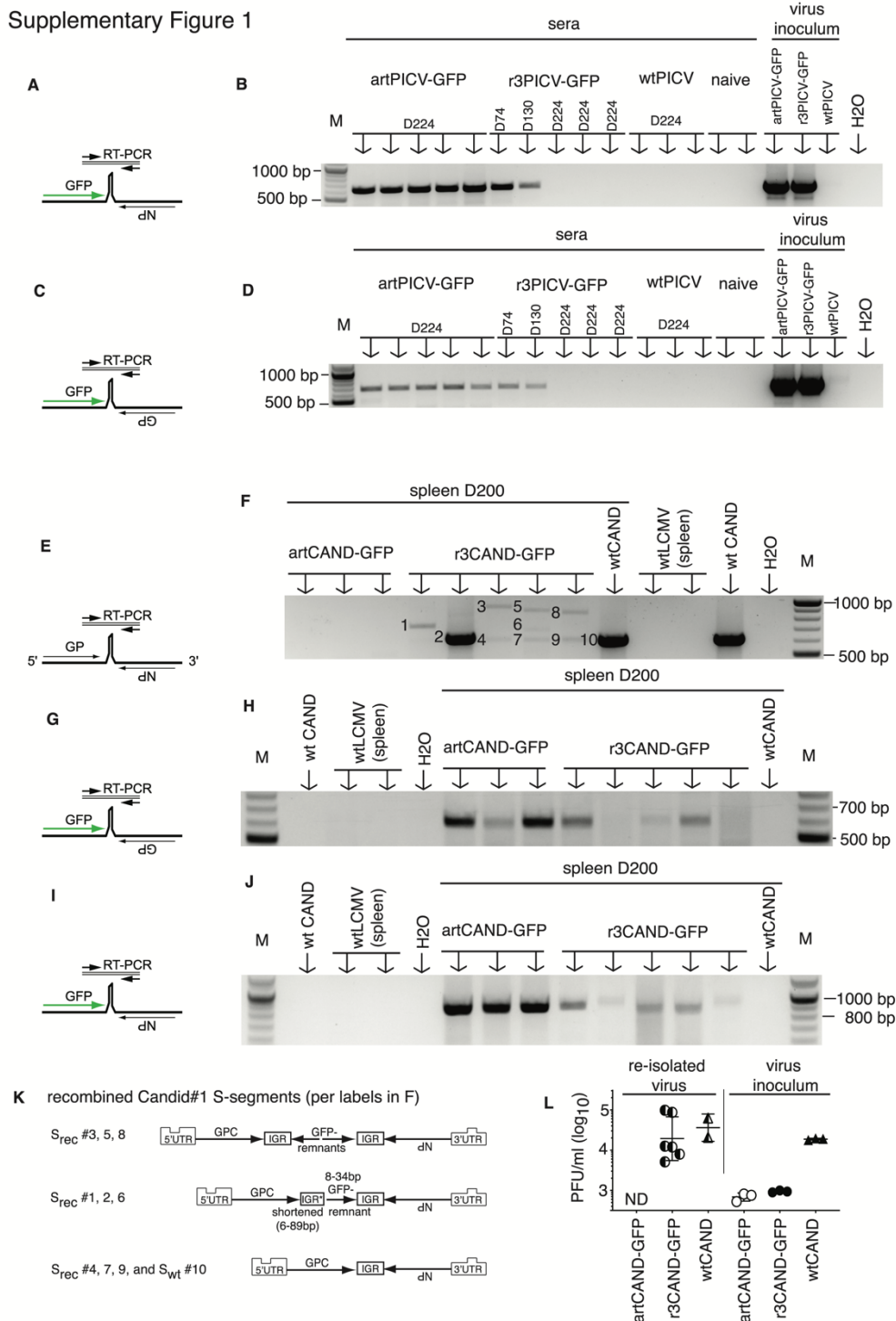
We implanted tumor cells subcutaneously in the flank of mice. A,C,E,G,L: DBA/2 mice, P815 tumor cells. B,D,F: C57BL/6 mice, TC-1 tumor cells. When animals exhibited palpable tumor masses on d9 (P815) or when tumors had reached an average volume of  $\sim 100 \text{ mm}^3$  on d8 (TC-1), mice were randomly assigned to the indicated prime-boost regimens administered i.v. on d9 and d16 (P815) or d8 and d18 (TC-1).

A, B: Symbols show tumor volumes (mean $\pm$ SEM) from two (A) and one (B) independent experiments. The curves end when >50% of animals in a group have reached humane endpoints. Entire tumor volume curves were statistically compared as described in Methods. C, D: Kaplan-Meier survival curves of the animals, with median survival and percent long-term survivors indicated. (A, C): n = 21 (untreated), 21 (artLCMV-P1A – artLCMV-P1A), 8 (artPICV-P1A – artPICV-P1A), 22 (artPICV-P1A – artLCMV-P1A) and 8 (artPICV-GFP – artLCMV-GFP). (B, D): n=8. \* p<0.05 by two-tailed chi-square test. E, F: Animals, which had rejected their tumors (“cured”) and tumor-naïve controls were subcutaneously re-challenged with tumor cells on d160 and d140 (E) or d118 (F) after primary tumor implantation. Re-challenged mice did not form palpable tumors (not shown). E: Combined data from tumor-free mice (n=5) and tumor-naïve mice (n=10) in two independent experiments. F: Tumor-free mice (n=3) and tumor-naïve mice (n=5) from one experiment.

G-L: We analyzed TILs in P815 tumors on day 20 (d4 after artARENA-P1A vector boost). Total CD8<sup>+</sup> TILs (G), P1A-specific CD8<sup>+</sup> TILs (H), amongst them Ki67<sup>+</sup> (I) or granzyme B expressing cells (J) and also NP118-specific TILs (K) were enumerated. The P1A : NP118 epitope dominance ratio was calculated (L). Symbols represent individual mice, bars show the mean, error bars indicate SEM. Boxes display the minimal and maximal values.

## 2.10 Results-Supplementary Figures

Supplementary Figure 1



S 2-1 Genetic and phenotypic stability of artARENA and r3ARENA vectors. Related to Figure 2-1

A-D: RT-PCR strategy (A) to amplify non-recombined  $S_{NP}$  (B) and RT-PCR strategy (C) to amplify  $S_{GP}$  segment (D) RNA species of both artPICV-GFP and r3PICV-GFP from the samples of the experiment shown in Fig. 1H-N. Gel electrophoresis image of RT-PCR products (B, D) obtained from serum samples collected on the indicated time points. Each lane represents an individual mouse. Sera from uninfected mice (“naive”), from three wtPICV infected mice and water were included as negative controls. Virus inocula served as reference.

E-L: We infected AGRAG mice with artCAND-GFP, r3CAND-GFP or CANDwt and collected spleen tissue 200 days later. E,F: RT-PCR strategy (E) applied to amplify recombined wildtype-like CAND S segment RNA species re-uniting NP and GP sequences (F). Gel electrophoresis image of RT-PCR products (F) obtained from spleen samples collected on the indicated time points after infection of AGRAG mice. Water and spleen tissue of AGRAG mice infected with LCMVwt served as negative control. Spleen tissue from a wtCAND-inoculated AGRAG mouse and wtCAND inoculum virus served as positive controls. Each lane with a spleen sample represents an individual mouse.

G-J: RT-PCR strategy (G) to amplify non-recombined S<sub>GP</sub> (H) and RT-PCR strategy (I) to amplify S<sub>NP</sub> segment (J) RNA species of both artCAND-GFP and r3CAND-GFP. Gel electrophoresis image of RT-PCR products (H,J) obtained from spleen samples collected on d200. Each lane represents an individual mouse. Spleen tissue from AGRAG mice infected with wtCAND or wtLCMV as well as wtCAND virus from cell culture and water were included as negative controls in the assay.

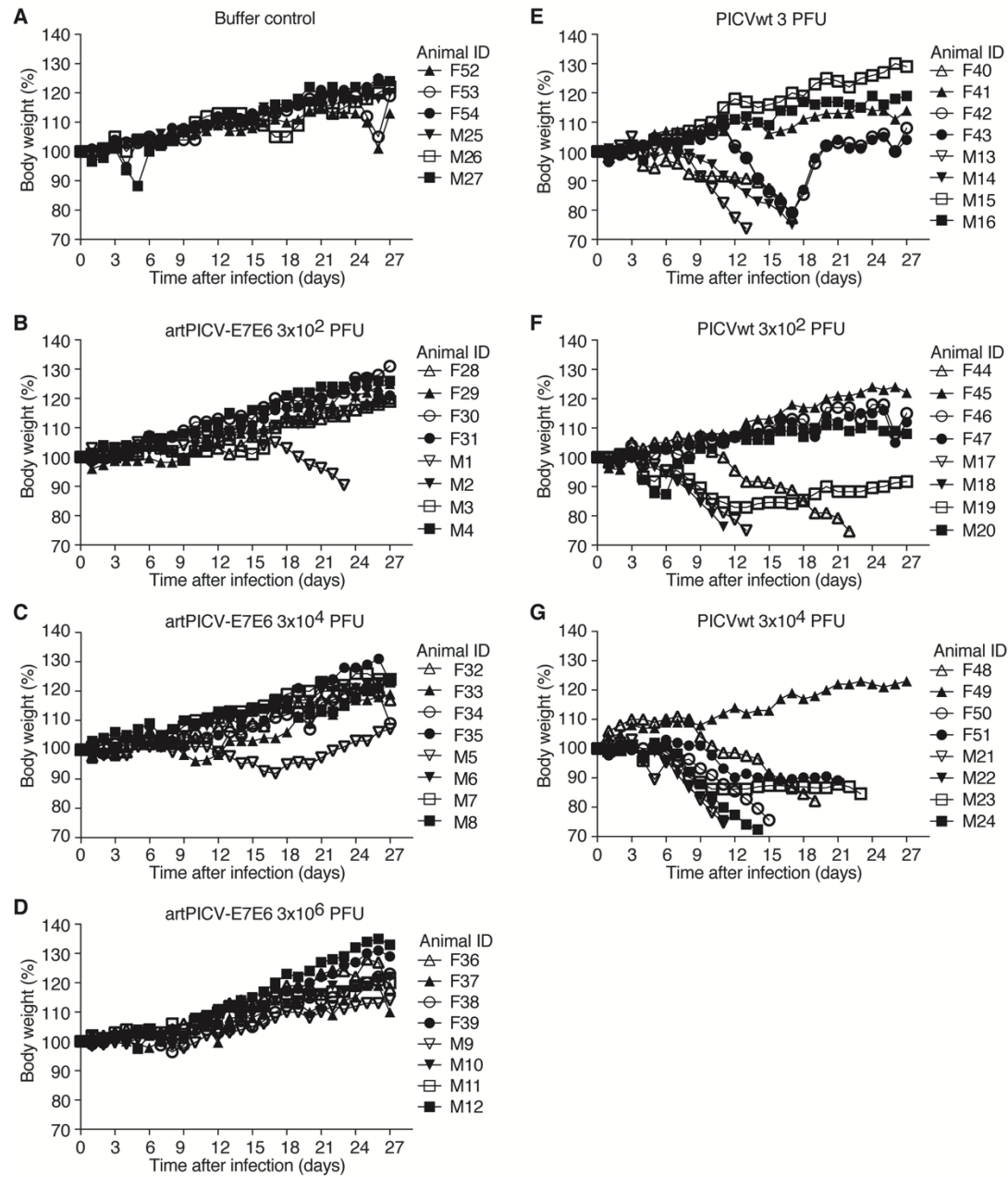
K: Sequence analysis of the bands numbered in (F) suggested viral recombination products as schematically depicted in (K).

IGR: S segment intergenic region; IGR\*: truncated S segment intergenic region; UTR: untranslated region

L: 293T cells were infected at MOI=0.001 with viruses re-isolated from individual AGRAG mice on d200 of the experiment in (E-K) or with the inoculum used to infect the animals. Titers after 72h are shown. Symbols represent individual viral cultures from one mouse each (re-isolated virus) or from replicate cultures (virus inoculum). Mean±SD is indicated. We failed to re-isolate infectious virus from artCAND-infected mice (ND).



Supplementary Figure 2

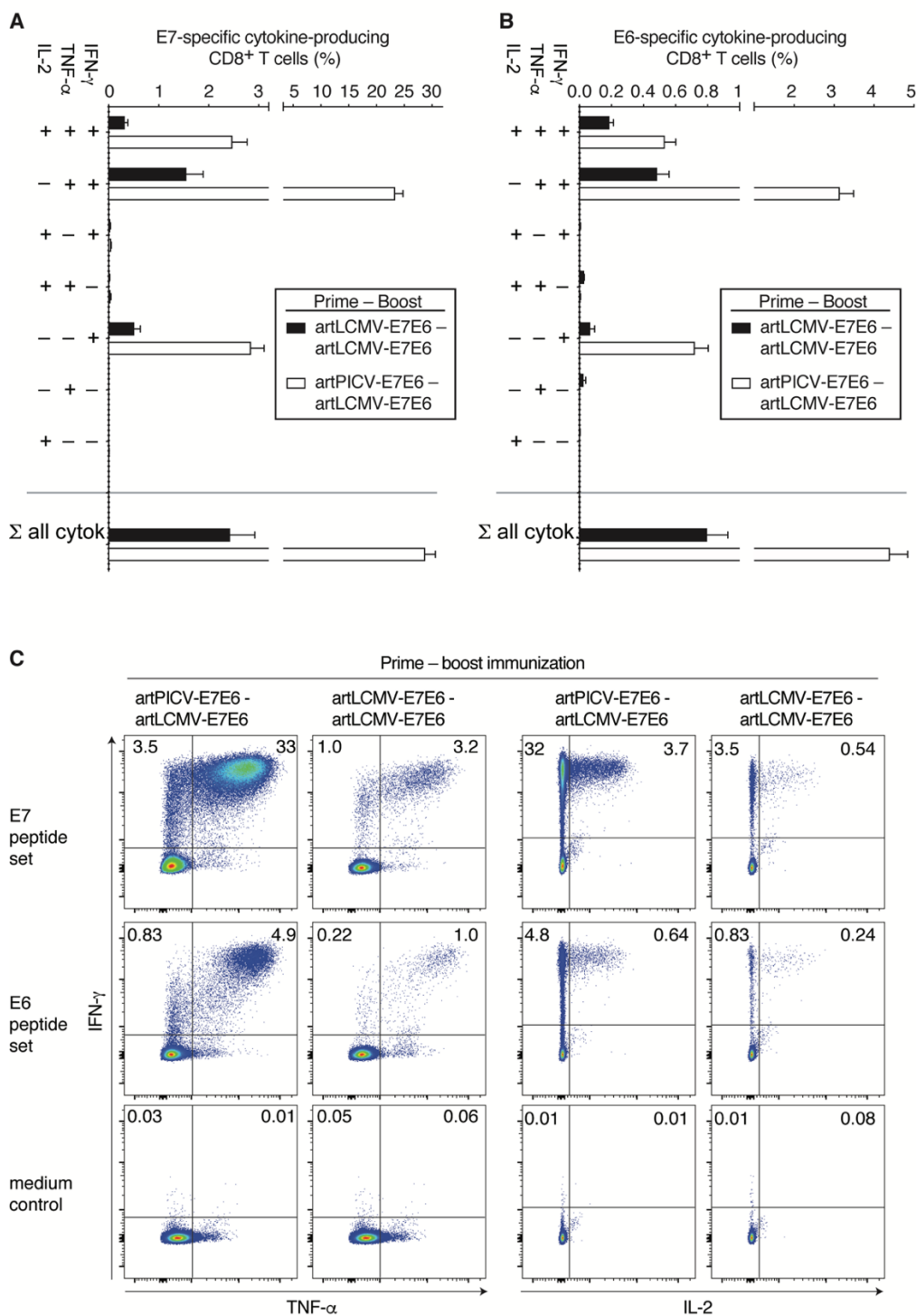


S 2-2 artARENA vectors are attenuated in guinea pigs. Related to Figure 2-2

We infected groups of 8 adult Hartley guinea pigs, four of each sex (F: female; M: male), with either artPICV-E7E6 or PICVwt at the indicated doses intraperitoneally and monitored body weight over time. A group of six control animals (three of each sex) was administered diluent. Data are from the same experiment as in Fig. 2-2 A-H.



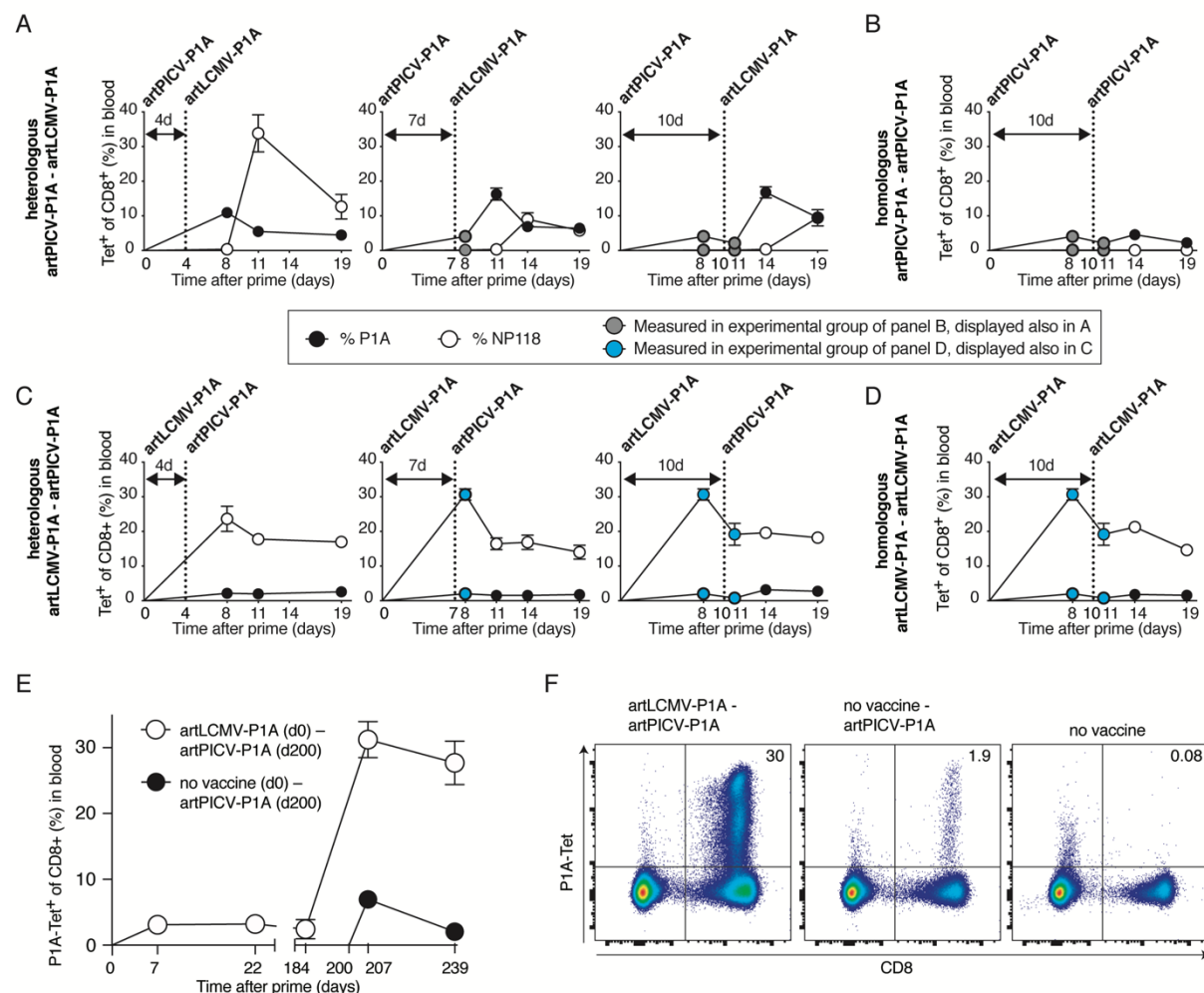
Supplementary Figure 3



S 2-3 Functionality of CD8 T cell response to heterologous artARENA prime – boost vaccination. Related to Figure 2-3

A-E: On d0 and d13 C57BL/6 mice were given i.v. vaccination with artPICV-E7E6 and artLCMV-E7E6, either as homologous or heterologous prime – boost, as indicated. On d51 the animals were sacrificed to determine E7- (A) and E6-specific (B) cytokine-secreting cells in spleen, respectively. Cytokine secretion was measured by intracellular cytokine staining upon restimulation with overlapping peptide sets spanning the E7 and E6 proteins, respectively. Bars represent the mean $\pm$ SEM of 5 mice per group. Representative FACS plots are shown in (C). Numbers indicate the percentage of cells falling into the respective quadrants.

Supplementary Figure 4

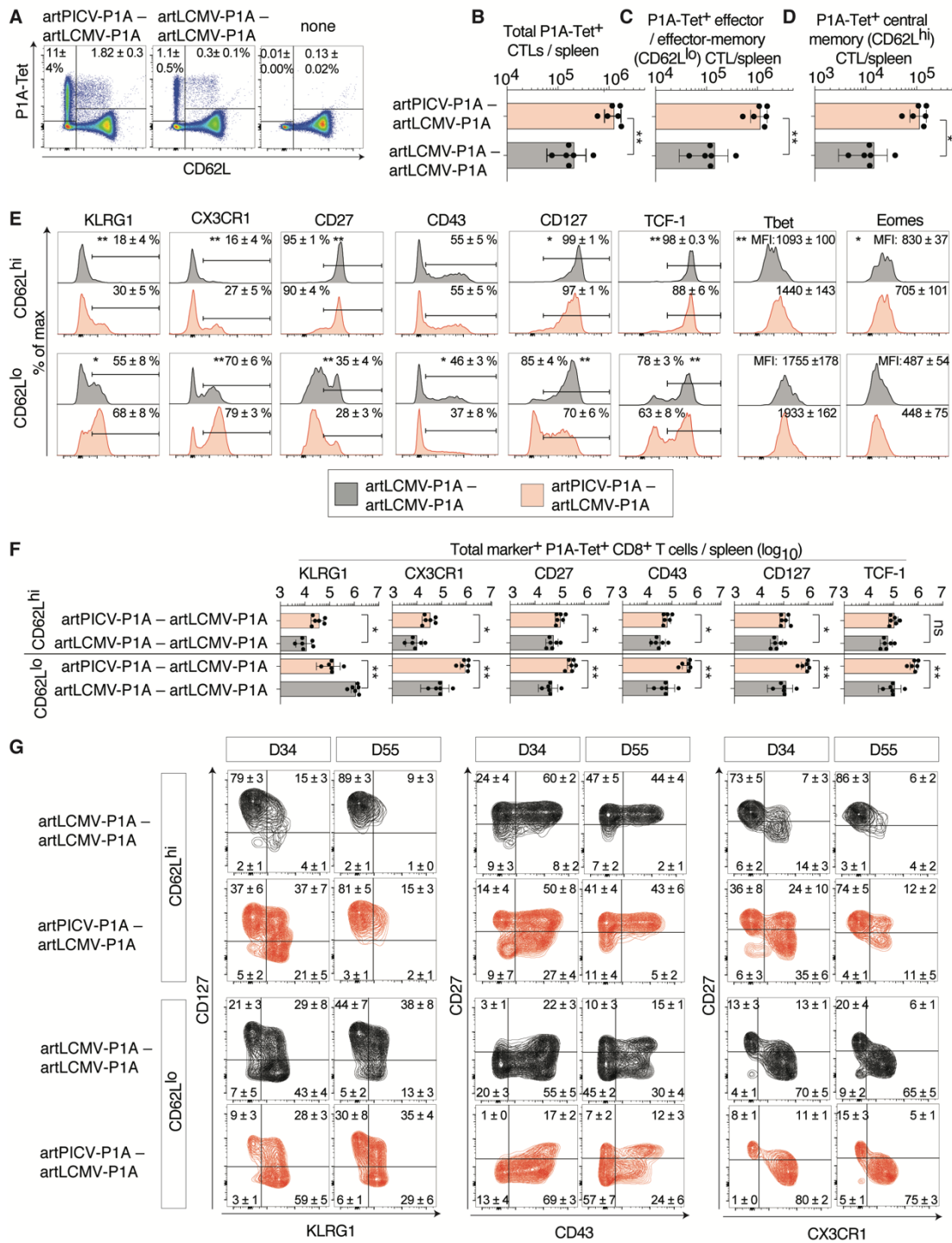


S 2-4 Impact of heterologous artARENA vector prime – boost interval on CTL responses, and efficient artPICV boost of artLCMV-primed responses after a long interval. Related to Figure 2-3

A-D: We immunized DBA/2 mice using artLCMV-P1A and artPICV-P1A in heterologous (A,C) or homologous (B,D) prime – boost combinations and at intervals of 4, 7 or 10 days as indicated. P1A-specific and NP118-specific CTL responses in peripheral blood were determined at the indicated time points. Grey and blue symbols are included in the graphs to panels (A,C) for reference only: Grey symbols in (A,B) indicate values determined in the group displayed in (B) upon single artLCMV-P1A prime, blue symbols in (C,D) indicate values determined in the group displayed in (D) upon single artLCMV-P1A prime. Symbols represent the mean±SEM of n=3-4 mice per group.

E-F: We immunized BALB/c mice with artLCMV-P1A on d0 and left controls without immunization. On d200 both groups were given artPICV-P1A for booster or prime immunization, respectively. P1A-specific CD8<sup>+</sup> T cell frequencies in peripheral blood were determined over time. Symbols in (E) represent the mean±SD of n=3 mice per group. Representative FACS plots from d239 are shown in (F), including also a naïve mouse as technical control (“no vaccine”). Values in (F) indicate the percentage of P1A-tetramer-binding cells amongst CD8<sup>+</sup> T cells.

Supplementary Figure 5

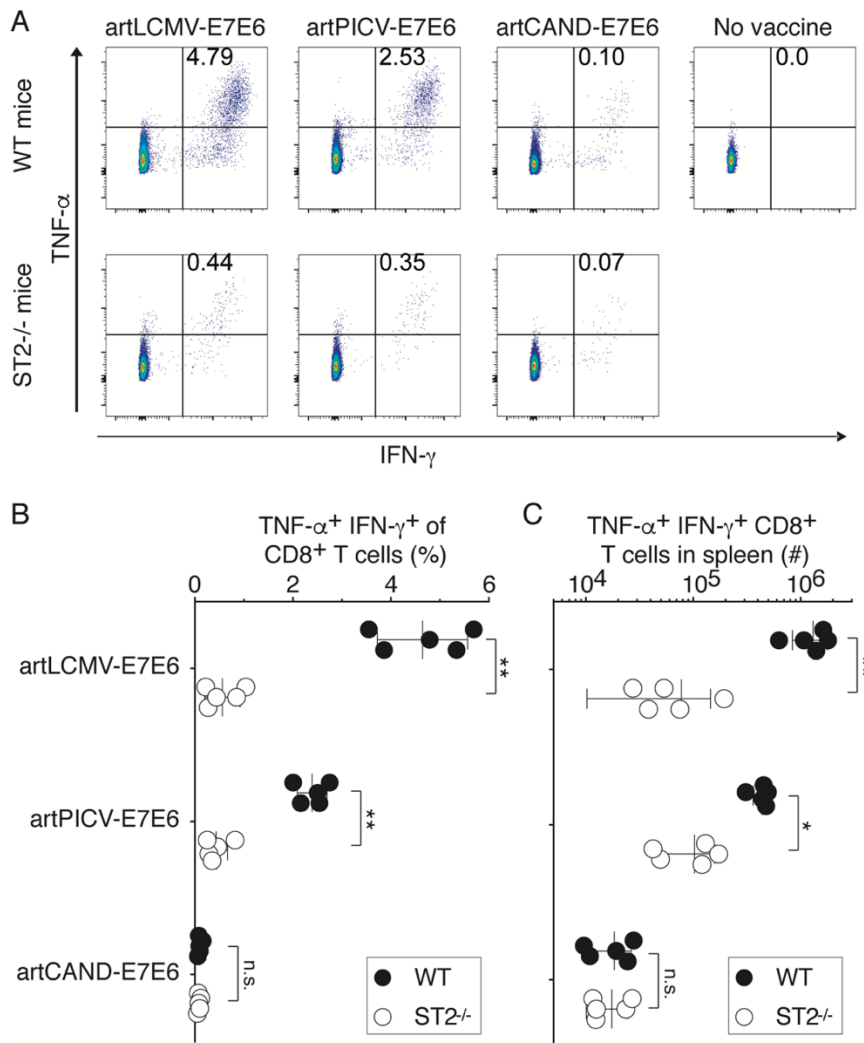


S 2-5 Phenotype of artARENA-induced CTLs one month after boost. Related to Figure 2-4

We immunized BALB/c mice with artPICV-P1A and artLCMV-P1A in homologous or heterologous prime – boost vaccination i.v. on d0 and d27. On d34 (G, same experimental data set as shown in Fig. 4A-F) and d55 (A-G) we analyzed P1A-Tet-binding and CD62L expression by splenic CD8<sup>+</sup> T cells (A, gated on CD8<sup>+</sup>B220<sup>-</sup> lymphocytes). Unimmunized control mice are shown for comparison in (A) only. Numbers in (A) indicate the percentage of cells in the respective quadrant. Total P1A-Tet<sup>+</sup> CTLs (B), P1A-specific effector/effector-memory CTLs (CD62L<sup>lo</sup>, C) and P1A-specific central memory CTLs (CD62L<sup>hi</sup>, D) were enumerated in spleen. In both subsets of P1A-specific CTLs, CD62L<sup>hi</sup> and CD62L<sup>lo</sup>, we determined the surface expression of KLRG1, CX3CR1, CD27, CD43 and CD127 as well as the master transcription factors Tcf-1, Tbet and Eomes

(E). Total numbers of marker-expressing P1A-specific CTLs were enumerated in (F). Co-expression of CD127, KLRG1, CD27, CD43 and CX3CR1 in combinations as indicated are shown in (G). (A) shows representative FACS plots from individual mice, (G) shows combined events from 6 mice. Symbols in (B-D, F) represent individual mice, bars in (B-D, F) indicate the mean±SD. Numbers in (A,E,G) indicate the percentage of gated cells (mean±SD) or the mean fluorescence intensity (MFI±SD). Means were calculated from six mice per immunization group (A-G) or from three unimmunized controls (A). \*\* p<0.01, \* p<0.05 by unpaired two-tailed Student's *t* test.

### Supplementary figure 6



S 2-6 Dependence of artARENA-induced CTL responses on IL-33 – ST2 alarmin signaling. Related to Figure 2-4

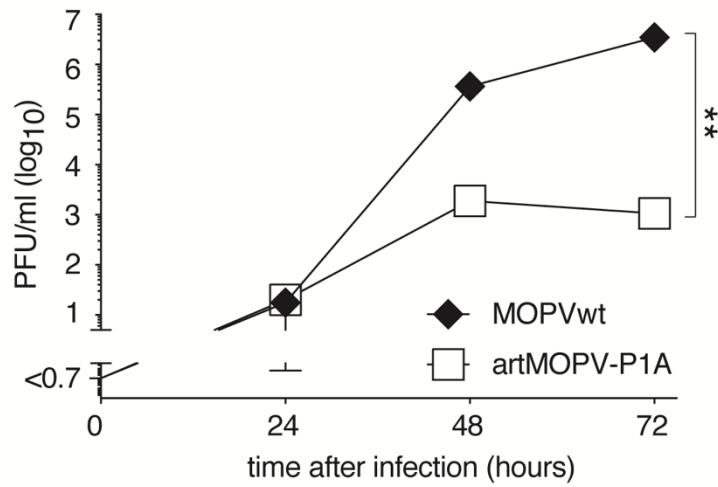
We immunized ST2<sup>-/-</sup> and wt mice on d0 with artLCMV-E7E6, artPICV-E7E6 or artCAND-E7E6 i.v. Wt controls were left unimmunized (“no vaccine”). E7<sub>49-57</sub> peptide-specific cytokine-secreting cells were determined on d9.

A: Representative FACS plots are shown.

B, C: TNF-α and IFN-γ co-producing CD8<sup>+</sup> T cells were enumerated and expressed as percentage of the total splenic CD8<sup>+</sup> T cell compartment (B) or as absolute number per spleen (C). Symbols in (B, C) represent individual mice with mean±SD. N=2.

\*\* p<0.01 by two-way ANOVA with Sidak's post-test.

### Supplementary figure 7



S 2-7 Cell culture growth curve of artMOPV-P1A. Related to Figure 2-5

We infected BHK-21 cells at MOI=0.01 with artMOPV-P1A or with MOPVwt and determined infectious titers in the supernatant at the indicated time points. Symbols represent the mean±SD of three independent cell culture wells (error bars mostly hidden within the symbol size). \*\* p<0.01 by unpaired two-tailed Student's *t* test.

## 2.11 Material and Methods

### 2.11.1 Animals and ethics statement

AGRAG mice (*IFN $\alpha$ / $\beta$ R<sup>-/-</sup>*, *IFN $\gamma$ R<sup>-/-</sup>*, *RAG1<sup>-/-</sup>* triple-deficient) (309), B cell-deficient JHT mice (310) and ST2-deficient *Il1rl1<sup>-/-</sup>* mice on C57BL/6J background have been described (59, 311) and they were bred at the Laboratory Animal Sciences Center (LASC) of the University of Zurich, Switzerland. C57BL/6J, BALB/c and DBA/2 wild-type mice were either purchased from Charles River and Janvier Labs or were bred at LASC and at the University of Geneva, Switzerland, under specific pathogen-free (SPF) conditions. TC-1 tumor therapy studies in mice were performed at Hookipa Biotech GmbH using C57BL/6N mice purchased from Charles River, Sulzfeld, Germany. These experiments were approved by the Austrian authorities and were carried out in accordance with the approved guidelines for animal experiments at Hookipa Biotech GmbH.

All other mouse experiments were performed at the Universities of Basel and Geneva in accordance with the Swiss law for animal protection. Permission was granted by the Veterinäramt Basel-Stadt and by the Direction générale de la santé, Domaine de l'expérimentation animale, of the Canton of Geneva, respectively. Animals in experimental groups were sex- and age-matched. In general, adult animals of both genders were used to reduce the number of animals bred for research purposes. P1A-specific immunogenicity assessments and P815 tumor control studies were conducted in female mice. Mice in tumor therapy experiments were assigned to groups in a manner to assure even distribution of tumor volumes between groups at the time of tumor therapy. In accordance with the Swiss law for animal protection mice exhibiting wounds on the tumor or displaying signs of distress (evident namely in lethargy, hunchback, piloerection, emaciation and agonal breathing) were immediately euthanized irrespective of tumor size and diameter. Study sample sizes in animal experiments were chosen based on experience in our labs with respect to group sizes readily revealing biologically significant differences in the experimental models used. The groups were neither randomized nor were experiments conducted in a blinded fashion.

The PICV virulence study in guinea pigs was conducted at Meditox (Czech Republic) and was approved by the Institutional Animal Care and Use Committee (IACUC) and the Committee for Animal Protection of the Ministry of Health of the Czech Republic. Dunkin Hartley guinea pigs were from Charles River, France, and weighed 370 – 520 g at the start of the study.

### 2.11.2 Cell lines

BHK-21 cells, HEK293T cells were purchased from ECACC (Clone 13, Cat #85011433), P815 mastocytoma cells (TIB-64), NIH 3T3 and BSC40 cells from ATCC. FreeStyle 293-F suspension culture cells were purchased from Invitrogen/ThermoFisher. LCMV-GP-expressing BHK-21 cells (BHK-21-GP) and 293T-GP cells have previously been described (267). All cell lines were regularly tested for mycoplasma

and were negative. Owing to their origin from renowned international repositories and vendors they were not authenticated.

### **2.11.3 Viruses, titration and neutralization test**

The titration of LCMV, PICV, MOPV and derived vectors by immunofocus assay has been described (58, 230) and was performed using NIH 3T3 cells as a substrate, CAND and derived vectors were titrated using HEK293T cells by analogous techniques. For detection of GFP-expressing artPICV and r3PICV infectivity by immunofocus assay we used rat-anti-GFP antibody (Biolegend) (58). To quantify PICV and derived vectors by immunofocus assays, monoclonal antibody (mAb) 17.2.E4-2 (312) served as primary antibody. mAb 17.1.C6-9 (312) was used for detection of CAND and mAb 2B5 (313) for MOPV. LCMV, PICV and derived vectors batches were produced on BHK-21 cells and 293F cells, MOPV and artMOPV-P1A on BHK-21, CAND and derived vectors on 293T cells.

Recombinant vaccinia viruses expressing the NP396 miniepitope or lacZ, respectively (VACC-NP396, VACC-lacZ) have been described (314, 315). They were grown and titrated on BSC40 cells.

The neutralizing capacity of immune serum was determined by immunofocus reduction assays (230).

### **2.11.4 Viral virulence testing**

Intracranial LCMV infection was administered through the skull and mice developing signs of terminal disease were euthanized in accordance with the Swiss law.

The wellbeing of guinea pigs undergoing PICV or artPICV infection was monitored twice daily during the entire study and clinically scored. Moribund animals were sacrificed. Humane endpoints were hypothermia (body temperature  $<35^{\circ}\text{C}$ , determined at two independent monitoring time points) and/or body weight loss  $\geq 20\%$ .

### **2.11.5 Tumor implantation and tumor measurement**

P815 cells ( $10^6$  per mouse) were implanted subcutaneously in the right flank. Tumor growth was assessed three times per week. The longest and the shortest diameter were determined using a caliper. Tumor volumes ( $\text{mm}^3$ ) were calculated as  $\frac{1}{2} (\text{length} \times \text{width}^2)$ . When tumor volumes exceeded  $1500 \text{ mm}^3$  or when the longest median tumor diameter exceeded 20 mm, mice were euthanized in accordance with the Swiss law.

TC-1 cells expressing HPV 16 E6 and E7 (316) were obtained from Johns Hopkins University. For tumor implantation,  $10^5$  cells were injected subcutaneously into the flank of C57BL/6 mice and, in accordance with the Austrian law, the experiment was terminated when tumor sizes exceeded 20 mm in any dimension.



### 2.11.6 Virus engineering, infection and immunization

The reverse genetic engineering of LCMVwt, r3LCMV and artLCMV vectors using a polymerase I- / polymerase II-based plasmid system has been described (48). PICV-based, CAND-based and MOPV-based vectors and the corresponding cDNA-derived wt viruses were generated using analogous expression cassettes and transfection procedures using BHK-21-GP cells as a cell substrate. In brief, we transfected  $5 \times 10^5$  cells, seeded the day before into an M6 cell culture well, with 0.8  $\mu\text{g}$  of each pol-I-driven S segment expression plasmid, 1  $\mu\text{g}$  of pol-I-driven L segment, 1.4  $\mu\text{g}$  of pol-II-driven L ORF expression plasmid and 0.8  $\mu\text{g}$  of pol-II-driven NP expression plasmid using 12  $\mu\text{l}$  Lipofectamine 2000. Six hours after transfection for the rescue of CAND and derived vectors,  $10^5$  293T-GP cells were added to each well. 72 hours after transfection, the cells were trypsinized and transferred to a T75 tissue culture flask. Virus- and vector-containing supernatants, respectively, were harvested 6-10 days after transfection. Wildtype CAND virus serving as a template for vector generation was generously provided by R. Charrel, Marseille, France. Its sequence was determined by RT-PCR Sanger sequencing and was identical to Genbank accession numbers HQ126698 and HQ126699. Genbank accession numbers EF529747.1 and EF529746.1 of the guinea pig-virulent PICV strain p18 (317) were used for vector generation. Silent point mutations were designed into ORFs to delete BsmBI, BbsI and BamHI restriction sites, enabling molecular cloning strategies for transgene insertion as described (318). cDNAs encoding for the L and NP ORFs as well as for the full-length L and S segments of CAND and PICV were synthesized by Genscript, The Netherlands, and were ligated into polymerase-II- and polymerase-I-driven expression cassettes, respectively (48). MOPV cDNAs for virus and vector rescue (Genbank accession numbers JN561685.1 and JN561684.1) were generated by RT-PCR cloning (L and wt S segment, NP and L ORFs) and by gene synthesis (transgenic S segments of vectors). cDNAs of the full-length cancer-testis antigen P1A (comprising the immunodominant LPYLGWLVF epitope), a non-oncogenic fusion protein consisting of the complete HPV16 E7 and E6 sequences (comprising the immunodominant epitope RAHYNIVTF) (277), GFP or Tomato (TOM), were used for insertion into the respective vectors and viruses using a seamless cloning strategy previously described in detail (318).

Infections and immunizations of mice with arenaviruses and arenavirus-based vectors were performed at a dose of  $10^5$  PFU i.v. unless specified otherwise. Vaccinia virus vectors were given at an intravenous dose of  $2 \times 10^6$  PFU.

### 2.11.7 Assessment of blood-brain-barrier integrity

Blood-brain-barrier leakage was assessed by detecting IgG deposits in mouse brain parenchyma. Cryosections of  $10 \mu\text{m}$  were fixed with 4% PFA for 15 min, endogenous peroxidases were inactivated and tissue sections were incubated with HRP-labelled-anti-mouse-IgG (Dako, K4001). Bound peroxidase polymers were visualized using polymerized 3,3'-diaminobenzidine (DAB, Dako, K5001).



The stained sections were scanned using a Panoramic Digital Slide Scanner 250 Flash II at 200x magnification. Quantifications were performed on scanned slides applying a custom-programmed script to detect the DAB<sup>+</sup> area in Cognition Network Language (Definiens Developer D software). For representative images, white balance was adjusted and contrast was linearly enhanced using the tools “levels”, “curves”, “brightness” and “contrast” in Photoshop CS6 (Adobe).

### **2.11.8 Virus sequencing and genealogy tree building**

Viral RNA was extracted from cell culture supernatant and from serum of infected mice using the QIAamp Viral RNA Mini Kit (QIAGEN, Cat No. 52906). RNA from spleens of mice was extracted using Tri Reagent (Sigma Aldrich). Reverse-transcription PCR was performed with the One Step RT-PCR kit (Qiagen) and gene-specific primers. Amplified products were gel-purified for Sanger sequencing (Microsynth).

A mammarenavirus genealogy tree was built based on S segment sequences of the following viruses and Genbank accession numbers: Allpahuayo virus (AY081210.1), Amapari virus (AF485256.1), Junin virus (AY358023), Bear Canyon virus (AY924391), Sabia virus (U41071), Pichinde virus (K02734), Chapare virus (EU260463), Cupixi virus (AF512832), Flexal virus (AF512831), Gairo virus (KJ855308), Guanarito virus (AY129247), Ippy virus (DQ328877), Lassa virus (AF181854.1), Latino virus (AF512830), Loei River virus (KC669698), Lujo virus (FJ952384), Luna virus (AB586644), Lunk virus (AB693150), Machupo virus (AY129248), Mariental virus (KM272987), Merino Walk virus (GU078660), Mobala virus (AY342390), Mopeia virus (AY772170), Okahandja virus (KM272988), Oliveros virus (U34248), Parana virus (AF485261), Pirital virus (AF485262), Ryukyu virus (KM020191), Solwezi virus (AB972428), Souris virus (KP050227), Tacaribe virus (M20304), Tamiami virus (AF485263), Wenzhou virus (KJ909794), Whitewater Arroyo virus (AF228063). To build the phylogenetic tree, we used the software package BEAST2 (319) with a TN93 site model (the corresponding .xml -file will be deposited for further reference). The MCMC chain ran for 10<sup>7</sup>000<sup>7</sup>000 steps. All ESS were well above the critical threshold. The maximum credibility tree was constructed with TreeAnnotator and the phylogeny displayed with FigTree v1.4.4 (320).

### **2.11.9 Flow cytometry**

Antibodies against CD8 (53-6.7 or Ly-3.2), CD45R/B220 (RA3-6B2), Klrg1 (2F1), CD127 (A7R34), CX3CR1 (SA011F11), CD27 (LG3A10), CD43 (1B11), GrzB (GB12), Ki67 (solA15), IFN- $\gamma$  (XMG1.2), TNF (MP6-XT22), IL-2 (JES6-5H4) CD11b (M1/70) CD11c (HL3) CD19(1D3) Nkp46 (29A1.4) and CD4 (RM4-5) were from Biolegend, BD Biosciences/Pharmingen and eBioscience/ThermoFisher. To assess intracellular levels of the transcription factor Tcf1, primary antibody binding (C63D8, Cell Signaling) was detected using donkey anti-rabbit IgG PE (Poly4064-eBioscience). Eomes (Dan11mag) and T-bet (4B10) were detected using the eBioscience<sup>TM</sup> FOXP3 transcription factor staining kit (Invitrogen).

Dead cells were excluded with Zombie UV Fixable Viability Kit (Biolegend, Cat. #423108). P1A epitope- (LPYLGWLVF), B8R epitope- (TSYKFESV) and NP396 epitope- (FQPQNGQFI) specific CTLs were identified by peptide-MHC class I tetramers after gating on CD8+B220<sup>+</sup> lymphocytes. The H-2Db tetramer loaded with the NP396 epitope and conjugated to PE was obtained through the NIH Tetramer Core Facility, the H-2Ld tetramer loaded with the P1A epitope and conjugated to PE as well as the H-2Kb tetramer loaded with the B8R epitope and conjugated to PE were purchased from the University of Lausanne Tetramer core facility. For tumor-infiltrating CTL analyses, cells expressing CD11b, CD11c, CD19 or NKp46 were excluded. For detection of E7- (RAHYNIVTF epitope) and NP118- (RPQASGVYM epitope) specific CTLs the corresponding dextramers (Immudex) were used analogously (for simplicity referred to as “tetramer” in the text). Splenic single-cell suspensions were prepared by mechanical disruption and were counted using the respective single-use chambers in a Immunospot S6 device (C.T.L.). Total numbers of peptide-MHC tetramer-binding CTLs were back calculated. Cytokine profiles after restimulation with overlapping peptide sets spanning the E7 and E6 proteins of HPV16, respectively (JPT) were determined in intracellular cytokine assays as previously described (59). Samples were measured on BD LSRIIFortessa flow cytometers and were analyzed using FlowJo software (Becton Dickinson).

For TIL analysis, tumors were dissected and digested with accutase (Sigma Aldrich), Collagenase IV (Worthington), Hyaluronidase (Sigma Aldrich) and DNaseI (Sigma Aldrich) for 60 min at 37°C, followed by red blood cell lysis. Single cell suspensions were filtered using a cell strainer (70 µM).

### 2.11.10 Statistical testing

For statistical analysis, GraphPad Prism software (Version 9.0, GraphPad Software) was used unless stated otherwise. Differences between two groups were generally assessed using unpaired two-tailed Student's *t* tests. To compare one group against multiple other groups we used one-way Analysis Of Variance (ANOVA), followed by Dunnett's *post hoc* test (Fig. 7G-J). Two-way ANOVA with Sidak's post-test was used to compare multiple cytokine-producing T cell subpopulations of two groups.

Tumor volume curves were compared as described (321). In brief, the area under the curve (AUC) for each individual animal was calculated using GraphPad Prism software and groups were compared pair-wise by two-tailed Mann-Whitney tests. To calculate AUCs for all groups and animals throughout the 41d and 60d periods in Figs. 7A and 7B, respectively, animals reaching humane endpoints of tumor volume were assigned either the maximally permitted tumor volume (1500 mm<sup>3</sup>, termination criterion for Fig. 7A) or the maximally reached tumor (2815 mm<sup>3</sup> for Fig. 7B) for time points after sacrifice. For comparison of long-term survival rates chi-square tests were performed using the GraphPad QuickCalcs online tool.

*P* values of  $p < 0.05$  were considered significant (\*),  $p < 0.01$  (\*\*) as highly significant.

### **3. Alarmins and type I interferon synergistically potentiate antiviral CD8 T cell responses by promoting stemness**

Anna-Friederike Marx<sup>1</sup>, Sandra M. Kallert<sup>1</sup>, Weldy V. Bonilla<sup>1</sup>, Patricia Aparicio-Domingo<sup>2</sup>, Tobias M. Brunner<sup>3</sup>, Min Lu<sup>1</sup>, Florian Geier<sup>4</sup>, Leo Scarpellino<sup>2</sup>, Melanie Charmoy<sup>6</sup>, Karsten Stauffer<sup>1</sup>, Florian Kreppel<sup>5</sup>, Werner Held<sup>6</sup>, Max Löhning<sup>3</sup>, Sanjiv A. Luther<sup>2</sup> and Daniel D. Pinschewer<sup>1‡</sup>

<sup>1</sup> Department of Biomedicine, Division of Experimental Virology, University of Basel, Basel, Switzerland

<sup>2</sup> Department of Biochemistry, University of Lausanne, Epalinges, Switzerland

<sup>3</sup> Experimental Immunology, Department of Rheumatology and Clinical Immunology, Charité-Universitätsmedizin Berlin, 10117, Berlin, Germany

<sup>4</sup> Department of Biomedicine, Bioinformatics Core Facility, University Hospital Basel, 4031 Basel, Switzerland

<sup>5</sup> Witten/Herdecke University (UW/H), Faculty of Health/School of Medicine, Stockumer Str. 10, Witten, 58453, Germany

<sup>6</sup> Department of Oncology UNIL CHUV, University of Lausanne, 1066 Epalinges, Switzerland

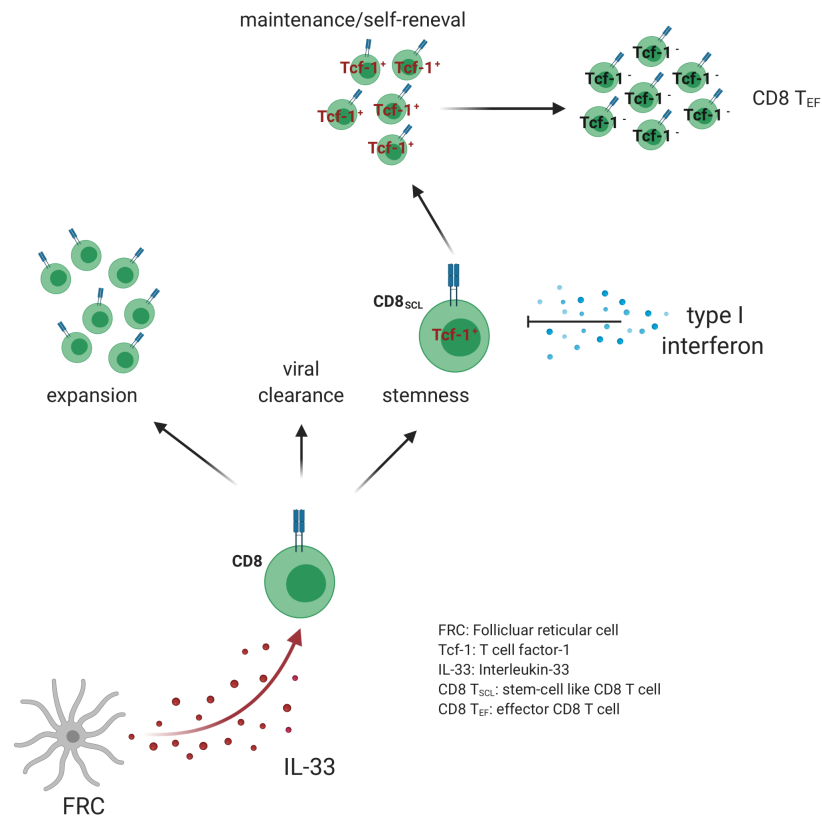
‡ Corresponding author and lead contact:

Daniel D. Pinschewer, M.D.

Email: Daniel.Pinschewer@unibas.ch

Phone: +41-79-543 39 70

**Keywords:** IL-33, antiviral stem-like CD8 T cells, chronic viral infection, type I interferon



Graphical abstract 3-1 Alarmins and type I interferon synergistically potentiate antiviral CD8 T cell responses by promoting stemness

(Generated with biorender.com)

### 3.1 Abstract

T-cell factor 1 (Tcf-1) expressing CD8 T cells with stem-like self-renewing capacity (CD8 T<sub>SCL</sub>) are pivotal for sustained immune defense against chronic viral infection and cancer. Accordingly, CD8 T<sub>SCL</sub> are crucial for the maintenance of the viral-specific CD8 T cell pool as well as their effector functions. Thus, strategies which can augment the pool of CD8 T<sub>SCL</sub> are urgently needed. So far, only type I interferon (IFN-I) blockade has been described to enhance the expansion as well as maintenance of CD8 T<sub>SCL</sub> cells. Given the pleiotropic effects associated with IFN-I blockade, a deeper and more precise molecular understanding is lacking.

The alarmin IL-33 has been identified as an important factor driving the expansion of antiviral CD8 T cells. In this work, we show that in a mouse model of chronic viral infection, antigen specific CD8 T cells missing the IL-33 receptor showed impaired differentiation into CD8 T<sub>SCL</sub>. Additionally, transfer of CD8 T<sub>SCL</sub> cells into IL-33<sup>-/-</sup> recipients clearly showed that IL-33 is crucial for CD8 T<sub>SCL</sub> to retain their proliferative potential, undergo self-renewal and generate effector cells (CD8 T<sub>EF</sub>). Overall, we were able to show that IL-33 is critical to augment and sustain the proliferation of Tcf-1 expressing cells during chronic antigen stimulation, by counterbalancing the suppressive effect of IFN-I stimuli on CD8 T<sub>SCL</sub>.

### 3.2 Introduction

The generation of a potent and sustainable CD8 T cell response during persistent viral infection is a cornerstone requirement to hasten viral clearance and confer long-lasting protective immunity. Upon a viral infection, the activation of virus specific CD8 T cells needs antigenic signals which are then balanced with the surrounding cytokine milieu (127, 130, 322). Specifically, a delicate equilibrium exists between anti- and pro-inflammatory cytokines which can tilt an efficient CD8 T cell response. As such, defining the constituent cytokines that influence the developmental choices of antiviral antigen specific CD8 T cells is fundamental for the generation and characterization of therapeutic approaches. Infection of mice with Lymphocytic choriomeningitis (LCMV) is one of the best studied model systems of viral infection that shares many common immunological features with persistent human infections (323, 324).

In 2016, a series of publications have reported on a novel subset of CD8 T cells present in chronic LCMV infection that are characterized by having self-renewing capacity and a central memory T cell phenotype, thus being sometimes referred as stem-like CD8 T cells (CD8 T<sub>SCL</sub>) (120, 121, 325). These CD8 T<sub>SCL</sub> were subsequently found in most settings of chronic inflammation such as persistent viral infection or cancer in both mice and humans, hinting at their important role in these conditions (117, 120, 121, 124, 325-329). A defining feature of CD8 T<sub>SCL</sub> is the transcription Tcf-1 (encoded by the *Tcf7* gene), a downstream transcription factor of the canonical Wnt signaling pathways, which is crucial for their self-renewal capacity. Tcf-1 is expressed by all non-activated T cells as well as the majority of memory T cells present after resolved infection (330). Their pluripotency allows for long-term self-renewal as well as for providing a regenerative pool that can terminally differentiate into effector cells upon loss of Tcf-1 expression and upregulation of CX3CR1 expression (99, 331). Importantly, several studies have highlighted that the proliferative potential of CD8 T cells resides in the Tcf-1 expressing CD8 T cell population (120, 121, 325, 326).

The transcriptional (120, 121) and epigenetic programs (122) of CD8 T<sub>SCL</sub> diverge from their terminally differentiated counterparts already on day 5 of chronic LCMV infection suggesting an early bifurcation of these population (116). However, the molecular pathways that assure the maintenance of CD8 T<sub>SCL</sub> are still not fully understood. Despite the extensive description of transcription factors regulating Tcf-1 expression (117-119), the upstream cytokine milieu that leads to the expansion and sustenance of Tcf-1 expressing CD8 T cells is yet to be described. Currently, only IFNAR blockade (117) has been shown to augment the pool of CD8 T<sub>SCL</sub> in chronic viral infection in an IL-27 dependent manner (332). However, the highly inherent viral infectious risks of depleting I-IFN in humans makes such an approach unviable for therapeutic purposes (189). Moreover, from a practical perspective, type I interferon is reaching the maximum level 24h after virus inoculum (174, 186), an event that commonly goes unnoticed. Therefore, strategies in counterbalancing the IFN-I effects on Tcf-1 expression are urgently needed and pathways leading to the generation of CD8 T<sub>SCL</sub> must be defined.

The alarmin IL-33, a member of the IL-1 family (131), has been identified as an essential driver of antiviral CD8 T cell responses to several RNA and DNA viruses (59, 258, 333). IL-33 is signaling through its receptor

named ST2 (131, 334). In the past years, we and others were able to highlight the importance of IL-33 to i) trigger the expansion, cytotoxicity and cytokine production of CD8 T cells and ii) to augment vaccination-induced CD8 T cell responses by exogenous administration (58, 59).

Recently, it was reported that the efficiency of immunotherapy arenavirus-based vectors in CD8 T cell mediated cancer immunotherapy correlates with the infection of IL-33 expressing lymphoid stromal cells, thus suggesting a dependency on the IL-33 signaling (58). In lymph nodes, the fibroblastic reticular cells (FRC) were identified as the major producers of IL-33 upon LCMV infection (58, 335). Further studies reported that IL-33 co-delivered in DNA vaccines or triggered by viral vectors can be considered as a promising immunoadjuvant at improving antiviral as well as tumor T cell immunity (58, 164-167).

Besides the effect of IL-33 in augmenting CD8 T cell responses during acute infection, the absence of IL-33 in chronic viral infection results in an impaired CD8 T cell expansion combined with defective viral control, through a poorly defined mechanism (59, 335).

Transcriptome analysis of ST2-deficient CD8 T cells showed that genes used to distinguish Tcf-1 expressing self-renewal T cells from their Tcf-1 non expressing counterparts (116), were significantly downregulated. Based on these results, we uncovered a role of IL-33 signaling in promoting the differentiation of CD8 T cells towards the CD8 T<sub>SCL</sub> phenotype. Upon transfer into naïve congenic recipients, followed by secondary challenge with LCMV, IL-33 sustained the pool of transferred CD8 T<sub>SCL</sub>. Moreover, we found that IL-33 signaling is counterbalancing IFN-I to maintain CD8 T cell stemness.

These findings highlight the ability of IL-33 to promote and improve the stemness of CD8 T<sub>SCL</sub> during chronic antigen stimulation which can have broader implications for immunotherapy of persistent infections.

### 3.3 Material and Methods

#### 3.3.1 Mice and animal experimentation

All mouse experiments were performed at the University of Basel or at the University of Lausanne in accordance with the SWISS law for animal protection. Animals in experiments were between 6-20 weeks old and sex-matched. Animals were bred at the Laboratory Animal Science Center (LACS) of the University of Zürich, at the ETH Phenomics Center (EPIC) at the ETH or at Animal Facility Bio Park 1060 at the University of Basel.

ST2-deficient *I11rl1*<sup>-/-</sup> (59, 311), *IL-33*<sup>-/-</sup> mice (336) (obtained through the RIKEN Center for Developmental Biology-Acc. No: CDB0631K), *IFNAR*<sup>-/-</sup> (179), *Tcf*<sup>EGFP</sup> mice (120) (provided by Prof. Dr. Werner Held), P14 TCR transgenic mice (183), *CCL19 Cre* (337), *IFNAR* fl/fl (338) (provided by Prof. Dr. Ulrich Kalinke) and *IL-33* fl/fl (339) mice have been described. P14 *ST2*<sup>-/-</sup>, P14 *IFNAR*<sup>-/-</sup>, *CCL19 Cre IFNAR* fl/fl and *CCL19 Cre IL-33* fl/fl mice were obtained by intercrossing with the respective parental lines. *C57BL/6J* (Wt) mice were bred at the at the Laboratory Animal Science Center (LACS) of the University of Zürich or

at the ETH Phenomics Center (EPIC) at the ETH. Mice that were used as donors were backcrossed to C57BL/6J mice. C57BL/6J background of ST2<sup>-/-</sup> mice was confirmed by SNIP typing (Taconic Biosciences).

### 3.3.2 Viruses, virus titrations, infections and immunizations

LCMV Cl-13 (34) was produced by infecting BHK-21 cells at a multiplicity of infection (MOI) of 0.01. The supernatant was harvested 48h later and viral titers were determined by focus forming assay on 3T3 cells as described (59, 230).

Mice were infected with  $2 \times 10^6$ - $1 \times 10^7$  PFU of LCMV Cl-13 intravenously (i.v.).

LCMV strain Armstrong expressing the LCMV strain WE glycoprotein (rArm-WEGP) was engineered as described (48).

The Ad vector described here is an Ad5-based E1 deleted first generation vector. The vector was generated by transfection of the corresponding infectious plasmids into the E1-transcomplementing 293 cell line followed by subsequent vector amplification with increasing cell numbers. The two transgenes (LCMV-WE glycoprotein (full length) and a green fluorescent protein (GFP)) were expressed under the cytomegalovirus (CMV) promoter that replaced the E1 gene of Ad5. The vector was purified by double discontinuous CsCl density gradient centrifugation and the physical titer was determined by OD260.

For measuring viremia of mice, 1 blood drop was collected in 950  $\mu$ l of BSS-heparin (Na-heparin, Braun, 1 IE/ml final), mixed and stored at -80°C before further measurements.

### 3.3.3 Flow cytometry and intracellular staining for transcription factors

Single-cell suspensions of spleens were prepared by mechanical disruption using metal mesh. Surface staining was performed at 4°C in the dark for 30 mins. All staining's were done in FACS buffer (FACS buffer (PBS, 2% FCS, 5mM EDTA, 0.05% sodium azide).

For the detection of GP33 specific CD8 T cells, peptide MHC Class I tetramers (H-2D<sup>b</sup> tetramers loaded with the LCMV GP<sub>33-41</sub> peptide-KAVYNFATM) obtained from the NIH-Core Facility or the University of Lausanne Tetramer core facility were used. Unspecific binding was excluded by pre-gating on B220<sup>-</sup> CD4<sup>-</sup> CD8<sup>+</sup> cells. Tetramer staining was performed at RT for 30 mins in the dark.

Antibodies against CD8 (53-6.7), CD4 (IM7 or RM4-5), B220 (RA3-6B2), CD45.1 (A20), CD45.2 (104), Ter-119 (TER-119; dilution: 1:10), GP38-Podoplanin (8.1.1; dilution: 1:250), CD31 (390), Ly108 (330-AJ), CD62L (MEL-14), CX3CR1 (SA01F11), PD-1 (29F.1A12) and Tim-3 (5D12) were obtained from Biolegend, eBioscience/ThermoFisher or BDBioscience/PharMingen. All fluorescently labelled monoclonal antibodies were, if not otherwise indicated, diluted 1:100.

Dead cells were excluded with either 7-AAD or Zombie UV Fixable Viability Kit (Biolegend) according to manufactures instructions.



In case of staining of peripheral blood cells, samples were fixed and lysed by adding 1 ml/sample of eBioscience 1-step Fix/Lyse Solution and incubated at RT for 5min. Afterwards, the reaction was stopped by adding FACS-buffer.

To detect intracellular levels of the transcription factors Eomes (Dan11mag), T-bet (4B10) or Tox (TXRX10), we followed the protocol from eBioscience™ FOXP3 transcription factor staining kit (Invitrogen). The transcription factor Tcf-1 was detected by incubating first with a primary antibody (C63D8, Cell Signaling, dilution:1: 200) followed by adding a donkey anti-rabbit IgG PE (Poly4064-eBioscience).

For the detection of ST2 on splenocytes, cells were stained with digoxigenin-coupled anti-mouse ST2 antibody (DJ8). As a secondary antibody, a PE-coupled anti-digoxigenin Fab (Roche) antibody was used. To further amplify the signal, two rounds of amplification using the PE-FASER Kit (Miltenyi Biotec) were performed.

To isolate stroma cells from spleens, the organs were cut into small pieces and incubated in RPMI (2% vol/vol FCS; containing 1mg/ml Collagenase IV (Worthington) and 40 µg/ml DNaseI (Roche)) for 30 minutes at 37°C stirring at a speed of 250 rpm. To stop the enzymatic reaction, FACS buffer was added. Erythrocytes were lysed by adding 1ml/spleen of ACK Lysis Buffer (0.15 M NH<sub>4</sub>Cl, 10mM KHCO<sub>3</sub>, 0.1 mM EDTA), the reaction (RT) was stopped after 60 sec by adding FACS buffer. Hematopoietic CD45<sup>+</sup> cells were depleted by using anti-CD45 beads (Miltenyi Biotec).

For analysis of stroma cells, erythrocytes (Ter119<sup>+</sup>) and hematopoietic cells (CD45<sup>+</sup>) were excluded. To distinguish between fibroblastic reticular cells (FRC) and blood endothelial cells (BEC), we used the endothelial marker CD31 and the fibroblast marker gp38 (Podoplanin) (see Figure S 3-5).

Samples were measured on BDLSRFortessa flow cytometer. FlowJo Software (Becton Dickinson) was used for analysis.

### 3.3.4 Next generation RNA sequencing and bioinformatic data analyses

For RNA-seq of co-transferred P14 Wt and P14 ST2<sup>-/-</sup> CD8 T cells, 1x10<sup>3</sup> MACS-purified P14 Wt and 3x10<sup>3</sup> MACS-purified P14 ST2<sup>-/-</sup> CD8 T cells were co-transferred (see Fig. S 3-2). Such an experimental set-up allowed an equalized number of both CD8 T cell subsets at day 6 p.i.. Cells were sorted on FASCARIA II (Becton Dickinson). Cells were directly sorted into Trizol LS (Sigma-Aldrich) and stored by -80°C until RNA-extraction. RNA was extracted using the Direct-zol™ RNA MicroPrep kit (Zymo research).

RNA quality was checked on the Bioanalyzer instrument (Agilent Technologies, Santa Clara, CA, USA) using the RNA 6000 Pico Chip (Agilent, Cat# 5067-1513) - Average RIN (RNA Integrity Number) was quantified by Fluorometry using the QuantiFluor RNA System (Cat# E3310, Promega, Madison, WI, USA). Library preparation was performed, starting from 35ng total RNA, using the TruSeq Stranded mRNA Library Kit (Cat# 20020595, Illumina, San Diego, CA, USA) and the TruSeq RNA UD Indexes (Cat# 20022371, Illumina, San Diego, CA, USA). 15 cycles of PCR were performed.



Libraries were quality-checked on the Fragment Analyzer (Advanced Analytical, Ames, IA, USA) using the Standard Sensitivity NGS Fragment Analysis Kit (Cat# DNF-473, Advanced Analytical) revealing excellent quality of libraries (average concentration was  $63 \pm 12$  nmol/L and average library size was  $317 \pm 4$  base pairs).

Samples were pooled to equal molarity. The pool was quantified by Fluorometry using the QuantiFluor ONE dsDNA System (Cat# E4871, Promega, Madison, WI, USA). Libraries were sequenced Single-reads 76 bases (in addition: 8 bases for index 1 and 8 bases for index 2) using the NextSeq 500 High Output Kit 75-cycles (Illumina, Cat# FC-404-1005) loaded at 2.0pM, and including 1% PhiX.

Primary data analysis was performed with the Illumina RTA version 2.11.13. The NextSeq run yielded on average per sample:  $19.7 \pm 1.6$  millions pass-filter reads.

Reads were aligned to the mouse genome (UCSC version mm10) with STAR (version 2.7.0c) using the multi-map settings '-outFilterMultimapNmax 10 --outSAMmultNmax 1'. Mapped reads were assigned to genes based on the ensembl gene annotation (version 96) using the function featureCounts (Subread package, version 1.6.4) and extra options '-O --read2pos 5 -M -s 2 -p -B'. Only genes with biotypes "protein coding", "long non-coding" or "short non coding" were considered in the analysis. Additionally, only genes with a  $\log\text{CPM} > 1$  in at least 5 samples were retained resulting in  $n=11032$  detected genes. Differential gene expression analysis between the genotypes relied on functions from the R/Bioconductor package edgeR. Specifically, function 'estimateDisp' was used for estimating gene-wise dispersions, and functions 'glmQLFit' and 'glmQLFTest' were used for testing the contrast of interest. Differential regulation of all hallmark gene sets from MSigDB (version 7.0) was evaluated using the function 'camera' from edgeR with extra options 'inter.gene.cor = 0.01'. The average absolute log fold change of a gene set was used as a proxy for its strength of regulation. Specific gene sets published in (116) were tested using the function 'cameraPR' with using the logFC as a ranking statistic (see Fig. 3-1-L). The ComplexHeatmap package was used to draw heatmaps (340).

### 3.3.5 Adoptive cell transfer and FACS sorting

For adoptive cell transfer, donor P14 CD8 T cells were MACS (Miltenyi Biotec naïve CD8 T cell isolation kit, mouse) purified and administered i.v. For co-transfers, equal numbers of both cell populations were transferred. For analysis on day 4 p.i.  $10^4$  cells were injected, for analysis on day 6 mice received  $10^3$  cells of each population. For analysis from day 9 onwards, mice received 500 cells to stay in the physiological range of the precursor frequency of gp-33<sup>+</sup> specific CD8 T cells (341). To avoid rejection of transferred cells, donor T cells from male or female were transferred into male recipients. The two transferred populations could be differentiated from each other and from the recipient's CD8 T cells by means of their congenic CD45 markers.

For adoptive transfer experiments,  $1 \times 10^6$  P14 Tcf7<sup>gfp</sup> and P14 ST2<sup>-/-</sup> Tcf7<sup>gfp</sup> were separately transferred into Wt mice followed by LCMV CI-13 infection. 4 days later, transferred cells were sorted on FASCARIA II (Becton Dickinson) in Lymphocytic medium (RPMI, 10 % FCS, 1% P/S).

Equal numbers of cells ( $\sim 1 \times 10^3$  -  $1 \times 10^4$ ) were re-transferred into Wt mice. Secondary recipients were either infected the same day with LCMV CI-13 or 14 days later with rAd/GP (see Fig. 3-5).

### 3.3.6 *In vivo* antibody blockade

Mice were depleted of type I interferon by intraperitoneal (i.p.) injection of 1 mg of  $\alpha$ -IFNAR (MAR-1-5A3, BioXcell) one day before infection. Control groups were treated with 1 mg of isotype control (MOPC-21, BioXcell) one day before infection.

For transfer of P14 IFNAR<sup>-/-</sup> as well as P14 ST2<sup>-/-</sup> IFNAR<sup>-/-</sup>, NK cells were depleted as described in (342). Depletion was performed by i.p. injection of 300  $\mu$ g of  $\alpha$ -NK.1.1 (clone PK136, BioXcell) 1 day before and 1 day after infection.

### 3.3.7 *In vitro* activation of P14 Wt cells with or without IL-33

These data correspond to Fig. 3-2 C. The data were generated by Tobias Brunner.

Naive CD62L<sup>+</sup> CD44<sup>-</sup> CD8<sup>+</sup> T cells were flow cytometrically sorted from spleens of LCMV-TCR<sup>tg</sup> P14 mice and cultured with a 4-fold excess of irradiated (3000 Gy) Tcr $\beta\delta$ <sup>-/-</sup> splenocytes in RPMI1640 + GlutaMax I (Thermo Scientific) culture medium supplemented with fetal calf serum (10% v/v, Thermo Scientific), penicillin (100 U/ml, Thermo Scientific), streptomycin (100  $\mu$ g/ml, Thermo Scientific), gentamycin (10  $\mu$ g/ml, Thermo Scientific), and  $\beta$ -mercaptoethanol (50 ng/ml, Sigma-Aldrich). For activation of P14 Wt cells, cognate LCMV-GP33 peptide (1  $\mu$ g/ml, KAVYNFATM, Genscript), IL-12 (5 ng/ml, Miltenyi), IL-2 (5 ng/ml, Miltenyi) and anti-IL-4 (10  $\mu$ g/ml, clone: 11B11, DRFZ) were added. T cells were split after 3 days of culture in a 1:3 ratio with fresh medium containing IL-2 (5 ng/ml). After 5 days, P14 were harvested by histopaque (1083 g/ml, Sigma-Aldrich) density centrifugation and replated for a second round of culture with fresh APCs in identical conditions. At day 10 of culture, activated P14 cells were harvested, and live cells were seeded in culture medium containing IL-2 (5 ng/ml, Miltenyi) and IL-7 (5 ng/ml, Miltenyi) without cognate peptide. After 3 days (day 13 of culture), IL-12 (5 ng/ml, Miltenyi) was added to one condition to induce IL-33 receptor expression and 16 h later (day 14 of culture), live P14 cells were harvested, replated in conditioned culture medium, and stimulated with IL-33 (10 ng/ml, R&D Systems) for 2 h or left untreated. Approximately  $5 \times 10^5$  P14 cells were lysed in RA-1 buffer (Macherey & Nagel) and immediately frozen in liquid nitrogen for storage at -80°C. Total RNA was purified using the Nucleospin RNA XS Micro kit (Macherey & Nagel) according to manufacturer's instructions, without addition of carrier RNA. For qRT-PCR analysis, up to 1  $\mu$ g of RNA was transcribed into cDNA utilizing Taqman Reverse Transcription Reagents (Applied Biosystems) according to manufacturer's instructions. cDNA was

subjected to qRT-PCR analysis using Taqman Fast Advanced Mastermix reagents (Applied Biosystems). Amplification was performed in a Quantstudio 7 device (Applied Biosystems) and Tcf7 (Assay ID: Mm00493445\_m1, Thermo Scientific) expression levels were quantified with the  $\Delta\Delta C_t$ -method by normalizing to expression of Hprt (Assay ID: Mm00446968\_m1, Thermo Scientific).

### 3.3.8 Histology

Immunofluorescence staining was performed in the group of Prof. Sanjiv Luther at the University of Lausanne. Spleens were harvested and fixed in 1 % PFA overnight. The following day, the tissue was saturated in 30 % sucrose and embedded on 100 % OCT Tissue-Tek freezing medium. Cryosections were cut (8  $\mu\text{m}$ ) and stained with an antibody specific for IL-33 (primary antibody: AF3626, R&D Systems; followed by a secondary antibody donkey-anti-goat IgG Alexa 647, ThermoFisher) and DAPI to stain DNA. Images were treated using Adobe Photoshop and quantified using Fiji software. Images were acquired with an upright Zeiss Axiovision microscope. White pulps were defined automatically using Fiji using the analyze particle function (50'000-infinity). IL-33 protein densities (signal intensities multiplied by signal-positive areas) were measured within the white pulp regions. Day 0 values were obtained from non-infected, non-treated mice. Exposure and image processing were identical for all three mouse groups.

### 3.3.9 Statistical analysis

For statistical analysis, GraphPad Prism software (Version 9.0, Graph Pad Software) was used. Differences between two groups were assessed by using an unpaired two-tailed Student's t-test. Differences between 2 cell populations within in the same host (co-transfer set-up) were assessed by using a paired two-tailed Student's t-test. For single measurement comparison of more than two groups one-way ANOVA with Tukey's or Sidak's post-test was performed. For multiple comparisons of more than one parameter between more than two groups, two-way ANOVA with either Tukey's or Sidak's post-test was used. Ns: not significant; \*:  $p < 0.05$ ; \*\*:  $p < 0.01$ .

Illustrations were created with BioRender.com

### 3.4 Results

#### 3.4.1 The expansion and fate of CD8 T cells depends on IL-33 signaling

To assess the impact of ST2 signaling on CD8 T cells responding to chronic infection we inoculated ST2<sup>-/-</sup> and C57BL/6J (Wt) control mice with LCMV CI-13 high dose (Fig. 3-1 A). On day 9 after infection, ST2<sup>-/-</sup> mice exhibited a ~10-fold reduction in splenic numbers of gp-33<sup>+</sup> specific CD8 T cells, respectively (Fig. 3-1 B), and these differences persisted in peripheral blood throughout day 28 (supplementary Fig S 3-1). As reported earlier (59, 335), impaired CD8 T cell responses manifested in prolonged viremia of ST2<sup>-/-</sup> mice (Fig. 3-1 C).

To selectively assess the CD8 T cell-intrinsic role of ST2 signaling, we performed an adoptive co-transfer with LCMV gp33-specific T cell receptor (TCR)-transgenic CD8 T cells (I83) (P14 cells) deficient or sufficient for the ST2 receptor (P14 ST2<sup>-/-</sup>; P14 Wt, Fig. 3-1 D). While P14 ST2<sup>-/-</sup> cells transiently outnumbered P14 Wt cells on day 4 after infection, P14 Wt cells were more abundant at later time points of the response (Fig. 3-1 E). These findings showed that CD8 T cell-intrinsic IL-33 signaling is essential for the response to chronic LCMV infection.

The fraction of P14 Wt cells expressing ST2 peaked around day 4-8 and remained in the 20 percent range throughout day 22 (Fig. 3-1 F). This finding parallel earlier findings from lymph nodes showing loss of IL-33 protein expression within the first week suggesting cytokine release (136).

In line with the hypothesis that IL-33 is predominantly available to T cells at the onset of the infection, P14 Wt and P14 ST2<sup>-/-</sup> cells expanded similarly when they were transferred on day 14 after LCMV CI-13 infection instead of prior to infection (Fig. 3-1 G-H). Overall, these data suggest that the bioavailability of IL-33 for antiviral CD8 T cell responses is largely confined to an early time window after infection.

To assess the impact of ST2 signals on CD8 T cell gene expression programs in chronic infection, we performed whole genome RNA sequencing on P14 Wt and P14 ST2<sup>-/-</sup> cells recovered on day 6 after LCMV infection (Fig. 3-1 I). Among the top genes most significantly down-regulated in ST2<sup>-/-</sup> deficient CD8 T cells, we found Tcf-1, Prickle1 and Kit, thus hallmark genes of the recently identified population of stem-like CD8 T cells (121) (Fig. 3-1 J). Further Gene Set Enrichment analysis showed in ST2-deficient CD8 T cells a pronounced inflammation-related hallmark gene sets such as interferon- $\alpha$  response (adj. p-value: 7.74e-14) and inflammatory response (adj. p-value: 0.03) (Fig. 3-1 K). Given that the P14 Wt and P14 ST2<sup>-/-</sup> CD8 T cells analyzed here responded to LCMV in the same recipient and thus were exposed to the same infection context (see experimental set-up in Fig. 3-1 I), these data raised the possibility that ST2 signaling attenuated IFN-I gene signatures at the level of individual CD8 T cells. Further comparison to published CD8 T cell gene expression data sets (116) showed that ST2<sup>-/-</sup> CD8 T cells significantly downregulate CD8 T<sub>SCL</sub> gene signatures (Fig. 3-1 L). In summary, the gene profile of ST2-deficient CD8 T cells at the onset of chronic LCMV infection reflected reduced stemness and an enhanced IFN-I signature.

### 3.4.2 IL-33 signaling promotes the formation of stem-like CD8 T cells

First, we studied the effects of ST2 signaling on CD8 T cell differentiation by co-transferring ST2-sufficient and -deficient P14 cells to Wt recipients and infecting them with LCMV. Six days later, ST2-deficient cells exhibited a clear reduction in the stemness-promoting transcription factor Eomes (343) as well as in the expression of PD-1 (Fig. 3-2 A). In contrast, neither the transcription factors T-bet or Tox nor the effector-like CD8 T cell marker CX3CR1 (331) seemed affected by ST2 deficiency.

To directly investigate a potential link between IL-33-ST2 signaling and Tcf-1 expression we relied on a green fluorescent Tcf7 reporter strain (Tcf7<sup>gfp</sup>) (120), which we crossed to P14 TCR transgenic mice to obtain P14 Wt Tcf7<sup>gfp</sup> mice. P14 Wt Tcf7<sup>gfp</sup> CD8 T cells were transferred to Wt recipient mice undergoing LCMV CI-13 infection to analyze whether ST2 expression correlated with Tcf-1 expression. On day 6 and even more on day 14 a higher proportion of ST2-positive than of ST2-negative P14 Wt Tcf7<sup>gfp</sup> cells reported Tcf-1 (Fig. 3-2 B). To study direct IL-33 effects on Tcf-1 expression we turned to an infection-independent culture system of peptide-stimulated P14 Wt cells. Intriguingly, the addition of exogenous IL-33 resulted in >30-fold higher Tcf-1 mRNA levels within 2 hours, highlighting that IL-33 signals promote Tcf-1 transcription independently of the infectious context (Fig. 3-2 C).

To confirm on the protein level that ST2-deficient CD8 T cells express less Tcf-1 (compare Fig. 3-1 J), we performed flow cytometry on day 4 and day 6 after LCMV CI-13 infection (Fig. 3-2 D). By day 4, the proportion of Tcf-1<sup>+</sup> P14 ST2<sup>-/-</sup> CD8 T cells was reduced 2-3-fold as compared to P14 Wt cells (Fig. 3-2 E), and by day 6, Tcf-1-expressing P14 Wt cells outnumbered Tcf-1<sup>+</sup> P14 ST2<sup>-/-</sup> cells in spleen ~10-fold (Fig. 3-2 F). These differences were also evident when analyzing the stem-like Ly108<sup>+</sup> Tcf-1<sup>+</sup> and Tcf-1<sup>+</sup> Tim-3<sup>-</sup> CD8 T cell subsets (Fig. 3-2 G-H). In a complementary experimental approach, we found that Tcf-1 reporting of P14 Wt Tcf7<sup>gfp</sup> CD8 T cells was reduced when LCMV challenge was performed in IL-33<sup>-/-</sup> hosts instead of Wt recipients (Fig. S 3-3).

Finally, we crossed P14 ST2<sup>-/-</sup> mice to Tcf7<sup>gfp</sup> reporter animals (P14 ST2<sup>-/-</sup> Tcf7<sup>gfp</sup> mice). These ST2-deficient CD8 T cells, when transferred to naïve recipients and challenged with LCMV, exhibited a lower proportion of GFP reporting cells than it was found amongst co-transferred ST2-sufficient P14 Tcf7<sup>gfp</sup> cells (Fig. 3-2 I-K). Taken together, these findings indicated that ST2 antagonized the downregulation of Tcf-1, which typically accompanies CD8 T cell terminal differentiation (344), to preserve a stem-like CD8 T cell population.

### 3.4.3 IL-33 signaling balances IFN-I effects to maintain CD8 T cell stemness

Our gene expression data had suggested that ST2 signaling attenuates IFN-I gene signatures in CD8 T cells (compare Fig. 3-1 K), which prompted us to investigate how IFN-I effects contribute to the phenotype of ST2-deficient CD8 T cells in chronic viral infection. We treated recipient mice with  $\alpha$ -IFN-I receptor ( $\alpha$ IFNAR) blocking antibody or isotype antibody (Fig. 3-3 A) (day-1), followed by adoptive co-transfer of

P14 Wt and P14 ST2<sup>-/-</sup> CD8 T cell and LCMV infection the next day (day 0). The expansion of P14 ST2<sup>-/-</sup> cells was significantly impaired in isotype-treated mice on day 6, 9 and 28 after infection, as expected (Fig. 3-3 B-C). In remarkable contrast, the population size of ST2-deficient and -sufficient P14 cells was equalized when LCMV challenge was performed in IFNAR-blocked recipients. In addition, IFNAR blockade normalized the magnitude of polyclonal gp33<sup>+</sup> specific CD8 T cell responses in ST2<sup>-/-</sup> mice (Fig. S 3-4).

Importantly, restoration of P14 ST2<sup>-/-</sup> CD8 T cell expansion by IFNAR blockade was accompanied by normal differentiation into stem-like T cell subsets (Fig. 3-3 D-F). When analyzed in isotype-treated mice on day 4 or day 6, a comparably small percentage of P14 ST2<sup>-/-</sup> cells exhibited a stem-like Tcf-1<sup>+</sup> Tim-3<sup>-</sup> phenotype (Fig. 3-3 D-E), whereas the percentage and absolute number of Tcf-1<sup>+</sup> Tim-3<sup>-</sup> progeny formed by P14 ST2<sup>-/-</sup> cells was identical to P14 Wt cells when tested in IFNAR-blocked recipients (Fig. 3-3 F). In keeping with this finding, IFNAR-blockade restored also Eomes expression by P14 ST2<sup>-/-</sup> cells (Fig. 3-3 G-H).

IFNAR blockade has a profound impact on the systemic inflammatory response to LCMV Cl-13 (229), with previously unknown effects on IL-33 bioavailability. To test a potential  $\alpha$ IFNAR effect on IL-33 expression levels, we analyzed LCMV-infected IL-33<sup>gfp/wt</sup> mice, reporting IL-33 transcription as green fluorescence, but did not observe any impact of IFNAR blockade on day 3 after infection (Fig. 3-3 I-J). In line with these results, a histological assessment of spleen tissue on day 3 after LCMV infection showed that IL-33 protein levels were unaffected by IFNAR blockade (Fig. 3-3 K and supplementary Figure S 3-3 6).

To directly address the possibility that IFN-I sensing by FRCs modulates IL-33 bioavailability, we relied on mice with an FRC-specific IFNAR deletion (CCL19<sup>Cre</sup>IFNAR<sup>fl/fl</sup> mice). As a readout for IL-33 bioavailability we adoptively co-transferred P14 Wt and P14 ST2<sup>-/-</sup> CD8 T cells and determined the cells' response to LCMV challenge. P14 Wt and P14 ST2<sup>-/-</sup> CD8 T cells expanded comparably when triggered in IL-33<sup>-/-</sup> mice, as expected. In CCL19<sup>Cre</sup>IFNAR<sup>fl/fl</sup> mice and in Wt recipients, however, P14 Wt cells were >10-fold more abundant than P14 ST2<sup>-/-</sup> CD8 T cells indicating unimpaired IL-33 bioavailability in the absence of IFNAR sensing by FRCs (Fig. 3-3 L). In contrast and in line with our previous report (335), CCL19<sup>Cre</sup>IL-33<sup>fl/fl</sup> mice lacking IL-33 selectively in FRCs annihilated the differential expansion of ST2-deficient and sufficient P14 cells, corroborating the role of FRCs as the primary source of IL-33 for antiviral CD8 T cell responses (Fig. 3-3 L). Finally, ST2 expression by IFNAR-sufficient and -deficient P14 CD8 T cells was comparable (Fig. 3-3 M), as suggested by our earlier work (168).

These several lines of evidence argued therefore, against significant IFN-I effects on IL-33 bioavailability or on ST2 receptor expression by antiviral CD8 T cells. Taken together, the present data suggested therefore, that ST2 signals to antiviral CD8 T cells promoted the cells' population expansion and stemness by balancing type I interferon effects.

### 3.4.4 IL-33 balances IFN-I effects for efficient expansion and self-renewal of early CD8 T<sub>SCL</sub> cells

IL-33 release by FRC is known to occur within the first days after LCMV infection (136) and we had observed that ST2 effects on Tcf-1 expression by CD8 T cells were evident by day 4 after infection (compare Fig. 3-1 F and Fig. 3-2 D-H), raising the possibility of an early ST2 effect on T cell stemness. First, we tested whether Tcf-1 expression early in the response differentiated already a stem-like, self-regenerative pool of antiviral CD8 T cells. For this we sorted Tcf7<sup>gfp+</sup> and Tcf7<sup>gfp-</sup> P14 Tcf7<sup>gfp</sup> CD8 T cells on day 4 after LCMV infection and re-transferred them individually yet at equal numbers into Wt recipients that were simultaneously challenged with LCMV (Fig. 3-4 A). P14 Wt Tcf7<sup>gfp+</sup> CD8 T cells underwent ~10-fold more robust expansion than P14 Wt Tcf7<sup>gfp-</sup> cells (Fig. 3-4 B) and they yielded ~20-fold more Tcf-1<sup>+</sup> Tim-3<sup>-</sup> and GFP<sup>+</sup> Ly108<sup>+</sup> progeny (Figs. 3-4 C, D). In contrast, the output in CX3CR1<sup>+</sup> GFP<sup>-</sup> effector cells were not different between the two transferred cell subsets (Fig. 3-4 E). Altogether, these observations indicated that both Tcf7<sup>gfp+</sup> and Tcf7<sup>gfp-</sup> cell subsets retained the ability to proliferate and produce effector T cells (Fig. 3-4 E). Already on day 4 after LCMV infection, however, stem-like capacity with the ability to produce further Tcf7<sup>gfp+</sup> cells resided almost exclusively in the Tcf7<sup>gfp+</sup> subset (“early stem-like CD8 T cells”).

Next, we investigated whether such early stem-like CD8 T cells remained responsive to and depended on further IL-33 signals for continued expansion. We sorted Tcf7<sup>gfp+</sup> P14 Wt T cells on day 4 after LCMV infection and transferred them into either Wt or IL-33<sup>-/-</sup> recipients, followed by immediate LCMV challenge (Fig. 3-4 F). A lack of IL-33 signal in the IL-33<sup>-/-</sup> recipients reduced the transferred cells’ overall expansion ~10-fold (Fig. 3-4 G), with a ~30-fold reduction in progeny Tcf1<sup>gfp+</sup> Ly108<sup>+</sup> stem-like CD8 T cells (Fig. 3-4 H) and similarly curtailed Tcf1<sup>-</sup> CX3CR1<sup>+</sup> effector cell yields (Fig. 3-4 I).

The IL-33 dependence of early stem-like CD8 T cells for self-renewal (Fig. 3-4 G-I) prompted us to investigate whether, analogously to naïve CD8 T cells (compare Fig. 3-3), early stem-like CD8 T cells required IL-33 to balance IFN-I signals. We sorted Tcf7<sup>gfp+</sup> P14 Wt T cells on day 4 after LCMV infection and transferred them into Wt and IL-33<sup>-/-</sup> animals, which were either IFNAR-blocked or control-treated. The cell's expansion and differentiation was analyzed 9 days later (Fig. 3-4 J). In line with the experiment in Fig. 3-4 G-I, the total population expansion and, in particular, the formation of Tcf7<sup>gfp+</sup> and Tcf7<sup>gfp+</sup> Ly108<sup>+</sup> stem-like progeny was significantly impaired when isotype control-treated hosts were IL-33-deficient. Strikingly though, these pronounced differences between IL-33-deficient and -sufficient recipients were annihilated when IFNAR was blocked. Altogether, these findings indicated that not only the formation of early stem-like Tcf1<sup>+</sup> cells were driven by IL-33 (compare Fig. 3-3) but that also these early stem-like Tcf-1<sup>+</sup> CD8 T cells depended on further IL-33 signals to balance IFN-I effects on their further clonal expansion and self-renewal.



### 3.4.5 IL-33 signals at the onset of infection impact the quality of emerging CD8 T<sub>SCL</sub> cells

We considered the possibility that IL-33 signals to antiviral CD8 T cells impact not only the cells' propensity to form Tcf-1-expressing progeny but might additionally influence stemness qualities of the resulting Tcf-1<sup>+</sup> cells. P14 Wt cells expanded ~10-fold more than P14 ST2<sup>-/-</sup> cells when triggered by recombinant LCMV Arm expressing WE-GP (rArmWEGP), whereas responses to a recombinant adenovirus vector expressing the LCMV glycoprotein (rAd/GP) were ST2-independent (Fig. 3-5 A-B), as expected (58, 59). This feature of rAd immunization allowed us to compare the self-renewal and re-expansion capacity early Tcf-1<sup>+</sup> stem-like CD8 T cells without confounding effects of IL-33 signaling during recall. To this end, we relied on an established experimental approach for determining T cell stemness (345) and adapted it for use with rAd/GP. We sorted Tcf7<sup>gfp+</sup> and Tcf7<sup>gfp-</sup> P14 Wt cells on day 4 after LCMV infection and transferred them into Wt recipients (Fig. 3-5 C). Upon two weeks of resting, the cells were challenged with rAd-GP to determine P14 CD8 T cell expansion 7 days later. Approximately 30-fold more progeny from Tcf7<sup>gfp+</sup> than from Tcf7<sup>gfp-</sup> P14 Wt cells (Fig. 3-5 D, E) corroborated our conclusion that Tcf7<sup>gfp</sup> reporting on day 4 after LCMV infection identified early stem-like CD8 T cells (compare Fig. 3-4 B). Moreover, it validated the rAd/GP-based experimental design.

Next, we set out to compare the stemness of ST2-deficient and -sufficient early Tcf1<sup>+</sup> stem-like CD8 T cells. On day 4 after LCMV infection we sorted the P14 Wt Tcf7<sup>gfp+</sup> and P14 ST2<sup>-/-</sup> Tcf7<sup>gfp+</sup> cells and re-transferred them into naïve Wt recipients (Fig. 3-5 H). After two weeks of resting, the animals were challenged with rAd/GP and P14 cell expansion was monitored. Intriguingly, the progeny of Tcf7<sup>gfp+</sup> P14 Wt cells were ~10-fold more abundant than their ST2-deficient counterpart (Fig. 3-5 I, J). Moreover, a clear reduction in the number of GFP<sup>+</sup> cells was observed when ST2 deficient CD8 T cells were used (Fig. 3-5 K-L). This indicated that IL-33 signals transmitted in the first four days of LCMV infection influenced not only the number of emerging early stem-like CD8 T cells but exerted also a profound impact on the cells' stemness beyond their mere expression of Tcf-1.



### 3.5 Discussion

Although many studies have characterized the transcription factors (117-119) guiding or repressing (326, 346-348), the differentiation of CD8 T cells into CD8 T<sub>SCL</sub>, a profound understanding of the molecular signals is still incomplete. Currently, recombinant IL-27 treatment (332) and IFNAR blockade (117) remain the only available strategies to foster the pool of stem-like CD8 T cells. Thus, an alternate safer strategy is urgently needed.

In this publication, we were able to identify the alarmin IL-33 as an important factor to augment Tcf-1 expression and is thereby promoting CD8 T<sub>SCL</sub> formation during chronic infection. As shown by the use of a re-transfer systems (Fig. 3-4), we were able to demonstrate that antigen specific CD8 T<sub>SCL</sub>, defined by Tcf-1 expression, have significantly impaired expansion when re-challenged in an IL-33 deficient environment. Such deficit, not only resulted in an impaired repertoire of CD8 T<sub>SCL</sub>, but also the inability to produce CD8 T<sub>EF</sub>, emphasizing the importance of IL-33 for a sustained CD8 T cell response. Indeed, these data corroborate the previous work by Baumann et al, (168) deciphering the importance of IL-33 for efficient secondary expansion of memory CD8 T cells. Our data speaks towards the theory that the IL-33 impairment of memory T cell recall might be linked to a reduced pool of Tcf-1 expressing cells, given that Tcf-1<sup>-/-</sup> CD8 T cells have limited expansion upon secondary challenge (349). By this, our data not only provide new insights into the role of IL-33 in a chronic viral infection but also further elucidate the role of IL-33-ST2 signaling on the CD8 T cell recall response to recurrent viral infections which is critically dependent on Tcf-1 expression.

Beyond the critical role of IL-33 in both CD8 T cell maintenance and secondary expansion, it appears to have a lasting imprint effect on the CD8 T cells. Indeed, the remarkable expansion differences between P14 ST2<sup>-/-</sup> Tcf7<sup>gfp</sup> and P14 WT Tcf7<sup>gfp</sup> (shown in Fig. 3-5) upon antigen re-encounter in an IL-33 independent environment (infection with rAdGP) point out towards an imprint mechanism within the first 4 days upon LCMV CI-13 infection. Such data together with earlier reports (136) and the data presented in Fig. 3-1 G-H suggest that IL-33 is released and mediates most of its effects within the first days of infection, despite having long-term consequences on the differentiation of CD8 T cells.

In addition, we were able to demonstrate that IL-33 counterbalances type I interferon CD8 T cell terminal differentiation through Tcf-1 repression (117). The concept that IL-33 and IFN-I have opposing effects on the formation of Tcf-1 expressing cells highlights the interplay between danger signals and alarmins. Since LCMV is triggering a strong type I interferon response (174, 186), it is possible that the link between IL-33 and CD8 T<sub>SCL</sub> formation is of greater importance in a highly inflammatory milieu. However, the *in vitro* data shown in Fig. 3-2 C demonstrate that IL-33 can equally trigger CD8 T<sub>SCL</sub> through an inflammation-independent mechanism.

The observation that Tcf-1 expressing cells are formed under type I interferon blockade in an IL-33 independent manner (shown in Fig. 3-3) is raising the possibility that the IFN-I induced inflammatory milieu might alter survival and/or differentiation signals (174, 186, 229) that are compensated by IL-33 signaling.

A major clinical implication of these findings would be the use of IL-33 adjuvanted vaccines to improve vaccination regimens and enhance tumor as well as antiviral immunotherapy as already depicted in previous reports of our group (58, 59) and others (167, 350-352). However, as for many other cytokines with immunomodulatory properties, IL-33 can be classified as pro- or anti-tumorigenic cytokine (353, 354) and targeting strategies should be considered with caution.

In the past years, we and others have made several contributions to corroborate and mechanistically decipher the role of IL-33 – ST2 signaling for the formation of a potent anti-viral CD8 T cell response. However, a true biological understanding was still missing. With this work, we mechanistically elucidate how IL-33 potentiate anti-viral CD8 T cell response, by tying the importance of IL-33 with the formation of the Tcf1<sup>+</sup> CD8 T<sub>SCL</sub> population. Moreover, the data presented above reveal a molecular circuitry in which IL-33 signaling governs the early CD8 T<sub>SCL</sub> fate decision by repressing an opposing cell fate of terminal effector cells induced by type I interferon.

Such findings can have a profound impact in the future development of CD8 T cell-based immunotherapies, by contributing to the understanding on how effective CD8 T cell responses can be induced and maintained.

3.6 Figures

Figure 1

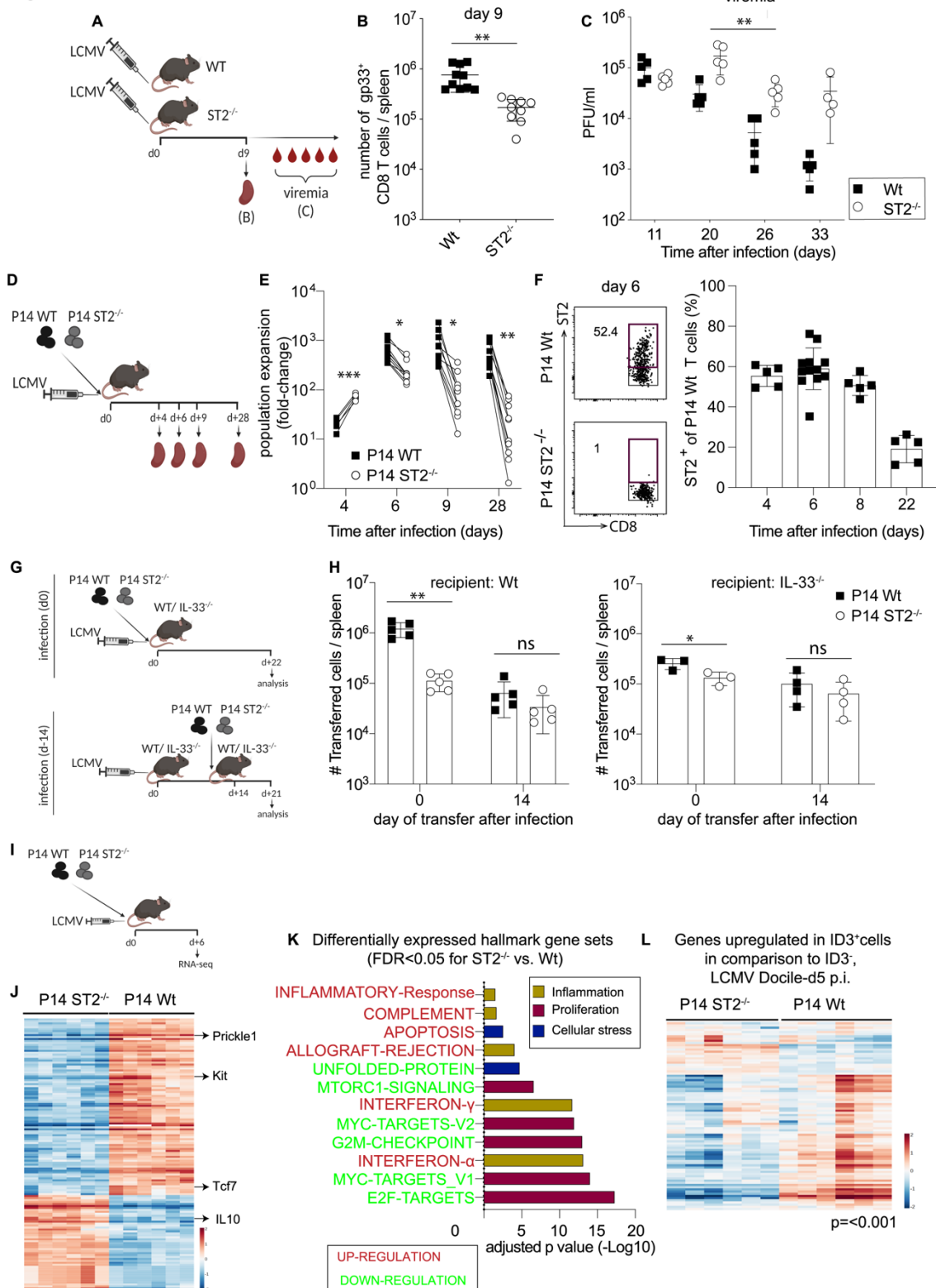


Figure 3-1 CD8 T cell-intrinsic IL-33 signaling is essential for the response to chronic viral infection

A: Experimental set-up used in B-C. Wt and ST2<sup>-/-</sup> mice were infected with LCMV CI-13 high dose. Spleens were harvested day 9 p.i. and analyzed for number of gp-33<sup>+</sup> CD8 T cells.

C: Virus titers were determined at the indicated time-points in the blood. D: Experimental set-up used in E-F. Equal numbers of P14 Wt (CD45.1) and P14 ST2<sup>-/-</sup> (CD45.1/2) CD8 T cells were transferred in Wt (CD45.2) recipient mice followed by LCMV CI-13 high dose infection. E: Population expansion (fold change) of P14 Wt and P14 ST2<sup>-/-</sup> cells at the indicated time-points in the spleen.

F: Representative FACS Plot showing ST2 receptor expression of P14 Wt cells on day 6 p.i. As control, ST2 staining was performed with P14 ST2<sup>-/-</sup> CD8 T cells. Numbers on FACS plots indicate the frequency of each gated population. Bar graphs summarizing the percentage of ST2 expression on P14 Wt cells at the indicated time-points. G: Schematic of the experimental design to H. Co-transfer of P14 Wt and P14 ST2<sup>-/-</sup> CD8 T cells into Wt and IL-33<sup>-/-</sup> mice that were either infected the same day (infection d0) or received the infection 14 days (infection d-14) before cell transfer. H: Bar graphs summarizing the number of P14 Wt and P14 ST2<sup>-/-</sup> CD8 T cells 8 days upon cell-transfer. I: Experimental set-up used in J-L: Co-transfer of P14 Wt and P14 ST2<sup>-/-</sup> CD8 T cells into Wt mice infected with LCMV CI-13. Bulk-RNA sequencing of transferred cells P14 Wt and P14 ST2<sup>-/-</sup> was performed 6 days after infection (see supplementary Fig. S-3-2).

J: Heat-map of hierarchically clustered top differentially expressed genes (displayed by P value; abs (logFC)>1.5; FDR<0.05) between P14 Wt and P14 ST2<sup>-/-</sup> CD8 T cells. Genes with important functions for CD8 T<sub>SCL</sub> differentiation are highlighted. K: Hallmark gene sets, which are significantly differentially expressed (FDR<0.05) between P14 Wt and P14 ST2<sup>-/-</sup> CD8 T cells, displayed are the adjusted p-values. L: Heatmap demonstrating a significant enrichment of CD8 T<sub>SCL</sub> gene signature within P14 Wt cells but not in P14 ST2<sup>-/-</sup> CD8 T cells. The CD8 T<sub>SCL</sub> gene sets was constructed from available datasets by taking the genes upregulated (FDR>1) in CD8 T<sub>SCL</sub> (ID3<sup>+</sup>) in comparison to non CD8 T<sub>SCL</sub> (ID3<sup>-</sup>). ID3<sup>+</sup> and ID3<sup>-</sup> CD8 T cells were sorted on day 5 after LCMV-Docile infection (see Supplementary Table 1 of reference (116)).

Data are representative of 1 (H) to 2 (B, C, E and F) independent experiments with at least 5 mice per group. B and E as well as day 6 (F) show data pooled from 2 independent experiments. Statistical comparison of experimental groups in B were performed using unpaired two-tailed Student's *t* test, for C a time-course one-way ANOVA test was performed, statistical comparison of experimental groups in E and H were performed using 2-way ANOVA with Sidak's post test. Ns: not significant; \*:  $p<0.05$ ; \*\*:  $p<0.01$ .

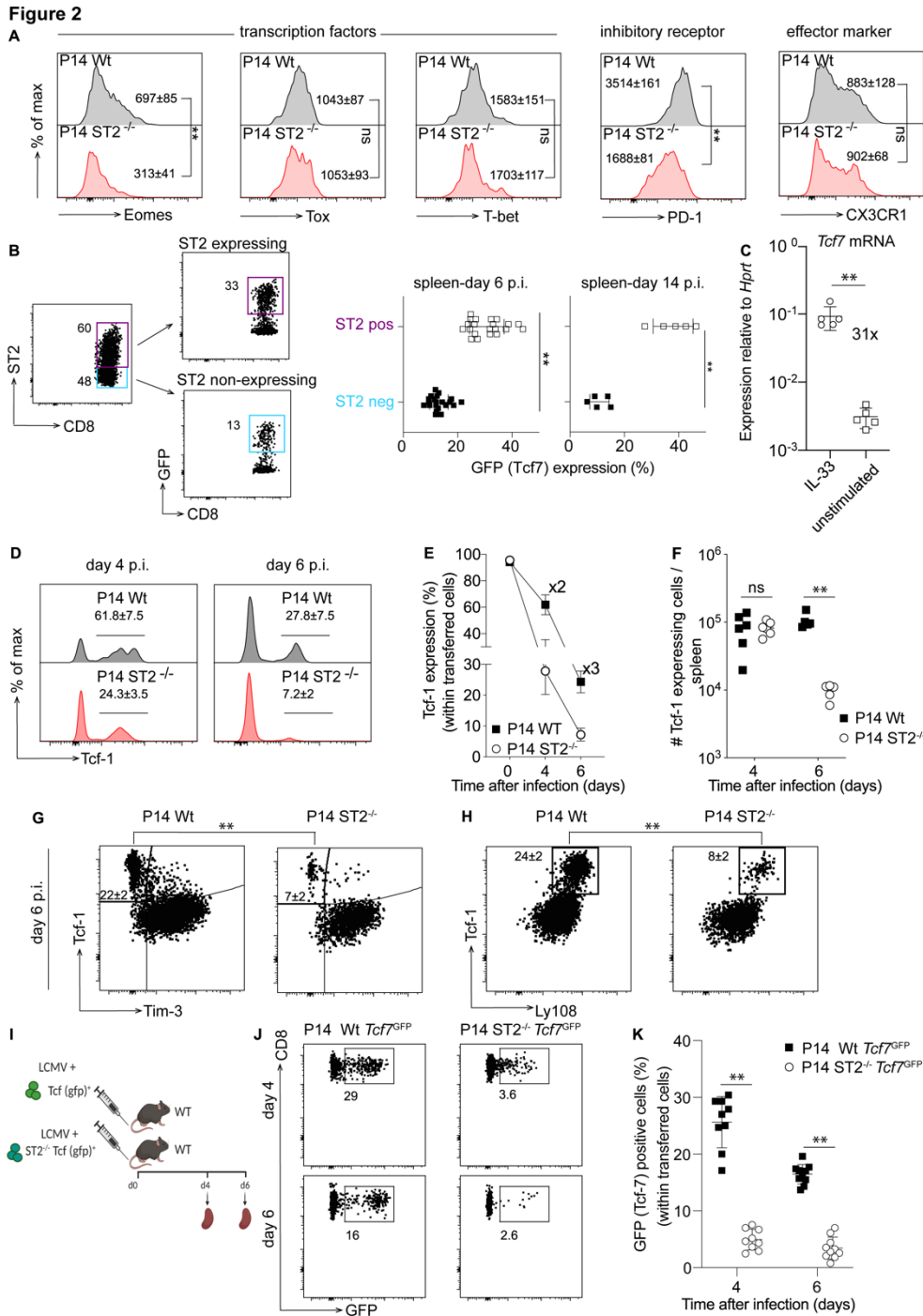


Figure 3-2 IL-33 is required to preserve the *Tcf-1* expressing population

A: Representative flow cytometry plots showing MFI (mean  $\pm$  SD) of the indicated transcription factors and surface markers by P14 Wt (grey) or P14 ST2<sup>-/-</sup> (red) cells on day 6 p.i. B: P14 Wt Tcf7<sup>gfp</sup> were transferred into Wt mice, which were infected with LCMV CI-13. 6 and 14 days later, P14 Wt Tcf7<sup>gfp</sup> CD8 T cells were analyzed for ST2 expression. Representative FACS Plots illustrating gating strategy. Numbers on FACS plots indicate the frequency of each gated population. Percentage of GFP<sup>+</sup> expression pre-gated on P14 ST2<sup>+</sup> cells. P14 ST2<sup>-/-</sup> Tcf7<sup>gfp</sup> CD8 T cells were used as staining control. Data from day 6 are pooled from 2 independent experiments. C: *In vitro* activated P14 Wt cells were stimulated with recombinant IL-33 for 2h. *Tcf7* mRNA expression levels relative to *Hprt*.

D: Tcf-1 expression by P14 Wt (grey) and P14 ST2<sup>-/-</sup> (red) cells at d4 and d6 after LCMV Cl-13 infection. E: Percentage of Tcf-1 expressing P14 Wt/ P14 ST2<sup>-/-</sup> cells d4/d6 p.i.. F: number of Tcf-1<sup>+</sup> P14 Wt and Tcf-1<sup>+</sup> P14 ST2<sup>-/-</sup> cells on d4 and d6 p.i. G-H: Representative flow cytometry plots showing co-expression of Tcf-1 and Tim-3 or Tcf-1 and Ly108 (Slamf6) in P14 Wt and P14 ST2<sup>-/-</sup> cells. Corresponding percentage values are shown as mean ± SD.

I-K: P14 Wt Tcf7<sup>gfp</sup> and P14 ST2<sup>-/-</sup> Tcf7<sup>gfp</sup> cells were transferred into Wt mice infected with LCMV Cl-13. I: Representative FACS Plots showing GFP expression level on d4 and d6 p.i.. Numbers on flow plots indicate the frequency of each gated population. K: Percentage of GFP<sup>+</sup> cells among transferred P14-Tcf7<sup>gfp</sup> and P14 ST2<sup>-/-</sup> Tcf7<sup>gfp</sup> cells. Data are pooled from 2 independent experiments.

Data are representative of two (B, C, J-K) to three (A, D-H) independent experiments with at least 4 mice per group. Symbols and bars represent means±SEM. Paired t-test (A, B, D-H). Un-paired t-test (C, K). Ns: not significant; \*:  $p<0.05$ ; \*\*:  $p<0.01$ .

**Figure 3**

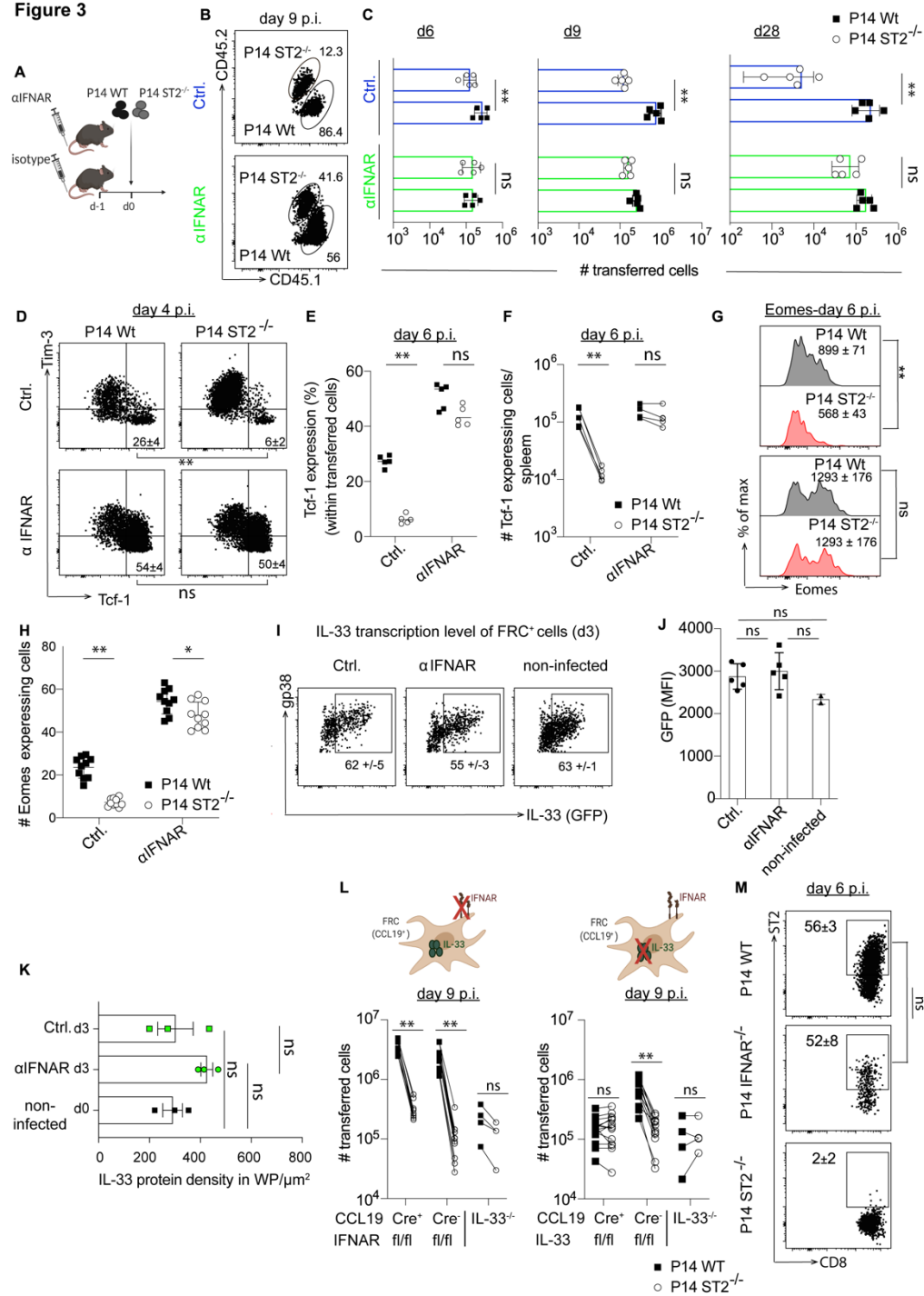


Figure 3-3 Upon type I interferon exposure, IL-33 signaling enables differentiation of CD8 T cells into CD8 T<sub>sc1</sub>

A: Experimental set-up for B-H; Co-transfer of equal numbers of P14 Wt (CD45.1) and P14 ST2<sup>-/-</sup> (CD45.1/2) CD8 T cells into isotype or  $\alpha$ IFNAR treated Wt (CD45.2) recipients. Antibodies were administered 1d before infection.

Mice were infected with a high dose of LCMV Cl-13. B: Representative FACS Plot showing the frequency of P14 Wt and P14 ST2<sup>-/-</sup> cells day 9 p.i.; pre-gated on transferred cells (CD45.1<sup>+</sup> cells). Numbers on FACS plots indicate the frequency of each gated population.

C: Splenocytes were harvested at the indicated time-points (d6, d9 and week 4 p.i.) and analyzed for the number of transferred cells.

D: Representative FACS plots showing the expression of Tcf-1 and Tim-3 by P14 Wt and P14 ST2<sup>-/-</sup> cells at d4 after infection. Corresponding percentage values are shown as mean ± SD. Percentage (E) and number (F) of Tcf-1<sup>+</sup> P14 Wt and P14 ST2<sup>-/-</sup> CD8 T cells day 6 p.i. G: P14 Wt and P14 ST2<sup>-/-</sup> CD8 T cells were harvested on day 6 p.i. and intracellularly stained for Eomes. Shown are representative histograms of P14 ST2<sup>-/-</sup> (red) CD8 T cells in comparison to P14 Wt (grey) cells. Numbers indicated the MFI of Eomes (Mean ± SD). H: Graph summarizing the percentage of Eomes<sup>+</sup> cells within P14 Wt or P14 ST2<sup>-/-</sup> CD8 T cells obtained from isotype or αIFNAR treated recipients.

I: IL-33<sup>gfp/wt</sup> mice were infected with LCMV Cl-13. Type I interferon was blocked by administration of an αIFNAR antibody 1d before infection. 3 days after infection, spleens were harvested and single-cell suspensions were prepared by collagenase digestion. Representative FACS Plot of the GFP profile of FRCs (gated on live CD45.2<sup>+</sup>, Ter119<sup>-</sup>, CD31<sup>-</sup> gp38<sup>+</sup>; see gating strategy shown in Fig. S 3-5). Corresponding percentage values are shown as mean ± SD. J: Quantification of the GFP-expression levels (MFI). L: Representative examples of Immunofluorescence staining of spleen sections for IL-33 protein. IL-33<sup>gfp/wt</sup> mice were infected with LCMV Cl-13 (d0). Type I interferon was blocked by administration of αIFNAR Ab 1 day before infection. Control mice were treated with isotype Ab. Spleens were harvested day 3 after infection. Quantification of immunofluorescence staining shown in Fig. S 3-6 for IL-33 protein density (signal intensities multiplied by signal-positive areas) per white pulp. Per mouse spleen 2 different cuts were analyzed. Each dot represents the mean of the experimental replicate.

L: IFNAR receptor was deleted on FRCs (CCL19<sup>+</sup> cells) by crossing IFNAR<sup>fl/fl</sup> mice with CCL19<sup>Cre+</sup> mice. As control IFNAR<sup>fl/fl</sup> CCL19<sup>Cre-</sup> as well as IL-33<sup>-/-</sup> mice were used. Furthermore IL-33 deletion by FRCs was achieved by crossing CCL19<sup>Cre+</sup> mice with IL-33<sup>fl/fl</sup> mice. Graph is summarizing the number of transferred P14 Wt and P14 ST2<sup>-/-</sup> CD8 T cells per group. Analysis was performed on day 9 p.i.. Data are pooled from 2 independent experiments. M: ST2 receptor expression was determined on P14 Wt and P14 IFNAR<sup>-/-</sup> CD8 T cells. In parallel P14 ST2<sup>-/-</sup> CD8 T cells were stained to substrate background signaling. NK-cells were depleted in all recipient mice (see Material and Methods: 3.3.6)

Data are representative of either one (K), two (B, C, I-J, L, M) or three (D-H) independent experiments with at least 4 mice per group.

Statistical comparison of experimental groups in B-H and M were performed using two-way ANOVA with post-hoc Sidak's multiple comparison test. J, L and N: one-way ANOVA with post-hoc Tukey's test for multiple comparisons. Ns: not significant; \*:  $p < 0.05$ ; \*\*:  $p < 0.01$ .



Figure 4

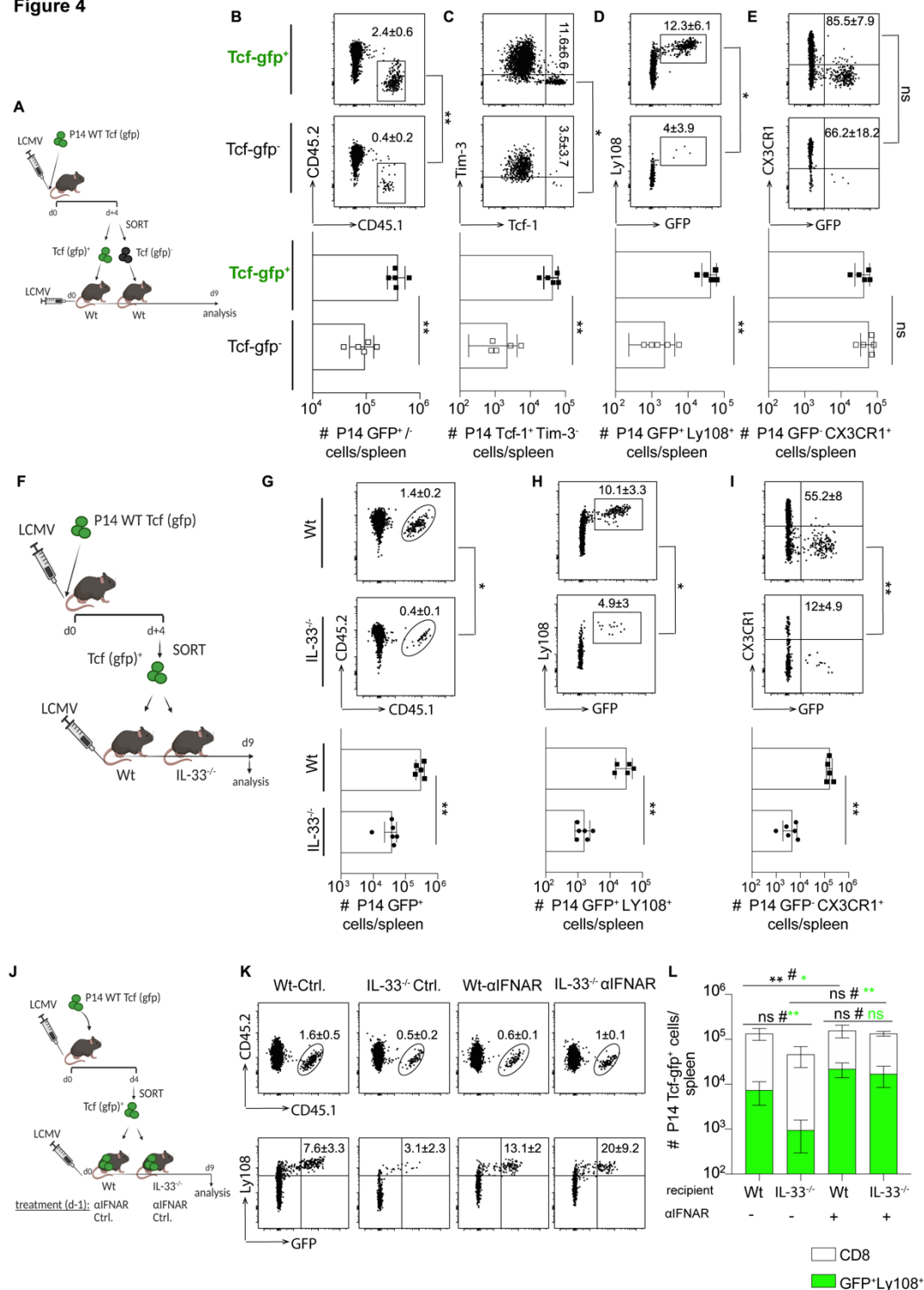


Figure 3-4 The proliferative as well as the generation capacity of CD8 T<sub>sc1</sub> cells and the differentiation into effector CD8 T cells is clearly IL-33 dependent

A: Experimental setup used in Fig. B-E. Naïve P14 Wt Tcf7<sup>gfp</sup> CD8 T cells were transferred into Wt mice followed by LCMV CI-13 infection. 4 Days later, transferred cells were flow-sorted into GFP<sup>+</sup> and GFP<sup>-</sup> cells. 1x10<sup>3</sup> cells of each population were re-transferred into secondary recipients followed by infection with LCMV CI-13. Secondary recipients were analyzed 9 days after transfer. B: (Top) Representative FACS Plot showing the percentage of transferred cells. Corresponding percentage values are shown as mean ± SD. (Bottom) Total number of P14 Wt Tcf7<sup>gfp</sup><sup>+</sup> and P14 Wt Tcf7<sup>gfp</sup><sup>-</sup> cells. C: (Top) Representative

FACS Plot showing the expression of Tcf-1<sup>+</sup> and Tim-3<sup>-</sup>. Numbers indicate mean  $\pm$  SD. (Bottom) Total number of Tcf-1<sup>+</sup> Tim-3<sup>-</sup> P14 Wt Tcf7<sup>gfp+</sup> and P14 Wt Tcf7<sup>gfp-</sup> cells.

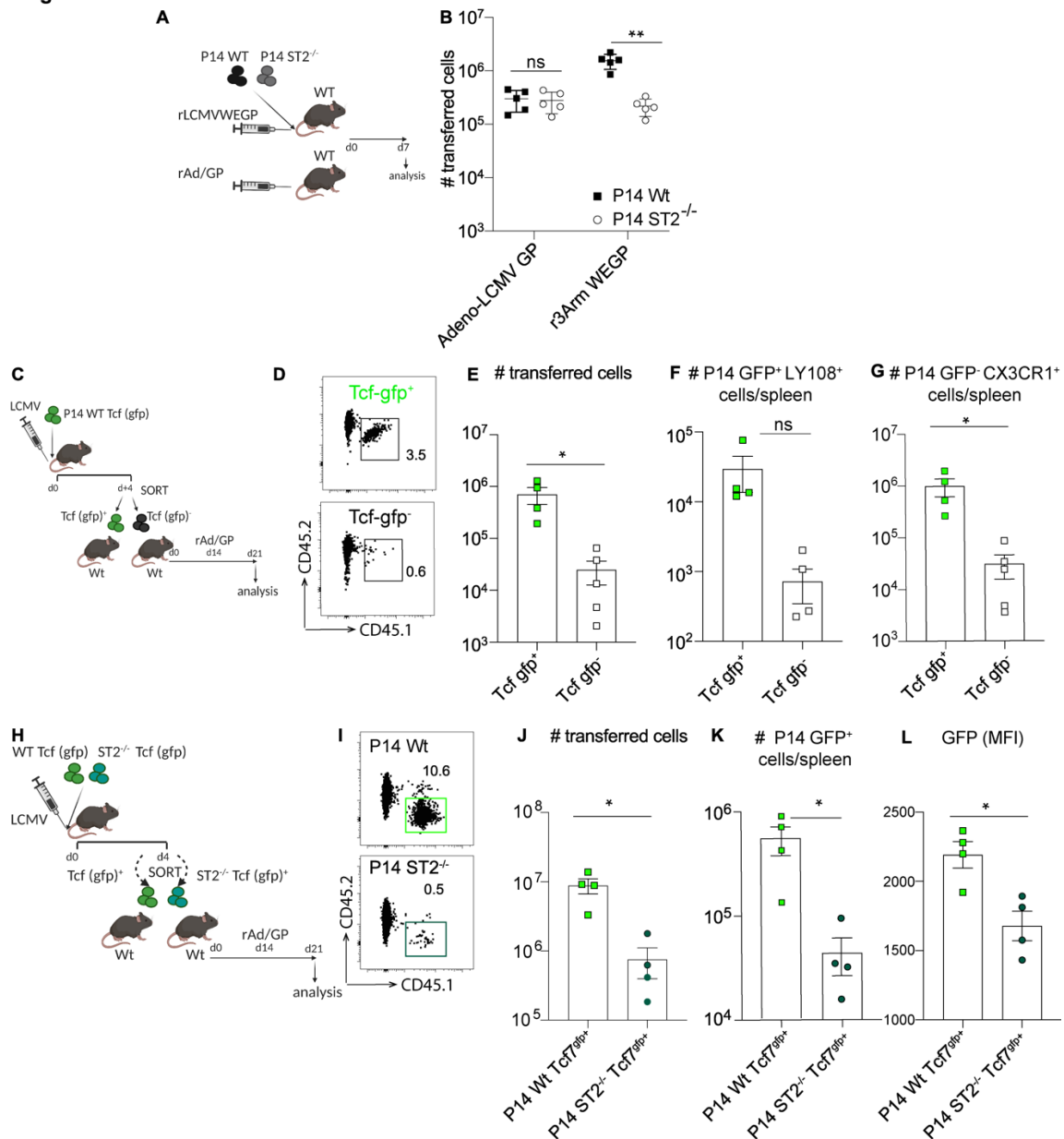
D: (Top) Representative FACS Plot showing the co-expression of GFP and Ly108. Numbers indicate mean  $\pm$  SD (Bottom): Total number of GFP<sup>+</sup> Ly108<sup>+</sup> P14 Wt Tcf7<sup>gfp+</sup> and P14 Wt Tcf7<sup>gfp-</sup> cells. E: (Top) P14 Wt Tcf7<sup>gfp+</sup> and P14 Wt Tcf7<sup>gfp-</sup> cells were analyzed for the expression of GFP and CX3CR1. Numbers in FACS Plots indicate percentages mean  $\pm$  SD. (Bottom) Total number of CX3CR1<sup>+</sup> GFP<sup>+</sup> P14 Wt Tcf7<sup>gfp+</sup> and P14 Wt Tcf7<sup>gfp-</sup> cells. F: Experimental setup used in Fig. G-I. Naïve P14 Wt Tcf7<sup>gfp</sup> CD8 T cells were transferred into Wt mice followed by LCMV CI-13 infection. 4 Days later, transferred cells were flow-sorted for expression of GFP.  $1 \times 10^3$  P14 Tcf7<sup>gfp+</sup> cells were transferred into Wt and IL-33<sup>-/-</sup> secondary recipients followed by infection with LCMV CI-13. Secondary recipients were analyzed 9 days after transfer. G: (Top) Representative FACS Plot showing the percentage of transferred cells. Numbers in FACS Plots indicate percentages mean  $\pm$  SD. (Bottom) Total number of P14 Wt Tcf7<sup>gfp+</sup>. H: (Top) Representative FACS Plot showing the co-expression of GFP and Ly108. Numbers in FACS Plots indicate percentages mean  $\pm$  SD. (Bottom) Total number of GFP<sup>+</sup> Ly108<sup>+</sup> P14 Wt Tcf7<sup>gfp+</sup> transferred in Wt or IL-33<sup>-/-</sup> mice. I: (Top) P14 Wt Tcf7<sup>gfp+</sup> cells were analyzed for the expression of GFP and CX3CR1. Numbers indicate mean  $\pm$  SD. Bottom: Total number of CX3CR1<sup>+</sup> GFP<sup>+</sup> P14 Wt Tcf7<sup>gfp+</sup> present in the spleen of Wt and IL-33<sup>-/-</sup> mice. Numbers in FACS Plots indicate percentages mean  $\pm$  SD.

J: Experimental setup used in Fig. K-L. Naïve P14 Wt Tcf7<sup>gfp</sup> CD8 T cells were transferred into Wt mice followed by LCMV CI-13 infection. 4 Days later, transferred cells were flow-sorted for expression of GFP.  $1 \times 10^3$  P14 Wt Tcf7<sup>gfp+</sup> cells were transferred into Wt and IL-33<sup>-/-</sup> secondary recipients pre-treated d-1 with isotype or  $\alpha$ IFNAR Ab followed by infection with LCMV CI-13. K: (Top) FACS plots showing the frequency of transferred P14 Wt Tcf7<sup>gfp+</sup> cells in the spleen of secondary recipients. Numbers in FACS Plots indicate percentages mean  $\pm$  SD. (Bottom) Representative FACS Plots showing the co-expression of GFP and Ly108. Numbers in FACS Plots indicate percentages mean  $\pm$  SD. L: Graph summarizing the number of GFP<sup>+</sup> Ly108<sup>+</sup> expressing (green bar) and total number of P14 Wt Tcf7<sup>gfp+</sup> cells in the spleen of secondary recipients (open bar).

Statistical analysis: Unpaired t-test (B-E, G-I). (L) # Ordinary one-way ANOVA with post-hoc Tukey's multiple comparison test for total CD8 T cell numbers. # Ordinary one-way ANOVA with post-hoc Tukey's multiple comparison test for total number of GFP<sup>+</sup> Ly108<sup>+</sup> CD8 T cells. Data are representative of one (L) to two (B-E, G-I) independent experiments with at least 4 recipients per group.

Ns: not significant; \*:  $p < 0.05$ ; \*\*:  $p < 0.01$ .

Figure 5

Figure 3-5 Self-generation of CD8 T<sub>SCL</sub> as well as the proliferative capacity rely on IL-33 signaling within the first 4 days

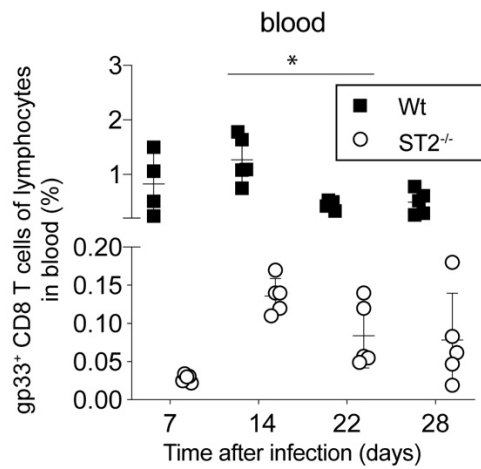
**A:** Experimental set-up used in **B**: P14 Wt and P14 ST2<sup>-/-</sup> CD8 T cells were transferred into Wt mice infected with rLCMV-WEGP or rAdGP. **B:** Number of transferred cells were analyzed on day 7 p.i. **C:** Experimental set-up used in **D-G**. Naïve P14 Wt Tcf7<sup>gfp</sup> CD8 T cells were transferred into Wt mice followed by LCMV CI-13 infection. 4 Days later, transferred cells were flow-sorted into GFP<sup>+</sup> and GFP<sup>-</sup> cells. 1x10<sup>3</sup> cells of each population were re-transferred into secondary recipients (Wt mice). Secondary recipients were infected 14 days later with rAdGP. Final time-point was 21 days after transfer. **D:** Representative FACS Plot showing the percentage of transferred cells. Numbers on FACS plots indicate the frequency of each gated population. **E:** Total number of P14Wt Tcf7<sup>gfp+</sup> and P14 Wt Tcf7<sup>gfp-</sup> cells. **F:** Total number of GFP<sup>+</sup> Ly108<sup>+</sup> P14 Wt Tcf7<sup>gfp+</sup> and GFP<sup>+</sup> Ly108<sup>+</sup> P14 Wt Tcf7<sup>gfp-</sup> cells. **G:** Total number of GFP<sup>+</sup> CX3CR1<sup>+</sup> P14 Wt Tcf7<sup>gfp+</sup> and GFP<sup>+</sup> CX3CR1<sup>+</sup> P14 Wt Tcf7<sup>gfp-</sup> cells. **H:** Experimental set-up used in **I-L**: Naïve P14 Wt Tcf7<sup>gfp</sup> CD8 T cells and naïve P14 ST2<sup>-/-</sup> Tcf7<sup>gfp</sup> CD8 T cells were transferred separately into Wt mice followed by LCMV CI-13 infection. 4 Days later, transferred cells were flow-sorted for GFP expression. 1x10<sup>3</sup> cells of each population were re-transferred into secondary recipients (Wt mice).

Secondary recipients were infected 14 days later with rAdGP. Final time-point was 21 days after transfer. I: Representative FACS Plot showing the percentage of transferred cells. Numbers on FACS plots indicate the frequency of each gated population. J: Total number of P14 Wt Tcf7<sup>gfp+</sup> and P14 ST2<sup>-/-</sup> Tcf7<sup>gfp+</sup> cells. K: Total number of GFP<sup>+</sup> P14 Wt Tcf7<sup>gfp+</sup> and GFP<sup>+</sup> P14 ST2<sup>-/-</sup> Tcf7<sup>gfp+</sup> cells. L: MFI of GFP pre-gated on P14 Wt Tcf7<sup>gfp+</sup> and P14 ST2<sup>-/-</sup> Tcf7<sup>gfp+</sup> CD8 T cells.

Data are representative of 2 independent experiments with at least 4 mice per group. Numbers indicate mean  $\pm$  SEM. Statistical analysis: Unpaired t-test (E-G, J-L). Ns: not significant; \*:  $p < 0.05$ ; \*\*:  $p < 0.01$ .

### 3.7 Supplementary Figures

**Figure S1**

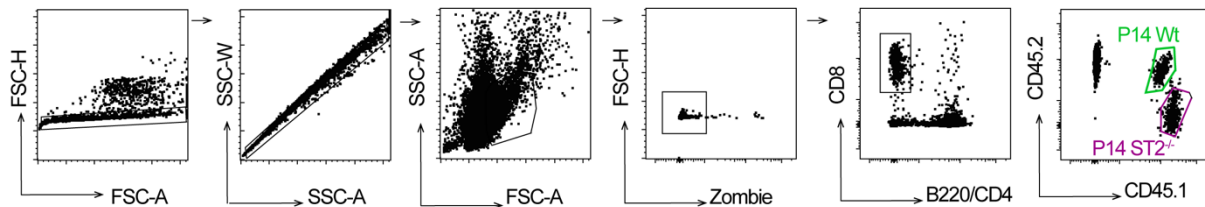


*S 3-1 Impaired T cell maintenance in the absence of IL-33*

Wt and ST2<sup>-/-</sup> mice were infected with LCMV Cl-13 high dose. The fraction of T cells specific for gp33 was determined using MHC Class I tetramers at the indicated time-points in blood. Data are representative of 2 independent experiments with at least 5 mice per group. Numbers indicate mean  $\pm$  SEM. Values indicate gp33<sup>+</sup> CD8 T cells as a percentage of lymphocytes. Statistical analysis: time course one way ANOVA. Ns: not significant; \*:  $p < 0.05$ ; \*\*:  $p < 0.01$

**Figure S2**

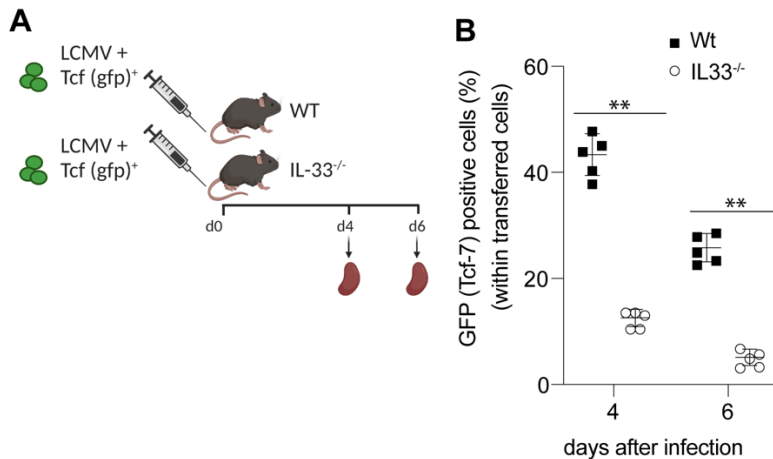
**Gating strategy for sorting of P14 Wt and P14 ST2<sup>-/-</sup> CD8 T cells for bulk-RNA sequencing**



*S 3-2 Gating strategy for FACS sorting of P14 Wt and P14 ST2<sup>-/-</sup> CD8 T cells*

Sorting strategy for FACS sorting of P14 Wt/ P14 ST2<sup>-/-</sup> CD8 T cells (related to Fig. 3-1 I-L). Co-transfer of P14 Wt and P14 ST2<sup>-/-</sup> CD8 T cells into Wt mice followed by LCMV Cl-13 infection. On d6 post infection, cells were sorted based on the expression of their congenic markers. A dump gate exclusion contained B220 and CD4.

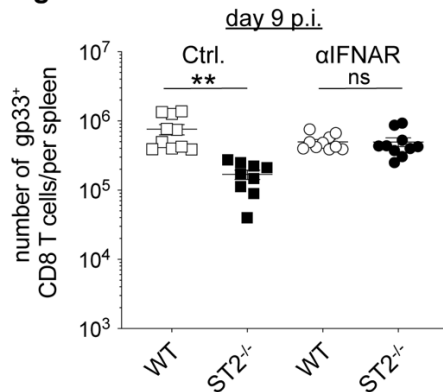
**Figure S3**



*S 3-3 Impaired Tcf-1 expression in the absence of IL-33 signaling*

A: Experimental set-up for B: P14 Wt Tcf7<sup>gfp</sup> CD8 T cells were transferred into Wt and IL-33<sup>-/-</sup> mice followed by LCMV CI-13 high dose infection. For analysis on day 4- 1x10<sup>4</sup> P14 Wt Tcf7<sup>gfp</sup> CD8 T cells were transferred, for analysis on day 6 1x10<sup>3</sup> P14 Wt Tcf7<sup>gfp</sup> CD8 T cells were used as input. Spleens were harvested 4 and 6 days later and analyzed for the expression of GFP. B: Percentage of GFP<sup>+</sup> cells among transferred P14 Wt Tcf7<sup>gfp</sup> and P14 ST2<sup>-/-</sup> Tcf7<sup>gfp</sup> cells. Data are representative of 1 independent experiments with at least 5 mice per group. Numbers indicate mean ± SEM. Statistical analysis: For each time-point an unpaired t-test was performed. Ns: not significant; \*: *p*<0.05; \*\*: *p*<0.01.

**Figure S4**

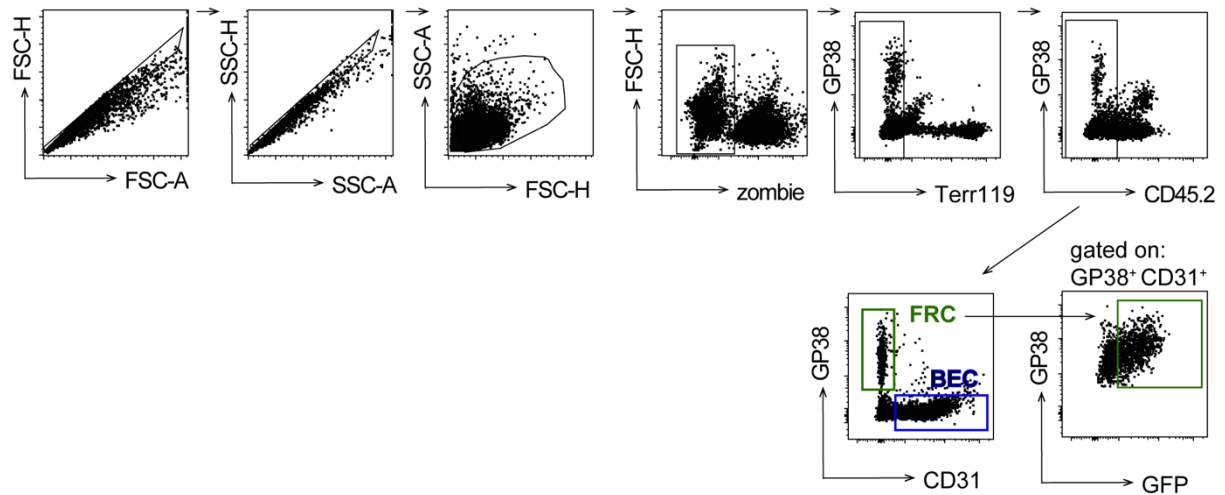


*S 3-4 Upon type I interferon exposure, the antigen-specific repertoire of antigen-specific CD8 T cells in Wt and ST2<sup>-/-</sup> mice is equalized*

Wt and ST2<sup>-/-</sup> mice were infected with LCMV CI-13 high dose. Type I interferon was depleted by treatment with αIFNAR 1 day before infection. Control mice received equal amount of isotype control. 9 days after infection, spleens were harvested and gp33<sup>+</sup> CD8 T cells were determined via MHC class I tetramer staining. Data show 2 independent experiments with 5 mice per group/experiment. Numbers indicate mean ± SEM. Statistical analysis: One way ANOVA with Tukey's post-test for multiple comparisons. Ns: not significant; \*: *p*<0.05; \*\*: *p*<0.01.

## Figure S5

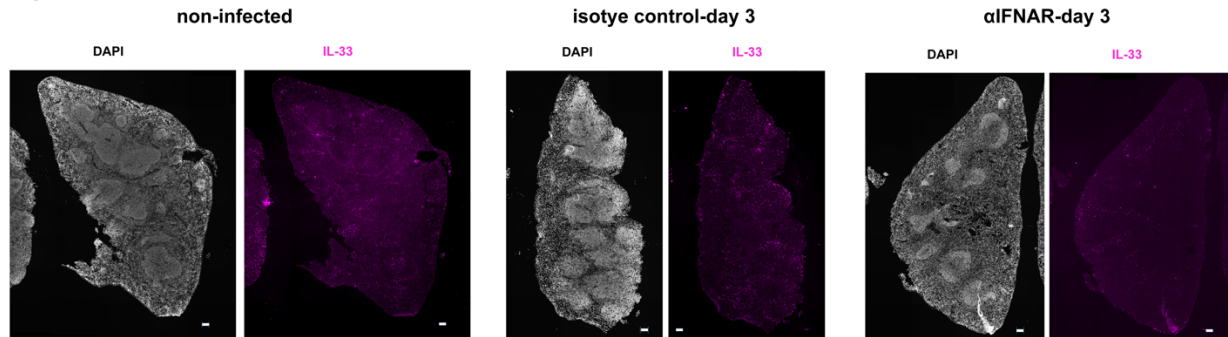
### B Gating strategy for IL-33 reporting stroma cells in the spleen



#### S 3-5 Gating strategy for IL-33 reporting stroma cells in the spleen

(Corresponding to Fig. 3-3 I-J) Gating strategy for the identification of GFP expression by the FRCs of IL-33 reporting mice. FRCs were defined as gp38<sup>+</sup> CD31<sup>-</sup>, BECs were defined as gp38<sup>-</sup> CD31<sup>+</sup>. A dump gate exclusion contained Terr119 and CD45.2. Analysis was performed with IL-33<sup>gfp/wt</sup> mice on day 3 after infection.

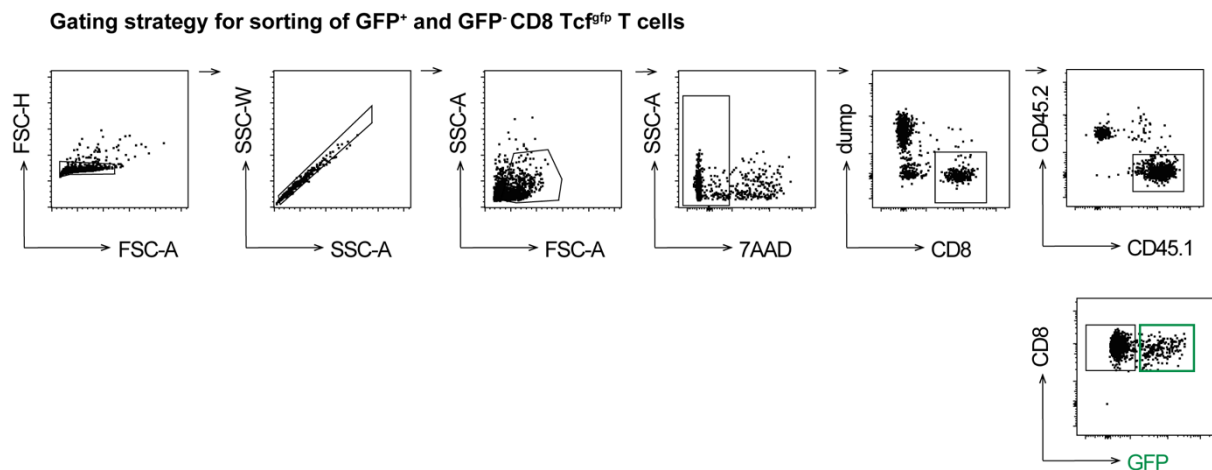
## Figure S6



#### S 3-6 IL-33 protein levels are unaffected upon IFN-I blockade

(Corresponding to Fig. 3-3 K) Representative examples of Immunofluorescence staining of spleen sections for DAPI (left) and IL-33 protein (purple-right). IL-33<sup>gfp/wt</sup> mice were infected with LCMV CI-13 (d0). Type I interferon was blocked by administration of  $\alpha$ -IFNAR Ab 1 day before infection. Control mice were treated with isotype Ab. Spleens were harvested day 3 after infection. Magnification bars: 100  $\mu$ m.

## Figure S7



S 3-7 Gating strategy for sorting of GFP<sup>+</sup> and GFP<sup>-</sup> CD8 Tcf7<sup>gfp</sup> T cells

Naïve P14 Wt Tcf7<sup>gfp</sup> and P14 ST2<sup>-/-</sup> Tcf7<sup>gfp</sup> cells were transferred into Wt mice followed by LCMV CI-13 infection. Day 4 after infection, cells were sorted based on their GFP expression. A dump gate exclusion contained B220 and CD4.

### 3.8 Author contributions

A.F.M., S.M.K., W.V.B, P.A.D., T.M.B., F.G, M.L., S.L. and D.D.P, contributed to experimental conception and design; A.F.M., S.M.K., W.V.B, P.A.D., T.M.B., F.G, M.L., S.L., K.S., M.L., M.C., L.S. and D.D.P acquired, analyzed and/or interpreted the data; A.F.M. and D.D.P. drafted or critically revised the article for important intellectual content.

### 3.9 Acknowledgements

We would like to thank the entire Experimental Virology lab for helpful discussions. We wish to thank Telma Lopes, Danny Labes, Lorenzo Raeli and Emmanuel Traunecker from the DBM flow cytometry core facility for outstanding FACS-sorting and Philippe Demougin from the Life Sciences Training Facility of the University of Basel Pharmacenter for bulk RNA sequencing.

Special thank goes to Tiago Abreu Mota for his help to assemble the first manuscript draft and critical discussions.



## **4. Supplementary data for: Alarmins and type I interferon synergistically potentiate antiviral CD8 T cell responses by promoting stemness**

**Keywords:** IL-33, antiviral stem-like CD8 T cells, chronic infection, type I interferon, intrinsic-extrinsic component

### **4.1 Introduction**

This chapter includes further data that were produced during my PhD but were not included in the manuscript for brevity's sake. However, this data further complements the work here discussed and aided on reaching the overall conclusions of this work.

CD8 T cells play crucial roles in limiting persistent infections and conferring life-long protective immunity. For the fate and differentiation pathways of antiviral CD8 T cells, signals provided by cytokines play an important role (*127*). Understanding the stage dependent effects as well as the interplay of cytokines enables modulation of their biological action that might help improving viral control and immunity.

In the beginning of the infection, cytokines such as IFN-I and IL-33 operate as immunological warning signs that inform about the presence of an infection but also influence the developmental choices of the antiviral CD8 T cells.

In our prior work (chapter 3), we were able to highlight that IL-33 signaling tilts the CD8 T cell fate decision towards CD8 T<sub>SCL</sub> differentiation early in chronic infection. Moreover, this effect was shown to be linked to IL-33's capability of counterbalancing type I interferon which operates by preferentially fostering the differentiation of effector CD8 T cells (*117*).

Considering the far-reaching inflammatory effects of type I interferon (*186, 229*), two important questions remained: a) Does ST2 signaling antagonizes CD8 T cell differentiation by an intrinsic or extrinsic effect, or both simultaneously, on the target CD8 T populations? and b) Given the pleotropic indirect effects that IFN-I blockade entails, is the observed effect on CD8 T cell expansion due to a different inflammatory milieu caused by IFNAR blockade on a specific cellular compartment?

## 4.2 Material and Methods

### 4.2.1 Mice and animal experimentations

All mouse experiments were performed at the University of Basel. Animals in experiments were between 6-20 weeks old and sex-matched. Animals were bred at the Laboratory Animal Science Center (LACS) of the University of Zürich, at the ETH Phenomics Center (EPIC) at the ETH or at Animal Facility Bio Park 1060 at the University of Basel.

ST2-deficient *Il1r1*<sup>-/-</sup> (59, 311), *IFNAR*<sup>-/-</sup> (179), P14 TCR transgenic mice (183), *IL10*<sup>-/-</sup> (355), *IFNAR* fl/fl (338) (provided by Ulrich Kalinke), *CD11c* Cre (356), *LysM*Cre (357), *CD4* Cre (358) and *CD19* Cre (359) have been described. P14 *ST2*<sup>-/-</sup>, P14 *IFNAR*<sup>-/-</sup> and P14 *ST2*<sup>-/-</sup> *IFNAR*<sup>-/-</sup> mice, *CD11c* Cre *IFNAR* fl/fl, *LysM* Cre *IFNAR* fl/fl, *CD4* Cre *IFNAR* fl/fl and *CD19* Cre *IFNAR* fl/fl mice were obtained by intercrossing with the respective parental lines. C57BL/6J (Wt) mice were bred at the at the Laboratory Animal Science Center (LACS) of the University of Zürich or at the ETH Phenomics Center (EPIC) at the ETH. Mice that were used as donors were backcrossed to C57BL/6J mice. Confirmation of C57BL/6J background by SNP typing (Taconic Biosciences).

### 4.2.2 Viruses

LCMV Cl-13 (34) was produced by infecting BHK-21 cells at a multiplicity of infection (MOI) of 0.01. The supernatant was harvested 48h later and viral titers were determined by focus forming assay on 3T3 cells as described (59, 230).

Mice were infected with  $2 \times 10^6$ - $1 \times 10^7$  PFU of LCMV Cl-13 i.v. to establish a chronic infection.

### 4.2.3 Flow cytometry and intracellular staining for cytokines

Single-cell suspensions of spleens were prepared by mechanical disruption using metal mesh. Surface staining was performed at 4°C in the dark for 30 mins. All staining's were done in FACS buffer (FACS buffer (PBS, 2% FCS, 5mM EDTA, 0.05% sodium azide).

Antibodies against CD8 (53-6.7), CD4 (IM7 or RM4-5), B220 (RA3-6B2), CD45.1 (A20), CD45.2 (104), Ly108 (330-AJ), CX3CR1(SA01F11), PD-1 (29F.1A12) and Tim-3 (5D12) were from Biolegend, eBioscience/ThermoFisher or BDBioscience/PharMingen. All fluorescently labelled monoclonal antibodies were, if not otherwise indicated, diluted 1:100.

For the detection of GP33 specific CD8 T cells, peptide MHC Class I tetramers (H-2D<sup>b</sup> tetramers loaded with the LCMV GP<sub>33-41</sub> peptide-KAVYNFATM) obtained from the NIH-Core Facility or the University of

Lausanne Tetramer core facility were used. Unspecific binding was excluded by pre-gating on B220<sup>-</sup> CD4<sup>-</sup> CD8<sup>+</sup> cells. Tetramer staining was performed at RT for 30 mins in the dark.

Dead cells were excluded with Zombie UV Fixable Viability Kit (Biolegend) according to manufactures instructions.

To detect intracellular levels of Tcf-1 we followed the protocol form eBioscience™ FOXP3 transcription factor staining kit (Invitrogen). The transcription factor Tcf-1 was detected by incubating first with a primary antibody (C63D8, Cell Signaling, dilution:1:200) followed by adding a donkey anti-rabbit IgG PE (Poly4064-eBioscience).

Samples were measured on BDLSRFortessa flow cytometer. FlowJo Software (Becton Dickinson) was used for analysis.

#### **4.2.4 Adoptive cell transfer**

For adoptive cell transfer, donor P14 CD8 T cells were MACS (Miltenyi Biotec-naïve CD8 T cell isolation kit, mouse) purified and administered i.v. For co-transfers, equal numbers of both cell populations were transferred. For analysis on day 6 p.i. 10<sup>4</sup> cells were injected. For analysis from day 8 onwards, mice received 500 cells to stay in the physiological range of the precursor frequency of gp-33<sup>+</sup> specific CD8 T cells (341). To avoid rejection of transferred cells, donor T cells from male or female were transferred into male recipients. The two transferred populations could be differentiated from each other and from the recipient's CD8 T cells by means of their congenic CD45 markers.

#### **4.2.5 Bone marrow chimeric mice**

Wt and IFNAR<sup>-/-</sup> recipients were lethally irradiated (a dose of twice 5.5 gray was given in a 6-hour interval). One day later, recipients were reconstituted with ~ 1x10<sup>7</sup> wt or IFNAR<sup>-/-</sup> BM cells and splenocytes.

After 5 weeks, a co-transfer of purified P14 Wt and P14 ST2<sup>-/-</sup> CD8 T cells was performed. Mice were infected the same day with LCMV CI-13 high dose. 9 days later, spleens were harvested and analyzed for the expansion capacity of the transferred cells. Transferred P14 Wt cells were distinguished from the endogenous CD8 T cells by gp33 MHC Class I tetramer staining.

#### **4.2.6 *In vivo* antibody blockade**

Mice were depleted of type I interferon by intraperitoneal (i.p.) injection of 1 mg of anti-IFNAR (MAR-1-5A3, BioXcell) one day before infection. Control groups were treated with 1mg of MOPC-21 (MOPC-21, BioXcell) one day before infection.

For transfer of P14 IFNAR<sup>-/-</sup> as well as P14 ST2<sup>-/-</sup> IFNAR<sup>-/-</sup>, NK cells were depleted as described in (342); depletion was performed by i.p. injection of 300 µg of α-NK.1.1 (clone PK136, BioXcell) 1 day before and after infection.

#### 4.2.7 Statistics

For comparison of one parameter between multiple groups, one-way analysis of variance (ANOVA) was used. Two-way ANOVA for comparison of multiple parameters between 2 or more groups. ANOVA was followed by Tukey's post-test for multiple comparisons. To compare multiple groups to a control group, Sidak's post-test was used. Data were analyzed using GraphPad Prism software (version 9).

### 4.3 Results

#### 4.3.1 The interplay of type I interferon and IL-33 in fostering an effective CD8 T cell response upon chronic antigen exposure

In chapter 3.3, we were able to show that besides its role in favoring Tcf-1 expression, IL-33 signaling is counterbalancing IFN-I. Moreover, we could show that IFN-I equalized the expansion of both transferred CD8 T cell populations (see Fig. 3-3 B-C). Thus, we were wondering to which extent the IFN-I driven proliferation was connected to an intrinsic component. For this, a co-transfer of P14 Wt and P14 ST2<sup>-/-</sup> CD8 T cells into IFNAR<sup>-/-</sup> was performed (Fig. 4-1 A). Under such conditions, only the transferred cells are able to respond to type I interferon. Interestingly, at day 8 of infection, there was a massive expansion of both ST2<sup>-/-</sup> and Wt P14 populations compared to Wt as well as α-IFNAR treated recipients. Despite the large increase of ST2<sup>-/-</sup> P14 cells in IFNAR recipients, these were still significantly lower than their Wt P14 counterparts (Fig. 4-1 B).

Since, type I interferon was shown to dampen Tcf-1 expression (117), it is important to understand whether IL-33 has any cross-talk on this effect on a CD8 T cell intrinsic level. For this, we generated a P14 ST2<sup>-/-</sup> IFNAR<sup>-/-</sup> mouse to have a deficiency in both signaling pathways. Importantly, based on the fact that NK cells were shown to mediate killing of activated P14 IFNAR<sup>-/-</sup> cells (185), NK cells were depleted. To measure the expansion capacity, same numbers of P14 Wt, P14 ST2<sup>-/-</sup>, P14 IFNAR<sup>-/-</sup> and P14 ST2<sup>-/-</sup> IFNAR<sup>-/-</sup> were transferred separately into NK-cell depleted Wt recipients (Fig. 4-2 A). Spleen cell analysis day 6 after infection showed the same impaired expansion capacity of P14 ST2<sup>-/-</sup> and P14 ST2<sup>-/-</sup> IFNAR<sup>-/-</sup> cells (Fig. 4-2 B). To make sure that P14 ST2<sup>-/-</sup> IFNAR<sup>-/-</sup> cells have similar functional properties, we performed a transfer of those cells into type I interferon blocked mice (Fig.4-2 C).

As shown in Fig.4-2 D, P14 ST2<sup>-/-</sup> IFNAR<sup>-/-</sup> cells expanded to the same extent as P14 Wt cells as soon as IFN-I was blocked. Thus, we concluded that P14 ST2<sup>-/-</sup> IFNAR<sup>-/-</sup> cells were not intrinsically impaired in their *in vivo* response.

Further analysis of all four transferred CD8 T cell populations clearly showed differences in their capacity to differentiate into CD8<sub>SCL</sub> cells (as determined by expression of Tcf-1<sup>+</sup> Tim-3<sup>-</sup> or co-expression of Tcf-1 and Ly108) (Fig. 4-2 E-G). As described by (117), P14 IFNAR<sup>-/-</sup> CD8 T cells showed the highest percentage of Tcf-1<sup>+</sup> Tim-3<sup>-</sup> cells (Fig. 4-2 E-F). Importantly, P14 ST2<sup>-/-</sup> IFNAR<sup>-/-</sup> cells showed in comparison to P14 IFNAR<sup>-/-</sup> CD8 T cells a clear reduction; the percentage of Tcf-1<sup>+</sup> Tim-3<sup>-</sup> cells was similar to the one observed in P14 ST2<sup>-/-</sup> CD8 T cells.

Moreover, both P14 IFNAR<sup>-/-</sup> as well as P14 ST2<sup>-/-</sup> IFNAR<sup>-/-</sup> CD8 T cells showed a significant reduction in the frequency of CX3CR1<sup>+</sup> Tcf-1<sup>-</sup> cells (Fig. 4-2 H).

#### **4.3.2 IFN-I sensing by hematopoietic cells results in an inflammatory environment in which ST2<sup>-/-</sup> CD8 T cells expand poorly**

To address the question whether hematopoietic or non-hematopoietic IFNAR sensing impaired the expansion of ST2<sup>-/-</sup> CD8 T cells, we performed an adoptive P14 co-transfer using bone marrow chimeric mice as recipients (Fig. 4-3 A). Interestingly, the expansion of P14 ST2<sup>-/-</sup> cells was largely restored when the hematopoietic compartment of the recipient was IFNAR<sup>-/-</sup> (Fig. 4-3 B). In contrast, IFNAR-deficiency of the radioresistant compartment did not restore P14 ST2<sup>-/-</sup> expansion. To further dissect how IFNAR signaling in various immune cell types contribute to the expansion of ST2-deficient CD8 T cells, we tested the expansion of P14 Wt and P14 ST2<sup>-/-</sup> CD8 T cells in recipients with cell-type specific IFNAR deletion. As shown in Fig. 4-3 C, IFNAR deletion in T cells (CD4<sup>Cre</sup>), B cells (CD19<sup>Cre</sup>), myeloid cells (LysM<sup>Cre</sup>) or dendritic cells (CD11c<sup>Cre</sup>) showed no clear effect. Although a statistically significant effect can be observed in CD19<sup>Cre</sup> IFNAR<sup>fl/fl</sup> as well as in LysM<sup>Cre</sup> IFNAR<sup>fl/fl</sup> mice, this effect is due to a lower proliferation of P14 Wt cells in these recipient mice, whereas the expansion capacity of P14 ST2<sup>-/-</sup> cells is not affected.

#### **4.3.3 The impaired expansion of ST2<sup>-/-</sup> CD8 T cell cannot be explained by a higher sensitivity towards the immunosuppressive cytokine IL-10**

One reason postulated for the enhanced viral control observed in type I interferon blocked mice is the downregulation of IL-10 producing suppressor cells (174). Indeed, blockade of IL-10 during early LCMV Cl-13 infection resulted in viral clearance (101, 102). Although the success of IL-10 blockade critically depends on the virulence of the infecting strain (360), IL-10 blockade may provide a novel therapeutic target to potentially enhance CD8 T cell responses (361).

Based on these data, we were wondering whether a crosstalk between IL-33 and IL-10 is existing (Fig. 4-4 A). Thus, we tested the expansion capacity of P14 ST2<sup>-/-</sup> CD8 T cells transferred into IL-10<sup>-/-</sup> recipients (Fig. 4-4 B). At day 9 after infection, transferred P14 ST2<sup>-/-</sup> CD8 T cells showed the same impaired expansion in IL-10<sup>-/-</sup> mice as it is observed for Wt mice. Thus, IL-10 cannot be seen as a factor restricting the expansion capacity of ST2<sup>-/-</sup> CD8 T cells.

#### 4.4 Discussion

In this chapter, we were able to gain further insight about the interplay of IL-33 and type I interferon in the context of a chronic infection.

Based on the fact that the different expansion potential between P14 Wt and P14 ST2<sup>-/-</sup> CD8 T cells converged when transferred into either IFNAR<sup>-/-</sup> or  $\alpha$ IFNAR treated mice, the impact of IFNAR blockade and ST2 signaling in CD8 T cells appears to be multifactorial. The fact that both CD8 T cell populations expanded to a higher extent in IFNAR<sup>-/-</sup> recipients points out that the higher availability of type I interferon present in these mice contribute to higher proliferation of transferred cells independently of the ST2 receptor expression. However, given that ST2<sup>-/-</sup> cells still proliferated to a lower extent than P14 Wt cells clearly suggest the importance of IL-33 to sustain a higher level of proliferation (Fig. 4-1 B). Moreover, these data are in line with the data presented in chapter 3.3 and support the concept of an IFN-I independent effect on IL-33 bioavailability. Yet, the pleiotropic differences in IFNAR<sup>-/-</sup> recipients do not allow us to exclude the possibility that the different inflammatory milieu present in these mice might have compensatory effects on IL-33 signaling deficiency.

The data obtained from studying the phenotype of P14 IFNAR<sup>-/-</sup> ST2<sup>-/-</sup> (Fig. 4-2) clearly point out that on a single cell level, the impaired Tcf-1 expression levels observed in ST2 deficient CD8 T cells cannot be compensated by intrinsic IFN-I blockade. By this, IL-33 can be defined as the dominant factor to ensure Tcf- 1 expression on a cell-intrinsic basis.

In accordance with data obtained from studying the phenotype of P14 IFNAR<sup>-/-</sup> in an acute infection, P14 IFNAR<sup>-/-</sup> showed lower levels of CX3CR1<sup>+</sup> effector-like CD8 T cells in the context of a chronic infection. Similar results were seen with P14 IFNAR<sup>-/-</sup> ST2<sup>-/-</sup> cells, whereas P14 ST2<sup>-/-</sup> CD8 T cells showed still higher levels of CX3CR1. These data point out that IFN-I function as a potent adjuvant for the generation of CD8<sub>EF</sub>. In summary, IFN-I is acting directly on CD8 T cells by tilting programming balance from CD8<sub>SCL</sub> towards CD8<sub>EF</sub>. Such data suggests that while IFN-I blockade maintains a stem-like CD8 T cell population, as it was proposed by (117), it also prevents efficient differentiation of CD8 T<sub>SCL</sub> cells into CD8 T<sub>EF</sub>. The higher CD8 T<sub>SCL</sub> arising upon IFN-I blockade thus appear to be functionally impaired by developmental arrestment. To clearly address the question to which extent IFNAR<sup>-/-</sup> CD8 T<sub>SC</sub> cells are able to differentiate into CD8 T<sub>EF</sub>, an adoptive transfer of sorted P14 IFNAR<sup>-/-</sup> Tcf<sup>tgfp+</sup> and P14 Tcf<sup>tgfp+</sup> Wt counterparts in naïve mice challenged with LCMV Cl-13 would be an option.

Furthermore, we were able to highlight that the effects of IFN-I on the expansion of ST2<sup>-/-</sup> CD8 T cells are based on hematopoietic IFNAR sensing (Fig. 4-3). To further dissect how IFNAR signaling in various

immune cell types is affecting the expansion of ST2-deficient CD8 T cells, cell-type specific IFNAR deletion models were used. As shown in Fig. 4-3 C, neither of the cell-type specific IFNAR deletion models phenocopied the data observed in IFNAR<sup>-/-</sup> or  $\alpha$ IFNAR-treated mice. Although, lineage-specific Cre deletion models have certain limitations (362), the presented data suggest that the different expansion kinetics of P14 ST2<sup>-/-</sup> CD8 T cells observed in type I interferon blocked mice, might result from IFNAR sensing by two or more hematopoietic cell types and cannot be restricted to a single cell compartment.

Nevertheless, it is possible that an unstudied cell compartment might be responsible for the observed effect such as NK cells that are known to be fully activated upon IFNAR signaling (363). Such hypothesis could be tested by transferring P14 Wt and P14 ST2<sup>-/-</sup> CD8 T cells into Ncr-1 Cre IFNAR fl/fl mice. In these mice, Cre-mediated deletion was shown to be tightly restricted to NK cells (364).

Importantly, cell numbers of both P14 Wt and P14 ST2<sup>-/-</sup> CD8 T cells in CD4<sup>Cre</sup> IFNAR<sup>fl/fl</sup> mice, which are IFNAR-deficient in both CD4 and CD8 T cell compartments, are comparable to Wt controls (Fig. 4-3 C). As such, the rescue of P14 ST2<sup>-/-</sup> observed in IFNAR<sup>-/-</sup> recipient mice cannot be explained by a higher competitiveness over the endogenous, IFNAR<sup>-/-</sup> T cell compartment.

Based on the fact that IFN-I is regulating IL-10 expression and having the anti-proliferative effects of IL-10 in mind (101, 102), strongly suggested that IL-10 might be dispensable for the type I interferon effect on expansion of ST2-deficient CD8 T cells. However, in comparison to Wt mice, no phenotypic differences were observed in an IL-10 free environment.

Collectively, these data highlight the overall complexity of type I interferon. Due to its broad spectrum on several immune mechanisms, it is indeed challenging to understand whether the observed extrinsic effects of IFN - I on CD8 T cells are a direct consequence of IFNAR signaling in certain immune cell compartments or whether it is due to a shift in downstream signaling cascades in these cells.

Moreover, we provide fundamental insight into the T-cell intrinsic role of IL-33 for the compensation of type I interferon. On a single cell-level, IL-33 can be considered as the dominant factor regulating Tcf-1 expression. By this, our data favor IL-33 stimulation over IFN-I blockade as the prime candidate to enable the generation of a stable pool of fully functional CD8 T<sub>SCL</sub> cells which are critically needed in chronic diseases where high antigenic load is present.

## 4.5 Figures

**Figure 1**

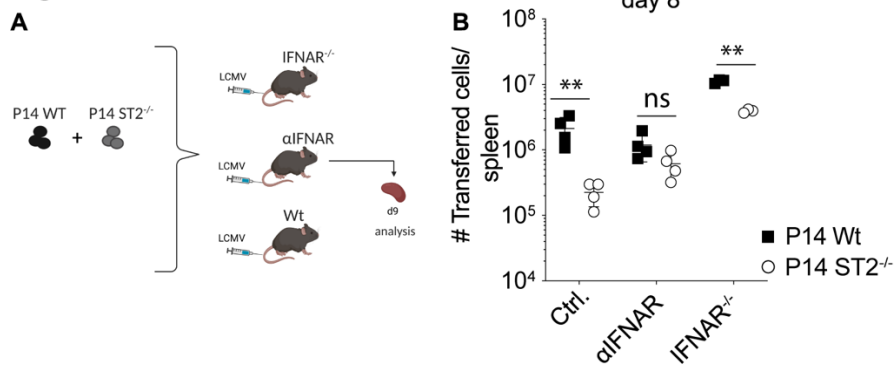


Figure 4-1 Comparison of the expansion kinetics of P14 Wt and P14 ST2<sup>-/-</sup> CD8 T cells in type I interferon depleted mice in comparison to IFNAR<sup>-/-</sup> mice

A: Experimental set-up used in B. Co-transfer of P14 Wt and P14 ST2<sup>-/-</sup> CD8 T cells into IFNAR<sup>-/-</sup>, Wt and type I interferon blocked mice followed by LCMV CI-13 infection. B: Total number of P14 Wt and P14 ST2<sup>-/-</sup> cells day 8 after infection. Statistical analysis: Two-way ANOVA with Sidak's test for multiple comparison. Ns: not significant; \*:  $p < 0.05$ ; \*\*:  $p < 0.01$ . Data are representative for one experiment. Symbols ( $n=4$  per group) with mean  $\pm$  SEM.



**Figure 2**

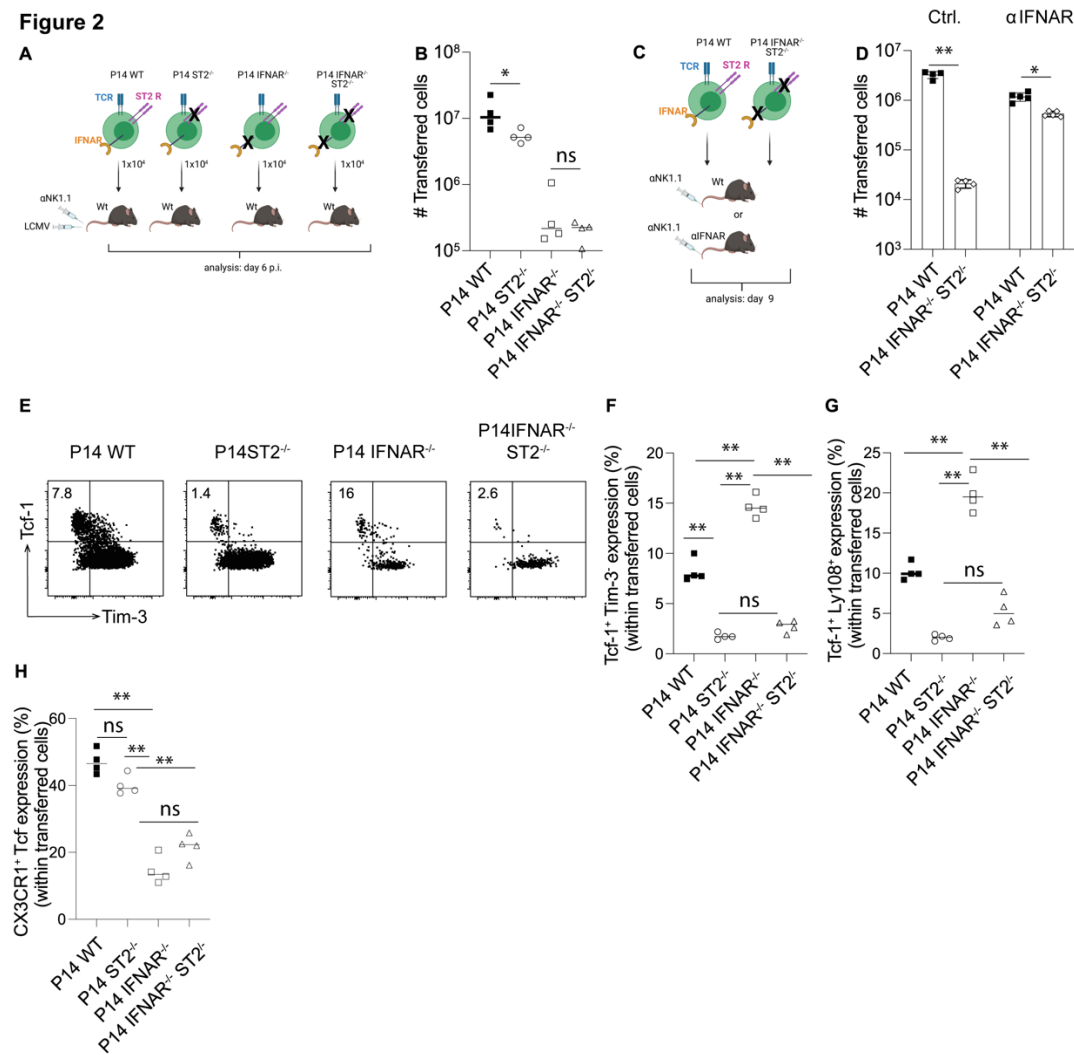
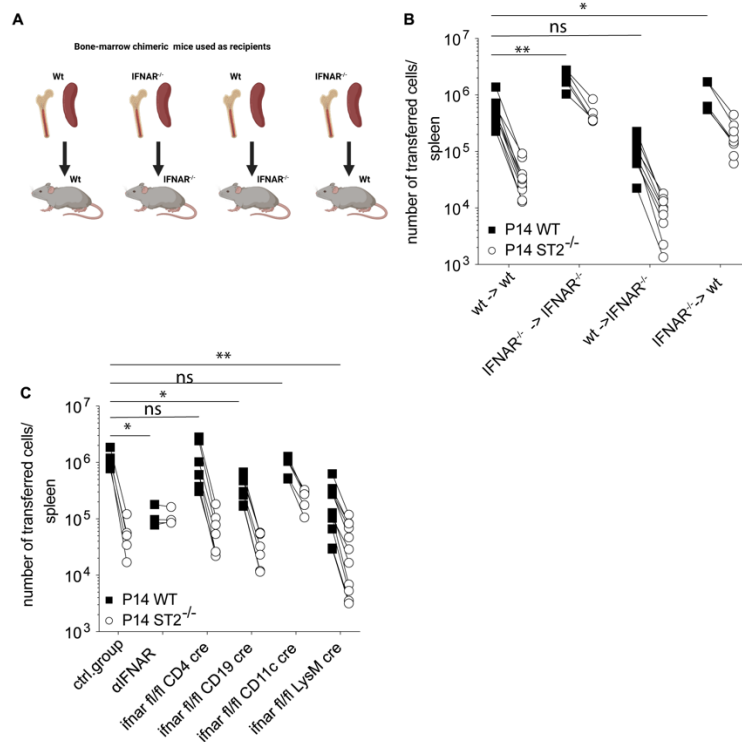


Figure 4-2 IL-33 signaling is compensating IFN-I signaling on a single cell level

A: Experimental set-up used in B, E-H. Single transfer of P14 Wt, P14 ST2<sup>-/-</sup>, P14 IFNAR<sup>-/-</sup> and P14 ST2<sup>-/-</sup> IFNAR<sup>-/-</sup> in Wt mice followed by LCMV Cl-13 infection. B: Total number of transferred cells day 6 p.i. All recipients were NK-cell depleted as described in material and methods. C: Experimental set-up used in C: Co-transfer of P14 Wt and P14 ST2<sup>-/-</sup> IFNAR<sup>-/-</sup> in either type I interferon blocked mice or isotype treated mice. All recipients were NK-cell depleted. D: Total numbers of transferred cells on day 9 after LCMV Cl-13 infection. E: Representative FACS plots showing the expression of Tcf-1 and Tim-3 by P14 Wt, P14 ST2<sup>-/-</sup>, P14 IFNAR<sup>-/-</sup> and P14 ST2<sup>-/-</sup> IFNAR<sup>-/-</sup> cells on day 6 after infection. Numbers on FACS plots indicate the frequency of each gated population. F: Percentage of Tcf-1<sup>+</sup> Tim-3<sup>-</sup> CD8 T cells shown for the indicated CD8 T cell populations. G: Percentage of Tcf-1<sup>+</sup> Ly108<sup>+</sup> CD8 T cells shown for the indicated CD8 T cell populations. H: Percentage of CX3CR1<sup>+</sup> Tcf-1<sup>+</sup> CD8 T cells shown for the indicated CD8 T cell populations. Statistical analysis: (B, F-H) Two-way ANOVA with Sidak's test for multiple comparison. D: One-way ANOVA with Tukey's test for multiple comparisons. Ns: not significant; \*:  $p < 0.05$ ; \*\*:  $p < 0.01$ .

Data are representative for one (D) to two (B, E, F, G and H) experiments. Symbols (n=5 per group) with mean ± SEM.

**Figure 3**



*Figure 4-3 Understanding the role of hematopoietic and non-hematopoietic IFNAR signaling for the expansion of P14 ST2<sup>-/-</sup> CD8 T cells*

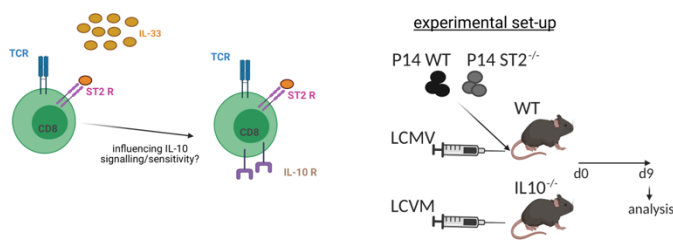
A: Experimental set-up used in B. Generation of reciprocal Wt and IFNAR<sup>-/-</sup> BM chimeras. B: Co-transfer of P14 Wt and P14 ST2<sup>-/-</sup> CD8 T cells into reciprocal Wt and IFNAR<sup>-/-</sup> BM chimeras. Final analysis was done 9 days after LCMV Cl-13 high dose infection. C: Co-transfer of P14 Wt and P14 ST2<sup>-/-</sup> CD8 T cells into recipients with cell-type specific IFNAR deletion. Analysis was done 9 days after LCMV Cl-13 high dose infection.

Statistical analysis: (B) Two-way ANOVA with Dunnett's multiple comparison test. Wt->Wt group was used as reference. C: Two-way ANOVA with Dunnett's multiple comparison test. Each data set was compared to Ctrl. Group. Ns: not significant; \*:  $p < 0.05$ ; \*\*:  $p < 0.01$ .

Data are representative for two independent experiment. Both graphs show the results from both experiments. Symbols (n=5 per group and experiment) with mean  $\pm$  SEM.

## Figure 4

**A**



**B**

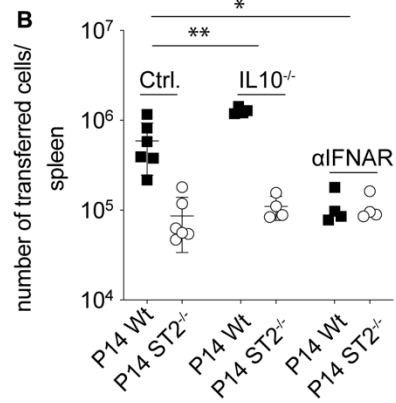


Figure 4-4 Comparison of the expansion kinetics of P14 Wt and P14 ST2<sup>-/-</sup> CD8 T cells in IL-10<sup>-/-</sup> mice compared to Wt recipients

A: Schematic overview summarizing potential link between IL-33 and IL-10 signaling. B: Co-transfer of P14 Wt and P14 ST2<sup>-/-</sup> CD8 T cells into reciprocal Wt and IL10<sup>-/-</sup> mice followed by LCMV CI-13 infection. Analysis was performed day 9 after infection. Statistical analysis: (B) Two-way ANOVA with Dunnett's test for multiple comparison. Ctrl. group was used as reference. Ns: not significant; \*:  $p < 0.05$ ; \*\*:  $p < 0.01$ .

Data are representative for one experiment. Symbols (n=4-5 per group) with mean  $\pm$  SEM.

### III. Global Discussion and Perspectives

For the development of new therapeutic approaches for chronic microbial diseases and cancer, a profound understanding of the molecular signals directing the immune response is of high importance. Besides inflammatory signals, both the amount and form of antigen-presentation are key components for a proper activation of the adaptive immune response. However, it is still poorly understood to which extent viral antigenic presence is modulating the ongoing immune response after a replicating viral infection is resolved (365). Moreover, a more profound knowledge on how the signaling pathways present in the initial inflammatory milieu affects the long-term immune differentiation is equally warranted. Both of these phenomena are of crucial importance for rational vaccine design, as well as having a better understanding on how the immune system can be further manipulated for greater treatment efficiency. Indeed, besides the revolutionary impact of the checkpoint inhibitor therapy (366), a more complete understanding of the molecular signaling pathways are key for the improvement of several immune therapies already in clinical use, such as CAR-T cell engineering (367), platforms for cytokine delivery (368) or inhibition (369), and enhancing antigenic availability (370-372). By the use of the LCMV infection model both these questions could be addressed simultaneously throughout this thesis.

In the first part, we were able to highlight how in transiently CD4 T cell depleted mice, residual antigen can still shape the virus-specific B cell response after a replicating LCMV infection is eliminated. A more detailed analysis showed that the LCMV antigen-depots were capable of inducing a robust LCMV-plasma cell differentiation, whereas the generation of LCMV-specific memory B-cells was impaired.

In the second part, we were able to demonstrate that a heterologous prime-boost combination of two distantly related arenavirus-vectors expressing a tumor-antigen provided a long-term anti-tumor CD8 T cell response capable of tumor growth control.

Finally, in the third part, we demonstrate that the IL-33/ST2 axis plays a critical role in driving a potent anti-viral CD8 T cell response in the context of a chronic LCMV infection.

As demonstrated in chapter 1, despite the fact that an acute LCMV infection is controlled in the first 8 days after inoculation, the generation of antigenic-depots continued to modulate immune differentiation, in particular B cells, long after active viral replication. Such findings were independent of CD4 T cell and B cell priming at the infection onset, since CD4 T cells were transiently depleted immediately before infection. The proliferation of LCMV GP specific B cells transferred in recipient mice which had long cleared an acute LCMV infection, pointed out that sufficient antigenic availability had to be provided. Similar results were shown for the endogenous NP specific B cell response. Such data strongly corroborates the generation of long lived antigenic-depots even in the context of an acute LCMV infection. Moreover, since CD4 T cells were transiently depleted upon acute infection, the proliferation of NP specific B cells cannot be attributed to an ongoing germinal center response generated during active infection. Upon a closer look into the NP specific B cell response, a striking phenotypic differentiation can be appreciated between transiently CD4 T depleted mice and the control group. Whereas the memory B cell formation was intact in the control group,

such compartment was clearly reduced in anti-CD4 T cell treated mice. Such findings suggest that the initial priming of the CD4 T cell help is crucial for the development of a memory B cell response, while the repopulating CD4 T cells cannot shepherd newly activated B cells towards memory B cell formation. Additionally, in CD4 T cell depleted mice later B cell proliferation is critically dependent on the newly generated CD4 T cells since in MHC-II deficient mice the B cell response is absent (compare Fig. S 1-3). As such, this data points out that antigen specific CD4 T cells primed under the initial inflammatory milieu of a LCMV infection can instruct broader developmental choices of activated B cells, whereas B cells instructed by the repopulating antigen specific CD4 T cells are developmentally constricted. Indeed, IL-33, a key cytokine in the early phase of LCMV infection, was shown to enhance the expansion of polyfunctional anti-viral CD4 T cells (152). At the time-point of CD4 T cell repopulation, IL-33 or other equally relevant cytokines (e.g. IL-21 (206)) might be no longer available, thus giving rise to a functionally different CD4 T cell population. Besides the inflammatory milieu the lower antigen level might also be a key determinant for the developmental choices of the repopulating CD4 T cells in comparison with the early primed CD4 T cells (373). To differentiate between these two theories, a protein immunization experiment at the timepoint of CD4 T cell repopulation would provide further insight about this data.

As previously shown, the IL-33 pathway is one of the key components for an effective CD8 T cell response after a LCMV infection. Moreover, the ability of IL-33 to stimulate an effective CD8 T response is also observed in the context of a viral vectored immunization such as artARENA-vector cancer therapy (58) (shown in chapter 2). Indeed, IL-33 dependent vectors were shown to better induce a functional CD8 T cell response in comparison to IL-33 independent vectors. Based on this, it was of further interest to study the IL-33 dependency for other Arenavirus-based vectors as potential vaccine candidates. Interestingly, IL-33 dependency was not observed in all Arenavirus-candidates tested. In comparison to artPICV, artCAND immunization showed no dependency on IL-33 for CD8 T cell expansion. However, the CD8 T cell expansion upon artCAND administration was severely limited, thus further strengthening the role of IL-33 for an efficient CD8 T cell expansion in vector immunization.

Such data raises the more general question of which parameters lead to the induction of an IL-33 dependent antiviral CD8 T cell response. Is the mere release of IL-33 sufficient for a more potent antiviral CD8 T cell response or is it the interplay between IL-33 and the surrounding inflammatory milieu? A significant hurdle is the fact that IL-33 is constitutively expressed in the nucleus of most cells thus greatly limiting the ability to distinguish between nucleus stored IL-33 from exogenous IL-33 (released). Despite the limited knowledge, there are several possible explanations: (see Fig. S 0-1)

Firstly, ST2 receptor induction. As shown by (168), ST2 receptor expression on CD8 T cells is strictly dependent on STAT-4 signaling. Cytokines that activate STAT-4 are IL-12, IFN- $\gamma$ , IL-23, IL-2, IL-27 and IL-35 (374). To which extent the virus of interest provides the inflammatory environment that leads to STAT-4 pathway stimulation on CD8 T cells resulting in ST2 receptor upregulation is not known.

Secondly, as shown by (58) artLCMV vectors target IL-33 expressing stromal cells, which results in an IL-33 enhanced CD8 T cell response. In this regard, differences in the capacity of the involved virus/vector to activate IL-33 expressing cells might play a role, since replication deficient vectors are not detectable in IL-33 expressing cells.

Thirdly, besides the tropism/invasiveness of the virus strain, the antigen-dose can be considered as another factor. IL-33 has a very short biological half-life since extracellular IL-33 is rapidly inactivated upon extracellular release by oxidation which results in the formation of two disulfide bridges in the IL-1-like cytokine domain (145). The limited availability of biologically active IL-33 speaks thus towards the theory that IL-33 signaling must occur in a very short time window. The antigen-presenting capacity of FRCs might thereby play an important role. If the antigen-dose is too low and a prolonged and stable surface presentation of MHC complexes is not enabled, the chance of IL-33 binding is quite low. Besides the antigen-dose itself, the number of virus-presenting FRCs might be another important aspect. T cells and antigen-presenting cells (APC) are interacting in a very intimate fashion (immunological synapse) (375, 376), moreover it is well described that high numbers of APCs could provide a more efficient and sustained signal. Thus, it might be possible that one requirement is that the whole layer of FRCs has to be infected to provide a stable T cell FRC interaction. However, it is not presently known whether an antigen presenting FRC is also releasing IL-33.

Fourthly, as pointed out in chapter 3 and 4, IL-33 is counterbalancing IFN-I signaling to assure differentiation into CD8 T<sub>SCL</sub> cells. Upon IFN-I blockade, IL-33 signaling has no enhancing effect, based on the fact that the phenotypically differences between Wt and ST2<sup>-/-</sup> CD8 T cells are annulled. Such data points towards the conclusion that IFN-I sensing might be one of the main criteria that defines the anti-viral CD8 T cell expansion dependency on IL-33. Indeed, replication deficient LMCV-based vaccine vectors are poor inducers of IFN-I (58) and induce identical CD8 T cell responses in Wt and ST2<sup>-/-</sup> mice (59). However, such a correlation could not be made for Wt Vaccinia Virus (VV), which showed an impaired CD8 T cell response in ST2<sup>-/-</sup> mice. Since Vaccinia has evolved sophisticated strategies to strongly inhibit IFN-I signaling (377), IFN-I cannot be seen as the only determinant for IL-33 driven CD8 T cell expansion.

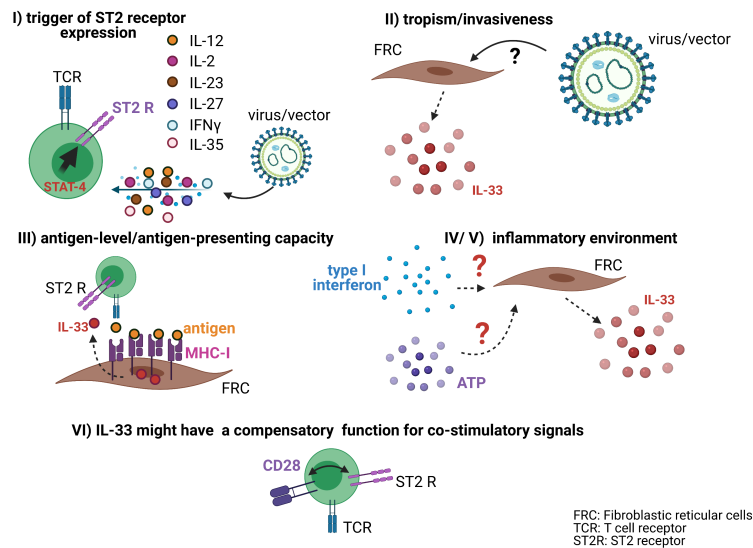
Fifthly, the release might be caused by the inflammatory environment such as by other damage-associated molecular patterns (DAMP). Indeed, it was shown that ATP, that is considered as a classical DAMP released by stressed cells, is inducing the release of IL-33 by human bronchial airway epithelial cells in cell culture (378). However, whether such observations can be applied to a more physiological stimuli, such as a viral infection, remain to be determined.

Sixthly, in general, one could argue that the dependency on IL-33 for the induction of an antiviral CD8 T cell response might be due to a compensatory function for co-stimulatory signals on CD8 T cells. In this regard, we excluded the possibility of a compensatory effect of IL-33 for CD28. In the course of an LCMV infection, CD8 T cells do not require CD28 signaling (379, 380). To exclude that IL-33 might have a compensatory effect, we transferred P14 CD28<sup>-/-</sup> cells into Wt and IL-33<sup>-/-</sup> mice infected with LCMV (unpublished data-generated with Dr. Weldy Bonilla). Since there were no differences in the expansion of

both cell populations, the possibility that CD28 co-stimulation is a critical factor in determining the requirement for IL-33 signaling can thus be ruled out.

Overall, it is possible that the inflammatory, antigenic load, and replication kinetics of the virus might play an important role for IL-33 release.

In conclusion, despite the limited knowledge, pathogen-specific conditions appear to differentially and uniquely dictate the need of the IL-33/ST2 axis for shaping effector CD8 T cell differentiation.



S 0-1 Schematic overview summarizing the potential parameters leading to the induction of an IL-33 dependent antiviral CD8 T cell response

(generated with biorender.com)

Upon release IL-33 is besides IL-21 (381, 382) the only cytokine that shows an enhancing function on the survival of antigen-specific CD8 T cells upon chronic infection. With the data presented in this thesis, we could highlight the importance of IL-33 for the generation of Tcf-1 expressing cells. To exclude the possibility that the observed link might be due to the infectious context, an *in vitro* system was established. The *in vitro* activated CD8 T cells showed higher Tcf-1 expression upon IL-33 stimulus, thus pointing towards an infection independent effect. In this context, it should be mentioned that the link seems to exist exclusively for CD8 T cells based on the fact that the differentiation of CD4 T cells that rely on Tcf-1 expression (e.g. Tfh) (383) is not affected by the absence of IL-33 (unpublished data-generated with Dr. Tiago Abreu Mota).

Our data are not only providing a new mechanism on how IL-33 is influencing the differentiation of CD8 T cells in a chronic infection but also allow to re-interpret previous data. As reported by (168), IL-33 is required for efficient secondary expansion. Tcf<sup>-/-</sup> CD8 T cells showed an impaired recall response upon infection (349, 384) and by this recapitulate to a certain extent the phenotype of ST2<sup>-/-</sup> CD8 T cells. Overall, one could conclude that the impaired recall response in the absence of IL-33 is linked to an impaired Tcf-1 expression.

But does the reduction in Tcf-1 expressing compartment explains the dramatic expansion defect of ST2<sup>-/-</sup> CD8 T cells?

In the setting of an acute infection, Tcf-1 deficient mice have been reported to show a comparable CD8 T cell response (349). Conversely, the transfer of TCR transgenic CD8 T cells as shown in (384) showed a clear defect in terms of expansion pointing towards a CD8 T cell intrinsic deficiency.

In the context of a chronic LCMV infection, controversial data were published. Groups using Tcf fl/fl-CD4 Cre (385) or Rosa26<sup>GFP</sup>Tcf7<sup>fl/fl</sup>hCD2-Cre<sup>+</sup> (121) mice reported a reduced population size in the early phase of the infection. Others have reported that Tcf-1 expression is not influencing the CD8 T cell expansion and is more important for the T cell maintenance (120). In this particular publication, the Tcf-1 deficient mouse that was used was generated by disrupting the murine Tcf-1 gene, thus the findings might not be readily comparable (386). To clearly make a statement towards the link between Tcf-1 and the reported expansion defect of ST2-deficient CD8 T cells, it would be of importance to further study the Tcf-1 deficient CD8 T cell models.

Exogenous supplementation with IL-33 may augment/potentiate stem-like CD8 T cell responses in chronic infection. To experimentally address such a question two main aspects, have to be considered: Firstly, at which time-points should the treatment start? Based on the presented data as well as on previous results (136), IL-33 release seems to occur within the first days of infection, coinciding with the peak of ST2 receptor expression (around day 6/8 p.i.). Nevertheless, we were able to show that antiviral CD8 T cells do express the ST2 receptor, albeit at a lower level, on later time-points of the infection. Transfer of P14 Wt/P14 ST2<sup>-/-</sup> CD8 T cells in preinfected mice pointed out that the effect of ST2 deficiency on CD8 T cell expansion is only of importance during the first 15 days or even less. Such data are speaking towards two different theories: i) Early IL-33 signaling may have an imprinting effect or ii) a prolonged IL-33 stimulus is influencing the behavior of the cells.

To gain an idea at which time-points IL-33 has an impact on the CD8 T cells, we generated an inducible ST2-knock-out mouse. The phenotypic characterization of such mouse by inducing the deletion of the receptor at several time-points would provide further insight. Yet, the data obtained from the adoptive transfer experiments would rather speak towards an imprint mechanism. Although exogenously provided IL-33 could further elucidated whether a continues effect of IL-33 on CD8 T cell differentiation exists, such an experimental set up is not without caveats, since IL-33 has a pleotropic effect and might not rely on a direct CD8 T cell effect. Indeed, based on the fact that IL-33 was shown to also stimulate antigen-presenting cells such as DCs to upregulate MHC class II expression and other co-stimulatory signals (156) the IL-33 therapy can accelerate LCMV chronic infection clearance independently of its direct effect on anti-viral CD8 T cells.

Secondly, how can we sustain an exogenous IL-33 stimulus *in vivo* given the short half-life of IL-33? One idea would be to deliver IL-33 in form of an adeno-associated vector (AAV), as previously shown for IL-2. If we would succeed in enhancing the differentiation/maintenance of stem-like CD8 T cells, a logical next step would consist in the generation of ST2-agonistic monoclonal antibodies as a therapeutic modality.



Moreover, based on the fact that different isoforms of full-length IL-33 and spliced variants of mature IL-33 (166) show different biological activities, a ST2-agonistic monoclonal antibody could overcome such biological variability.

Taking into account the dual role of IL-33 in the cancer field, IL-33 targeting therapies should be considered with caution. Indeed, several studies proposed cancer immunotherapy strategies based on exogenous IL-33 administration (167, 351, 387), whereas others suggested to block IL-33 as a novel anticancer strategy (388-390). The opposing roles in tumorigenesis might also be applied to viral infection as discussed in (391).

In conclusion, the dependency on IL-33 for anti-viral and anti-tumor immunotherapies might depend on the site of infection, the duration of the disease and the cytokine milieu.

Overall, this thesis provides fundamental insight how CD8 T cells are functionally differentiated after infection. By dissecting the critical role of IL-33 in inducing the formation of the CD8 T<sub>SCL</sub> population, which is responsible for producing and maintaining the effector CD8 T cell response throughout a chronic condition, a new therapeutical candidate can be considered in immunotherapy. Without the CD8 T<sub>SCL</sub> population, major immunomodulatory therapies currently in use, such as checkpoint inhibitors and other therapies targeting the reversion of CD8 T cell exhaustion would not be possible. Thus, defining the pathways that safeguard the generation of CD8 T<sub>SCL</sub> cells is defining new immunomodulatory therapeutical approaches for chronic diseases.

## IV. References

1. J. C. de la Torre, Molecular and cell biology of the prototypic arenavirus LCMV: implications for understanding and combating hemorrhagic fever arenaviruses. *Ann N Y Acad Sci* 1171 Suppl 1, E57-64 (2009).
2. S. R. Radoshitzky *et al.*, Past, present, and future of arenavirus taxonomy. *Arch Virol* 160, 1851-1874 (2015).
3. S. F. Emonet, J. C. de la Torre, E. Domingo, N. Sevilla, Arenavirus genetic diversity and its biological implications. *Infect Genet Evol* 9, 417-429 (2009).
4. R. N. Charrel, X. de Lamballerie, S. Emonet, Phylogeny of the genus Arenavirus. *Curr Opin Microbiol* 11, 362-368 (2008).
5. N. D. N *et al.*, Evidence of lymphocytic choriomeningitis virus (LCMV) in domestic mice in Gabon: risk of emergence of LCMV encephalitis in Central Africa. *J Virol* 89, 1456-1460 (2015).
6. R. N. Charrel *et al.*, New insights into the evolutionary relationships between arenaviruses provided by comparative analysis of small and large segment sequences. *Virology* 317, 191-196 (2003).
7. K. G. Andersen *et al.*, Clinical Sequencing Uncovers Origins and Evolution of Lassa Virus. *Cell* 162, 738-750 (2015).
8. L. Zeitlin *et al.*, Monoclonal antibody therapy for Junin virus infection. *Proc Natl Acad Sci U S A* 113, 4458-4463 (2016).
9. J. I. Maiztegui *et al.*, Protective efficacy of a live attenuated vaccine against Argentine hemorrhagic fever. AHF Study Group. *J Infect Dis* 177, 277-283 (1998).
10. D. A. Enria, J. G. Barrera Oro, Junin virus vaccines. *Curr Top Microbiol Immunol* 263, 239-261 (2002).
11. J. B. McCormick, in *Encyclopedia of Virology (Third Edition)*, B. W. J. Mahy, M. H. V. Van Regenmortel, Eds. (Academic Press, Oxford, 2008), pp. 203-212.
12. K. Rosenke *et al.*, Use of Favipiravir to Treat Lassa Virus Infection in Macaques. *Emerg Infect Dis* 24, 1696-1699 (2018).
13. L. L. Barton, C. J. Peters, T. G. Ksiazek, Lymphocytic choriomeningitis virus: an unrecognized teratogenic pathogen. *Emerg Infect Dis* 1, 152-153 (1995).
14. D. J. Bonthius, Lymphocytic choriomeningitis virus: an underrecognized cause of neurologic disease in the fetus, child, and adult. *Semin Pediatr Neurol* 19, 89-95 (2012).
15. S. Drager *et al.*, Lymphocytic choriomeningitis virus meningitis after needlestick injury: a case report. *Antimicrob Resist Infect Control* 8, 77 (2019).
16. S. A. Fischer *et al.*, Transmission of lymphocytic choriomeningitis virus by organ transplantation. *N Engl J Med* 354, 2235-2249 (2006).
17. M. M. Sheinbergas, Hydrocephalus due to prenatal infection with the lymphocytic choriomeningitis virus. *Infection* 4, 185-191 (1976).
18. L. L. Barton *et al.*, Congenital lymphocytic choriomeningitis virus infection in twins. *Pediatr Infect Dis J* 12, 942-946 (1993).
19. G. M. Komrower, B. L. Williams, P. B. Stones, Lymphocytic choriomeningitis in the newborn; probable transplacental infection. *Lancet* 268, 697-698 (1955).
20. S. Cordey *et al.*, Analytical validation of a lymphocytic choriomeningitis virus real-time RT-PCR assay. *J Virol Methods* 177, 118-122 (2011).
21. K. A. Eberhardt *et al.*, Ribavirin for the treatment of Lassa fever: A systematic review and meta-analysis. *Int J Infect Dis* 87, 15-20 (2019).

22. M. Mendenhall *et al.*, T-705 (favipiravir) inhibition of arenavirus replication in cell culture. *Antimicrob Agents Chemother* 55, 782-787 (2011).
23. M. Mendenhall *et al.*, Effective oral favipiravir (T-705) therapy initiated after the onset of clinical disease in a model of arenavirus hemorrhagic fever. *PLoS Negl Trop Dis* 5, e1342 (2011).
24. D. Safronetz *et al.*, The broad-spectrum antiviral favipiravir protects guinea pigs from lethal Lassa virus infection post-disease onset. *Sci Rep* 5, 14775 (2015).
25. R. M. Zinkernagel, P. C. Doherty, H-2 compatibility requirement for T-cell-mediated lysis of target cells infected with lymphocytic choriomeningitis virus. Different cytotoxic T-cell specificities are associated with structures coded for in H-2K or H-2D. *J Exp Med* 141, 1427-1436 (1975).
26. E. J. Wherry, T cell exhaustion. *Nat Immunol* 12, 492-499 (2011).
27. P. C. Doherty, R. M. Zinkernagel, T-cell-mediated immunopathology in viral infections. *Transplant Rev* 19, 89-120 (1974).
28. D. L. Barber *et al.*, Restoring function in exhausted CD8 T cells during chronic viral infection. *Nature* 439, 682-687 (2006).
29. P. S. Ohashi *et al.*, Ablation of "tolerance" and induction of diabetes by virus infection in viral antigen transgenic mice. *Cell* 65, 305-317 (1991).
30. M. B. Oldstone, M. Nerenberg, P. Southern, J. Price, H. Lewicki, Virus infection triggers insulin-dependent diabetes mellitus in a transgenic model: role of anti-self (virus) immune response. *Cell* 65, 319-331 (1991).
31. K. E. Pauken, E. J. Wherry, Overcoming T cell exhaustion in infection and cancer. *Trends Immunol* 36, 265-276 (2015).
32. K. Catakovic, E. Klieser, D. Neureiter, R. Geisberger, T cell exhaustion: from pathophysiological basics to tumor immunotherapy. *Cell Commun Signal* 15, 1 (2017).
33. C. J. Pfau, J. K. Valenti, D. C. Pevear, K. D. Hunt, Lymphocytic choriomeningitis virus killer T cells are lethal only in weakly disseminated murine infections. *J Exp Med* 156, 79-89 (1982).
34. R. Ahmed, A. Salmi, L. D. Butler, J. M. Chiller, M. B. Oldstone, Selection of genetic variants of lymphocytic choriomeningitis virus in spleens of persistently infected mice. Role in suppression of cytotoxic T lymphocyte response and viral persistence. *J Exp Med* 160, 521-540 (1984).
35. A. Bergthaler *et al.*, Viral replicative capacity is the primary determinant of lymphocytic choriomeningitis virus persistence and immunosuppression. *Proc Natl Acad Sci U S A* 107, 21641-21646 (2010).
36. M. Salvato, E. Shimomaye, P. Southern, M. B. Oldstone, Virus-lymphocyte interactions. IV. Molecular characterization of LCMV Armstrong (CTL+) small genomic segment and that of its variant, Clone 13 (CTL-). *Virology* 164, 517-522 (1988).
37. M. Matloubian, T. Somasundaram, S. R. Kolhekar, R. Selvakumar, R. Ahmed, Genetic basis of viral persistence: single amino acid change in the viral glycoprotein affects ability of lymphocytic choriomeningitis virus to persist in adult mice. *J Exp Med* 172, 1043-1048 (1990).
38. W. Cao *et al.*, Identification of alpha-dystroglycan as a receptor for lymphocytic choriomeningitis virus and Lassa fever virus. *Science* 282, 2079-2081 (1998).
39. N. Sevilla *et al.*, Immunosuppression and resultant viral persistence by specific viral targeting of dendritic cells. *J Exp Med* 192, 1249-1260 (2000).
40. N. Sevilla, D. B. McGavern, C. Teng, S. Kunz, M. B. Oldstone, Viral targeting of hematopoietic progenitors and inhibition of DC maturation as a dual strategy for immune subversion. *J Clin Invest* 113, 737-745 (2004).

41. D. Moskophidis *et al.*, Role of virus and host variables in virus persistence or immunopathological disease caused by a non-cytolytic virus. *J Gen Virol* 76 ( Pt 2), 381-391 (1995).
42. E. J. Wherry, J. N. Blattman, K. Murali-Krishna, R. van der Most, R. Ahmed, Viral persistence alters CD8 T-cell immunodominance and tissue distribution and results in distinct stages of functional impairment. *J Virol* 77, 4911-4927 (2003).
43. E. J. Wherry *et al.*, Molecular signature of CD8<sup>+</sup> T cell exhaustion during chronic viral infection. *Immunity* 27, 670-684 (2007).
44. F. Lehmann-Grube, J. Lohler, O. Utermohlen, C. Gegin, Antiviral immune responses of lymphocytic choriomeningitis virus-infected mice lacking CD8<sup>+</sup> T lymphocytes because of disruption of the beta 2-microglobulin gene. *J Virol* 67, 332-339 (1993).
45. M. A. de La Vega, G. P. Kobinger, Safety and immunogenicity of vesicular stomatitis virus-based vaccines for Ebola virus disease. *Lancet Infect Dis* 20, 388-389 (2020).
46. C. A. Larocca, N. R. LeBoeuf, A. W. Silk, H. L. Kaufman, An Update on the Role of Talimogene Laherparepvec (T-VEC) in the Treatment of Melanoma: Best Practices and Future Directions. *Am J Clin Dermatol* 21, 821-832 (2020).
47. M. Saxena, T. T. H. Van, F. J. Baird, P. J. Coloe, P. M. Smooker, Pre-existing immunity against vaccine vectors--friend or foe? *Microbiology (Reading)* 159, 1-11 (2013).
48. L. Flatz, A. Bergthaler, J. C. de la Torre, D. D. Pinschewer, Recovery of an arenavirus entirely from RNA polymerase I/II-driven cDNA. *Proc Natl Acad Sci U S A* 103, 4663-4668 (2006).
49. A. B. Sanchez, J. C. de la Torre, Rescue of the prototypic Arenavirus LCMV entirely from plasmid. *Virology* 350, 370-380 (2006).
50. X. de Lamballerie, C. F. Fulhorst, R. N. Charrel, Prevalence of antibodies to lymphocytic choriomeningitis virus in blood donors in southeastern France. *Transfusion* 47, 172-173 (2007).
51. C. B. Stephensen *et al.*, Prevalence of serum antibodies against lymphocytic choriomeningitis virus in selected populations from two U.S. cities. *J Med Virol* 38, 27-31 (1992).
52. L. Lledo, M. I. Gegundez, J. V. Saz, N. Bahamontes, M. Beltran, Lymphocytic choriomeningitis virus infection in a province of Spain: analysis of sera from the general population and wild rodents. *J Med Virol* 70, 273-275 (2003).
53. R. Sommerstein *et al.*, Arenavirus Glycan Shield Promotes Neutralizing Antibody Evasion and Protracted Infection. *PLoS Pathog* 11, e1005276 (2015).
54. H. C. Probst, J. Lagnel, G. Kollias, M. van den Broek, Inducible transgenic mice reveal resting dendritic cells as potent inducers of CD8<sup>+</sup> T cell tolerance. *Immunity* 18, 713-720 (2003).
55. R. M. Steinman, Lasker Basic Medical Research Award. Dendritic cells: versatile controllers of the immune system. *Nat Med* 13, 1155-1159 (2007).
56. L. Flatz *et al.*, Development of replication-defective lymphocytic choriomeningitis virus vectors for the induction of potent CD8<sup>+</sup> T cell immunity. *Nat Med* 16, 339-345 (2010).
57. S. F. Emonet, L. Garidou, D. B. McGavern, J. C. de la Torre, Generation of recombinant lymphocytic choriomeningitis viruses with trisegmented genomes stably expressing two additional genes of interest. *Proc Natl Acad Sci U S A* 106, 3473-3478 (2009).
58. S. M. Kallert *et al.*, Replicating viral vector platform exploits alarmin signals for potent CD8(+) T cell-mediated tumour immunotherapy. *Nat Commun* 8, 15327 (2017).
59. W. V. Bonilla *et al.*, The alarmin interleukin-33 drives protective antiviral CD8(+) T cell responses. *Science* 335, 984-989 (2012).
60. S. Lu, Heterologous prime-boost vaccination. *Curr Opin Immunol* 21, 346-351 (2009).

61. S. Biswas, G. S. Reddy, V. A. Srinivasan, P. N. Rangarajan, Preexposure efficacy of a novel combination DNA and inactivated rabies virus vaccine. *Hum Gene Ther* 12, 1917-1922 (2001).
62. M. A. Egan *et al.*, Priming with plasmid DNAs expressing interleukin-12 and simian immunodeficiency virus gag enhances the immunogenicity and efficacy of an experimental AIDS vaccine based on recombinant vesicular stomatitis virus. *AIDS Res Hum Retroviruses* 21, 629-643 (2005).
63. S. L. Hu *et al.*, Protection of macaques against SIV infection by subunit vaccines of SIV envelope glycoprotein gp160. *Science* 255, 456-459 (1992).
64. I. Magalhaes *et al.*, rBCG induces strong antigen-specific T cell responses in rhesus macaques in a prime-boost setting with an adenovirus 35 tuberculosis vaccine vector. *PLoS One* 3, e3790 (2008).
65. W. V. Bonilla *et al.*, Heterologous arenavirus vector prime-boost overrules self-tolerance for efficient tumor-specific CD8 T cell attack. *Cell Rep Med* 2, 100209 (2021).
66. M. Schwendinger *et al.*, A Randomized Dose-Escalating Phase I Trial of a Replication-Deficient Lymphocytic Choriomeningitis Virus Vector-Based Vaccine Against Human Cytomegalovirus. *J Infect Dis*, (2020).
67. F. Lehmann-Grube, D. Moskophidis, J. Lohler, Recovery from acute virus infection. Role of cytotoxic T lymphocytes in the elimination of lymphocytic choriomeningitis virus from spleens of mice. *Ann N Y Acad Sci* 532, 238-256 (1988).
68. C. M. Walsh *et al.*, Immune function in mice lacking the perforin gene. *Proc Natl Acad Sci U S A* 91, 10854-10858 (1994).
69. S. M. Kaech *et al.*, Selective expression of the interleukin 7 receptor identifies effector CD8 T cells that give rise to long-lived memory cells. *Nat Immunol* 4, 1191-1198 (2003).
70. S. M. Kaech, E. J. Wherry, R. Ahmed, Effector and memory T-cell differentiation: implications for vaccine development. *Nat Rev Immunol* 2, 251-262 (2002).
71. B. Youngblood *et al.*, Effector CD8 T cells dedifferentiate into long-lived memory cells. *Nature* 552, 404-409 (2017).
72. M. Matloubian, R. J. Concepcion, R. Ahmed, CD4<sup>+</sup> T cells are required to sustain CD8<sup>+</sup> cytotoxic T-cell responses during chronic viral infection. *J Virol* 68, 8056-8063 (1994).
73. M. A. Brundler *et al.*, Immunity to viruses in B cell-deficient mice: influence of antibodies on virus persistence and on T cell memory. *Eur J Immunol* 26, 2257-2262 (1996).
74. M. Recher *et al.*, Deliberate removal of T cell help improves virus-neutralizing antibody production. *Nat Immunol* 5, 934-942 (2004).
75. B. Eschli *et al.*, Early antibodies specific for the neutralizing epitope on the receptor binding subunit of the lymphocytic choriomeningitis virus glycoprotein fail to neutralize the virus. *J Virol* 81, 11650-11657 (2007).
76. T. Straub *et al.*, Nucleoprotein-specific nonneutralizing antibodies speed up LCMV elimination independently of complement and FcγR3. *Eur J Immunol* 43, 2338-2348 (2013).
77. K. Richter, A. Oxenius, Non-neutralizing antibodies protect from chronic LCMV infection independently of activating FcγR3 or complement. *Eur J Immunol* 43, 2349-2360 (2013).
78. D. Stoycheva *et al.*, Non-neutralizing antibodies protect against chronic LCMV infection by promoting infection of inflammatory monocytes in mice. *Eur J Immunol*, (2021).



79. P. S. Kim, R. Ahmed, Features of responding T cells in cancer and chronic infection. *Curr Opin Immunol* 22, 223-230 (2010).
80. B. Fallet *et al.*, Chronic Viral Infection Promotes Efficient Germinal Center B Cell Responses. *Cell Rep* 30, 1013-1026 e1017 (2020).
81. H. W. Virgin, E. J. Wherry, R. Ahmed, Redefining chronic viral infection. *Cell* 138, 30-50 (2009).
82. D. Moskophidis, F. Lechner, H. Pircher, R. M. Zinkernagel, Virus persistence in acutely infected immunocompetent mice by exhaustion of antiviral cytotoxic effector T cells. *Nature* 362, 758-761 (1993).
83. A. Gallimore *et al.*, Induction and exhaustion of lymphocytic choriomeningitis virus-specific cytotoxic T lymphocytes visualized using soluble tetrameric major histocompatibility complex class I-peptide complexes. *J Exp Med* 187, 1383-1393 (1998).
84. J. D. Sears, K. J. Waldron, J. Wei, C. H. Chang, Targeting metabolism to reverse T-cell exhaustion in chronic viral infections. *Immunology* 162, 135-144 (2021).
85. D. R. Sen *et al.*, The epigenetic landscape of T cell exhaustion. *Science* 354, 1165-1169 (2016).
86. K. E. Pauken *et al.*, Epigenetic stability of exhausted T cells limits durability of reinvigoration by PD-1 blockade. *Science* 354, 1160-1165 (2016).
87. H. T. Jin *et al.*, Cooperation of Tim-3 and PD-1 in CD8 T-cell exhaustion during chronic viral infection. *Proc Natl Acad Sci U S A* 107, 14733-14738 (2010).
88. P. K. Gupta *et al.*, CD39 Expression Identifies Terminally Exhausted CD8<sup>+</sup> T Cells. *PLoS Pathog* 11, e1005177 (2015).
89. K. Richter, P. Agnellini, A. Oxenius, On the role of the inhibitory receptor LAG-3 in acute and chronic LCMV infection. *Int Immunol* 22, 13-23 (2010).
90. S. D. Blackburn *et al.*, Coregulation of CD8<sup>+</sup> T cell exhaustion by multiple inhibitory receptors during chronic viral infection. *Nat Immunol* 10, 29-37 (2009).
91. R. J. Johnston *et al.*, The immunoreceptor TIGIT regulates antitumor and antiviral CD8(+) T cell effector function. *Cancer Cell* 26, 923-937 (2014).
92. A. C. Anderson, N. Joller, V. K. Kuchroo, Lag-3, Tim-3, and TIGIT: Co-inhibitory Receptors with Specialized Functions in Immune Regulation. *Immunity* 44, 989-1004 (2016).
93. K. D. Cook, J. K. Whitmire, LAG-3 Confers a Competitive Disadvantage upon Antiviral CD8<sup>+</sup> T Cell Responses. *J Immunol* 197, 119-127 (2016).
94. N. Patsoukis *et al.*, PD-1 alters T-cell metabolic reprogramming by inhibiting glycolysis and promoting lipolysis and fatty acid oxidation. *Nat Commun* 6, 6692 (2015).
95. B. Bengsch *et al.*, Bioenergetic Insufficiencies Due to Metabolic Alterations Regulated by the Inhibitory Receptor PD-1 Are an Early Driver of CD8(+) T Cell Exhaustion. *Immunity* 45, 358-373 (2016).
96. R. V. Parry *et al.*, CTLA-4 and PD-1 receptors inhibit T-cell activation by distinct mechanisms. *Mol Cell Biol* 25, 9543-9553 (2005).
97. K. Richter, T. Brocker, A. Oxenius, Antigen amount dictates CD8<sup>+</sup> T-cell exhaustion during chronic viral infection irrespective of the type of antigen presenting cell. *Eur J Immunol* 42, 2290-2304 (2012).
98. R. D. Aubert *et al.*, Antigen-specific CD4 T-cell help rescues exhausted CD8 T cells during chronic viral infection. *Proc Natl Acad Sci U S A* 108, 21182-21187 (2011).
99. R. Zander *et al.*, CD4(+) T Cell Help Is Required for the Formation of a Cytolytic CD8(+) T Cell Subset that Protects against Chronic Infection and Cancer. *Immunity* 51, 1028-1042 e1024 (2019).

100. I. Sandu, D. Cerletti, M. Claassen, A. Oxenius, Exhausted CD8(+) T cells exhibit low and strongly inhibited TCR signaling during chronic LCMV infection. *Nat Commun* 11, 4454 (2020).
101. D. G. Brooks *et al.*, Interleukin-10 determines viral clearance or persistence in vivo. *Nat Med* 12, 1301-1309 (2006).
102. M. Ejrnaes *et al.*, Resolution of a chronic viral infection after interleukin-10 receptor blockade. *J Exp Med* 203, 2461-2472 (2006).
103. M. O. Li, S. Sanjabi, R. A. Flavell, Transforming growth factor-beta controls development, homeostasis, and tolerance of T cells by regulatory T cell-dependent and -independent mechanisms. *Immunity* 25, 455-471 (2006).
104. A. Schietinger, P. D. Greenberg, Tolerance and exhaustion: defining mechanisms of T cell dysfunction. *Trends Immunol* 35, 51-60 (2014).
105. P. Fusicaro, C. Boni, V. Barili, D. Laccabue, C. Ferrari, Strategies to overcome HBV-specific T cell exhaustion: checkpoint inhibitors and metabolic re-programming. *Curr Opin Virol* 30, 1-8 (2018).
106. P. Fusicaro *et al.*, Targeting mitochondrial dysfunction can restore antiviral activity of exhausted HBV-specific CD8 T cells in chronic hepatitis B. *Nat Med* 23, 327-336 (2017).
107. N. H. Gruener *et al.*, Sustained dysfunction of antiviral CD8+ T lymphocytes after infection with hepatitis C virus. *J Virol* 75, 5550-5558 (2001).
108. P. Shankar *et al.*, Impaired function of circulating HIV-specific CD8(+) T cells in chronic human immunodeficiency virus infection. *Blood* 96, 3094-3101 (2000).
109. S. Kostense *et al.*, Persistent numbers of tetramer+ CD8(+) T cells, but loss of interferon-gamma+ HIV-specific T cells during progression to AIDS. *Blood* 99, 2505-2511 (2002).
110. H. Frebel *et al.*, Programmed death 1 protects from fatal circulatory failure during systemic virus infection of mice. *J Exp Med* 209, 2485-2499 (2012).
111. J. E. Schmitz *et al.*, Control of viremia in simian immunodeficiency virus infection by CD8+ lymphocytes. *Science* 283, 857-860 (1999).
112. X. Jin *et al.*, Dramatic rise in plasma viremia after CD8(+) T cell depletion in simian immunodeficiency virus-infected macaques. *J Exp Med* 189, 991-998 (1999).
113. S. C. Wei, C. R. Duffy, J. P. Allison, Fundamental Mechanisms of Immune Checkpoint Blockade Therapy. *Cancer Discov* 8, 1069-1086 (2018).
114. S. J. Im, S. J. Ha, Re-defining T-Cell Exhaustion: Subset, Function, and Regulation. *Immune Netw* 20, e2 (2020).
115. C. Kim, J. Jin, C. M. Weyand, J. J. Goronzy, The Transcription Factor TCF1 in T Cell Differentiation and Aging. *Int J Mol Sci* 21, (2020).
116. D. T. Utzschneider *et al.*, Early precursor T cells establish and propagate T cell exhaustion in chronic infection. *Nat Immunol* 21, 1256-1266 (2020).
117. T. Wu *et al.*, The TCF1-Bcl6 axis counteracts type I interferon to repress exhaustion and maintain T cell stemness. *Sci Immunol* 1, (2016).
118. M. V. Kim, W. Ouyang, W. Liao, M. Q. Zhang, M. O. Li, The transcription factor Foxo1 controls central-memory CD8+ T cell responses to infection. *Immunity* 39, 286-297 (2013).
119. F. Alfei *et al.*, TOX reinforces the phenotype and longevity of exhausted T cells in chronic viral infection. *Nature* 571, 265-269 (2019).
120. D. T. Utzschneider *et al.*, T Cell Factor 1-Expressing Memory-like CD8(+) T Cells Sustain the Immune Response to Chronic Viral Infections. *Immunity* 45, 415-427 (2016).

121. S. J. Im *et al.*, Defining CD8<sup>+</sup> T cells that provide the proliferative burst after PD-1 therapy. *Nature* 537, 417-421 (2016).
122. R. R. Jadhav *et al.*, Epigenetic signature of PD-1<sup>+</sup> TCF1<sup>+</sup> CD8 T cells that act as resource cells during chronic viral infection and respond to PD-1 blockade. *Proc Natl Acad Sci U S A* 116, 14113-14118 (2019).
123. C. Petrovas *et al.*, Follicular CD8 T cells accumulate in HIV infection and can kill infected cells in vitro via bispecific antibodies. *Sci Transl Med* 9, (2017).
124. I. Siddiqui *et al.*, Intratumoral Tcf1(+)PD-1(+)CD8(+) T Cells with Stem-like Properties Promote Tumor Control in Response to Vaccination and Checkpoint Blockade Immunotherapy. *Immunity* 50, 195-211 e110 (2019).
125. B. C. Miller *et al.*, Subsets of exhausted CD8(+) T cells differentially mediate tumor control and respond to checkpoint blockade. *Nat Immunol* 20, 326-336 (2019).
126. S. Kurtulus *et al.*, Checkpoint Blockade Immunotherapy Induces Dynamic Changes in PD-1(-)CD8(+) Tumor-Infiltrating T Cells. *Immunity* 50, 181-194 e186 (2019).
127. M. A. Cox, S. M. Kahan, A. J. Zajac, Anti-viral CD8 T cells and the cytokines that they love. *Virology* 435, 157-169 (2013).
128. L. L. Lau, B. D. Jamieson, T. Somasundaram, R. Ahmed, Cytotoxic T-cell memory without antigen. *Nature* 369, 648-652 (1994).
129. K. Murali-Krishna *et al.*, Persistence of memory CD8 T cells in MHC class I-deficient mice. *Science* 286, 1377-1381 (1999).
130. M. Hashimoto, S. J. Im, K. Araki, R. Ahmed, Cytokine-Mediated Regulation of CD8 T-Cell Responses During Acute and Chronic Viral Infection. *Cold Spring Harb Perspect Biol* 11, (2019).
131. J. Schmitz *et al.*, IL-33, an interleukin-1-like cytokine that signals via the IL-1 receptor-related protein ST2 and induces T helper type 2-associated cytokines. *Immunity* 23, 479-490 (2005).
132. R. Kakkar, H. Hei, S. Dobner, R. T. Lee, Interleukin 33 as a mechanically responsive cytokine secreted by living cells. *J Biol Chem* 287, 6941-6948 (2012).
133. G. Haraldsen, J. Balogh, J. Pollheimer, J. Sponheim, A. M. Kuchler, Interleukin-33 - cytokine of dual function or novel alarmin? *Trends Immunol* 30, 227-233 (2009).
134. C. Moussion, N. Ortega, J. P. Girard, The IL-1-like cytokine IL-33 is constitutively expressed in the nucleus of endothelial cells and epithelial cells in vivo: a novel 'alarmin'? *PLoS One* 3, e3331 (2008).
135. M. Pichery *et al.*, Endogenous IL-33 is highly expressed in mouse epithelial barrier tissues, lymphoid organs, brain, embryos, and inflamed tissues: in situ analysis using a novel Il-33-LacZ gene trap reporter strain. *J Immunol* 188, 3488-3495 (2012).
136. P. Aparicio-Domingo *et al.*, Fibroblast-derived IL-33 is dispensable for lymph node homeostasis but critical for CD8 T-cell responses to acute and chronic viral infection. *Eur J Immunol* 51, 76-90 (2021).
137. V. Carriere *et al.*, Endogenous IL-33 Deficiency Exacerbates Liver Injury and Increases Hepatic Influx of Neutrophils in Acute Murine Viral Hepatitis. *Mediators Inflamm* 2017, 1359064 (2017).
138. Y. S. Choi *et al.*, Nuclear IL-33 is a transcriptional regulator of NF-kappaB p65 and induces endothelial cell activation. *Biochem Biophys Res Commun* 421, 305-311 (2012).
139. A. Lingel *et al.*, Structure of IL-33 and its interaction with the ST2 and IL-1RAcP receptors--insight into heterotrimeric IL-1 signaling complexes. *Structure* 17, 1398-1410 (2009).
140. C. Cayrol, J. P. Girard, The IL-1-like cytokine IL-33 is inactivated after maturation by caspase-1. *Proc Natl Acad Sci U S A* 106, 9021-9026 (2009).



141. D. Talabot-Ayer, C. Lamacchia, C. Gabay, G. Palmer, Interleukin-33 is biologically active independently of caspase-1 cleavage. *J Biol Chem* 284, 19420-19426 (2009).
142. E. Lefrancais *et al.*, IL-33 is processed into mature bioactive forms by neutrophil elastase and cathepsin G. *Proc Natl Acad Sci U S A* 109, 1673-1678 (2012).
143. E. Lefrancais *et al.*, Central domain of IL-33 is cleaved by mast cell proteases for potent activation of group-2 innate lymphoid cells. *Proc Natl Acad Sci U S A* 111, 15502-15507 (2014).
144. G. Palmer, C. Gabay, Interleukin-33 biology with potential insights into human diseases. *Nat Rev Rheumatol* 7, 321-329 (2011).
145. E. S. Cohen *et al.*, Oxidation of the alarmin IL-33 regulates ST2-dependent inflammation. *Nat Commun* 6, 8327 (2015).
146. A. U. Luthi *et al.*, Suppression of interleukin-33 bioactivity through proteolysis by apoptotic caspases. *Immunity* 31, 84-98 (2009).
147. T. Pecaric-Petkovic, S. A. Didichenko, S. Kaempfer, N. Spiegl, C. A. Dahinden, Human basophils and eosinophils are the direct target leukocytes of the novel IL-1 family member IL-33. *Blood* 113, 1526-1534 (2009).
148. L. A. Monticelli *et al.*, Innate lymphoid cells promote lung-tissue homeostasis after infection with influenza virus. *Nat Immunol* 12, 1045-1054 (2011).
149. C. Schiering *et al.*, The alarmin IL-33 promotes regulatory T-cell function in the intestine. *Nature* 513, 564-568 (2014).
150. D. R. Moritz, H. R. Rodewald, J. Gheyselinck, R. Klemenz, The IL-1 receptor-related T1 antigen is expressed on immature and mature mast cells and on fetal blood mast cell progenitors. *J Immunol* 161, 4866-4874 (1998).
151. E. K. Brint *et al.*, ST2 is an inhibitor of interleukin 1 receptor and Toll-like receptor 4 signaling and maintains endotoxin tolerance. *Nat Immunol* 5, 373-379 (2004).
152. C. Baumann *et al.*, T-bet- and STAT4-dependent IL-33 receptor expression directly promotes antiviral Th1 cell responses. *Proc Natl Acad Sci U S A* 112, 4056-4061 (2015).
153. A. B. Molofsky, A. K. Savage, R. M. Locksley, Interleukin-33 in Tissue Homeostasis, Injury, and Inflammation. *Immunity* 42, 1005-1019 (2015).
154. F. Y. Liew, J. P. Girard, H. R. Turnquist, Interleukin-33 in health and disease. *Nat Rev Immunol* 16, 676-689 (2016).
155. M. Lohning *et al.*, T1/ST2 is preferentially expressed on murine Th2 cells, independent of interleukin 4, interleukin 5, and interleukin 10, and important for Th2 effector function. *Proc Natl Acad Sci U S A* 95, 6930-6935 (1998).
156. M. A. Rank *et al.*, IL-33-activated dendritic cells induce an atypical TH2-type response. *J Allergy Clin Immunol* 123, 1047-1054 (2009).
157. A. Yagami *et al.*, IL-33 mediates inflammatory responses in human lung tissue cells. *J Immunol* 185, 5743-5750 (2010).
158. I. G. Luzina *et al.*, Full-length IL-33 promotes inflammation but not Th2 response in vivo in an ST2-independent fashion. *J Immunol* 189, 403-410 (2012).
159. W. D. Xu, M. Zhang, Y. J. Zhang, D. Q. Ye, IL-33 in rheumatoid arthritis: potential role in pathogenesis and therapy. *Hum Immunol* 74, 1057-1060 (2013).
160. M. Li, Y. Li, X. Liu, X. Gao, Y. Wang, IL-33 blockade suppresses the development of experimental autoimmune encephalomyelitis in C57BL/6 mice. *J Neuroimmunol* 247, 25-31 (2012).
161. R. B. Werder *et al.*, Chronic IL-33 expression predisposes to virus-induced asthma exacerbations by increasing type 2 inflammation and dampening antiviral immunity. *J Allergy Clin Immunol* 141, 1607-1619 e1609 (2018).

162. M. A. Stanczak *et al.*, IL-33 expression in response to SARS-CoV-2 correlates with seropositivity in COVID-19 convalescent individuals. *Nat Commun* 12, 2133 (2021).
163. W. P. Arend, G. Palmer, C. Gabay, IL-1, IL-18, and IL-33 families of cytokines. *Immunol Rev* 223, 20-38 (2008).
164. D. Dominguez *et al.*, Exogenous IL-33 Restores Dendritic Cell Activation and Maturation in Established Cancer. *J Immunol* 198, 1365-1375 (2017).
165. D. O. Villarreal *et al.*, Molecular adjuvant IL-33 enhances the potency of a DNA vaccine in a lethal challenge model. *Vaccine* 33, 4313-4320 (2015).
166. D. O. Villarreal, D. B. Weiner, IL-33 isoforms: their future as vaccine adjuvants? *Expert Rev Vaccines* 14, 489-492 (2015).
167. D. O. Villarreal *et al.*, Alarmin IL-33 acts as an immunoadjuvant to enhance antigen-specific tumor immunity. *Cancer Res* 74, 1789-1800 (2014).
168. C. Baumann *et al.*, Memory CD8(+) T Cell Protection From Viral Reinfection Depends on Interleukin-33 Alarmin Signals. *Front Immunol* 10, 1833 (2019).
169. T. Suprunenko, M. J. Hofer, Complexities of Type I Interferon Biology: Lessons from LCMV. *Viruses* 11, (2019).
170. F. McNab, K. Mayer-Barber, A. Sher, A. Wack, A. O'Garra, Type I interferons in infectious disease. *Nat Rev Immunol* 15, 87-103 (2015).
171. L. B. Ivashkiv, L. T. Donlin, Regulation of type I interferon responses. *Nat Rev Immunol* 14, 36-49 (2014).
172. S. Zhou *et al.*, Induction and inhibition of type I interferon responses by distinct components of lymphocytic choriomeningitis virus. *J Virol* 84, 9452-9462 (2010).
173. L. Martinez-Sobrido, E. I. Zuniga, D. Rosario, A. Garcia-Sastre, J. C. de la Torre, Inhibition of the type I interferon response by the nucleoprotein of the prototypic arenavirus lymphocytic choriomeningitis virus. *J Virol* 80, 9192-9199 (2006).
174. J. R. Teijaro *et al.*, Persistent LCMV infection is controlled by blockade of type I interferon signaling. *Science* 340, 207-211 (2013).
175. Y. Wang *et al.*, Timing and magnitude of type I interferon responses by distinct sensors impact CD8 T cell exhaustion and chronic viral infection. *Cell Host Microbe* 11, 631-642 (2012).
176. J. Louten, N. van Rooijen, C. A. Biron, Type 1 IFN deficiency in the absence of normal splenic architecture during lymphocytic choriomeningitis virus infection. *J Immunol* 177, 3266-3272 (2006).
177. M. Huber *et al.*, IRF9 Prevents CD8(+) T Cell Exhaustion in an Extrinsic Manner during Acute Lymphocytic Choriomeningitis Virus Infection. *J Virol* 91, (2017).
178. K. Sandberg *et al.*, Altered tissue distribution of viral replication and T cell spreading is pivotal in the protection against fatal lymphocytic choriomeningitis in mice after neutralization of IFN-alpha/beta. *J Immunol* 153, 220-231 (1994).
179. U. Muller *et al.*, Functional role of type I and type II interferons in antiviral defense. *Science* 264, 1918-1921 (1994).
180. R. Lindqvist *et al.*, Fast type I interferon response protects astrocytes from flavivirus infection and virus-induced cytopathic effects. *J Neuroinflammation* 13, 277 (2016).
181. J. Wei *et al.*, Alpha/beta interferon receptor deficiency in mice significantly enhances susceptibility of the animals to pseudorabies virus infection. *Vet Microbiol* 203, 234-244 (2017).
182. G. A. Kolumam, S. Thomas, L. J. Thompson, J. Sprent, K. Murali-Krishna, Type I interferons act directly on CD8 T cells to allow clonal expansion and memory formation in response to viral infection. *J Exp Med* 202, 637-650 (2005).

183. H. Pircher, K. Burki, R. Lang, H. Hengartner, R. M. Zinkernagel, Tolerance induction in double specific T-cell receptor transgenic mice varies with antigen. *Nature* 342, 559-561 (1989).
184. P. Aichele *et al.*, CD8 T cells specific for lymphocytic choriomeningitis virus require type I IFN receptor for clonal expansion. *J Immunol* 176, 4525-4529 (2006).
185. H. C. Xu *et al.*, Type I interferon protects antiviral CD8<sup>+</sup> T cells from NK cell cytotoxicity. *Immunity* 40, 949-960 (2014).
186. E. B. Wilson *et al.*, Blockade of chronic type I interferon signaling to control persistent LCMV infection. *Science* 340, 202-207 (2013).
187. A. Audige, U. Hofer, U. Dittmer, M. van den Broek, R. F. Speck, Evaluation of the immunomodulatory and antiviral effects of the cytokine combination IFN- $\alpha$  and IL-7 in the lymphocytic choriomeningitis virus and Friend retrovirus mouse infection models. *Viral Immunol* 24, 375-385 (2011).
188. B. M. Sullivan, J. R. Tejjaro, J. C. de la Torre, M. B. Oldstone, Early virus-host interactions dictate the course of a persistent infection. *PLoS Pathog* 11, e1004588 (2015).
189. N. G. Sandler *et al.*, Type I interferon responses in rhesus macaques prevent SIV infection and slow disease progression. *Nature* 511, 601-605 (2014).
190. L. Cheng *et al.*, Blocking type I interferon signaling enhances T cell recovery and reduces HIV-1 reservoirs. *J Clin Invest* 127, 269-279 (2017).
191. P. Cordero-Ruiz *et al.*, Long-term follow-up of patients with chronic hepatitis C treated with alpha-interferon and ribavirin antiviral therapy: clinical and fibrosis impact of treatment response. *Eur J Gastroenterol Hepatol* 29, 792-799 (2017).
192. A. S. J. Woo, R. Kwok, T. Ahmed, Alpha-interferon treatment in hepatitis B. *Ann Transl Med* 5, 159 (2017).
193. J. C. Hafalla, G. Sano, L. H. Carvalho, A. Morrot, F. Zavala, Short-term antigen presentation and single clonal burst limit the magnitude of the CD8(+) T cell responses to malaria liver stages. *Proc Natl Acad Sci U S A* 99, 11819-11824 (2002).
194. A. Oxenius, M. F. Bachmann, R. M. Zinkernagel, H. Hengartner, Virus-specific MHC-class II-restricted TCR-transgenic mice: effects on humoral and cellular immune responses after viral infection. *Eur J Immunol* 28, 390-400 (1998).
195. I. Misumi *et al.*, Differential T cell responses to residual viral antigen prolong CD4<sup>+</sup> T cell contraction following the resolution of infection. *J Immunol* 191, 5655-5668 (2013).
196. D. L. Turner, L. S. Cauley, K. M. Khanna, L. Lefrancois, Persistent antigen presentation after acute vesicular stomatitis virus infection. *J Virol* 81, 2039-2046 (2007).
197. D. M. Jelley-Gibbs *et al.*, Unexpected prolonged presentation of influenza antigens promotes CD4 T cell memory generation. *J Exp Med* 202, 697-706 (2005).
198. D. J. Zammit, D. L. Turner, K. D. Klonowski, L. Lefrancois, L. S. Cauley, Residual antigen presentation after influenza virus infection affects CD8 T cell activation and migration. *Immunity* 24, 439-449 (2006).
199. I. F. Hermans, D. S. Ritchie, J. Yang, J. M. Roberts, F. Ronchese, CD8<sup>+</sup> T cell-dependent elimination of dendritic cells in vivo limits the induction of antitumor immunity. *Journal of immunology* 164, 3095-3101 (2000).
200. P. Wong, E. G. Pamer, Feedback regulation of pathogen-specific T cell priming. *Immunity* 18, 499-511 (2003).
201. T. S. Kim, M. M. Hufford, J. Sun, Y. X. Fu, T. J. Braciale, Antigen persistence and the control of local T cell memory by migrant respiratory dendritic cells after acute virus infection. *The Journal of experimental medicine* 207, 1161-1172 (2010).

202. R. Ahmed, L. D. Butler, L. Bhatti, T4+ T helper cell function in vivo: differential requirement for induction of antiviral cytotoxic T-cell and antibody responses. *Journal of virology* 62, 2102-2106 (1988).
203. C. Dow *et al.*, Lymphocytic choriomeningitis virus infection yields overlapping CD4+ and CD8+ T-cell responses. *Journal of virology* 82, 11734-11741 (2008).
204. D. Homann, L. Teyton, M. B. Oldstone, Differential regulation of antiviral T-cell immunity results in stable CD8+ but declining CD4+ T-cell memory. *Nature medicine* 7, 913-919 (2001).
205. J. J. Moon *et al.*, Naive CD4(+) T cell frequency varies for different epitopes and predicts repertoire diversity and response magnitude. *Immunity* 27, 203-213 (2007).
206. M. A. Rasheed *et al.*, Interleukin-21 is a critical cytokine for the generation of virus-specific long-lived plasma cells. *J Virol* 87, 7737-7746 (2013).
207. M. K. Slifka, M. Matloubian, R. Ahmed, Bone marrow is a major site of long-term antibody production after acute viral infection. *Journal of virology* 69, 1895-1902 (1995).
208. A. Bergthaler, D. Merkler, E. Horvath, L. Bestmann, D. D. Pinschewer, Contributions of the lymphocytic choriomeningitis virus glycoprotein and polymerase to strain-specific differences in murine liver pathogenicity. *The Journal of general virology* 88, 592-603 (2007).
209. L. Hangartner *et al.*, Antiviral immune responses in gene-targeted mice expressing the immunoglobulin heavy chain of virus-neutralizing antibodies. *Proceedings of the National Academy of Sciences of the United States of America* 100, 12883-12888 (2003).
210. J. M. Ahearn *et al.*, Disruption of the Cr2 locus results in a reduction in B-1a cells and in an impaired B cell response to T-dependent antigen. *Immunity* 4, 251-262 (1996).
211. R. A. Barrington, O. Pozdnyakova, M. R. Zafari, C. D. Benjamin, M. C. Carroll, B lymphocyte memory: role of stromal cell complement and FcγRIIB receptors. *The Journal of experimental medicine* 196, 1189-1199 (2002).
212. Y. Fang, C. Xu, Y. X. Fu, V. M. Holers, H. Molina, Expression of complement receptors 1 and 2 on follicular dendritic cells is necessary for the generation of a strong antigen-specific IgG response. *Journal of immunology* 160, 5273-5279 (1998).
213. D. Qin *et al.*, Fc gamma receptor IIB on follicular dendritic cells regulates the B cell recall response. *Journal of immunology* 164, 6268-6275 (2000).
214. D. Radoux *et al.*, Retention of immune complexes by Fc receptors on mouse follicular dendritic cells. *Scandinavian journal of immunology* 21, 345-353 (1985).
215. D. A. Croix *et al.*, Antibody response to a T-dependent antigen requires B cell expression of complement receptors. *The Journal of experimental medicine* 183, 1857-1864 (1996).
216. D. T. Fearon, R. H. Carter, The CD19/CR2/TAPA-1 complex of B lymphocytes: linking natural to acquired immunity. *Annual review of immunology* 13, 127-149 (1995).
217. K. M. Haas *et al.*, Complement receptors CD21/35 link innate and protective immunity during *Streptococcus pneumoniae* infection by regulating IgG3 antibody responses. *Immunity* 17, 713-723 (2002).
218. K. Pracht *et al.*, A new staining protocol for detection of murine antibody-secreting plasma cell subsets by flow cytometry. *European journal of immunology* 47, 1389-1392 (2017).
219. R. J. Benjamin, H. Waldmann, Induction of tolerance by monoclonal antibody therapy. *Nature* 320, 449-451 (1986).



220. J. Goronzy, C. M. Weyand, C. G. Fathman, Long-term humoral unresponsiveness in vivo, induced by treatment with monoclonal antibody against L3T4. *The Journal of experimental medicine* 164, 911-925 (1986).
221. J. J. Goronzy, C. M. Weyand, Persistent suppression of virus-specific cytotoxic T cell responses after transient depletion of CD4<sup>+</sup> T cells in vivo. *Journal of immunology* 142, 4435-4440 (1989).
222. N. L. Gutstein, W. E. Seaman, J. H. Scott, D. Wofsy, Induction of immune tolerance by administration of monoclonal antibody to L3T4. *Journal of immunology* 137, 1127-1132 (1986).
223. P. Vieira, K. Rajewsky, Persistence of memory B cells in mice deprived of T cell help. *International immunology* 2, 487-494 (1990).
224. N. M. Provine *et al.*, Transient CD4<sup>+</sup> T Cell Depletion Results in Delayed Development of Functional Vaccine-Elicited Antibody Responses. *Journal of virology* 90, 4278-4288 (2016).
225. C. M. Snapper, W. E. Paul, Interferon-gamma and B cell stimulatory factor-1 reciprocally regulate Ig isotype production. *Science* 236, 944-947 (1987).
226. R. M. Zinkernagel, What if protective immunity is antigen-driven and not due to so-called "memory" B and T cells? *Immunological reviews* 283, 238-246 (2018).
227. M. Maruyama, K. P. Lam, K. Rajewsky, Memory B-cell persistence is independent of persisting immunizing antigen. *Nature* 407, 636-642 (2000).
228. M. F. Franssen *et al.*, A Restricted Role for FcγR2b in the Regulation of Adaptive Immunity. *Journal of immunology* 200, 2615-2626 (2018).
229. B. Falset *et al.*, Interferon-driven deletion of antiviral B cells at the onset of chronic infection. *Sci Immunol* 1, (2016).
230. M. Battegay *et al.*, Quantification of lymphocytic choriomeningitis virus with an immunological focus assay in 24- or 96-well plates. *J Virol Methods* 33, 191-198 (1991).
231. M. M. McCausland, S. Crotty, Quantitative PCR technique for detecting lymphocytic choriomeningitis virus in vivo. *Journal of virological methods* 147, 167-176 (2008).
232. A. Cossarizza *et al.*, Guidelines for the use of flow cytometry and cell sorting in immunological studies. *European journal of immunology* 47, 1584-1797 (2017).
233. L. Zhang *et al.*, Intratumoral T cells, recurrence, and survival in epithelial ovarian cancer. *N Engl J Med* 348, 203-213 (2003).
234. F. Pages *et al.*, Effector memory T cells, early metastasis, and survival in colorectal cancer. *N Engl J Med* 353, 2654-2666 (2005).
235. J. Galon *et al.*, Type, density, and location of immune cells within human colorectal tumors predict clinical outcome. *Science* 313, 1960-1964 (2006).
236. P. C. Tumeh *et al.*, PD-1 blockade induces responses by inhibiting adaptive immune resistance. *Nature* 515, 568-571 (2014).
237. A. D. Kosinska, T. Bauer, U. Protzer, Therapeutic vaccination for chronic hepatitis B. *Curr Opin Virol* 23, 75-81 (2017).
238. P. Romero *et al.*, The Human Vaccines Project: A roadmap for cancer vaccine development. *Sci Transl Med* 8, 334ps339 (2016).
239. C. J. M. Melief, Cancer: Precision T-cell therapy targets tumours. *Nature* 547, 165-167 (2017).
240. P. W. Kantoff *et al.*, Sipuleucel-T immunotherapy for castration-resistant prostate cancer. *N Engl J Med* 363, 411-422 (2010).
241. J. F. Vansteenkiste *et al.*, Efficacy of the MAGE-A3 cancer immunotherapeutic as adjuvant therapy in patients with resected MAGE-A3-positive non-small-cell lung

- cancer (MAGRIT): a randomised, double-blind, placebo-controlled, phase 3 trial. *Lancet Oncol* 17, 822-835 (2016).
242. C. Butts *et al.*, Tecemotide (L-BLP25) versus placebo after chemoradiotherapy for stage III non-small-cell lung cancer (START): a randomised, double-blind, phase 3 trial. *Lancet Oncol* 15, 59-68 (2014).
  243. J. L. Gulley *et al.*, Phase III Trial of PROSTVAC in Asymptomatic or Minimally Symptomatic Metastatic Castration-Resistant Prostate Cancer. *J Clin Oncol* 37, 1051-1061 (2019).
  244. S. A. Rosenberg, J. C. Yang, N. P. Restifo, Cancer immunotherapy: moving beyond current vaccines. *Nat Med* 10, 909-915 (2004).
  245. T. F. Gajewski, H. Schreiber, Y. X. Fu, Innate and adaptive immune cells in the tumor microenvironment. *Nat Immunol* 14, 1014-1022 (2013).
  246. J. A. Joyce, D. T. Fearon, T cell exclusion, immune privilege, and the tumor microenvironment. *Science* 348, 74-80 (2015).
  247. D. Zamarin *et al.*, Localized oncolytic virotherapy overcomes systemic tumor resistance to immune checkpoint blockade immunotherapy. *Sci Transl Med* 6, 226ra232 (2014).
  248. K. Y. Tsang *et al.*, Generation of human cytotoxic T cells specific for human carcinoembryonic antigen epitopes from patients immunized with recombinant vaccinia-CEA vaccine. *J Natl Cancer Inst* 87, 982-990 (1995).
  249. P. W. Kantoff *et al.*, Overall survival analysis of a phase II randomized controlled trial of a Poxviral-based PSA-targeted immunotherapy in metastatic castration-resistant prostate cancer. *J Clin Oncol* 28, 1099-1105 (2010).
  250. M. A. Morse *et al.*, An alphavirus vector overcomes the presence of neutralizing antibodies and elevated numbers of Tregs to induce immune responses in humans with advanced cancer. *J Clin Invest* 120, 3234-3241 (2010).
  251. L. Aurisicchio *et al.*, Safety, tolerability and immunogenicity of V934/V935 hTERT vaccination in cancer patients with selected solid tumors: a phase I study. *J Transl Med* 18, 39 (2020).
  252. clinicaltrials.gov, A Phase 1 Study To Evaluate Escalating Doses Of A Vaccine-Based Immunotherapy Regimen For Prostate Cancer (PrCa VBIR). <https://clinicaltrials.gov/ct2/show/NCT02616185>.
  253. S. M. Pollack *et al.*, First-in-Human Treatment With a Dendritic Cell-targeting Lentiviral Vector-expressing NY-ESO-1, LV305, Induces Deep, Durable Response in Refractory Metastatic Synovial Sarcoma Patient. *J Immunother* 40, 302-306 (2017).
  254. M. J. Atherton *et al.*, Preclinical development of peptide vaccination combined with oncolytic MG1-E6E7 for HPV-associated cancer. *Vaccine* 36, 2181-2192 (2018).
  255. clinicaltrials.gov, This is a Trial of MG1-E6E7 With Ad-E6E7 and Atezolizumab in Patients With HPV Associated Cancers (Kingfisher). <https://www.clinicaltrials.gov/ct2/show/NCT03618953?term=maraba&draw=2&rank=3>.
  256. D. D. Pinschewer, Virally vectored vaccine delivery: medical needs, mechanisms, advantages and challenges. *Swiss Med Wkly* 147, w14465 (2017).
  257. T. Querec *et al.*, Yellow fever vaccine YF-17D activates multiple dendritic cell subsets via TLR2, 7, 8, and 9 to stimulate polyvalent immunity. *J Exp Med* 203, 413-424 (2006).
  258. M. Peine, R. M. Marek, M. Lohning, IL-33 in T Cell Differentiation, Function, and Immune Homeostasis. *Trends Immunol* 37, 321-333 (2016).
  259. P. R. Pittman *et al.*, Phase 3 Efficacy Trial of Modified Vaccinia Ankara as a Vaccine against Smallpox. *N Engl J Med* 381, 1897-1908 (2019).

260. T. M. Kundig, C. P. Kalberer, H. Hengartner, R. M. Zinkernagel, Vaccination with two different vaccinia recombinant viruses: long-term inhibition of secondary vaccination. *Vaccine* 11, 1154-1158 (1993).
261. M. J. McElrath *et al.*, HIV-1 vaccine-induced immunity in the test-of-concept Step Study: a case-cohort analysis. *Lancet* 372, 1894-1905 (2008).
262. S. Colloca *et al.*, Vaccine vectors derived from a large collection of simian adenoviruses induce potent cellular immunity across multiple species. *Sci Transl Med* 4, 115ra112 (2012).
263. E. Barnes *et al.*, Novel adenovirus-based vaccines induce broad and sustained T cell responses to HCV in man. *Sci Transl Med* 4, 115ra111 (2012).
264. D. A. Stanley *et al.*, Chimpanzee adenovirus vaccine generates acute and durable protective immunity against ebolavirus challenge. *Nat Med* 20, 1126-1129 (2014).
265. R. M. Zinkernagel, Lymphocytic choriomeningitis virus and immunology. *Curr Top Microbiol Immunol* 263, 1-5 (2002).
266. A. B. Sanchez, J. C. de la Torre, Rescue of the prototypic Arenavirus LCMV entirely from plasmid. *Virology*, (2006).
267. L. Flatz *et al.*, Development of replication-defective lymphocytic choriomeningitis virus vectors for the induction of potent CD8(+) T cell immunity. *Nat Med* 16, 339-345 (2010).
268. L. Flatz *et al.*, Gene-based vaccination with a mismatched envelope protects against simian immunodeficiency virus infection in nonhuman primates. *J Virol* 86, 7760-7770 (2012).
269. P. Penaloza MacMaster *et al.*, Development of novel replication-defective lymphocytic choriomeningitis virus vectors expressing SIV antigens. *Vaccine* 35, 1-9 (2017).
270. ClinicalTrials.gov, A Study of CMV Vaccine (HB-101) in Kidney Transplant Patients. NCT03629080.
271. R. Dhanwani *et al.*, A Novel Live Pichinde Virus-Based Vaccine Vector Induces Enhanced Humoral and Cellular Immunity after a Booster Dose. *J Virol* 90, 2551-2560 (2015).
272. ClinicalTrials.gov, A Study of HB-201 Alone or in Combination With a Checkpoint Inhibitor in Patients With Human Papillomavirus 16 Positive (HPV 16+) Confirmed Cancers'. NCT04180215.
273. M. Buchmeier, E. Adam, W. E. Rawls, Serological evidence of infection by Pichinde virus among laboratory workers. *Infect Immun* 9, 821-823 (1974).
274. C. Armstrong, Some recent research in the field of neurotropic viruses with especial reference to lymphocytic choriomeningitis and herpes simplex. *Milit. Surg.* 91, 129-146 (1942).
275. G. S. Stone, M. Glover, N. Jilg, M. M. Sfeir, Case 40-2019: A 26-Year-Old Returning Traveler with Headache. *N Engl J Med* 381, 2553-2560 (2019).
276. H. T. Souders, D. Byler, N. Marupudi, R. Patel, G. McSherry, Protracted symptoms in lymphocytic choriomeningitis: a case report. *J Child Neurol* 30, 644-647 (2015).
277. M. C. Cassetti *et al.*, Antitumor efficacy of Venezuelan equine encephalitis virus replicon particles encoding mutated HPV16 E6 and E7 genes. *Vaccine* 22, 520-527 (2004).
278. A. Bergthaler *et al.*, Envelope exchange for the generation of live-attenuated arenavirus vaccines. *PLoS Pathog* 2, e51 (2006).
279. D. D. Pinschewer *et al.*, T cells can mediate viral clearance from ependyma but not from brain parenchyma in a major histocompatibility class I- and perforin-independent manner. *Brain* 133, 1054-1066 (2010).

280. J. E. Christensen, C. de Lemos, T. Moos, J. P. Christensen, A. R. Thomsen, CXCL10 is the key ligand for CXCR3 on CD8<sup>+</sup> effector T cells involved in immune surveillance of the lymphocytic choriomeningitis virus-infected central nervous system. *J Immunol* 176, 4235-4243 (2006).
281. G. A. Cole, N. Nathanson, R. A. Prendergast, Requirement for theta-bearing cells in lymphocytic choriomeningitis virus-induced central nervous system disease. *Nature* 238, 335-337 (1972).
282. J. Derbinski, A. Schulte, B. Kyewski, L. Klein, Promiscuous gene expression in medullary thymic epithelial cells mirrors the peripheral self. *Nat Immunol* 2, 1032-1039 (2001).
283. C. Uyttenhove *et al.*, The expression of mouse gene P1A in testis does not prevent safe induction of cytolytic T cells against a P1A-encoded tumor antigen. *Int J Cancer* 70, 349-356 (1997).
284. I. J. Huijbers *et al.*, Minimal tolerance to a tumor antigen encoded by a cancer-germline gene. *J Immunol* 188, 111-121 (2012).
285. J. P. Bottcher *et al.*, Functional classification of memory CD8(+) T cells by CX3CR1 expression. *Nat Commun* 6, 8306 (2015).
286. C. Gerlach *et al.*, The Chemokine Receptor CX3CR1 Defines Three Antigen-Experienced CD8 T Cell Subsets with Distinct Roles in Immune Surveillance and Homeostasis. *Immunity* 45, 1270-1284 (2016).
287. J. A. Olson, C. McDonald-Hyman, S. C. Jameson, S. E. Hamilton, Effector-like CD8(+) T cells in the memory population mediate potent protective immunity. *Immunity* 38, 1250-1260 (2013).
288. N. S. Joshi *et al.*, Inflammation directs memory precursor and short-lived effector CD8(+) T cell fates via the graded expression of T-bet transcription factor. *Immunity* 27, 281-295 (2007).
289. D. Voehringer *et al.*, Viral infections induce abundant numbers of senescent CD8 T cells. *J Immunol* 167, 4838-4843 (2001).
290. J. Hendriks *et al.*, CD27 is required for generation and long-term maintenance of T cell immunity. *Nat Immunol* 1, 433-440 (2000).
291. W. Yu *et al.*, Clonal Deletion Prunes but Does Not Eliminate Self-Specific alphabeta CD8(+) T Lymphocytes. *Immunity* 42, 929-941 (2015).
292. L. M. McLane, M. S. Abdel-Hakeem, E. J. Wherry, CD8 T Cell Exhaustion During Chronic Viral Infection and Cancer. *Annu Rev Immunol*, (2019).
293. D. E. Speiser *et al.*, T cell differentiation in chronic infection and cancer: functional adaptation or exhaustion? *Nat Rev Immunol* 14, 768-774 (2014).
294. D. T. Utzschneider *et al.*, T cells maintain an exhausted phenotype after antigen withdrawal and population reexpansion. *Nat Immunol* 14, 603-610 (2013).
295. C. Larocca, J. Schlom, Viral vector-based therapeutic cancer vaccines. *Cancer J* 17, 359-371 (2011).
296. L. Zhang *et al.*, Delivery of viral-vectored vaccines by B cells represents a novel strategy to accelerate CD8(+) T-cell recall responses. *Blood* 121, 2432-2439 (2013).
297. A. R. Elbers *et al.*, Low prevalence of antibodies against the zoonotic agents *Brucella abortus*, *Leptospira* spp., *Streptococcus suis* serotype II, hantavirus, and lymphocytic choriomeningitis virus among veterinarians and pig farmers in the southern part of The Netherlands. *Vet Q* 21, 50-54 (1999).
298. E. N. Borducchi *et al.*, Ad26/MVA therapeutic vaccination with TLR7 stimulation in SIV-infected rhesus monkeys. *Nature* 540, 284-287 (2016).
299. D. M. Roberts *et al.*, Hexon-chimaeric adenovirus serotype 5 vectors circumvent pre-existing anti-vector immunity. *Nature* 441, 239-243 (2006).



300. C. L. Smith *et al.*, Immunodominance of poxviral-specific CTL in a human trial of recombinant-modified vaccinia Ankara. *J Immunol* 175, 8431-8437 (2005).
301. N. Frahm *et al.*, Human adenovirus-specific T cells modulate HIV-specific T cell responses to an Ad5-vectored HIV-1 vaccine. *J Clin Invest* 122, 359-367 (2012).
302. K. L. O'Brien *et al.*, Adenovirus-specific immunity after immunization with an Ad5 HIV-1 vaccine candidate in humans. *Nat Med* 15, 873-875 (2009).
303. A. M. Leen *et al.*, Identification of hexon-specific CD4 and CD8 T-cell epitopes for vaccine and immunotherapy. *J Virol* 82, 546-554 (2008).
304. R. M. Kedl *et al.*, T cells compete for access to antigen-bearing antigen-presenting cells. *J Exp Med* 192, 1105-1113 (2000).
305. V. Loyer *et al.*, The in vivo fate of APCs displaying minor H antigen and/or MHC differences is regulated by CTLs specific for immunodominant class I-associated epitopes. *J Immunol* 163, 6462-6467 (1999).
306. R. E. Hollingsworth, K. Jansen, Turning the corner on therapeutic cancer vaccines. *NPJ Vaccines* 4, 7 (2019).
307. M. M. Schuler, M. D. Nastke, S. Stevanovic, SYFPEITHI: database for searching and T-cell epitope prediction. *Methods Mol Biol* 409, 75-93 (2007).
308. K. Falk, O. Rotzschke, S. Stevanovic, G. Jung, H. G. Rammensee, Allele-specific motifs revealed by sequencing of self-peptides eluted from MHC molecules. *Nature* 351, 290-296 (1991).
309. P. Grob *et al.*, Role of the individual interferon systems and specific immunity in mice in controlling systemic dissemination of attenuated pseudorabies virus infection. *J Virol* 73, 4748-4754 (1999).
310. J. Chen *et al.*, Immunoglobulin gene rearrangement in B cell deficient mice generated by targeted deletion of the JH locus. *Int Immunol* 5, 647-656 (1993).
311. M. J. Townsend, P. G. Fallon, D. J. Matthews, H. E. Jolin, A. N. McKenzie, T1/ST2-deficient mice demonstrate the importance of T1/ST2 in developing primary T helper cell type 2 responses. *J Exp Med* 191, 1069-1076 (2000).
312. M. Nakauchi *et al.*, Characterization of monoclonal antibodies to Junin virus nucleocapsid protein and application to the diagnosis of hemorrhagic fever caused by South American arenaviruses. *Clin Vaccine Immunol* 16, 1132-1138 (2009).
313. F. T. Hufert, W. Ludke, H. Schmitz, Epitope mapping of the Lassa virus nucleoprotein using monoclonal anti-nucleocapsid antibodies. *Arch Virol* 106, 201-212 (1989).
314. H. C. Probst *et al.*, Immunodominance of an antiviral cytotoxic T cell response is shaped by the kinetics of viral protein expression. *J Immunol* 171, 5415-5422 (2003).
315. B. Ludewig *et al.*, Immunotherapy with dendritic cells directed against tumor antigens shared with normal host cells results in severe autoimmune disease. *J Exp Med* 191, 795-804 (2000).
316. K. Y. Lin *et al.*, Treatment of established tumors with a novel vaccine that enhances major histocompatibility class II presentation of tumor antigen. *Cancer Res* 56, 21-26 (1996).
317. S. Lan, L. McLay, J. Aronson, H. Ly, Y. Liang, Genome comparison of virulent and avirulent strains of the Pichinde arenavirus. *Arch Virol* 153, 1241-1250 (2008).
318. D. D. Pinschewer, M. Perez, A. B. Sanchez, J. C. de la Torre, Recombinant lymphocytic choriomeningitis virus expressing vesicular stomatitis virus glycoprotein. *Proc Natl Acad Sci U S A* 100, 7895-7900 (2003).
319. R. Bouckaert *et al.*, BEAST 2.5: An advanced software platform for Bayesian evolutionary analysis. *PLoS Comput Biol* 15, e1006650 (2019).
320. FigTree, Computer program distributed by author: <http://tree.bio.ed.ac.uk/software/figtree/>. (2018).

321. F. Duan *et al.*, Area under the curve as a tool to measure kinetics of tumor growth in experimental animals. *J Immunol Methods* 382, 224-228 (2012).
322. M. A. Cox, L. E. Harrington, A. J. Zajac, Cytokines and the inception of CD8 T cell responses. *Trends Immunol* 32, 180-186 (2011).
323. X. Zhou, S. Ramachandran, M. Mann, D. L. Popkin, Role of lymphocytic choriomeningitis virus (LCMV) in understanding viral immunology: past, present and future. *Viruses* 4, 2650-2669 (2012).
324. P. Klenerman, R. M. Zinkernagel, What can we learn about human immunodeficiency virus infection from a study of lymphocytic choriomeningitis virus? *Immunol Rev* 159, 5-16 (1997).
325. R. He *et al.*, Follicular CXCR5- expressing CD8(+) T cells curtail chronic viral infection. *Nature* 537, 412-428 (2016).
326. Y. A. Leong *et al.*, CXCR5(+) follicular cytotoxic T cells control viral infection in B cell follicles. *Nat Immunol* 17, 1187-1196 (2016).
327. D. Wieland *et al.*, TCF1(+) hepatitis C virus-specific CD8(+) T cells are maintained after cessation of chronic antigen stimulation. *Nat Commun* 8, 15050 (2017).
328. Q. Shan *et al.*, Ectopic Tcf1 expression instills a stem-like program in exhausted CD8(+) T cells to enhance viral and tumor immunity. *Cell Mol Immunol*, (2020).
329. R. Kratchmarov, A. M. Magun, S. L. Reiner, TCF1 expression marks self-renewing human CD8(+) T cells. *Blood Adv* 2, 1685-1690 (2018).
330. C. Boudousquie *et al.*, Differences in the transduction of canonical Wnt signals demarcate effector and memory CD8 T cells with distinct recall proliferation capacity. *J Immunol* 193, 2784-2791 (2014).
331. W. H. Hudson *et al.*, Proliferating Transitory T Cells with an Effector-like Transcriptional Signature Emerge from PD-1(+) Stem-like CD8(+) T Cells during Chronic Infection. *Immunity* 51, 1043-1058 e1044 (2019).
332. Z. Huang *et al.*, IL-27 promotes the expansion of self-renewing CD8(+) T cells in persistent viral infection. *J Exp Med* 216, 1791-1808 (2019).
333. Q. Yang *et al.*, IL-33 synergizes with TCR and IL-12 signaling to promote the effector function of CD8+ T cells. *Eur J Immunol* 41, 3351-3360 (2011).
334. S. Ali *et al.*, IL-1 receptor accessory protein is essential for IL-33-induced activation of T lymphocytes and mast cells. *Proc Natl Acad Sci U S A* 104, 18660-18665 (2007).
335. P. Aparicio-Domingo *et al.*, Fibroblast-derived IL-33 is dispensable for lymph node homeostasis but critical for CD8 T-cell responses to acute and chronic viral infection. *Eur J Immunol*, (2020).
336. K. Oboki *et al.*, IL-33 is a crucial amplifier of innate rather than acquired immunity. *Proc Natl Acad Sci U S A* 107, 18581-18586 (2010).
337. Q. Chai *et al.*, Maturation of lymph node fibroblastic reticular cells from myofibroblastic precursors is critical for antiviral immunity. *Immunity* 38, 1013-1024 (2013).
338. M. Prinz *et al.*, Distinct and nonredundant in vivo functions of IFNAR on myeloid cells limit autoimmunity in the central nervous system. *Immunity* 28, 675-686 (2008).
339. W. Y. Chen, J. Hong, J. Gannon, R. Kakkar, R. T. Lee, Myocardial pressure overload induces systemic inflammation through endothelial cell IL-33. *Proc Natl Acad Sci U S A* 112, 7249-7254 (2015).
340. Z. Gu, R. Eils, M. Schlesner, Complex heatmaps reveal patterns and correlations in multidimensional genomic data. *Bioinformatics* 32, 2847-2849 (2016).
341. J. N. Blattman *et al.*, Estimating the precursor frequency of naive antigen-specific CD8 T cells. *J Exp Med* 195, 657-664 (2002).

342. J. Crouse *et al.*, Type I interferons protect T cells against NK cell attack mediated by the activating receptor NCR1. *Immunity* 40, 961-973 (2014).
343. A. Banerjee *et al.*, Cutting edge: The transcription factor eomesodermin enables CD8+ T cells to compete for the memory cell niche. *J Immunol* 185, 4988-4992 (2010).
344. Z. Chen *et al.*, TCF-1-Centered Transcriptional Network Drives an Effector versus Exhausted CD8 T Cell-Fate Decision. *Immunity* 51, 840-855 e845 (2019).
345. M. Borsa *et al.*, Modulation of asymmetric cell division as a mechanism to boost CD8(+) T cell memory. *Sci Immunol* 4, (2019).
346. K. Man *et al.*, Transcription Factor IRF4 Promotes CD8(+) T Cell Exhaustion and Limits the Development of Memory-like T Cells during Chronic Infection. *Immunity* 47, 1129-1141 e1125 (2017).
347. Q. Shan *et al.*, The transcription factor Runx3 guards cytotoxic CD8(+) effector T cells against deviation towards follicular helper T cell lineage. *Nat Immunol* 18, 931-939 (2017).
348. M. Danilo, V. Chennupati, J. G. Silva, S. Siegert, W. Held, Suppression of Tcf1 by Inflammatory Cytokines Facilitates Effector CD8 T Cell Differentiation. *Cell Rep* 22, 2107-2117 (2018).
349. G. Jeannet *et al.*, Essential role of the Wnt pathway effector Tcf-1 for the establishment of functional CD8 T cell memory. *Proc Natl Acad Sci U S A* 107, 9777-9782 (2010).
350. V. Lucarini *et al.*, IL-33 restricts tumor growth and inhibits pulmonary metastasis in melanoma-bearing mice through eosinophils. *Oncoimmunology* 6, e1317420 (2017).
351. L. Qin *et al.*, Exogenous IL-33 overcomes T cell tolerance in murine acute myeloid leukemia. *Oncotarget* 7, 61069-61080 (2016).
352. J. E. McLaren *et al.*, IL-33 Augments Virus-Specific Memory T Cell Inflation and Potentiates the Efficacy of an Attenuated Cytomegalovirus-Based Vaccine. *J Immunol* 202, 943-955 (2019).
353. M. H. Wasmer, P. Krebs, The Role of IL-33-Dependent Inflammation in the Tumor Microenvironment. *Front Immunol* 7, 682 (2016).
354. J. J. Fournie, M. Poupot, The Pro-tumorigenic IL-33 Involved in Antitumor Immunity: A Yin and Yang Cytokine. *Front Immunol* 9, 2506 (2018).
355. R. Kuhn, J. Lohler, D. Rennick, K. Rajewsky, W. Muller, Interleukin-10-deficient mice develop chronic enterocolitis. *Cell* 75, 263-274 (1993).
356. M. L. Caton, M. R. Smith-Raska, B. Reizis, Notch-RBP-J signaling controls the homeostasis of CD8- dendritic cells in the spleen. *J Exp Med* 204, 1653-1664 (2007).
357. B. E. Clausen, C. Burkhardt, W. Reith, R. Renkawitz, I. Forster, Conditional gene targeting in macrophages and granulocytes using LysMcre mice. *Transgenic Res* 8, 265-277 (1999).
358. P. P. Lee *et al.*, A critical role for Dnmt1 and DNA methylation in T cell development, function, and survival. *Immunity* 15, 763-774 (2001).
359. R. C. Rickert, J. Roes, K. Rajewsky, B lymphocyte-specific, Cre-mediated mutagenesis in mice. *Nucleic Acids Res* 25, 1317-1318 (1997).
360. K. Richter, G. Perriard, A. Oxenius, Reversal of chronic to resolved infection by IL-10 blockade is LCMV strain dependent. *Eur J Immunol* 43, 649-654 (2013).
361. G. Ni *et al.*, Targeting interleukin-10 signalling for cancer immunotherapy, a promising and complicated task. *Hum Vaccin Immunother* 16, 2328-2332 (2020).
362. A. J. Song, R. D. Palmiter, Detecting and Avoiding Problems When Using the Cre-lox System. *Trends Genet* 34, 333-340 (2018).
363. S. Madera *et al.*, Type I IFN promotes NK cell expansion during viral infection by protecting NK cells against fratricide. *J Exp Med* 213, 225-233 (2016).

364. E. Eckelhart *et al.*, A novel *Ncr1*-Cre mouse reveals the essential role of STAT5 for NK-cell survival and development. *Blood* 117, 1565-1573 (2011).
365. C. Gaebler *et al.*, Evolution of antibody immunity to SARS-CoV-2. *Nature* 591, 639-644 (2021).
366. C. Robert, A decade of immune-checkpoint inhibitors in cancer therapy. *Nat Commun* 11, 3801 (2020).
367. J. Chen *et al.*, NR4A transcription factors limit CAR T cell function in solid tumours. *Nature* 567, 530-534 (2019).
368. A. Mullard, Restoring IL-2 to its cancer immunotherapy glory. *Nat Rev Drug Discov* 20, 163-165 (2021).
369. C. Monaco, J. Nanchahal, P. Taylor, M. Feldmann, Anti-TNF therapy: past, present and future. *Int Immunol* 27, 55-62 (2015).
370. R. S. Accolla, G. Tosi, Adequate antigen availability: a key issue for novel approaches to tumor vaccination and tumor immunotherapy. *J Neuroimmune Pharmacol* 8, 28-36 (2013).
371. A. O. Moguche *et al.*, Antigen Availability Shapes T Cell Differentiation and Function during Tuberculosis. *Cell Host Microbe* 21, 695-706 e695 (2017).
372. H. H. Tam *et al.*, Sustained antigen availability during germinal center initiation enhances antibody responses to vaccination. *Proc Natl Acad Sci U S A* 113, E6639-E6648 (2016).
373. L. M. Fahey *et al.*, Viral persistence redirects CD4 T cell differentiation toward T follicular helper cells. *J Exp Med* 208, 987-999 (2011).
374. C. Yang *et al.*, STAT4: an immunoregulator contributing to diverse human diseases. *Int J Biol Sci* 16, 1575-1585 (2020).
375. T. M. Kundig *et al.*, Duration of TCR stimulation determines costimulatory requirement of T cells. *Immunity* 5, 41-52 (1996).
376. A. Grakoui *et al.*, The immunological synapse: a molecular machine controlling T cell activation. *Science* 285, 221-227 (1999).
377. Z. Waibler *et al.*, Vaccinia virus-mediated inhibition of type I interferon responses is a multifactorial process involving the soluble type I interferon receptor B18 and intracellular components. *J Virol* 83, 1563-1571 (2009).
378. H. Kouzaki, K. Iijima, T. Kobayashi, S. M. O'Grady, H. Kita, The danger signal, extracellular ATP, is a sensor for an airborne allergen and triggers IL-33 release and innate Th2-type responses. *J Immunol* 186, 4375-4387 (2011).
379. S. P. Welten *et al.*, The viral context instructs the redundancy of costimulatory pathways in driving CD8(+) T cell expansion. *Elife* 4, (2015).
380. M. Suresh *et al.*, Role of CD28-B7 interactions in generation and maintenance of CD8 T cell memory. *J Immunol* 167, 5565-5573 (2001).
381. H. Elsaesser, K. Sauer, D. G. Brooks, IL-21 is required to control chronic viral infection. *Science* 324, 1569-1572 (2009).
382. A. Frohlich *et al.*, IL-21R on T cells is critical for sustained functionality and control of chronic viral infection. *Science* 324, 1576-1580 (2009).
383. T. Wu *et al.*, TCF1 Is Required for the T Follicular Helper Cell Response to Viral Infection. *Cell Rep* 12, 2099-2110 (2015).
384. X. Zhou *et al.*, Differentiation and persistence of memory CD8(+) T cells depend on T cell factor 1. *Immunity* 33, 229-240 (2010).
385. Y. Wang *et al.*, The Transcription Factor TCF1 Preserves the Effector Function of Exhausted CD8 T Cells During Chronic Viral Infection. *Front Immunol* 10, 169 (2019).
386. S. Verbeek *et al.*, An HMG-box-containing T-cell factor required for thymocyte differentiation. *Nature* 374, 70-74 (1995).

387. C. Duault *et al.*, IL-33-expanded human Vgamma9Vdelta2 T cells have anti-lymphoma effect in a mouse tumor model. *Eur J Immunol* 47, 2137-2141 (2017).
388. S. F. Chen *et al.*, The paracrine effect of cancer-associated fibroblast-induced interleukin-33 regulates the invasiveness of head and neck squamous cell carcinoma. *J Pathol* 231, 180-189 (2013).
389. M. Akimoto, R. Maruyama, H. Takamaru, T. Ochiya, K. Takenaga, Soluble IL-33 receptor sST2 inhibits colorectal cancer malignant growth by modifying the tumour microenvironment. *Nat Commun* 7, 13589 (2016).
390. K. Wang *et al.*, IL-33 blockade suppresses tumor growth of human lung cancer through direct and indirect pathways in a preclinical model. *Oncotarget* 8, 68571-68582 (2017).
391. V. Mehraj, R. Ponte, J. P. Routy, The Dynamic Role of the IL-33/ST2 Axis in Chronic Viral-infections: Alarming and Adjuvanting the Immune Response. *EBioMedicine* 9, 37-44 (2016).

## V. Appendix

### Lymphocytic choriomeningitis virus meningitis after needlestick injury: a case report#

Sarah Dräger<sup>1\*</sup>, Anna-Friederike Marx<sup>2</sup>, Fiona Pigny<sup>3</sup>, Pascal Cherpillod<sup>3</sup>, Philip Eisermann<sup>4</sup>, Parham Sendi<sup>1,5</sup> and Andreas F. Widmer<sup>1</sup>

<sup>1</sup>Infectious Diseases and Hospital Epidemiology, University Hospital Basel, Petersgraben 4, 4031 Basel, Switzerland.

<sup>2</sup>Department of Biomedicine – Haus Petersplatz, Division of Experimental Virology, University of Basel, 4009 Basel, Switzerland.

<sup>3</sup>Laboratory of Virology, Department of Genetic and Laboratory Medicine, University Hospitals of Geneva, Rue Gabrielle-Perret-Gentil 4, 1211, 14 Geneva, Switzerland.

<sup>4</sup>WHO Collaborating Centre for Arbovirus and Haemorrhagic Fever Reference and Research, Bernhard Nocht Institute for Tropical Medicine, Bernhard-Nocht-Strasse 74, 20359 Hamburg, Germany.

<sup>5</sup>Institute for Infectious Diseases, University of Bern, Freiburgstrasse 18, 3010 Bern, Switzerland.

\* Correspondence: [sarah.draeger@usb.ch](mailto:sarah.draeger@usb.ch)

# **Correction to:** Lymphocytic choriomeningitis virus meningitis after needlestick injury: a case report.

Dräger S, Marx AF, Pigny F, Cherpillod P, Eisermann P, Sendi P, Widmer AF. Antimicrob Resist Infect Control.2019 Aug 22; 8:141 PMID: 31463044

**Key words:** Lymphocytic choriomeningitis virus, Meningitis, Needlestick injury, Accidental infection, RT-PCR

This article has been published in

Antimicrob Resist Infect Control. 2019 May 20;8:77



## **V.1 Background**

Needlestick accidents while handling of infectious material in research laboratories can lead to life-threatening infections in laboratory personnel. In laboratories working with the lymphocytic choriomeningitis virus (LCMV), the virus can be transmitted to humans through needlestick injury and lead to serious acute illness up to meningitis.

## **V.2 Case presentation**

We report of a case of LCMV meningitis in a laboratory worker who sustained a penetrating needlestick injury with a LCMV-contaminated hollow needle whilst disposing of a used syringe into the sharps waste bin. Four days after needlestick injury the laboratory worker developed a systemic disease: 11 days after exposure, she was diagnosed with meningitis with clinical signs and symptoms of meningismus, photophobia, nausea and vomiting, requiring hospitalization. The PCR was positive for LCMV from the blood sample. 18 days after exposure, seroconversion confirmed the diagnosis of LCMV-induced meningitis with an increase in specific LCMV-IgM antibodies to 1:10'240 (day 42: 1:20'480). Ten weeks after exposure, a follow-up titre for IgM returned negative, whereas IgG titre increased to 1:20'480.

## **V.3 Conclusions**

This is the first case report of a PCR-documented LCMV meningitis, coupled with seroconversion, following needlestick injury. It highlights the importance of infection prevention practices that comprise particularly well-established safety precaution protocols in research laboratories handling this pathogenic virus, because exposure to LCMV can lead to a severe infection.

## **V.4 Author contribution**

I contributed to this article by providing the clinical data. Throughout the course of my PhD, there was an unfortunate incident while infection mice with LCMV Cl-13 that resulted in a self-inoculation of LCMV Cl-13. As you can read in the clinical report, although the first day's post infection were asymptomatic, I developed a meningitis soon after the incubation period. As a consequence, I had to be hospitalized for symptomatic treatment and support. Given the verity of well documented LCMV infections that include full information about the source and route of the inoculum in humans, it was my interest together with the clinicians to publish such a report. The clinical data, that I provided included a self-reported description about my symptoms from onset to termination.



## VI. Contributions to the work

The article “Residual antigen in transiently CD4<sup>+</sup> T cell depleted mice induces high levels of virus-specific antibodies but only limited B cell memory” was achieved in close collaboration of our lab with the group of Prof. Hanspeter Pircher at the University in Freiburg, Germany. This project was a continuation of my master thesis “Induction of virus specific antibodies after the acute phase of lymphocytic choriomeningitis infection”. Based on the preliminary data generated during my master thesis, further experiments were performed by Oliver Schweier and Ulrike Aichele. During my PhD in the group of Daniel Pinschewer, I could perform the experiment shown in Fig. 1-4.

For the article “Heterologous arenavirus vector prime-boost overrules self-tolerance for efficient tumor-specific CD8 T cell attack” I performed experiments and analyses, which contributed to Figure 2-4, Fig. S 2- 5 and Fig. S 2-6.

The big majority of experiments in Chapter 3 were done by myself with the following exceptions.

The *in vitro* data (experiment as well as analysis) shown in Fig. 3- 2 C were conducted in the laboratory of Prof. Max Löhning (Berlin) by Tobias Brunner.

The bioinformatic data analysis of RNA seq data from P14 Wt and P14 ST2<sup>-/-</sup> (Fig. 3-1 I-L) was done by Florian Geier (Department of Biomedicine, Bioinformatics Core Facility, Basel).

Immunofluorescence staining of spleen sections for IL-33 protein shown in Fig. 3-3 K and Fig. S 3-6 were conducted in the laboratory of Prof. Sanjiv Luther at the University of Lausanne by Leo Scarpellino and Melanie Charmoy (group Prof. Werner Held).

All data presented in Chapter 4 were done by myself. The generation of chimeric mice was done with the help of Weldy Bonilla Pinschewer (group Prof. Daniel Pinschewer).

## Curriculum vitae

# Anna-Friederike Marx

Markircherstrasse 54  
4055 Basel, Switzerland  
[a.marx@unibas.ch](mailto:a.marx@unibas.ch)  
Tel.: +41-766049486

### Personal Info

---

DATE OF BIRTH: 11<sup>th</sup> MARCH 1992  
PLACE OF BIRTH: BREMEN  
NATIONALITY: GERMAN  
SWISS RESIDENCE PERMIT: C

### Education

---

- 02/2017-06/2021
- **PhD in Medical-Biological Research (Dr.rer.nat)**  
University of Basel (Switzerland)
    - Dissertation: *The role of residual antigen and the alarmin IL-33 in shaping the antiviral immune response.*  
Advisor: Prof. Dr. Daniel Pinschewer  
Experimental Virology-Department of Biomedicine, Basel
    - Final grade: summa cum laude
- 10/2014-12/2018
- **Master of Science in Biology**  
Albert- Ludwig's-University of Freiburg (Germany)
    - Study emphases: Advanced Immunobiology
    - Master Thesis: *Induction of virus specific antibodies after the acute phase of lymphocytic choriomeningitis virus infection.* (Grade 1.0, excellent)  
Advisor: Prof. Dr. Hanspeter Pircher  
Institute of Immunology, Freiburg
    - Final grade: 1.3 (best=1, worst=5)

- 10/2011-06/2014
- **Bachelor of Science in Molecular Biology**  
Johannes Gutenberg Universität Mainz (Germany)
    - Study emphases: Molecular Genetics
    - Bachelor Thesis: *Kartierung unterschiedlicher Loci an Polytäanchromosomen von Chironomus*  
Advisor: Prof. Dr. Erwin Schmidt  
Institute of Molecular Genetics, Mainz
    - Final grade: 1.5 (best=1, worst=5)

## Work and Research experience

---

- 06/2021-present
- **Junior researcher/Postdoctoral scientist**  
University of Basel, Department of Biomedicine, Basel (Switzerland)  
Working Group Prof. Dr. Daniel Pinschewer  
Projects:
    - *Memory B cell longevity and origin*
    - *The alarmin interleukin-33 promotes the expansion and preserves the stemness of Tcf-1<sup>+</sup> CD8<sup>+</sup> T cells in chronic viral infection*
- 01/2017-02/2017
- **Research Assistant**  
University of Freiburg, Albert Ludwig's University (Germany)  
Working Group Prof. Dr. Hanspeter Pircher  
Projects:
    - *Characterization of virus-specific B cell responses upon initial CD4 T cell depletion*
- 04/2013-03/2014
- **Research Assistant**  
University of Mainz, Institute of Molecular Physiology (Germany)  
Working Group Prof. Dr. Harald Paulsen  
Teaching Course:
    - *Pflanzenphysiologisches Praktikum Institute of Molecular Physiology*

## Skills and Training

---

- Courses and Workshops**
- **Antelope Career Program of the University of Basel** (coaching sessions on the topics of funding and leadership/empowerment)  
University of Basel  
(04/2023-present)
  - **Laboratory Animal Welfare and Science FELASA B**  
University of Freiburg (Germany)  
(02/2016)

- **English Language Summer School**  
Summer School at Glyndwr-University Wrexham (Great Britain)  
(06/2014-07/2014)

**Languages**

- German (native), English (fluent), French (basic)

**Software**

- Microsoft Office, Endnote, Adobe Illustrator, GraphPad Prism, FlowJo

**Scientific Publications**

- 
- **Marx AF\***, Kallert SM\*, Brunner TM\*, Villegas JA, Geier F, Fixemer J, Abreu-Mota T, Reuther P, Bonilla WV, Fadejeva J, Kreutzfeldt M, Wagner I, Aparicio-Domingo P, Scarpellino L, Charmoy M, Utschneider DT, Hagedorn C, Lu M, Cornille K, Stauffer K, Kreppel F, Merkler D, Zehn D, Held W, Luther SA, Löhning M, Pinschewer DD. *The alarmin interleukin-33 promotes the expansion and preserves the stemness of Tcf-1<sup>+</sup> CD8<sup>+</sup> T cells in chronic viral infection.* **Immunity.** 2023 Feb 14;S1074-7613(23)00041-9. doi: <https://doi.org/10.1016/j.immuni.2023.01.029> PMID: 36809763. \*Shared first author
  - Ertuna YI, Fallet B, **Marx AF**, Dimitrova M, Kastner AL, Wagner I, Merkler D, Pinschewer DD. *Vectored antibody gene delivery restores host B and T cell control of persistent viral infection.* **Cell Rep.** 2021 Nov 30;37(9):110061. doi: <https://doi.org/10.1016/j.celrep.2021.110061>. PMID: 34852228.
  - Narr K, Ertuna YI, Fallet B, Cornille K, Dimitrova M, **Marx AF**, Martin K, Abreu Mota T, Künzli M, Schreiner D, Brunner TM, Kreutzfeldt M, Wagner I, Geier F, Bestmann L, Löhning M, Merkler D, King CG, Pinschewer DD. *Vaccine-elicited CD4 T cells prevent the deletion of antiviral B cells in chronic infection.* **Proc Natl Acad Sci U S A.** 2021 Nov 16;118(46):e2108157118. doi: <https://doi.org/10.1073/pnas.2108157118>. PMID: 34772811
  - Bonilla WV, Kirchhammer N \*, **Marx AF\***, Kallert SM, Krzyzaniak MA, Lu M, Darbre S, Schmidt S, Raguz J, Berka U, Vincenti I, Pauzuolis M, Kerber R, Hoepner S, Günther S, Magnus C, Merkler D, Orlinger KK, Zippelius A, Pinschewer DD. *Heterologous arenavirus vector prime-boost overrules self-tolerance for efficient tumor-specific CD8 T cell attack.* **Cell Rep Med.** 2021 Mar3;2 (3):100209 doi: <https://doi.org/10.1016/j.xcrm.2021.100209>. PMID: 33763654 \*Shared second author
  - Schweier, O.\*, Aichele, U. \*, **Marx, A.-F.\***, Straub, T., Verbeek, J.S., Pinschewer, D.D. and Pircher, H. (2019), *Residual LCMV antigen in transiently CD4<sup>+</sup> T cell-depleted mice induces high levels of virus-specific antibodies but only limited B-cell memory.* **Eur. J. Immunol.** 2019 Apr:49 (4):626-637 doi: <https://doi.org/10.1002/eji.201847772>. PMID: 30636035.\*Shared first author
  - Dräger S, **Marx AF**, Pigny F, et al. *Lymphocytic choriomeningitis virus meningitis after needlestick injury: a case report [published correction appears in Antimicrob Resist Infect Control. 2019 Aug 22;8:141].* **Antimicrob Resist Infect Control.** 2019 May 20;8:77. doi: <https://doi.org/10.1186/s13756-019-0524-4>. PMID: 31139360

## Acknowledgment

First, I would like to thank Daniel! *Daniel*, thanks for giving me the opportunity to work on such a fascinating project. Thank you very much for all your support! Throughout my PhD, I never felt that there were any restrictions in following my ideas conceptionally and experimentally. I thank you for your understanding, optimism, enthusiasm, encouragement and for pushing me further than I thought I could go. Especially thanks for your support during my hospitalization. I am really thankful for that!

I would also like to thank my tutors, Dr. Peter Aichele and Prof. Dr. Christoph Dehio, for their valuable guidance throughout my PhD and for evaluating my work.

*Peter*, recht herzlichen Dank für all die spannenden Diskussionen rund um IFNAR und ST2 sowie dein offenes Ohr und deinen grossen Optimismus!

A big THANK YOU to all present and past lab members-Mirela, Min, Yusuf, Peter, Mehmet, Kerstin, Karen, Weldy, Karsten, Tiago, Marianna, Katrin, Nicole and Mathias. It was a great time and it has been a great pleasure to work with all of you! For all your support many, many thanks!

Thanks especially to *Min(i)*! Thanks for always being supportive and helpful! I could always count on you- indeed you are our lab-mama!

Liebe *Katrin*, ich danke dir von Herzen für all die Unterstützung und all die vielen Cappuccino Pausen;) Ich konnte mich immer auf dich verlassen und du hast immer ein offenes Ohr gehabt! Die Freundschaft zu dir ist etwas ganz Besonderes!

Special thanks to *Yusi, Mati, Mehmet* and *Lena* Okidoki (and Christoph) for all the support and the funny moments we shared together.

*Lena*, vielen Dank für deine Hilfsbereitschaft und dein offenes Ohr sowie die Gründung einer AAV-Produktionsfirma☺!

*Karsten*, ich bedanke mich von Herzen für die unendliche Unterstützung im «Maus-Haus». Ohne dich, wären wir alle aufgeschmissen. Besonderen Dank für dein offenes Ohr und die grossartige Unterstützung beim Maus-Umzug;) Recht herzlichen Dank!

*Weldy*, ich danke dir von Herzen für all die Unterstützung im Labor. Ich danke dir auch für das Züchten unserer ST2 Maus-Linien! Ich konnte mich auf dich immer 100% verlassen und es hat mir immer Freude bereitet mit dir und Mini zu arbeiten. Ich denke noch heute gerne an die «CD28-story» zurück;)

*Sandra*, ich bedanke mich recht herzlich für all die Hilfe zu Beginn des Projektes. Du hast den Grundstein gelegt, auf dem ich aufbauen konnte!

Thanks to *Sonia* and *Nicole*, two persons that keep the lab running.

Many thanks to Prof. Max Löhning, Prof. Sanjiv Luther as well as Prof. Doron Merkler for all the “Synergia meetings”. Thanks especially to Sanjiv, Patricia, Tobias and Max for all the support.

Ein grosses Dankeschön an Prof. Hanspeter Pircher! *Hanspeter*, ich danke dir von Herzen für deine Unterstützung in jeglicher Hinsicht und dein offenes Ohr! Es hat mir immer grosse Freude gemacht zu dir

nach Freiburg zu fahren oder dich einfach anzurufen und stundenlang über Paper und Daten zu reden. Ich bedanke mich auch recht herzlich, dass du mein Masterprojekt weitergeführt hast, das war einfach Spitze! Meinen Freiburger Anna(nas) Mädels (*Siyu, Lena, Sandra* und *Judith*) danke ich für eine unvergessliche Zeit und für die vielen einzigartigen Momente! Ihr habt immer an mich geglaubt und mich unterstützt. Vielen Dank an *Judith* und *Sandra* für die Korrekturen.

Besonderen Dank an *Lena*: Du bist einfach klasse! Ich danke dir für all die gemeinsamen Urlaube und Aktivitäten! Ohne dich und dein Organisationstalent wäre ich/wären wir einfach aufgeschmissen! Ich kann mich auf dich 100 % verlassen, du wirst als Freundin für mich immer eine ganz wichtige Rolle spielen!

Liebe *Nadine*, ich danke dir von Herzen für diese tolle Freundschaft!! Du hast nie den Weg gescheut mich zu besuchen und wir konnten so über all die Jahre in Kontakt bleiben! Vielen Dank, dass ich mich auf dich einfach immer verlassen kann.

Ich danke recht herzlich meinen Eltern für all die Unterstützung! Ich kann mich auf euch immer verlassen, was mir eine enorme Sicherheit gibt! Ihr habt mir immer das Gefühl gegeben, dass ihr mich in jeglicher Hinsicht unterstützt! Vielen Dank für euren grossen Optimismus in jeder Lebenslage und den grossartigen Humor, der so viele Situationen einfacher macht! Auch recht herzlichen Dank an den Rest der Familie, besonders *Karen, Tobias, Daniel, Tante Heide* und natürlich *Oma*!

And last but not least I would like to thank Tiago!! Throughout the writing of this dissertation, I have received a great deal of support and assistance. This was just AMAZING! You`ve provided stimulating discussions as well as many, many happy moments.